IDENTIFICATION OF AMYOTROPHIC LATERAL SCLEROSIS DISEASE MECHANISMS BY CEREBROSPINAL FLUID PROTEOMIC PROFILING

by

Mahlon Angus Collins

B.S. in Neuroscience/Psychology, Central Michigan University, 2006

M.S. in Experimental Psychology, Central Michigan University, 2009

Submitted to the Graduate Faculty of

the School of Medicine in partial fulfillment

of the requirements for the degree of

PhD in Neurobiology

University of Pittsburgh

2016

UNIVERSITY OF PITTSBURGH

SCHOOL OF MEDICINE

This dissertation was presented

by

Mahlon Angus Collins

It was defended on

April 14, 2016

and approved by

Carey Balaban, PhD, Professor

Michael Gold, PhD, Professor

Teresa Hastings, PhD, Associate Professor

Janice Robertson, PhD, Associate Professor

Rebecca Seal, PhD, Assistant Professor

Dissertation Advisor: Robert Bowser, PhD, Adjunct Professor

IDENTIFICATION OF AMYOTROPHIC LATERAL SCLEROSIS DISEASE MECHANISMS BY CEREBROSPINAL FLUID PROTEOMIC PROFILING

Mahlon Angus Collins, PhD

University of Pittsburgh, 2016

Amyotrophic lateral sclerosis (ALS) is the most common form of adult-onset motor neuron disease. Heterogeneity in clinical, genetic, and pathological features of ALS suggest the disease is a spectrum of disorders each resulting in motor neuron degeneration. Molecular profiling of ALS patients is, therefore, a useful means of characterizing and stratifying the ALS population. To this end, mass spectrometric proteomic profiling was performed on cerebrospinal fluid (CSF) from ALS, healthy control (HC), and other neurological disease (OND) subjects. This resulted in the identification of 1,712 CSF proteins, 123 of which exhibited altered relative abundance in ALS CSF. Biological processes related to these 123 proteins included synaptic activity, extracellular matrix, and inflammation. The application of feature selection and machine learning methods to these CSF proteomic profiles resulted in a classifier that used relative levels of WDR63, APLP1, SPARCL1, and CADM3 to predict independent ALS, HC, and OND samples with 83% sensitivity and 100% specificity. To aid in the validation of selected CSF proteins, a Western blot loading control method was developed and validated using a reversible, iodine-based total protein stain. This method improves the accuracy and sensitivity of the relative quantification of CSF proteins via Western blot. As RNA binding protein (RBP) pathology/dysfunction is common to several forms of ALS, the largest CSF RBP alteration, that of RNA binding motif 45 (RBM45) protein, was validated externally. The results demonstrated that RBM45 pathology is common to several forms of ALS, frontotemporal lobar degeneration (FTLD), and Alzheimer's disease. To further understand the

biological functions of RBM45, immunoprecipitation coupled to mass spectrometry was performed to identify RBM45 protein-protein interactions (PPIs). RBM45 PPIs and associated pathways were most strongly associated with hnRNP proteins, RNA processing, and cytoplasmic translation. RBM45 also participates in the general cellular response to stress via association with nuclear stress bodies. This association is dependent on RNA binding, is upregulated in ALS/FTLD, and is sufficient to induce the aggregation of the protein. Collectively, these results illustrate the utility of CSF proteomic profiling for characterizing mechanisms of neurological disease and provide new insights into the contributions of RNA binding protein dysregulation to ALS/FTLD.

TABLE OF CONTENTS

LIST OF TABLES

LIST OF FIGURES

PREFACE

I would like to thank the patients who have participated in this and other research projects on ALS/FTLD by tissue and biofluid donation.

1.0 INTRODUCTION

Amyotrophic lateral sclerosis (ALS) is the most common form of adult-onset motor neuron disease. This progressive, fatal neurodegenerative disorder occurs in approximately 2 persons per 100,000[1-5]. Since the initial description of the symptoms and associated pathology in 1874, considerable insights into the genetic, molecular, and biochemical mechanisms of ALS have been gained. The pathological hallmark of ALS is the death of pyramidal motor neurons of the corticospinal pathway in the motor cortex and spinal column. This leads to a myriad of clinical symptoms, such as muscle weakness, muscle atrophy, and spasticity. Considerable variability in site of onset, rate of progression, and survival time occurs in ALS patients and underscores the overall heterogeneity of the disease. These observations have led to the hypothesis that ALS is actually a collection of disorders of distinct cause that produce similar pathological and clinical phenotypes. Nevertheless, molecular mechanisms of ALS tend to converge on the general themes of selective motor neuron vulnerability and non-cell autonomous influences. These themes have aided the development of molecular models that explain relevant clinical phenomena, such as spreading of motor dysfunction, age-related onset, and co-occurrence of cognitive dysfunction (e.g., dementia) in ALS.

Broadly, ALS can be separated into two categories based on disease etiology. The vast majority of cases are classified as sporadic ALS (sALS) and are of unknown cause. Approximately 5-10% of all ALS cases are a result of inherited genetic abnormalities and are thus classified as familial ALS (fALS). Although fALS cases are a small portion of the overall ALS population and

any single familial form of disease represents an even smaller fraction, considerable insight into disease mechanisms have been gained by studying these rare forms of ALS. As will be emphasized throughout this introduction, fALS cases and model systems based on these cases have proven highly valuable for the study of sALS, as well as fALS. These monogenic disease-causing variants provide a relatively straightforward approach to understanding how a triggering event (in this case a genetic abnormality) can produce a cascade of molecular events that ultimately lead to cell death. A thorough overview of the various mechanisms associated with ALS, combining evidence from the research on sALS (and, where appropriate, fALS) cases and model systems, thus provides a suitable framework for understanding current mechanistic models of ALS as well as areas where new advancements in our understanding of the disease may be made.

1.1 PROTEIN AGGREGATION AND INTRACELLULAR INCLUSION BODIES

The abnormal aggregation of proteins into inclusion bodies in motor neurons is a long-known pathological feature of sALS[6] and fALS[7]. The early characterizations of inclusions defined their filamentous, skein-like morphology, along with their eosinophilic core (and, hence, proteinaceous composition)[6-8]. Subsequent work revealed a variety of characteristic inclusion types in in ALS motor neurons, including larger skein-like inclusions reactive for ubiquitin, smaller filamentous inclusions containing neurofilament proteins, dense spheroids with a Lewy-body like appearance (compact inclusions [CIs]), and Bunina bodies, small granular inclusions of lysosomal origin[8]. Since the identification of inclusions as a pathological hallmark of ALS, considerable effort has been devoted to determining the protein constituents and neurotoxic mechanisms.

1.1.1 SOD1

The discovery that point mutations in the superoxide dismutase 1 (*SOD1*) gene can produce familial forms of ALS[9] (approximately 20% of all fALS cases[10]) led to the identification of inclusions positive for the mutant, misfolded protein. Subsequent work has shown that SOD1 pathology can also occur in sALS cases[11,12]. SOD1 catalyzes the conversion of the superoxide anion into hydrogen peroxide and molecular oxygen via the cylical reduction and oxidation of copper[13,14]. Despite altered enzymatic activity in many fALS-linked SOD1 mutant proteins, existing evidence suggests that loss of SOD1 function does not contribute to SOD1-linked fALS. Notably, disease progression and severity are not correlated with mutant SOD1 enzymatic activity in human patients[15,16] and mice lacking the SOD1 gene develop normally and do not develop motor deficits or SOD1 pathology[17], in contrast to mutant SOD1 expressing mice that develop progressive motor abnormalities and SOD1 aggregates[18,19]. fALS-linked mutant SOD1 aggregates into insoluble amyloid-like fibrils in vitro[20-22], in transgenic mutant SOD1 expressing mice[19,23] , and in human fALS patients[24,12]. The mutant SOD1 aggregation appears to be driven by mutation-induced misfolding, which can result from the protein sequence itself, reduced capacity to bind metal ions, or both[12,21,22].

While human ALS patients and transgenic SOD1 mice develop insoluble, ubiquitinated SOD1 aggregates in motor neurons, current models implicate soluble, misfolded SOD1, as the toxic species, similar to models proposed other aggregating proteins, such as amyloid beta. Soluble, misfolded SOD1 can form oligomeric pore structures and exerts many deleterious effects within the cell[25,20]. The protein is capable of inducing ER stress, which overwhelms the cell's capacity to provide normal clearance of cytoplasmic proteins and can ultimately lead to apoptotic cell death[26-28]. Mutant SOD1 also aberrantly accumulates in the mitochondrial intermembrane space, impairing normal mitochondrial function[27,29,30]. SOD1 localization to mitochondria promotes the association of

mutant SOD1 with BCL2[28], which is capable of inducing apoptosis in cell culture models. Where the mutation reduces metal ion binding, mutant SOD1 also promotes calcium dyshomeostasis, leading to enhanced susceptibility to cellular stress[31]. More recent work suggests that cells also secrete misfolded SOD1, which can then seed the aggregation SOD1 (mutant or WT native) in adjacent cells via a prion-like process[32,11], providing a possible mechanism for disease spreading.

1.1.2 TDP-43

Subsequent work demonstrated that many ubiquitinated, skein-like inclusions in sALS motor neurons were non-reactive to SOD1 antibodies. The identity of the constituent protein(s) of these inclusions remained elusive until 2006, when TDP-43 was identified as the main component[33]. Subsequent studies identified mutations in the *TARDBP* gene that could lead to familial forms of either disorder[34-37], each with extensive TDP-43 inclusion pathology. These discoveries led to the creation of the umbrella term "TDP-43 proteinopathy"[38] for forms of ALS, frontotemporal lobar degeneration (FTLD), and other disorders that exhibit characteristic TDP-43 inclusion pathology. Though phenotypically dissimilar, these disorders show a number of common TDP-43 modifications, the most prevalent of which is the incorporation of the protein into insoluble, ubiquitinated filamentous inclusions in neurons[38-41]. The protein is also frequently depleted from the cell nucleus, hyperphosphorylated, and cleaved into C-terminal fragments, though this latter phenomenon occurs in a CNS region-specific pattern[38-41].

The TDP-43 protein is a 43 kDa RNA binding protein that features two RNA recognition motifs (RRMs), a nuclear localization sequence (NLS), a nuclear export signal, a glycine-rich C-terminal domain, and a prion-like domain, the latter two of which are aggregation-prone and the location of the majority of ALS/FTLD-causing *TARDBP* mutations[42,43]. TDP-43 has many roles in

the regulation of gene expression. These include regulating transcription, RNA splicing, microRNA biogenesis, and mRNA transport and degradation[42,43]. The importance of this regulatory capacity is underscored by the observation that *TARDBP* null mice are embryonic lethal[44,45]. TDP-43 also undergoes transient nucleo-cytoplasmic transport in response to cellular stress[46,47]. The resultant association of the protein with cytoplasmic stress granules (SGs), stress-induced protein-RNA complexes containing stalled translational components, has emerged as a plausible mechanism for TDP-43 aggregate formation[48]. Association of RNA binding proteins, such as TDP-43, into stress granules results in their assembly into insoluble complexes that disassemble following the removal of the stressor. Chronic activation of stress-associated pathways, however, could result in irreversible aggregation of TDP-43. Evidence in support of this notion comes from the observation that SG proteins are frequently found in TDP-43 inclusions in ALS/FTLD patient tissue and that chronic stress produces TDP-43 aggregates in cell culture models[47-49]. Moreover, the TDP-43 protein (and, more specifically the C-terminal domain) of the protein are intrinsically aggregation prone[50].

Unlike SOD1, TDP-43 toxicity is mediated by both loss-of-function and toxic gain-of-function mechanisms[40,42]. Loss of the normal gene expression regulatory functions of TDP-43 may occur through hypofunction induced by mutation or post-translational modification (e.g., phosphorylation or C-terminal cleavage). Similarly, trapping of the protein in cytoplasmic aggregates is expected to contribute to loss of function by depleting the protein from the nucleus and impairing both normal nuclear and cytoplasmic TDP-43 functions. The importance of maintaining homeostatic TDP-43 levels to cell viability is highlighted by studies demonstrating TDP-43's ability to self-regulate its expression in cells via an auto-regulatory feedback loop[51] and the observation of neuronal and behavioral abnormalities in a variety of model systems over- or under-expressing TDP-43 (WT or mutant), including mice[44,52,53], drosophila[54-56], and zebrafish[57,58,].

In addition, misfolded, aberrantly modified TDP-43 displays toxic properties unrelated to its normal functions and these toxic properties are chiefly related to the cytoplasmic accumulation and processing of the protein. Increased cytoplasmic accumulation is an early event in human TDP-43 proteinopathies and is thought to precede inclusion formation[59]. When recapitulated in cell culture and animal models, the phenomenon induces TDP-43 aggregation/misfolding, proteasomal and autophagic activation, and is toxic to cultured neurons[60-62]. Cellular stress together with aberrant cytoplasmic localization of TDP-43 promotes cleavage of the protein into C-terminal fragments by the activation of caspases[63]. Such fragments are hyperphosphorylated and are toxic to cultured cells[64]. A unique property of C-terminal fragments is their confinement to the cytoplasm as a consequence of the location of the NLS in the protein's N-terminus. The generation of CTF's is enhanced by proteasomal inhibition or cell stress[63], though the precise function(s) of the fragments remains elusive. Likewise, the effects of TDP-43 phosphorylation and ubiquitination are not entirely clear, though these modifications are strongly associated with misfolded, insoluble forms of the protein[65]. Misfolded, cytoplasmic TDP-43 also appears capable of seeding further misfolding of endogenous TDP-43 in a prion-like manner as is observed for SOD1[66].

1.1.3 FUS

FUS/TLS is a related RNA binding protein also mutated in rare instances of fALS (approximately 3-5% of all fALS cases) and found in skein-like inclusions in fALS and sALS motor neurons[67-70]. Structurally, the protein contains an RNA recognition motif, a nuclear localization sequence, a nuclear export sequence, two arginine/glycine-rich regions, a zinc finger domain, a prion-like domain, and a glycine-rich domain. These latter two features confer a propensity for aggregation to the protein[71]. Like TDP-43, it has numerous roles in the regulation of gene expression, however, the

specific functions defined for FUS distinguish it from TDP-43[67,70]. FUS binding to DNA regulates transcription and the protein is recruited to sites of DNA damage, where it contributes to break repair[67]. FUS also regulates transcription by direct binding to DNA. With regard to RNA, FUS binds long intronic regions of pre-mRNAs[72] and thus contributes to splicing and the protein also regulates the subcellular localization of RNA molecules[67]. FUS, like TDP-43, is capable of nucleocytoplasmic shuttling by virtue of its structure and, when localized to the cytoplasm, associates with SGs[73]. As it does for TDP-43, this association provides a plausible mechanism for FUS inclusion formation.

Both loss of function and toxic gain of function mechanisms are thought to contribute to FUS-mediated neurodegeneration[67]. The trapping of FUS in inclusions is expected to impair the normal functions of FUS and neurons appear particularly sensitive to mutations that alter FUS levels or confine the protein to the cytoplasm. Like TDP-43, several ALS-causing *FUS* mutations are found in the glycine rich region of the protein, while, in contrast to TDP-43, numerous additional disease causing mutations have been found in the NLS[67,70]. This underscores the vital role of intranuclear FUS functions to cell viability and the toxic properties of excessive cytoplasmic FUS. Cytoplasmic-confined FUS forms inclusions and these are positive for ubiquitin and p62[49,74-76]. Intriguingly, these same inclusions are negative for TDP-43, implying separate mechanisms of inclusion formation, despite the association of both proteins with SGs. FUS inclusions are non-amyloid, though the protein can form fibrils in vitro[71]. Insoluble FUS can be found in human ALS tissue and FUS inclusions are frequently ubiquitinated[76]. More recent evidence suggests that FUS may also form intranuclear inclusions[77]. Collectively, these processes suggest that mis-localization of FUS, misfolding, and aggregation of the protein contribute to its neurotoxic effects in both FUS-linked fALS and sALS.

1.1.4 Neurofilament Proteins and Peripherin

The pathological aggregation of cytoskeletal intermediate filament proteins into inclusions in ALS motor neurons provides evidence of cell-structural mechanisms of ALS neurodegeneration. Spheroidal axonal aggregates, Lewy body-like inclusions, and hyaline conglomerate inclusions are frequently positive for peripherin and the neurofilament proteins in fALS and sALS cases[78-80]. These proteins are critical components of the neuronal cytoskeleton. Peripherin forms cytoskeleton-associated homopolymers that can also interact with other cytoskeletal proteins[81]. The expression of peripherin is neuron-specific, particularly in neurons extending to the peripheral nervous system, including spinal motor neurons. The neurofilaments comprise three subunit types: neurofilament light, neurofilament medium, and neurofilament heavy[78,82]. Protein function requires polymerization of the three subunit types and the light filament is essential for this process[83]. They are largely localized to the axon where they provide structural strength and regulate axonal diameter. The neurofilament cytoskeletal assembly is highly dynamic and the rate of transport of neurofilament proteins is inversely related to their phosphorylation state[83]. The abnormal accumulation and aggregation of these intermediate filament proteins occur in both the cell body and the axon of ALS motor neurons[78]. In the case of neurofilaments, the aggregated proteins are generally hyperphosphorylated, and hence, immobile. The accumulation and aggregation of these proteins lead to deficits in axonal transport and cytoskeletal abnormalities that appear to be early indicators of disease in ALS patients and SOD1 transgenic mice[84,85]. Genetic evidence for these mechanisms comes from the identification of rare mutations in the peripherin gene in ALS cases[86,87], ALS patients with mutations in the neurofilament heavy gene[88,89], and the observation that peripherin overexpressing mice develop intermediate filament protein inclusions and progressive motor neuron loss[90].

1.1.5 Bunina Bodies

A related form of protein aggregate unique to ALS is the Bunina body. These structures are small (3-5 μm), intraneuronal, globular inclusions[91]. They are found in motor neurons and are specific for ALS, occurring in approximately 90% of sALS cases[92]. The protein composition of Bunina bodies is unique in that they are typically not immunoreactive for ubiquitin, p62, TDP-43, FUS, or other ALS inclusion-associated proteins. Instead, the cysteine protease inhibitor cystatin C and the iron binding protein transferrin are the canonical marker proteins of these aggregates[93,94]. In addition to their protein composition, a further distinguishing feature of Bunina bodies is a homogeneous, electron-dense core surrounded by vesicular and tubular materials[91]. This has led to the suggestion that Bunina bodies are of ER or lysosomal origin. The presence of cystatin C in neuronal lysosomes lends support to a theory of lysosomal origin and suggests a neuroprotective role for Bunina bodies/cystatin C related to protein quality control[91].

1.1.6 Other Aggregating Proteins

In recent years, mutations in a number of genes have been found fALS cohorts. These include mutations in the *TARDBP*, *FUS*, *UBQLN2*, *OPTN*, *SQSTM1*, *VCP*, *HNRNPA1*, and *PFN1* genes[8]. Despite diverse functions of each protein, aggregates of the mutant form are consistently found in fALS cases. Moreover, recent work has shown that non-ATG translation of the fALS-associated *C9ORF72* repeat expansion leads to the expression of dipeptide repeat proteins that are aggregated in fALS tissue and model systems. These findings underscore the preponderant role of protein aggregation in motor neuron degeneration, especially when considered together with the observation that similar aggregates of these proteins are frequently found in sALS cases[8]. Moreover, some fALS

genes encode proteins associated with the ubiquitin proteasome system, demonstrating the indispensable role of protein quality control and degradation in maintaining neuronal viability. While the protein composition of aggregates in sALS and fALS varies considerably, proteasomal stress and impairment of normal cellular trafficking of biomolecules are expected to occur widely in the various forms the disorder takes and, thus, these processes represent promising therapeutic targets for future drug development and clinical trials. A schematic of the contributions of intracellular protein aggregation to motor neuron degeneration is shown in Figure 1.1.

1.2 INTRACELLULAR STRESS

Intracellular stress occurring in motor neurons is widely recognized as a cause of ALS pathology and motor neuron death. Studies in human ALS tissues and model systems have documented the occurrence of multiple forms of intracellular stress occurring within motor neurons and the ways these stressors may contribute to cell death. Though it is likely that multiple cellular stresses contribute to cell death in concert, understanding the effects of a single cellular stressor is valuable in defining the time course of events that lead to cell death and in identifying potential therapeutic targets. This has proven especially true for fALS-linked mutations in stress-response genes, as documented below.

1.2.1 Stress Granules

Cytoplasmic stress granules (SGs) are protein-RNA complexes that form in response to a variety of cellular stressors. The onset of cellular stress causes a rapid cessation of mRNA translation. The

stalled translational complex rapidly disassembles and the components coalesce into SGs. The purpose of SGs appears to be two-fold: (1) To prioritize translation of mRNAs that favor the cellular response to stress and (2) remove other mRNAs and RNA binding proteins from the harmful cellular environment and stop their translation[95,96]. Evidence for the former purpose comes from studies showing selective increases in translation of stress-related mRNAs and selective decreases in translation of unrelated mRNAs[96,97]. Evidence for the latter comes from studies showing that certain housekeeping gene transcripts are reliably recruited to stress granules following the onset of a variety of stressors[98]. SGs are dynamic, transient structures that dissipate following the removal of the stressor and a constant turnover of protein and mRNA occurs during the life of the SG. Multiple lines of evidence now suggest SG formation and duration are vital determinants of cell fate decisions following stressor onset or in disease[95,96,99,100].

The notion that this adaptive response has a role in ALS pathogenesis has roots in two discoveries, (1) the finding that TDP-43 is a primary component of ubiquitinated inclusions in ALS/FTLD patients[33] and (2) the finding that TDP-43 translocates from the nucleus and associates with SGs during conditions of cellular stress[47]. Subsequent identification of FUS as a component of inclusions[76], mutations in its gene in fALS[68], and its association with stress granules[74] furthered the notion that stress granules represent potential sites of inclusion formation. Analysis of the domain structure of TDP-43 and FUS (and other SG-associated proteins) provided evidence of the structural elements mediating the association of these proteins with SGs, as well as the mechanisms by which these proteins may be irreversibly converted from a transient SG assembly into insoluble aggregates. TDP-43 incorporation into SGs requires RRM1 and the glycine-rich C-terminal component of the protein[49]. For FUS, the protein's zinc finger RNA binding domain is required and the degree of association is mediated by the protein's RRM and glycine-rich domain[49]. The necessity of intact

RNA binding for incorporation of both proteins suggests that their association with SGs is part of the normal cellular response to stress and that loss of this function adversely affects motor neuron viability.

Further domain analysis of both TDP-43 and FUS identified prion-like domains that are essential for their aggregation[46,49,71,101]. Prion-like domains are sequence elements within proteins with sequence similarity to the domains of yeast prion proteins (e.g., Sup35) necessary for self-templating of fold conversion and subsequent aggregation. The general sequence composition of such domains is rich in asparagine, glutamine, tyrosine, and glycine residues and they are typically 60 amino acids or more in length[102]. These regions tend to be unstructured and capable of taking on a variety of conformations[95]. Namely, prion domains can self-associate, forming soluble oligomers, soluble aggregates, amyloidogenic oligomers, and amyloid fibrils[95]. In some of these conformations, the proteins access a hydrogel-like state that may serve as intermediary between soluble monomers and insoluble aggregates. Though the aggregation of proteins into fibrils can serve beneficial functions in yeast in certain environments, the persistent association of TDP-43, FUS, and other RNA binding proteins in SGs in ALS is thought to result in the generation of toxic oligomers and fibrils and the loss of DNA/RNA binding functions by misfolding and removal of these proteins from their normal cellular milieu. Moreover, emerging evidence suggests that a host of RNA binding proteins may participate in this process. Analysis of prion-like domain harboring proteins in the human proteome shows a striking enrichment for DNA/RNA binding proteins, with as many as 20% of proteins with prion-like domains having RNA binding function[102]. The identification of mutations in the genes encoding these proteins (e.g., *HNRNPA1*[103], *TAF15*[104]) in fALS cases and the association of these proteins with SGs provides additional evidence in support of this concept. Thus, the combination of persistent RNA binding protein association with SGs and aggregation-prone

prion-like domain structures in these proteins likely contributes to ALS pathogenesis by both toxic loss of normal function and toxic gain of function.

1.2.2 Autophagy and Proteasomal Stress

Autophagy is a degradative pathway by which intracellular materials, including proteins and organelles, are enveloped and degraded via fusion with lysosomes. The function of autophagy and the observation of numerous types of proteinaceous inclusions in ALS motivated investigations of the role of autophagy in the disease process. Such studies consistently find defects in autophagy, and protein clearance more generally, in human ALS and ALS model systems. These findings are in keeping with views of autophagy as a crucial component of the cellular response to stress[105] and views of ALS as a disease of numerous cellular stressors[106]. The autophagic process proceeds via a series of well-defined and evolutionarily conserved steps. The process begins with the generation of a phagophore, a double membrane structure that can emerge from ER, Golgi, mitochondria, or plasma membrane, depending on the cytoplasmic component to be degraded[107,105]. The phagophore encapsulates the components to be degraded and these components collectively define the autophagosome. Subsequent fusion of the autophagosome with a lysosome produces an autolysosome that degrades the components of the autophagosome, releasing them into the cytosol, where they may be used for the metabolic or protein synthetic needs of the cell[105]. Numerous signaling molecules mediate various steps in autophagy and among the more well-characterized are phosphatidylinositol 3-kinase signaling during autophagosome formation and p62/SQSTM1 tagging of proteins/structures targeted for degradation[108,109]. Induction of autophagy results from numerous forms of cellular stress. A lack of intracellular nutrient or amino acid availability are signaled to the cell via mTOR signaling, which results in autophagic protein degradation. Autophagy is also crucial

for the clearance of misfolded or aggregated proteins and is activated by the unfolded protein response (UPR). The protein targets of autophagy appear to be relatively long-lived proteins, which includes RNA binding proteins, in contrast with the ubiquitin/proteasome system, which is relatively specific for short-lived proteins[110].

Autophagic clearance of proteins and organelles is particularly important for neuronal homeostasis and survival, as neurons have considerable metabolic needs and are acutely sensitive to the presence of misfolded or aggregated proteins. Consistent with this, mice lacking the Atg7 gene, which is essential for autophagy, show progressive neurodegeneration and motor deficits[111]. Human ALS patients show accumulation of p62-positive inclusions in motor neurons and glia[8], suggesting insufficient clearance of misfolded and aggregated proteins is a contributing factor to the disease process. The identification of mutations in genes encoding autophagy-associated proteins as causative factors in subsets of the fALS population have shown that motor neurons are acutely sensitive to defects in autophagy. Mutations in *OPTN*, the gene encoding optineurin, a membrane trafficking protein and autophagy receptor for damaged mitochondria[112], cause rare forms of fALS[113]. *OPTN*-linked fALS cases harbor optineurin-positive inclusions, which also contain TDP-43, p62, and ubiquitin. Optineurin-positive inclusions are relatively rare in sALS cases[114] and fALS-linked *OPTN* mutations affect the protein's autophagic functions[113], suggesting that loss of autophagic function is the primary contributing factor to motor neuron degeneration in *OPTN*-linked fALS and sALS. Mutations in the *VCP* gene, which encodes valosin-containing protein, are likewise found in subsets of fALS patients[115]. Initial estimates indicated that such mutations account for 1-2% of fALS cases, suggesting that *VCP* mutations are a relatively rare event. Nevertheless, the finding adds important insights into role of autophagy in both fALS and sALS, as the VCP protein is essential for autophagy and loss of VCP function (either via expression of a non-functional mutant

protein or gene silencing) leads to the accumulation of unfused autophagosomes and neurodegeneration[116,117]. Intriguingly, *OPTN* and *VCP* mutation-induced loss of autophagic function also leads to the accumulation of cytoplasmic, aggregated TDP-43, suggesting that autophagic hypofunction is sufficient to promote TDP-43 nuclear translocation, aggregation, and ultimately, cell death. Notably then, sALS and fALS are united by the common motor neuron susceptibility factor of impaired or overwhelmed autophagic function and TDP-43 aggregation (Figure 1.1). Loss of autophagic function is further supported as the primary pathogenic mechanism of *VCP* mutations by the consistent finding that mutant forms of VCP do not incorporate into inclusion bodies in human ALS patients or model systems[117,118]. fALS-causing mutations in the genes for the autophagy receptor protein p62[119] (*SQSTM1*), the UPS and autophagy-associated protein ubiquilin 1[120] (*UBQLN1*), and the endosomal trafficking component charged multivesicular protein 2B[121] (*CHMP2B*) and the recent description of the *C9ORF72*-encoded protein as a regulator of endosomal sorting[122] provide further evidence that impaired protein/organelle clearance and vesicular trafficking can contribute to motor neuron death in ALS patients and model systems.

ALS-associated proteins influence the balance of autophagy in motor neurons. Transgenic mice expressing mutant SOD1 show elevated autophagy[123]. Mutant SOD1 is, however, cleared from motor neurons via autophagy at a lower rate than in muscle cells[124]. This reduced clearance rate is sufficient to induce SOD1 aggregation and cause impaired proteasomal function not seen in muscle cells, providing further evidence of autophagic function as a susceptibility factor for motor neuron degeneration[124]. Transgenic mice induced to overexpress C-terminal fragments of TDP-43 (TDP-25) show reduced levels of several autophagy markers and cytoplasmic accumulation of TDP-25 (expected, due to the loss of the protein's NLS), suggesting that TDP-25 overexpression either overwhelms neuronal autophagic capabilities, results in reduced expression of autophagic markers,

or both[125]. Consistent with this, activation of autophagy via rapamycin reduces TDP-43 aggregation and ameliorates motor deficits in transgenic mice expressing TDP-43[126] and drosophila overexpressing the TDP-43 ortholog dTDP[127]. These results suggest that autophagy activation is a potential ALS therapeutic target. The results of rapamycin administration to SOD1-G93A mice, which accelerated motor neuron degeneration, suggest that some caution is necessary, however, in targeting autophagy therapeutically[128]. These studies collectively support the idea that autophagic balance, the relative rates of phagophore, autophagosome, and autolysosome formation and degradation are a key determinant of motor neuron health and survival in ALS model systems. This concept is supported by ultrastructural studies of human ALS spinal cord tissue, which show prominent deposition of autophagosomes and autolysosomes, particularly in degenerating motor neurons and around inclusion bodes[129]. Impaired autophagic balance, either by accumulation of misfolded proteins (such as TDP-43 or SOD1) or mutations in key autophagic proteins (as occurs in *VCP*/*OPTN*/*UBQLN1*/*SQSTM1*-linked fALS), are thus likely to make cells (and in particular motor neurons) susceptible to degeneration (Figure 1.1).

1.2.3 ER Stress

The endoplasmic reticulum (ER) is an integral component in the synthesis, folding, modification, and transport of proteins. The rough ER contains bound ribosomes translating mRNAs into proteins that are then brought into the luminal cisternae of the ER for further folding, processing, and modification. A large proportion of a cell's protein synthesis occurs at the level of the ER and ER-synthesized proteins are destined for one of three possible fates: (1) secretion via the secretory pathway, (2) membrane integration, or (3) luminal association with membrane-bound intracellular organelles, including ER, Golgi, lysosomes, etc….[130] Perturbation of normal ER function and,

particularly, the accumulation of un- or mis-folded proteins causes ER stress. ER stress signals that the normal capacity of the ER to modify and fold proteins has been saturated, which triggers the evolutionarily conserved reaction termed the unfolded protein response (UPR). Key components of the UPR include a general decrease in the rate of protein synthesis, an increase in the expression of ER-associated chaperone proteins, increased expression of folding-associated enzymes (chiefly, glycosylases and disulfide isomerases), and activation of the endoplasmic reticulum-associated (ERAD) protein degradation pathway and ER-induced autophagy[131,132]. ERAD initiates retrotranslocation of the misfolded protein into the cytoplasm for polyubiquitin tagging and proteasomal degradation.

ER function and stress are monitored by three ER membrane proteins with signaling functions: IRE1, PERK, and ATF6. The function of the latter two proteins is regulated by the ER chaperone BiP, which is normally bound to the luminal domains of PERK and ATF6[131,132]. The accumulation of misfolded proteins releases BiP and allows cytosolic translocation of active PERK and ATF6. PERK inhibits translation (reducing the folding load on the ER) by phosphorylating its target, eIF2α. ATF6 is proteolytically processed to a transcriptional activating form and translocates to the nucleus where it increases the transcription of ER folding-associated genes. IRE1 is activated by the direct binding of misfolded proteins and also undergoes cytosolic translocation[131,132]. Once in the cytosol, its now active RNAse domain leads to removal of an intron in the XBP1 transcript, leading to production of the associated protein, which is a transcriptional activator of ER fold-associated genes. The ER is also a major reservoir for intracellular Ca^{2+} and contains numerous calcium channels and sensors. Ca^{2+} signaling regulates a number of cellular processes related to the stress response and many folding enzymes in the ER lumen are Ca^{2+}-dependent. When the UPR and ERAD are insufficient to restore ER homeostasis, the above ER proteins and Ca^{2+} signaling can lead

to the induction of apoptosis[132,133]. Ca^{2+} signaling leads to mitochondrial Ca^{2+} overload. IRE1, PERK, and ATF6 are each capable of activating pro-apoptotic genes[132,134].

Accumulating evidence suggests that impaired UPR and excessive ER stress are contributing factors to motor neuron vulnerability in ALS and ALS model systems (Figure 1.1). ER abnormalities are common in sporadic ALS motor neurons, with irregularities in ER structure, chromatolysis of ER membrane, and ribosomal detachment from ER membrane evident[135]. Spinal cord motor neurons of sALS patients show several signs of ER stress, including enhanced PERK-induced eIF2α phosphorylation and increased expression of ER chaperone proteins, as well as oxidative damage to proteins[136]. These changes occur in sporadic ALS patients and are confined to motor neurons, suggesting that (1) ER stress is a general phenomenon in ALS and (2) that these changes are specific to motor neurons, implicating ER function as a susceptibility factor in motor neuron degeneration. Evidence for the former notion comes from studies showing that misfolded TDP-43 and FUS induce ER stress and associate with ER chaperone proteins following nucleocytoplasmic translocation[137,138]. In evidence of the latter notion, a P56S mutation in *VAPB*, a gene encoding a vesicular membrane trafficking protein that associates with the ER, causes a rare form of fALS in a Brazilian family[139]. The mutant protein forms inclusions in ER and cytosol[140] and is, unlike the wild type protein, incapable of activating IRE1 splicing of XBP1 mRNA[141], suggesting gain and loss of function mechanisms of toxicity both related to ER stress. Expression of the disease-associated protein also perturbs proteasomal function[142] , alters ER calcium homeostasis[143], and strongly inhibits ATF6 activity[144], suggesting that a global dysregulation of ER and UPR contributes to neurotoxicity in *VAPB*-linked fALS. Further evidence that ER homeostasis and UPR are component of selective motor neuron vulnerability comes from longitudinal studies of vulnerable and resistant motor neurons in SOD1 transgenic mice. Vulnerable motor neurons were consistently more susceptible to

the onset of ER stress and showed upregulation of UPR markers compared to resistant motor neurons, despite comparable accumulation of ubiquitnated cytosolic proteins[145].

Efforts to understand the mechanisms promoting ER stress and UPR in ALS model systems and mechanisms of toxicity of fALS-linked mutant proteins have largely focused on mutant SOD1. Though SOD1 is a primarily cytosolic protein, secretion of and expression of surface receptors for the secreted protein have been demonstrated[146]. These findings suggest a physiological role for the association of SOD1 with ER and a potential mechanism of disease spreading by secretion of prion-like misfolded SOD1[147]. Motor neurons seem particularly susceptible to SOD1-induced ER dysfunction, as NSC-34 motor neuron-like cells, but not neuronal PC12 or fibroblast COS-7 cells, express protein disulfide isomerase (PDI; a UPR-associated folding enzyme) in response to mutant SOD1 overexpression[148]. Mutant SOD1 is also secreted less efficiently than the wild-type protein and forms inclusions that are toxic to NSC-34, but not COS-7, cells[149]. Secretion of mutant SOD1 also activates microglia, resulting in non-cell autonomous neurotoxicity in motor neuron/microglial co-cultures[150].

These findings can be recapitulated in transgenic animal models of ALS. Transgenic mutant SOD1-expressing rats display upregulated UPR markers in spinal cord motor neurons, along with co-localization of PDI in SOD1 inclusions. Transgenic mice expressing mutant SOD1 likewise show elevated PDI expression and inhibition of PDI activity results in a greater motor neuron SOD1 inclusion burden[148]. Further evidence for the role of ER stress and UPR activation comes from the finding that symptomatic SOD1-G93A mice have concomitant elevations in the expression of UPR (PERK, IRE1, and ATF6) and apoptosis markers (CHOP expression and caspase cleavage) in motor neurons[148]. Cytoplasmic SOD inclusions in these mice are also positive for ER-resident chaperone proteins, suggesting that misfolded SOD1 accumulates in the ER, activates the UPR, and may

ultimately overwhelm its capacity, resulting in apoptotic cell death[151]. To test this idea, transgenic SOD1 mice lacking the XBP-1 gene (whose activation is a component of the UPR) were generated. Counterintuitively, mice lacking XBP-1 showed reduced cytoplasmic deposition of SOD1 aggregates and enhanced resistance to disease onset that was linked to clearance of SOD1 by elevations in macroautophagy[152]. This, together with evidence that the ER stress-reducing drug salubrinal, preserves neuromuscular function and increases survival in SOD1 transgenic mice argues that the role of ER stress and UPR in disease is complex. Maintenance of ER homeostasis is dependent on multiple sensor molecules and signaling pathways and the relative balance of these, together with other processes like proteasomal and autophagic protein degradation, likely determines whether UPR activation is beneficial or harmful to motor neurons in ALS. A schematic of the contributions of intracellular stressors to motor neuron degeneration is shown in Figure 1.1.

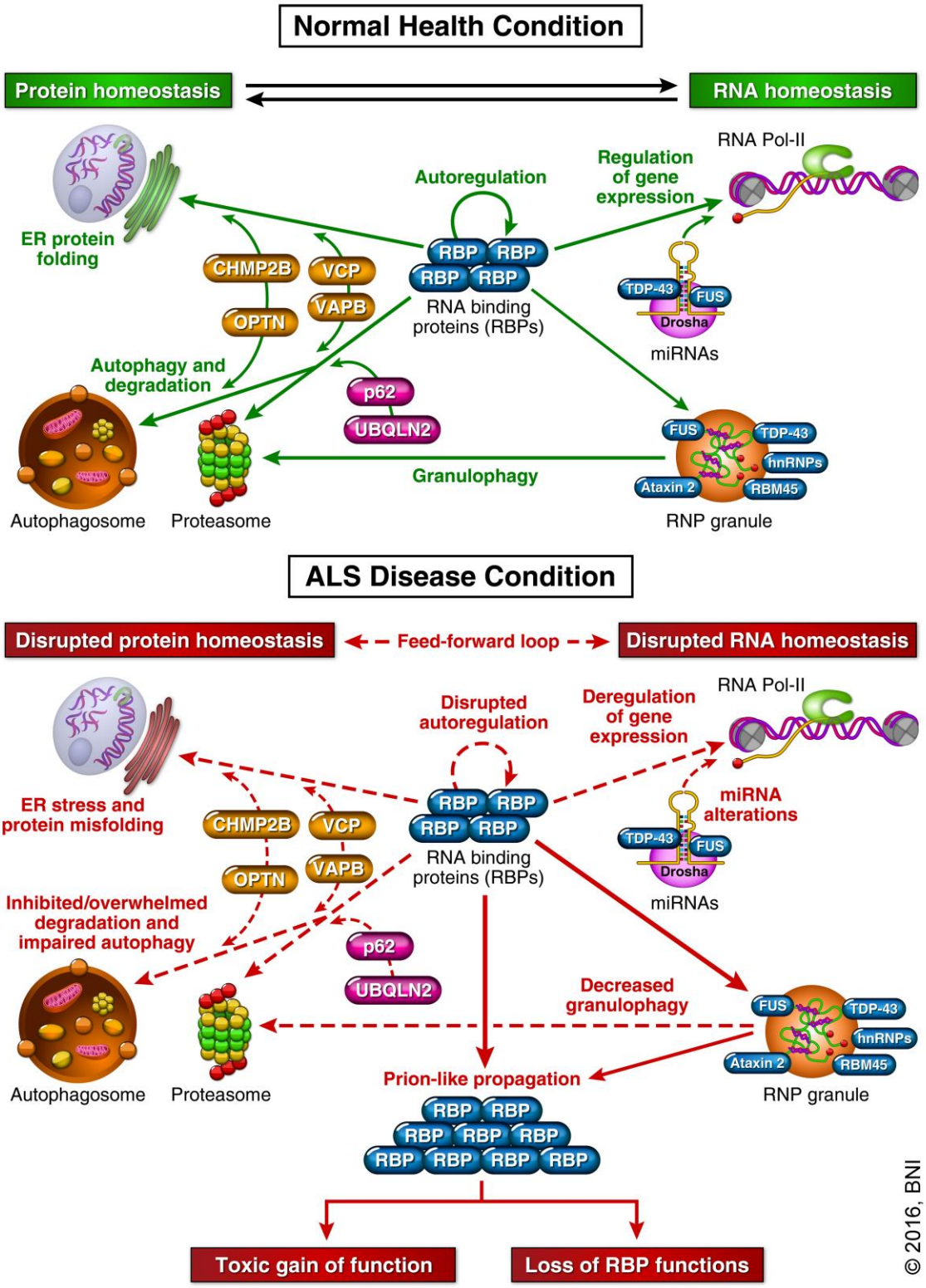
Normal Health Condition
Protein homeostasis
RNA homeostasis
ER protein folding
Autoregulation
Regulation of gene expression
RNA Pol-II
CHMP2B
VCP
VAPB
OPTN
RBP
RNA binding proteins (RBPs)
TDP-43
FUS
Drosha
miRNAs
Autophagy and degradation
p62
UBQLN2
Granulophagy
FUS
TDP-43
hnRNPs
Ataxin 2
RBM45
Autophagosome
Proteasome
RNP granule
ALS Disease Condition
Disrupted protein homeostasis
Feed-forward loop
Disrupted RNA homeostasis
ER stress and protein misfolding
Disrupted autoregulation
Deregulation of gene expression
RNA Pol-II
miRNA alterations
Inhibited/overwhelmed degradation and impaired autophagy
Decreased granulophagy
Prion-like propagation
Toxic gain of function
Loss of RBP functions
© 2016, BNI

Figure 1.1 Protein aggregation and intracellular stress in ALS. A schematic of protein/RNA homeostasis in the normal and ALS disease conditions are shown. Aggregation of RNA binding proteins in ALS impairs the normal gene expression regulatory effects of these proteins while also impairing protein clearance/degradation pathways. Motor neurons are acutely vulnerable to defective/overwhelmed protein clearance as shown by fALS-linked mutations in the indicated proteins/genes associated with ER protein folding, processing, and sorting, as well as mutations in autophagy and proteasomal proteins.

1.2.4 Evidence for RNA Binding Protein in the Disease Process

Since the initial discovery of the TAR DNA-binding protein (TDP-43) as a major component of neuronal cytoplasmic inclusions in ALS [153] and subsequent identification of genetic alterations in the *TARDBP* gene that cause familial forms of ALS and frontotemporal dementia (FTD)[154], the number of RNA/DNA binding proteins associated with ALS has continued to grow. TDP-43 positive neuronal inclusions are a pathologic hallmark of both ALS and FTLD. Mutations in *TARDBP* account for approximately 4% of familial cases and a small number of apparently sporadic ALS cases[155].

Shortly after the discovery of *TARDBP* mutations that cause ALS, missense mutations in the fused-in-sarcoma (*FUS*) gene were identified as the cause of chromosome 16p linked familial ALS[156,157]. Mutations in *FUS* also account for ~4% of familial ALS cases. The observed protein domain homology between TDP-43 and FUS, with both proteins containing multiple RNA binding motifs, suggested that RNA metabolism may play an important role in ALS. Other key structural elements include the presence of glycine-rich domains and prion-like domains that contribute to their pathological aggregation and impaired function in ALS. This latter element was used to predict other

RNA binding proteins associated with ALS. This led to the discovery of disease causing mutations in *TAF15, hnRNPA1,* and *hnRNPA2B1* in rare fALS kindreds[158,159]. Key functional properties linking these RNA binding proteins include association with stress granules and nucleocytoplasmic translocation during cellular stress.

Genetic studies have identified other RNA binding proteins linked to familial or sporadic forms of ALS. These include disease causing mutations in *SETX, ANG,* and *ELP3*[160-162], repeat expansion of *ATXN2* associated with increased risk of ALS[163], and others such as *RBM45* that are linked to ALS due to pathologic inclusions of the protein that occur in patients[164].

1.2.5 Altered RNA Splicing, Transport, and Translation

While most of the genetic alterations of RNA binding proteins impact their subcellular distribution and accumulation into stress granules and/or pathologic inclusions (see below), we will focus here on specific effects of disease causing mutations in TDP-43 and FUS on RNA metabolism (Figure 1.2). RNA binding proteins have diverse roles in the cell and function within many nuclear sub-structures and the cytoplasm. At present, the vast majority of evidence for impaired RNA processing in ALS has come from studies of TDP-43 and FUS. However many other RNA binding proteins linked to ALS interact with TDP-43 and/or FUS, and therefore likely impact RNA metabolism. Since both TDP-43 and FUS bind RNA/DNA (Figure 1.2), determining the specific binding sequences and effects on gene expression were crucial to understand how these proteins contribute to cell death in ALS. Using CLIP-SEQ, TDP-43 was shown to bind over 6,000 RNA targets in the brain, approximately 30% of the transcriptome[51,165-167]. TDP-43 binding to long introns (>100 kb) is required for the normal maturation and splice site selection of immature mRNA species [167,168]. TDP-43 binding to the 3' UTR of mRNAs may impact stability or transport, whereas binding to long

noncoding RNAs (ncRNAs) may influence their regulatory roles. Splicing of many RNA targets of TDP-43 are altered in ALS spinal cord tissue[169].

Likewise, FUS binds over 5,500 RNA targets in the brain[165], and its binding pattern to long introns suggests that FUS remains bound to pre-mRNAs until splicing is complete. Loss of FUS function results in changes of the splicing pattern or abundance in over 1,000 RNAs[165]. All three members of the FET gene family (FUS, EWSR1, and TAF-15) are implicated in ALS, suggesting that the functions of these proteins on global RNA splicing and metabolism are particularly important for motor neurons. In addition, both TDP-43 and FUS bind to the long ncRNAs (lncRNA) and influence their function and subcellular localization (Figure 1.2). Both proteins, for example, bind NEAT1[170], a lncRNA core component of nuclear paraspeckles, which function in cell stress responses and in the nuclear retention of hyperedited RNAs[171]. FUS directly regulates NEAT1 levels and decreasing FUS levels leads to reduced numbers of paraspeckles[172]. At the same time, FUS-positive inclusions contain other paraspeckle proteins, suggesting that pathological changes in FUS levels or function impair normal paraspeckle formation/function, thereby altering cellular homeostatic responses and increasing motor neuron vulnerability to degeneration.

Finally, both TDP-43 and FUS exhibit neuron-specific functions that further implicate them in neurodegenerative diseases. Both localize to dendrites in response to neuronal activity. Disease causing mutations that result in functional impairments and protein mis-localization therefore likely impact synaptic structure and function via loss of localized translation of specific mRNAs[173,174]. Given the remarkable functional diversity of RNA binding proteins such as TDP-43 and FUS, it is unsurprising that mutations that affect their structure and function confer numerous aberrant changes in the regulation of gene expression. Motor neurons, in particular, seem acutely vulnerable to alterations in the levels of ALS-linked RNA binding proteins by either loss of function, gain of toxic

function, or both. While much insight into the sequence targets, processing functions, and subcellular associations of ALS-associated RNA binding proteins have been gained in recent years, determining which of these properties contribute directly to motor neuron vulnerability/degeneration remains an unanswered question with considerable therapeutic implications. The collective functions of TDP-43, FUS, and other ALS-linked RNA binding proteins are shown in Figure 1.2.

1.2.6 ADAR2 RNA Editing

Further evidence for motor neuron-specific defects in RNA processing have come from studies of RNA editing of the GluA2 subunit of the l-α-amino-3-hydroxy-5-methyl-4-isoxazolepropionic acid (AMPA) receptor. Adenosine deaminase acting on RNA 2 (ADAR2)-mediated conversion of adenosine to inosine (A-to-I editing) of the GluA2 pre-mRNA results in replacement of glutamine with arginine in the translated protein. This editing normally occurs in all motor neurons and results in expression of Ca2+ impermeable AMPA receptors. ADAR2 levels, and consequently A-to-I editing, is dramatically reduced in sALS motor neurons[175]. The resultant enhancement of AMPA Ca2+ permeability leads to increased motor neuron vulnerability and the development of TDP-43 pathology[176].

1.2.7 miRNAs

Over the past decade, microRNAs (miRNAs) have been identified as significantly impacting overall gene expression by modulating the stability and/or translational repression of target mRNAs[177]. miRNAs are short non-coding RNAs (~22 nucleotides) and over 1,000 have been identified in humans, constituting a large class of regulators of gene expression. Approximately 60% of all

mammalian mRNAs are predicted targets of miRNAs[178]. miRNA binding to mRNA targets results in reduced protein expression from the specific bound mRNA. A single miRNA may have many mRNA transcript targets, therefore impacting expression of a large number of genes. Various types of cellular stressors impact the levels of miRNAs and therefore regulate how a cell responds to stress [179]. As ALS is a disorder of multiple stressors, miRNA alterations may represent an important pathogenic mechanism of disease. miRNAs are also essential to the overall ability of a cell to properly respond to acute or chronic stress conditions that exist during ALS and, therefore, modulating levels of stress-associated miRNAs may have therapeutic value in the treatment of ALS.

Recent studies have examined miRNA changes in ALS patients and model systems, including the G93A SOD1 transgenic mouse model, circulating monocytes, skeletal muscle, and lumbar spinal cord tissue from ALS patients, and serum from familial ALS patients and pre-manifest carriers with known ALS-linked genetic mutations[180-184]. Altered levels of miRNAs may have significant impact on gene expression during ALS (Figure 1.2) and studies of miRNA levels from multiple sources of origin in ALS patients find altered miRNA profiles. Moreover, modulating levels of certain miRNAs (namely, miRNAs 206 and 155) can slow disease progression in SOD1 mice[183,185]. Collectively, these observations support the notion that miRNA-based modulation of gene expression is a key determinant of motor neuron health. Nevertheless, perhaps due to differences in models, cell/tissue types, and analytical methods used in these studies, a common set of miRNA alterations has not been observed across studies of human ALS patients. However two studies detected increased levels of miR-146a and miR-155 in microglial cells[186,181]. In addition, increases in miR-146a were detected in two studies using either microglia or spinal cord tissue from ALS patients[181,182]. The results support further studies on miRNA changes in ALS using standardized approached and model systems, ideally in large collaborative research efforts.

Understanding the genes and biological pathways modulated by miRNAs associated with ALS may reveal new mechanisms of disease or provide novel targets for modulation of known ALS pathways. In addition, miRNAs may correlate with the rate of ALS disease progression, as miR-206 levels have been associated with the rate of disease progression in the G93A SOD1 mouse model[187]. Finally, both TDP-43 and FUS (and likely other RNA binding proteins implicated in ALS) impact miRNA biogenesis[188,189], linking ALS disease causing mutations to miRNA regulated gene expression.

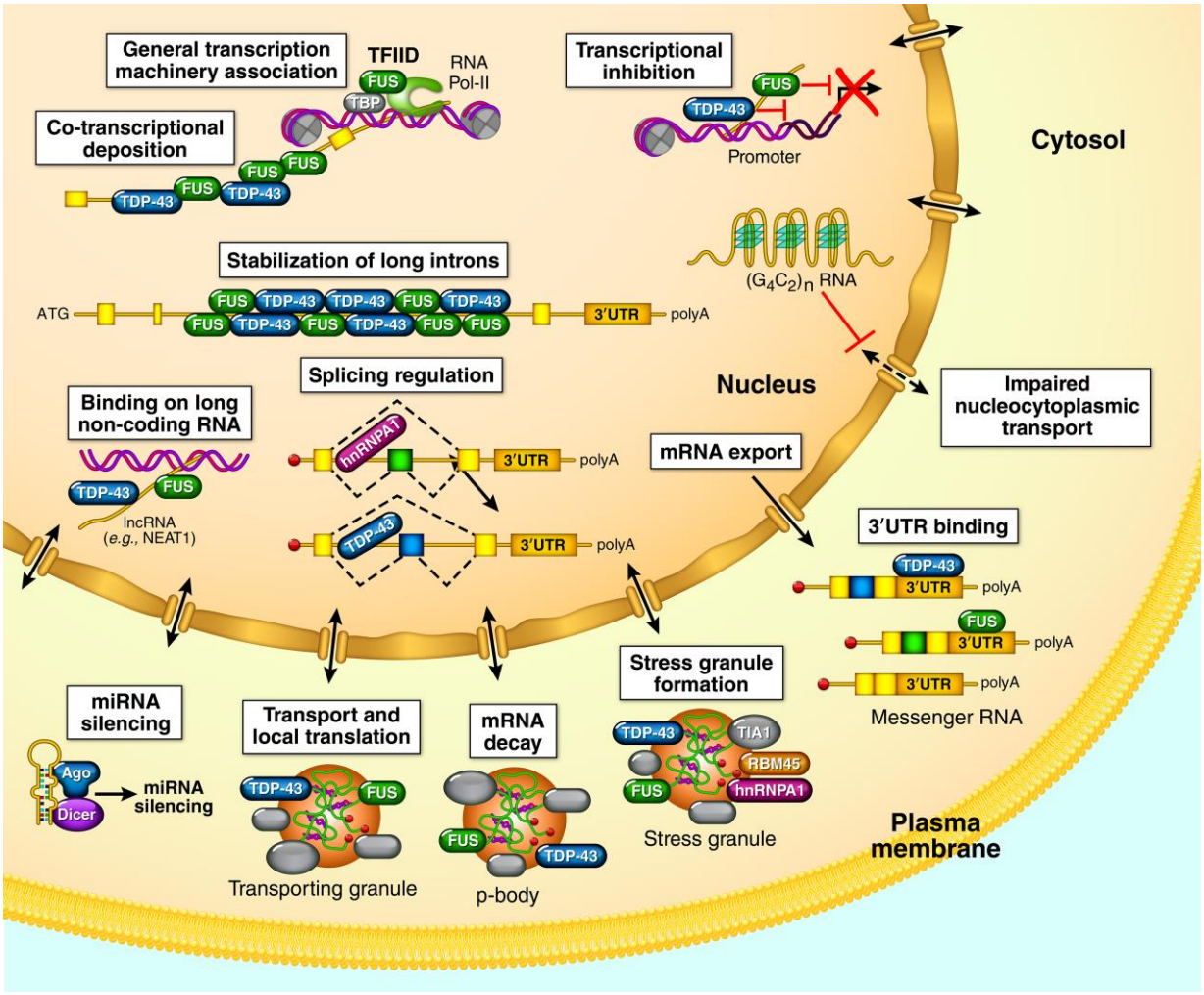

Figure 1.2 RNA processing functions of ALS-associated RNA binding proteins (RBPs). A schematic diagram of the RNA-related functions of ALS-linked RBPs is shown. These RBPs affect the transcription, processing, export, maturation, transport, and turnover of RNA molecules. ALS-linked RBPs influence which genes are transcribed, how transcripts are spliced, and the final subcellular location of the RNA molecule. In addition to their effects on normal transcription/translation, ALS RBPs participate in stress responses via stress granules and regulate levels and functions of miRNAs. Lastly, the *C9ORF72*-linked hexanucleotide repeat expansion (G_4C_2) may impair many of these processes via expansion-linked nucleocytoplasmic transport defects.

1.2.8 *C9ORF72* Hexanucleotide Repeat Expansion

The most common genetic cause of ALS and FTLD is a GGGGCC repeat expansion in the *C9ORF72* gene[190,191]. The *C9ORF72* repeat expansion is believed to underlie approximately 40% of fALS and 6-7% of sALS cases[192]. Patients with *C9ORF72* repeat expansions that develop disease display variable amounts of TDP-43 pathology and abundant TDP-43 negative, p62-positive neuronal and glial inclusions in multiple regions of the CNS, including the cerebellum[193]. At present, the function(s) of the *C9ORF72* protein is not fully characterized, however, the protein's high degree of homology with the DENN protein, a GDP/GTP exchange factor that acts on Rab-GTPases[194], and reported ability to regulate endosomal trafficking[122] suggests that the protein has multiple functions.

Proposed neurotoxic mechanisms of the repeat expansion include haploinsufficiency and a toxic gain-of-function. Studies of the former have produced conflicting results: Conditional knockout of the *C9ORF72* gene does not result in the development of motor neuron degeneration or an overt motor/behavioral phenotype in mice[195]; however, knockdown of the zebrafish orthologue (z*C9ORF72*) led to motor deficits and axonal pathology[196]. Differences in model system, genetic ablation strategy, and repeat expansion size in these studies could account for these discrepancies and underscore the complexity of C9-mediated neurodegeneration. Experimental evidence for a repeat expansion-induced toxic gain of function have implicated both the accumulation of RNA foci within the nucleus and cytoplasmic translation of dipeptide proteins via repeat-associated non-AUG translation (RAN) translation products and resultant accumulation of DPR cytoplasmic inclusions[197]. The presence of sense and antisense foci is a common observation in both patient tissues/cell lines and C9 model systems[198], and C9 transcripts are capable of forming G-quadruplex structures that may aberrantly influence gene expression by sequestering RNA binding proteins[199] (Figure 1.2). As noted above, *C9ORF72* fALS patients exhibit DPR cytoplasmic inclusions resulting from non-ATG

(RAN) translation of the repeat. DPRs are neurotoxic in a variety of ALS model systems[200] and co-culture of astrocytes taken from C9 patients with wild-type motor neurons results in extensive neuronal death[201], suggesting intracellular and non-cell autonomous mechanisms of neurodegeneration in C9-linked ALS. Studies in ALS patients, however, have noted the presence of DPR containing inclusions in regions of the CNS that do not degenerate in ALS[202], suggesting DPR inclusions are not directly neurotoxic.

Recent studies examining mechanisms of C9-mediated toxicity have consistently identified impairments in nucleocytoplasmic transport of proteins[203,204] (Figure 1.2). It remains unclear if all proteins that enter/exit the nucleus are equally impacted by C9 repeat expansion-induced transport defects. Therapeutic approaches that enhance nucleocytoplasmic transport or remedy defective transport-induced pathologies may thus be an effective treatment for C9-linked ALS. However nucleocytoplasmic transport deficits may be present from birth, whereas ALS or FTLD typically occurs in late to middle age, raising the question of whether additional factors cause disease and C9 repeat expansion induced nucleocytoplasmic transport defects merely make the cell more susceptible to further insult. Anti-sense oligonucleotides (ASOs) and small molecules that target production of C9 RAN proteins have also been identified as therapeutics with clinical potential[205,206]. ASOs have been shown to ameliorate or prevent the development of C9-associated pathology and pathophysiology in some model systems. However, since C9 repeat expansion BAC transgenic mice harbor both nuclear RNA foci and C9 RAN proteins throughout life yet exhibit no phenotype, the role of both RNA foci and C9 RAN protein inclusions in ALS neurodegeneration remains uncertain. Moreover, while loss of *C9ORF72* function does not induce motor neuron degeneration or impair CNS function, the necessity of the *C9ORF72* protein for the proper functioning of other organ systems/cell types has not been evaluated. Thus, while knockdown-based approaches (such as

ASOs) have shown early promise in model systems, much additional research is needed to determine their safety/efficacy.

1.3 GLIAL AND INFLAMMATORY MECHANISMS OF DISEASE

A host of non-cell autonomous mechanisms contribute to neurodegeneration in ALS. Among the most studied are those involving glial cells, specifically astrocytes, microglia, and oligodendrocytes, and the specialized extracellular matrix surrounding motor neurons, termed perineuronal nets (PNNs). More recent studies have also shown that regulatory T-cells and extracellular matrix breakdown also contribute to motor neuron degeneration.

1.3.1 Astrocytes

Astrocytes are the most abundant cell type in the CNS and serve numerous important roles in synaptic transmission and maintaining neuronal viability[207,208]. One of the most vital of these functions is establishing and maintaining a homeostatic environment for neurons and other CNS cells[209]. This is accomplished, in part, by astrocytic contacts with other CNS cells, including projections at synaptic sites. At the synapse, astrocytes provide considerable support to neurons in the regulation of synaptic activity and plasticity[209]. In addition to providing structural integrity to synapses, astrocytes regulate the concentration of neurotransmitters and other molecules both by uptake and release of neurotransmitters, ions, and other molecules in the synaptic space[208-211]. Astrocytes also aid in maintaining neuronal viability by secreting growth and trophic factors, the secretion of which may be increased in response to neuronal injury or stress[209-211].

Astrocytes contact many cell types in addition to neurons, including other astrocytes and cells of the vascular system. Astrocytic influence on the cerebrovascular system is extensive and comprises numerous functions. This influence is exerted chiefly by the extension of astrocytic endfeet to vascular epithelial cells. The resultant cell-cell contacts allow astrocytes to regulate brain vascular function[210]. This is, in part, accomplished is by the secretion of factors that influence the gap and tight junction protein expression in endothelial cells. In this way, the integrity and permeability of the blood brain barrier are directly influenced by astrocytes[210]. Similarly, astrocytic secretion of chemical factors can induce vasodilation or constriction, thus tailoring the regional blood flow to the needs of surrounding neurons. Astrocytes maintain contact with surrounding astrocytes via gap junctions, and though these connections, exchange various molecules[208,210]. Collectively, then, astrocytes act as an extensively connected support network that adapts its activities to the needs of adjacent neurons.

In addition to these homeostasis-promoting functions, astrocytes also participate in a defensive response to CNS injury or disease termed reactive gliosis[212-214]. Reactive gliosis, or reactive astrogliosis, comprises a series of morphological and functional changes that occur in astrocytes intended to respond to the initiating stimulus, minimize CNS tissue damage, and restore a homeostatic cellular environment (Figure 1.3). Perhaps the most pronounced and well-described change occurring in these cells during reactive gliosis is markedly enhanced expression of glial fibrillary acidic protein (GFAP), an astrocytic intermediate filament protein. This results in increased extension and branching of astrocytic processes to areas of CNS injury or disease and may ultimately lead to the formation of a glial scar, a dense interconnected astrocytic network that physically seals the afflicted area off from the rest of the CNS[211,215].

Several lines of evidence implicate astrocytes in the degeneration of motor neurons in ALS[213,214,216]. Dying motor neurons in the spinal cord and motor cortex of ALS patients are frequently surrounded by reactive astrocytes and astrocytes exhibit some of the pathological hallmarks of ALS motor neurons, including intracellular inclusion bodies. Astrocytes in ALS patients also show elevated expression of inflammatory markers, including nitric oxide synthase (NOS), TNFα, and NF-Kβ, suggestive of an astrocytic response to motor neuron degeneration[217-221]. The increased expression inflammatory markers and attendant decrease in trophic factor support highlight the complexity of the degenerative process, as studies targeting individual markers of either type have proven unsuccessful in ameliorating motor neuron degeneration in ALS clinical trials[222-224], even when they have provided benefit in ALS model systems[225-227]. Nevertheless, much of our understanding of the role of astrocytes in ALS is a result of studies using transgenic mutant SOD1 mice and primary cultures of neurons and glia thereof. One of the main findings of studies in mutant SOD1 transgenic mice is that astrocytes secrete numerous factors that predispose motor neurons toward apoptotic cell death[213]. Astrocytic production of nitric oxide via increased expression of NOS leads to uptake of the molecule by motor neurons, where it impairs mitochondrial function and can lead to cell death[218,228]. Likewise, transgenic mutant SOD1 mice show enhanced expression of receptors for p75 and TNFα[229-232]. Astrocytic secretion of NGF can activate p75 receptors and trigger apoptotic cell death[233,234]. TNFα expression is also increased in these mice and can similarly trigger apoptosis[234]. Despite well-defined increases in TNFα in motor neurons and glia in ALS transgenic mice and human patients, however, ablating TNFα signaling or even deleting the encoding gene do not stop disease progression, suggesting that TNFα may make only minor contributions to neurodegeneration in ALS[235,236]. Activated astrocytes also increase their expression of EAAT following brain injury and ischemia, which is thought to be a neuroprotective

mechanism[237,238]. In contrast, astrocytes in ALS patients show markedly reduced levels of EAAT2 due to mRNA splicing abnormalities[239,240] , thus contributing to glutamate excitotoxicity in ALS.

An important question for resolving the role of astrocytes in ALS is whether reactive astrogliosis is a cause of degeneration, consequence, or both. Conflicting reports from mutant SOD1 transgenic mouse lines have emerged, with reactive astrocytosis evident several weeks prior to symptom onset in $SOD1^{G37R}$ mice[241] and following motor neuron loss by several weeks in the more commonly used $SOD1^{G93A}$ mouse[242]. Further complicating matters is the observation that astrocytes overexpressing mutant TDP-43^{A315T} or lacking the *TARDBP* gene did not contribute to motor neuron death, either in vitro or following transplant into wild-type rats, in a recent study[243]. This same group later showed that inflammatory astrocytic activation with lipopolysaccharide (a known astrocytic activator), can lead to cytoplasmic accumulation of TDP-43 in astrocytes and motor neurons in A315T TDP-43 transgenic mice, though cell viability was not evaluated[244]. Taken together, these results imply that ALS-associated changes, such as a causative mutation or stressor, are sufficient to induce reactive astrocytosis and pathological changes in astrocytes, and that astrocytosis may speed the degeneration of ALS motor neurons. The interplay of motor neuron intracellular mechanisms and non-cell autonomous mechanisms, such as astrocytosis, is complex and the relative contributions of each and their time course are unknown in human ALS. Given the heterogeneity of the disease, it seems likely that a number of possibilities exist, wherein the initiation of a disease-promoting stimulus at either the level of the motor neuron of the astrocyte is sufficient to result in pathological changes, and perhaps eventually, cell death (Figure 1.3). The creation of numerous iPSC lines from sALS, fALS, and healthy control subjects offers tremendous promise towards delineating the contribution of astrocytes to neurodegeneration and identifying subtypes of ALS for which therapeutics targeting astrocytes may be effective[245].

The contribution of astrocytes to neurodegeneration in ALS can therefore be viewed as two-fold. First, the development of pathology within astrocytes (e.g., proteinaceous inclusions) is expected to impair their normal function of supporting neuronal health. Motor neurons, with their considerable energy demands, are likely to be particularly susceptible to impairment of the astrocytic network that maintains a homeostatic environment in the CNS. Second, activation of astrocytes by the secretion of chemical factors and misfolded proteins from dying motor neurons results in profound activation of astrocytes with accompanying reactive astrogliosis (Figure 1.3).

1.3.2 Microglia

Microglia are the resident macrophage cells of the CNS and are a key component of the CNS immune system. They have a small cell body with numerous branching processes that extend outwards from the soma. These processes extend to neuron cell bodies, dendrites, and axons and areas of the CNS vascular system. The processes are used as mobile probes to determine the local cellular environment and microglia express receptors for numerous types of molecules (e.g., complement proteins, cytokines, ions, plasma proteins, and neurotrophic factors) to aid this process[246,247]. Microglia exhibit considerable phenotypic heterogeneity in relation to such environmental signals and the density of microglia varies considerably throughout the CNS, with microglial numbers being particularly high in myelinated region[248,249]. Microglial activation results in phenotypic and morphological changes and occurs in response to signaling molecules (Figure 1.3). The nature and extent of activation depends on the molecules and their local concentration. More recent work has shown that microglia also monitor neuronal activity, with enhanced projection surveillance resulting from higher levels of neuronal activity[248]. Activation generally occurs in response to a pathological environmental change, such as infection, disease, or inflammation and is

associated with a thickening and retraction of processes and the assumption of a more rounded morphology[246,247]. This signaling can occur through either the presence of a molecule(s) that is normally absent (e.g., LPS signaling via toll-like receptors) or the absence of a molecule(s) that are normally present (e.g., CD-200 signaling via CD-200 receptor). Activated microglia also exhibit different "active" phenotypes based on the stimulating molecule(s). This concept is perhaps best illustrated by microglial activation response to the T-cell effector cytokines IFN-γ and IL-4. IFN-γ challenged microglia assume an activated phenotype that commonly produces cell death, while IL-4 challenge leads to a microglial response that favors neuroprotection. The response to IFN-γ may be viewed as M1 activation and is accompanied by microglial release of reactive oxygen species, nitric oxide, and inflammatory cytokines (Figure 1.3). In contrast, neuroprotective microglial activation (M2) is associated with greater phagocytic activity (e.g., for removing protein aggregates), release of trophic factors, and the uptake of potentially neurotoxic substances, (e.g., glutamate via GLT-1). Generally, the balance of pro- versus anti-inflammatory factors will determine the nature of the response (M1 or M2), time course, and extent of the response[246-249].

Given their roles in surveilling the CNS microenvironment and responding to homeostatic disturbances, it is perhaps unsurprising that microglia are implicated in the progression ALS in studies of both human patients and ALS transgenic mouse models. Studies in human ALS tissue consistently identify activated microglia in proximity to degenerating motor neurons and these microglia are frequently positive for inflammatory markers[250-253]. In human subjects, the level of microglial activation is greater with increasing disease severity, consistent with a microglial role in disease progression. In consideration of this, as with astrocytes, an important question is whether microglial activation is a consequence of the neurodegenerative process or a primary cause of neurodegeneration, and whether microglial responses can be modulated to favor neuroprotection.

Answers to these questions have largely come, as they have for astrocytes, from studies of mutant SOD1 transgenic mice.

Microglial activation is one of numerous features recapitulated in SOD1 transgenic mice, including elevation of inflammatory markers and microglial activation[253]. The creation of chimeric mice expressing mutant SOD1 in defined cell populations has helped clarify the role of microglia in ALS. Wild-type glial cells surrounding mutant SOD1 expressing motor neurons led to a significant decrease in neurodegeneration and absence of pathological abnormalities. By contrast, mutant SOD1 expressing non-neuronal cells adjacent to while type motor neurons led to ubiquitinated protein deposits forming in motor neurons[254]. These findings collectively underscore the contribution of non-cell autonomous effects to neurodegeneration. Further evidence for this phenomenon comes from the observation that expression of an ALS-associated mutant protein seems to shift microglia towards and inflammatory phenotype, as cultured microglia from SOD1 mice have enhanced inflammatory marker expression[255]. This phenotype can also be conferred by microglial uptake of secreted, misfolded SOD1[150,256], suggesting that the mutant SOD1 misfolded conformation is sufficient to activate microglia, independent of other ongoing degenerative processes. Similar results obtained for mutant, misfolded TDP-43 and TDP-43 C-terminal fragments[257], as well as amyloid beta[258], support this as a general mechanism and suggests that misfolded proteins contribute to microglial activation via NF-κβ signaling. Receptor-mediated NF-κβ signaling allows nuclear translocation of the NF-κβ protein, which induces a host of inflammation-related transcriptional responses. Recent evidence indicates that blocking NF-κβ signaling in microglia, but not in astrocytes, reduces motor neuron death and extends survival in SOD1 transgenic mice[221], suggesting a clear role for microglia in neurodegeneration and NF-κβ as a possible therapeutic target. Others have shown that knockdown of TDP-43 also causes activation of microglia with attendant

neurotoxicity[259], highlighting the general notion that several ALS-associated changes can lead to microglial activation and cell death.

Given the signal-dependent variability in microglial activation and response, determining whether microglial can be induced to assume a benign or neuroprotective phenotype in ALS is an important area of research. In vitro studies have convincingly shown that this approach is viable. Treatment of microglia with IL-4 antagonists following LPS activation reduces microglial-associated wild type motor neuron toxicity[260]. Co-culture of motor neurons and microglia in the presence of extracellular mutant SOD1 was used to test this idea in the context of ALS. Extracellular mutant SOD1 activates microglia and leads to motor neuron death (not seen in the absence of microglia) that can be attenuated by blocking signaling through CD14 and Toll-like receptors. Other studies have obtained similar results by attenuating signaling of M1 phenotype-inducing stimuli following nerve injury[261,262]. These studies are often performed using co-culture experiments and it is important to emphasize such systems do not fully capture the complexity the brain and spinal cord and associated signaling between multiple cell types. In ALS, neurons, glia, and astrocytes all simultaneously secrete numerous pro- and anti-inflammatory molecules as a result of the disease process, and the relative balance of these signals likely determines the phenotypic response of glial cells (M1 or M2) and motor neuron fate. Consequently, as with astrocytes, therapeutics targeting an individual signaling pathway are unlikely to prove valuable for the treatment of sporadic ALS[223,224].

1.3.3 Oligodendrocytes

Oligodendrocytes are a highly specialized form of glial cell found exclusively in the CNS. They ensheath neuronal axons in myelin, a hydrophobic lipid mixture with protein components, thus insulating them and markedly enhancing the speed and energetic efficiency of action potential

propagation by saltatory conduction. Because of the length of axons and the energy requirements of conducting action potentials, oligodendrocytes are also provide metabolic support to neurons directly at the level of myelin. Oligodendrocytes express the lactate transporter monocarboxylate transporter 1 (MCT1) and removal of the protein by antisense oligonucleotide leads axon damage and can produce neurodegeneration[263]. The axons of cortical and spinal motor neurons are among the longest in the CNS and demyelination, reduced metabolic support, and loss of normal oligodendrocyte function have accordingly been hypothesized as contributors to motor neuron selective vulnerability/degeneration in ALS.

Support for this hypothesis was found in studies of human ALS spinal cords, which showed inclusion pathology in oligodendrocytes[264-266]. MCT1 levels are also reduced in the spinal cords of ALS patients[263]. More direct evidence in favor of oligodendrocyte dysfunction has been obtained using transgenic animals expressing ALS mutant proteins. SOD-G93A transgenic rats showed extensive myelin abnormalities in early and late stages of disease[267]. Similarly, SOD1-G93A transgenic mice show reduced levels of MCT1[263]. In addition to compromising oligodendrocyte metabolic support of motor neurons, reduced MCT1 levels are also expected to contribute to myelination abnormalities, as lactate is an essential energy source for the production of myelin[268]. Such a metabolic impairment may lead to the secretion of inflammatory factors by both oligodendrocytes and motor neurons that trigger signaling cascades that ultimately result in non-cell autonomous contributions to cell death. SOD1-G93A exhibit morphological changes in oligodendrocytes, favoring an elongated and thickened morphology, prior to symptom onset and neurodegeneration and the number of cells with this altered morphology increases over the course of disease. Although oligodendrocytes frequently undergo apoptosis in this model, the number of oligodendrocytes in the cortex and spinal cord remains constant over the course of disease. This is a

result of the presence of a pool of undifferentiated $NG2^+$ oligodendrocyte precursor cells[266]. Replenishment of oligodendrocytes does not mitigate the degenerative phenotype, however, as the SOD1-G93A transgene expressing oligodendrocytes exhibit reduced capacity to generate myelin and reduced expression of MCT1, leading to metabolic impairments[266]. Promising results were recently obtained by selectively removing mutant SOD1 from oligodendrocytes. Though untreated mice (and ALS patients) showed extensive oligodendrocyte degeneration, when the mutant SOD1 was removed, disease onset was delayed and survival prolonged[84].

These results directly suggest that oligodendrocytes are a key contributor to motor neuron viability and that expression of ALS mutant proteins impairs their normal function and maturation to an extent sufficient to produce neurodegeneration. Future studies examining other ALS-associated proteins, such as TDP-43 and FUS, will address the generality of this mechanism and likely identify potential signaling pathways for therapeutic targeting in human ALS.

1.3.4 Perineuronal Nets and Extracellular Matrix Dysfunction

The extracellular matrix of the CNS is highly specialized and of a unique composition, consisting of chondroitin sulfate proteoglycans, fibronectin, hyaluronan, and several ECM-associated proteins, including tenascin R[269,270]. The protein components of PNNs are synthesized by both neuronal and glial cells and the type of neuron (e.g., glutamatergic, GABAergic, etc..), in part, determines the specific protein and glycan composition of the PNN. This compositional heterogeneity confers functional specificity to PNNs located in specific CNS regions. Consequently, considerable regional heterogeneity exists in the distribution of PNNs throughout the CNS. PNNs are highly abundant in motor regions of the brain and spinal cord and surround the soma, axons, and dendrites of motor neurons[269,270]. PNN development is dependent on neuronal activity and PNNs are vital to the

establishment of proper synaptic connectivity during development[271]. In adulthood, PNNs are known to be repellant to adjacent dendrites and axons, suggesting that PNNs function to maintain established synaptic networks and a homeostatic extracellular environment. Consistent with this latter point, PNNs entrap growth factors and aid in maintaining local ionic homeostasis[269,272]. The neuroprotective functions, together with the observation of PNN abnormalities in other neurodegenerative disorders, have led to the hypothesis that PNN abnormalities also contribute to ALS-associated neurodegeneration.

Evidence of PNN abnormalities in ALS have come from studies of human ALS patients and ALS model systems. Recent work in human subjects indicates that levels of numerous extracellular matrix proteins are decreased in the CSF of ALS patients[273]. This decrease could be correlated with a loss of tenascin R immunoreactivity around motor neurons in ALS patient spinal cord tissue. A similar loss of tenascin R immunoreactivity around motor neurons is observed in SOD1 transgenic rats[274], suggesting that PNN net abnormalities and degradation may be a common consequence of motor neuron degeneration irrespective of cause. A cause of PNN abnormalities in ALS is the well-characterized elevation in matrix metalloproteinases (MMPs) observed in ALS brain and spinal cord tissue[275] and in transgenic mouse models of ALS[276]. MMPs are zinc dependent endopeptidases capable of degrading ECM and PNN components. They can be activated by cytokines, reactive oxygen species, and other inflammatory factors secreted from activated microglia or reactive astrocytes[277], suggesting additional non-cell autonomous mechanisms of motor neuron dysfunction in ALS. Enhanced MMP expression and PNN degradation may reflect a compensatory response from dying neurons attempting to re-establish synaptic contacts. Conversely, MMP degradation of PNNs may be an initiating stimulus for an inflammatory glial reaction that ultimately predisposes motor neurons to death. Support for this latter proposition comes from a study showing that

administration of an MMP inhibitor extended survival in SOD1 transgenic mice[276]. In addition to MMPs, high-throughput profiling of ALS subjects at the protein, mRNA, and mRNA splicing level consistently demonstrates robust changes in PNN and ECM-associated components[273,278,279]. Despite this, PNN alterations in ALS and their contribution to selective motor neuron vulnerability remain a relatively understudied topic in the field of ALS research. Future studies addressing the time course of onset and mechanisms of PNN dysfunction in ALS will likely identify new mechanisms of motor neuron degeneration and therapeutic targets.

1.3.5 Inflammation and Regulatory T-Cells

Neuroinflammation within the CNS is a common pathologic feature in many neurodegenerative diseases, including ALS (reviewed in [214]). Both animal models of ALS and post-mortem tissue from ALS patients exhibit cellular signs of inflammation, namely activation of astrocytes and microglia within affected regions of the brain and spinal cord. Inflammation, therefore, has been a frequent therapeutic target for ALS. Many anti-inflammatory drugs have shown promise in the G93A SOD1 mouse model of disease, but all have failed human clinical trials. These include celecoxib, ceftriaxone, thalidomide, and minocycline[280-282]. Reasons may include inadequate powering of the clinical trial, suboptimal dosage, or administration to ALS patients after disease onset and therefore after closing of a therapeutic window. It is also possible that these therapies failed to reach the appropriate target, as pharmacodynamic biomarkers that demonstrate target engagement have only been recently introduced into ALS clinical trials. However not all neuroinflammation during ALS may be detrimental, as early inflammatory responses can be neuroprotective. Transfer of wild-type microglia into a transgenic SOD1 mouse model of ALS slows disease progression [283], suggesting

that supportive glial responses that release neurotrophic factors and decrease neuronal stress may be beneficial.

Recent evidence strongly implicates CNS-infiltrating immune cells via breakdown of the blood-brain barrier or via the choroid plexus contribute to ALS and other neurodegenerative diseases (Figure 1.3). Infiltrating T lymphocytes have been shown to play important roles in regulating progression and neuroprotection in mouse models of ALS[284]. Fox3p positive regulatory T cells (Tregs) infiltration in the CNS plays an important role in modulating the rate of disease progression, working together with M2 microglia to suppress inflammation[285]. Passive transfer of Tregs into G93A SOD1 mice lacking functional T lymphocytes prolonged survival and decreased Tregs in the blood of ALS patients correlated to more rapid disease progression. In addition, early reduced FoxP3 levels could be used to identify rapidly progressing ALS patients [286].

Nevertheless, in most chronic neurodegenerative diseases, the recruitment of these cells into the CNS seems to be insufficient or delayed, resulting in a pro-inflammatory response that contributes to the exacerbation of pathology[287]. Transport of these lymphocytes into the CNS appears to occur at the level of the choroid plexus[288,289]. Upon entry, Tregs and other infiltrating leukocytes could be transported via the CSF to infiltrate within the brain and spinal cord parenchyma. In addition, the CSF has recently been proposed to be a mechanism for spread of disease[290]. Therefore, both Tregs and the infiltration of other leukocytes into the CNS via the choroid plexus are therapeutic targets for ALS and offer new insight into the mechanisms of disease.

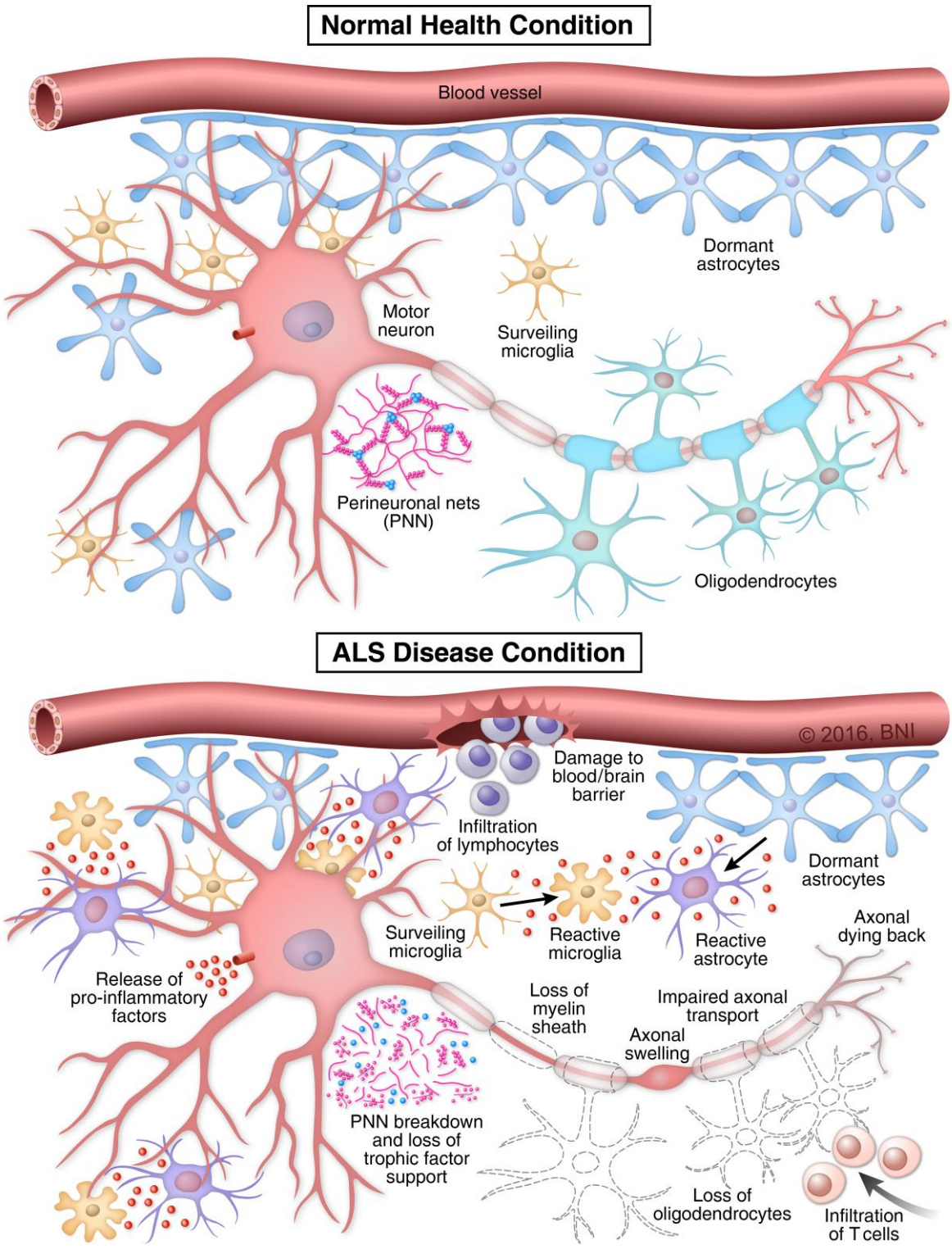

Figure 1.3 Non-cell autonomous mechanisms of ALS. A schematic diagram of non-neuronal cells surrounding motor neurons in normal and ALS disease states is shown. Under normal conditions,

astrocytes and microglia surveil the local environment and aid in homeostatic maintenance. Lymphocytes and T-cells are absent from the local environment and perineuronal nets provide structural and trophic support to motor neurons. Activation of microglia and astrocytes by secretion of inflammatory factors from neuronal and non-neuronal cells activates astrocytes and microglia in ALS, exacerbating the degenerative motor neuron phenotype. Oligodendrocyte hypofunction and degeneration, impaired axonal transport, and perineuronal net breakdown also contribute to motor neuron death. Lastly, infiltration of circulating T-cells and lymphocytes also occurs in ALS, which influences disease progression.

1.4 AXONAL TRANSPORT DEFECTS AND AXONOPATHY

Bi-directional transport of organelles and molecules along axons is a vital determinant of neuronal function, homeostasis, and survival. Synaptic activity at the level of the axon is energetically demanding and requires a diverse array of biochemical reactions, cellular organelles, and molecules for function. Anterograde axonal transport accomplishes this by transporting proteins, mRNAs, organelles, vesicles, and other signaling molecules to the axon terminal[291,292]. At the same time, the axon requires a means to retrogradely transport misfolded proteins, damaged organelles, vesicles, and signaling molecules from the axon to the cell soma. Both of these functions are accomplished by axonal transport driven by protein molecular motors. Because motor neuron axons may be up to 1 meter in length, they are particularly vulnerable to impairments in this process[292]. Collectively, evidence of impaired axonal transport in ALS model systems and evidence of a “dying back” mechanism of neurodegeneration have implicated axonal function as a key susceptibility factor in ALS.

1.4.1 Molecular Motor Proteins and the Neuronal Cytoskeleton

Active transport of proteins, molecules, vesicles, and organelles along the axon occurs via the movement of motor proteins along the microtubule cytoskeleton. Anterograde transport occurs via the ATP hydrolysis-driven stepwise motion of proteins of the kinesin superfamily (KIFs). KIFs proteins possess a globular motor domain that catalyzes ATP hydrolysis and binds to microtubules[293]. The motor domain may be accompanied by a long stalk that allows dimerization of kinesin molecules. KIF light chain proteins associate with these stalks and bind cargoes, making the classical kinesin unit a heterotetramer[293]. The protein sequence of KIFs members confer binding specificity for diverse cargo types and variability in transport velocity.

Retrograde transport along the axon is primarily accomplished by the molecular motor protein dynein. The functional dynein complex is a mixture of polypeptide subunits that includes dynein heavy, medium, intermediate light, and light subunits. The heavy chain subunit functions as a dimer and contains a globular motor domain that binds microtubules and catalyzes the hydrolysis of ATP to achieve molecular motion[294]. Like kinesin, dynein heavy chain stalks associate in a coiled structure that also interacts with intermediate, intermediate light, and light dynein polypeptides. The dynactin protein complex, composed of 11 different polypeptide subunits, mediates cargo recognition and binding and associates with the dynein complex to form the functional retrograde transport machinery[292,294].

Kinesin and dynein-mediated axonal transport occurs along the microtubule cytoskeleton. Microtubules are cylindrical structures built on heterodimers of α and β tubulin monomers that are extended linearly to form protofilaments[293]. Hollow, cylindrical filaments 25 nm in diameter comprising the functional microtubule are formed by the lateral association of 13 protofilaments[292]. Each microtubule has an inherent polarity conferred by the type of tubulin monomer found at each of

its ends; the "plus" end features protruding β tubulin monomers, while the "minus" end contains α tubulin monomers. Axonal microtubules feature a consistent polarity, with "plus" ends facing outward to the axon and "minus" ends facing towards the cell body[295]. This polarity confers directionality to the kinesin and dynein motor transport complexes. Microtubule structure is dynamic (particularly during development) and polymerization occurs faster at the plus end of microtubules to allow for adaptations in synaptic structure[292,295].

1.4.2 Anterograde Axonal Transport

Anterograde axonal transport serves important functions related to synaptic activity, axonal function, and axonal growth and structural integrity. Neurotransmitter containing secretory vesicles are transported via anterograde axonal transport where they subsequently undergo membrane fusion and synaptic transmitter release. Numerous additional cellular components are also transported via anterograde transport to the axon terminal, including mitochondria, RNA granules, transmembrane receptors, enzymes, and mRNAs[292]. Axon extension, growth, and structural integrity likewise require cytoskeletal proteins, including actin, tubulin, and neurofilaments, each of which are transported via kinesin-based anterograde transport[292]. Transport can be further subdivided based on rate, with transport of mitochondria and vesicles designated as "fast" transport and transport of cytoskeletal proteins, enzymes, and other proteins designated as "slow" transport[292,293]. The rates of transport for this diverse array of cargoes span an approximate range of 0.1 m to 10 m per day and transport often occurs intermittently, with cargoes stopping and starting or switching directions during the transport process[292]. Current evidence suggests that the combined rates of antero- and retrograde transport determine where and when a cargo is deposited[293]. Loss or impediment of

axonal transport function is sufficient to induce growth cone collapse in developing neurons or axonal dying back in adult neurons.

1.4.3 Retrograde Axonal Transport

Retrograde axonal transport serves important signaling and homeostatic functions for neurons. Neurotrophic factors, including BDNF and NGF, bind to axonal receptors and, upon internalization, are transported via the dynein-dynactin protein complex to the cell body where they provide trophic support to cells[292]. Similarly, following axonal injury, multiple signaling proteins, including transcription factors and nuclear transport proteins, are transported to the cell body to enable the neuron to sense and respond to injury. Retrograde transport of proteins and organelles destined for degradation is also carried out by the dynein-dynactin complex, which mediates transport of autophagosomes and other vesicles destined for lysosomal fusion[294].

1.4.4 Axonal Transport Defects in ALS

The remarkable length (up to 1 m) of motor neuron axons and the necessity of axonal transport for synaptic function implicate axonal transport as a point of susceptibility in motor neuron degeneration. Initial work showing that substances could bypass the blood brain barrier via axonal uptake at the neuromuscular junction led to the hypothesis of uptake of a peripheral toxic compound that resulted in a progressive dying back of motor neurons[296]. A dying back mechanism was further suggested by the identification of decreased retrograde transport in motor neuron axons from ALS patients[297]. This defect seems to be related to cytoskeletal abnormalities that occur in the axons of ALS patients. Notably, such neurons show axonal swelling and the accumulation of spheroidal

inclusions that are positive for neurofilament proteins[78,298]. Cytoskeletal abnormalities and associated impairments in axonal transport were further implicated as a susceptibility factor for motor neuron degeneration when mice overexpressing the human neurofilament heavy protein were found to develop selective, progressive motor neuron degeneration[299]. Findings from this model system also implicated anterograde transport, however, as the axon terminals of motor neurons lacked normal levels of several proteins and organelles[300]. Mice overexpressing dynamitin showed deficits in retrograde axonal transport related to the disassembly of the dynactin complex[301]. Taken together, these findings suggest that impairment of axonal transport in either direction are sufficient to cause motor neuron degeneration by either cytoskeletal-dependent or cytoskeletal-independent mechanisms.

The development of transgenic mice expressing mutant, ALS-linked SOD1 further demonstrated how impairments to axonal transport could contribute to motor neuron degeneration. Early studies in SOD1-G93A mice suggested a selective impairment in anterograde axonal transport as one of the earliest pathologic events occurring prior to symptom onset[302]. Further characterization showed selective impairments of slow anterograde transport, particularly of tubulin and neurofilament proteins, that led to axonal swellings containing these proteins[303]. Other studies have suggested specific impairments in fast axonal transport, showing that such impairments lead to depletion of axonal mitochondria, owing to intact retrograde transport[304]. Still other studies have implicated impaired retrograde axonal transport in SOD1-mediated neurodegeneration[305]. This notion was supported by the finding that mutant SOD1, but not the wild-type protein, interacts directly with the dynein complex[306]. Intriguingly, expression of mutant SOD1 seems to alter not simply the rate of retrograde transport, but the cargo as well. The dynein-associated fraction of axoplasm from mutant SOD1 transgenic mice shows a significant reduction in neurotrophic factors

(including NGF and BDNF) and significant increases in stress-associated signaling molecules (including capase 8 and P-JNK)[307]. Thus, the role of axonal transport in mutant SOD1-mediated neurodegeneration is complex and likely depends on numerous molecules and organelles. The discrepancies between studies are likely due, at least in part, to the use of different assays and preparations in measuring axonal transport, which range from nerve ligation in mice to isolated axoplasm taken from nerves. Nevertheless, these studies all indicate that impaired axonal transport is an early, presymptomatic event in transgenic SOD1 mice.

More recent work has demonstrated how impaired axonal transport may contribute to sporadic ALS. A genome-wide SNP analysis identified a polymorphism in the kinesin-associated protein 3 (KIFAP3) gene that led to reduced KIFAP3 protein levels and resulted in a 14 month enhancement of survival in sALS patients[308], although this finding was not replicated by a subsequent population-based study[309]. Others have found decreased expression of kinesin motor proteins KIF1Bβ and KIF3Aβ in the motor cortex of sALS patients[310]. Lastly, TDP-43, which is found in inclusions in motor neurons in almost all sALS cases, is also involved in trafficking of mRNA to the axon terminal. TDP-43 associates with mRNAs in the cytoplasm and is transported via slow axonal transport. fALS-linked mutant TDP-43 misfolds and reduces the net movement of mRNA granules and shifts the balance of transport in the retrograde direction[311]. Because TDP-43 is found misfolded and aggregated in inclusions in sALS patients, impaired trafficking of mRNA to axon terminals may also be a common pathology of sALS.

Thus, impaired axonal transport and cytoskeletal abnormalities at the level of the axon are susceptibility factors for motor neuron degeneration in ALS. Because of the considerable length of their axons relative to other neuronal populations, axonal transport defects and pathology may partially explain the selective loss of motor neurons that occurs in ALS. These factors confer both

loss and toxic gain of function mechanisms to motor neurons. The loss of normal cytoskeletal structure and trafficking of cargoes impairs neuronal function, while protein aggregates and enhanced stress signaling are associated with neuronal toxicity. Defects in axonal transport are consistently an early event in ALS model systems, suggesting it represents a potential preventative therapeutic target.

1.5 CURRENT THEORY AND OUTSTANDING CHALLENGES

As described above, many mechanisms have been proposed to contribute to motor neuron degeneration in various forms of ALS (Figure 1.4). Delineating which of these are primary, causative factors in the development of disease in human patients remains one of the great challenges for the field. This question is complicated by the simultaneous occurrence of many of the pathologies described above in sALS patients at the time of diagnosis . The observation that these mechanisms result in cell death/degeneration in ALS model systems only establishes the sufficiency of these processes to produce motor neuron death; it does not demonstrate that they are initiating stimuli or causal mechanisms of disease. Emerging evidence does suggest significant genetic contributions to the development of disease in apparently sporadic patients, with a current heritability estimate for sALS of approximately 20%[312]. Variability in multiple genomic regions is associated with increased risk of disease and approximately 25% of sALS patients exhibit polymorphisms in known fALS causative genes[313]. Thus, it is likely that a combination of genetic and non-genetic factors interact to produce a cumulative individual risk level that if exceeded leads to disease. While incomplete, our understanding of non-genetic factors that contribute to sporadic forms of disease continues to grow. The unique morphological and metabolic requirements of motor

neurons contribute to the cell-type specific degeneration seen in ALS. As described above, motor neurons are acutely vulnerable to defects in RNA processing, protein folding/clearance, and axonal transport. The accumulation of such defects, individually or concurrently, likely leads to further exacerbation of ongoing pathological processes, and, potentially, spread of disease to neighboring cells via secretion of toxic factors or misfolded proteins with prion-like properties and non-cell autonomous activity generated by this signaling. This accumulative model of disease is consistent with the middle to late age of onset observed in a majority of ALS patients. The identification of genetic loci that increase cumulative risk of disease, together with characterization of induced pluripotent stem cells (IPSCs) will provide insight into the initiation of sporadic ALS. Interplay between various mechanisms, genetic variants and/or mutations, and environmental factors likely contribute to the onset, progression rate and selective neurodegeneration observed in ALS (Figure 1.4). Due to the heterogeneity of the disease, a combination of drug treatments targeting multiple pathways, and possibly cell replacement strategies, will likely be necessary to effectively impact disease course within patients. Our ever-increasing understanding of ALS disease mechanisms is vital to designing and implementing these therapeutic approaches.

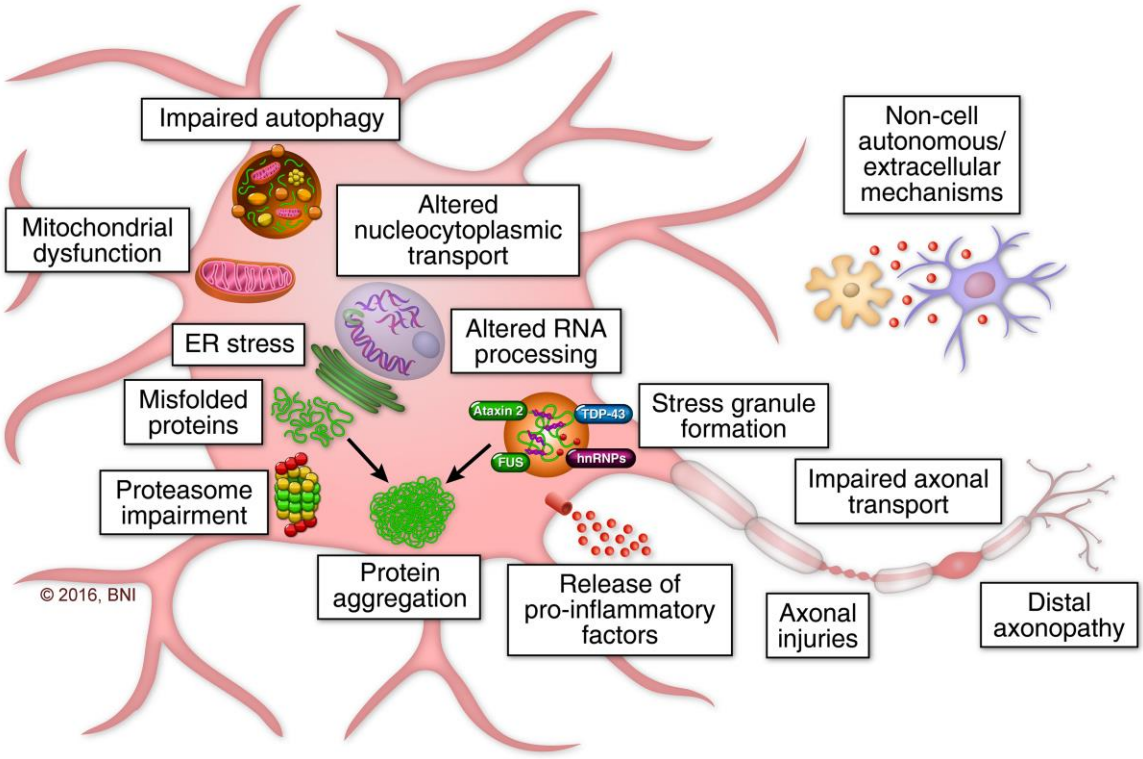

Figure 1.4 General overview of ALS disease mechanisms. Numerous intracellular mechanisms contribute to motor neuron death. Each indicated mechanism represents a point of motor neuron susceptibility, a concept supported by the fALS-linked mutations in genes associated with each mechanism described in the text. As indicated, motor neurons are acutely vulnerable to defects in protein processing/clearance, RNA processing/metabolism, and impaired cytoskeletal/axonal transport function. Each of these processes is capable of inducing inflammatory signaling cascades, which exacerbate impaired motor neuron function by the activation and recruitment of glial and other immune cells.

Despite considerable advances in our understanding of the risk factors, molecular mechanisms, and genetics of ALS, numerous outstanding issues limit our understanding and, consequently, impede the proper treatment, diagnosis, and prevention of ALS. Chief among these issues is determining the distinct etiologies and combinations thereof sufficient to result in the

occurrence of disease. ALS is currently viewed as a collection of disorders with diverse etiologies sharing clinical and neuropathological features[314,315]. This view of disease suggests that clinical phenotype alone is insufficient to properly stratify ALS sub-populations for research and clinical trials. Where familial inheritance is evident, genome sequencing has clear utility in diagnosis, creation of model systems, and in patient stratification for clinical trials. As noted, however, familial forms of ALS account for only approximately 10 percent of the ALS patient population. Genome-wide association studies (GWAS) in various ALS populations have identified genetic loci that increase the risk of sporadic ALS, although findings from these studies have often fared poorly in replication studies and the overall contribution of any given single nucleotide polymorphism (SNP) to risk of ALS is low, albeit statistically significant[316]. Thus, the majority of genetic influence on ALS remains unidentified. Moreover, the identification of SNPs influencing rate of progression and age at onset[316] suggest that fully elucidating the genetic aspects of ALS is a daunting challenge that will require considerable population-based sequencing efforts.

A complementary approach that may provide similar benefits in terms of stratification of the ALS population for research and clinical trials is the identification and validation of protein biomarkers for the disease[317,318]. Protein biomarkers may provide useful indices of the degeneration of motor neurons at various stages of the disease process. This would be particularly valuable for the early detection of disease, as clinical presentation of ALS occurs only after approximately 40 to 50% of motor neurons have been lost. Moreover, protein biomarkers could be used to stratify subsets of ALS patient for clinical trials and assess target engagement or efficacy by molecular therapeutics[318]. The source used for biomarker discovery is a vital determinant of outcome. For ALS numerous possibilities exist and include IPSCs, muscle tissue, blood/plasma, and cerebrospinal fluid (CSF), among others. Of these, CSF offers several distinct advantages. First, its proximity to the

disease/tissue microenvironment results in an increased concentration of motor neuron degeneration-associated proteins and factors[319]. Second, CSF is relatively easy to obtain and does not require extensive culturing/processing as compared to IPSCs or tissue biopsies. Lastly, studies have consistently shown that the protein composition of the CSF is diverse and contains proteins from a variety of intracellular organelles[320,321]. This suggests that monitoring CSF proteome alterations could provide biomarkers of multiple aspects of motor neuron degeneration, including secretion of toxic/inflammatory factors[322], glial/Treg activation[323], protein aggregation[324], and cytoskeletal abnormalities[323]. While studies have demonstrated the feasibility of this approach, they have typically done so in a targeted manner, examining a relatively small number of proteins, often from the same protein family. Given that the CSF proteome contains thousands of proteins and with considerable functional diversity[320,321], a global profiling strategy is necessary to fully capture the proteomic alterations accompanying ALS. We, therefore, hypothesized that comprehensive proteomic profiling of CSF from ALS, healthy control, and other neurological disease patients would lead to the identification of novel ALS disease biomarkers and provide insight to ongoing molecular mechanisms of disease.

2.0 LC-MS/MS PROTEOMIC PROFILING OF AMYTROPHIC LATERAL SCLEROSIS CEREBROSPINAL FLUID

2.1 CHAPTER SUMMARY

Analysis of the cerebrospinal fluid (CSF) proteome has proven valuable to the study of neurodegenerative disorders. To identify new protein/pathway alterations and candidate biomarkers for amyotrophic lateral sclerosis (ALS), we performed comparative proteomic profiling of CSF from sporadic ALS (sALS), healthy control (HC), and other neurological disease (OND) subjects using label-free liquid chromatography-tandem mass spectrometry (LC-MS/MS). A total of 1,712 CSF proteins were detected and relatively quantified by spectral counting. Levels of several proteins with diverse biological functions were significantly altered in sALS samples. Enrichment analysis was used to link these alterations to biological pathways, which were predominantly related to inflammation, neuronal activity, and extracellular matrix regulation. We then used our CSF proteomic profiles to create a support vector machines classifier capable of discriminating training set ALS from non-ALS (HC and OND) samples. Four classifier proteins, WD repeat-containing protein 63, amyloid-like protein 1, SPARC-like protein 1, and cell adhesion molecule 3 were identified by feature selection and externally validated. The resultant classifier distinguished ALS from non-ALS samples with 83% sensitivity and 100% specificity in an independent test set.

Collectively, our results illustrate the utility of CSF proteomic profiling for identifying ALS protein/pathway alterations and candidate disease biomarkers.

2.2 INTRODUCTION

Amyotrophic lateral sclerosis (ALS) is a progressive, fatal neurodegenerative disorder marked by the loss of motor neurons of the corticospinal pathway. ALS is the most common form of adult-onset motor neuron disease, with an overall incidence of approximately 2-3 per 100,000[325-327]. The disease is relentlessly progressive, with most patients dying from respiratory failure within 3-5 years of diagnosis[328-331].

At present, diagnosis of ALS is made clinically by use of the symptom-based El Escorial diagnostic criteria. While clinically stringent, the method does not take into account the underlying etiology of the disease. Numerous mechanisms have been proposed to cause motor neuron death in ALS, including oxidative stress, mitochondrial dysfunction, impaired RNA metabolism, protein aggregation, and proteasomal/autophagic dysfunction, among others[332-335]. These phenomena occur in a heterogeneous fashion in sporadic ALS cases, as do differences in site of onset and rate of disease progression. This has led to the suggestion that ALS is actually a constellation of disorders of diverse cause united by the death of motor neurons and common symptoms[336,337]. Thus, a more accurate understanding of the underlying protein/pathway alterations accompanying sporadic ALS could enhance diagnostic accuracy, identify novel therapeutic targets, provide relevant indices of disease progression/therapeutic response, and aid in stratification of the patient population for research studies and clinical trials.

Proteomic profiling of cerebrospinal fluid (CSF) offers considerable promise towards these ends. In the context of ALS, CSF is a proximal fluid to the site of disease[338], which gives it several advantages as a biomarker source over more distal fluids, such as plasma. One such advantage is its less expansive dynamic range of protein concentrations compared to plasma. By reducing levels of highly abundant proteins such as albumin, sensitive detection and relative quantification of low abundance, disease-associated proteins can be achieved[339,340]. CSF and other proximal fluids are also hypothesized to contain a higher concentration of disease-associated proteins as a result of proximity to the diseased tissue microenvironment, from which such proteins may be secreted or released. For example, CSF TDP-43, an RNA binding protein known to form inclusions in neurons in ALS and FTLD-TDP, has been suggested as a possible biomarker for these disorders[341-343]. Thus, pathological intracellular changes resulting from disease can be detected externally through proximal fluids, such as CSF. CSF has proven useful for identifying biomarkers for other neurodegenerative diseases, including Alzheimer's disease[344], Parkinson's disease[345], and multiple sclerosis[346]. CSF-based ALS biomarkers could likewise be used for several purposes, including identifying novel disease mechanisms, diagnostic testing[347], and evaluating drug efficacy[348].

The ability to detect and quantify the CSF proteome has been aided considerably by the development of label-free mass spectrometric comparative approaches, such as ion abundance and spectral counting[349-351]. Several studies have shown that the values produced by these label-free methods reliably correlate with overall protein abundance across orders of magnitude in complex samples. Following appropriate processing (including filtering and normalization[350]), robust statistical methods can be applied to identify proteins of differential abundance between samples, as well as associated pathways/processes from databases such as Gene Ontology, Reactome, or KEGG[352,353]. Moreover, when combined with an appropriate feature selection method[354], machine-

learning approaches can be applied to such datasets to build parsimonious classifiers that, e.g., distinguish healthy from diseased samples based on protein profiles[354-358]. Such methods have been used to define the normal human CSF proteome. A recent study identified 2,630 proteins from a group of healthy individuals using immunoaffinity depletion of abundant proteins, multiple liquid chromatography separations, and label-free quantitation[320]. Moreover, 56% of these proteins were CSF-specific. This study and others suggest that the CSF proteome is relatively stable across time and that inter-subject differences are considerably greater than intra-subject longitudinal differences[320,321], highlighting the utility of CSF for biomarker discovery.

Several previous studies have attempted to discover CSF-based biomarkers of ALS using mass-spectrometric methods[359-363]. A limitation of these studies is the small overall number of CSF samples and, consequently, proteins, peptides, or M/Z peaks detected, which can limit downstream data analysis and the detection of low-abundance, disease-associated proteins. The present study, by contrast, benefitted from an extensive patient and control population that dramatically enhanced our ability to identify CSF proteins. Subjects were segmented into groups based on age at symptom onset (< 40, 40-60, or > 60 years old) and, for ALS subjects, site of symptom onset (limb or bulbar). This grouping strategy was selected to reduce non-contributing inter-subject variability, while preserving disease-associated differences. Moreover, pooling of samples was used to maximize the sensitivity of protein detection.

The goals of this study, thus, were two-fold. First, we sought to use LC-MS/MS label-free methods to characterize the CSF proteome in ALS, healthy controls, and other neurologic disease subjects to identify disease-associated alterations in proteins and biological pathways. Second, we sought to identify CSF proteins that could distinguish sALS from both healthy control and other

neurological disease subjects by applying feature selection and machine learning methods to our CSF proteomic profiles.

2.3 MATERIALS AND METHODS

2.3.1 Subjects and CSF Collection

In the first phase of the study, CSF samples from 90 sporadic amyotrophic lateral sclerosis (sALS), 80 healthy control (HC), 20 multiple sclerosis (MS), 20 Alzheimer's disease (AD), 10 lower motor neuron disease (LMND), 10 upper motor neuron disease (UMND), and 15 familial ALS (fALS) subjects were collected. These samples were pooled into 9 sALS, 8 HC, 2 MS, 2 AD, 1 LMND, 1 UMND, and 2 fALS samples for discovery profiling (training set). Subjects were assigned to a given pool based on age and disease status, as indicated in Table 1, and all pools were gender matched. Each pool contained 200 µL of CSF from each subject in that pool. The MS, AD, LMND, and UMND samples were collectively grouped as "other neurological diseases" (OND, n=6) for subsequent statistical analyses. A separate set of 9 sALS, 7 fALS, and 4 HC CSF samples were individually processed for LC-MS/MS and used in the test set for validation of the classifier generated from our training set of pooled samples described above. The demographics of these individual samples are also described in Table 1.

Revised El Escorial criteria were used to diagnose all ALS subjects, with 18% diagnosed as definite ALS, 33% probable ALS, 24% probable/lab supported ALS, and 25% possible ALS. CSF samples were obtained by lumbar puncture from subjects at either the University of Pittsburgh

Medical Center (UPMC) or Massachusetts General Hospital (MGH) upon informed patient consent. The study was approved by both institutional review boards.

Following collection, all samples were spun at 3000 rpm at 4 °C for 10 minutes to remove any cells and debris, mixed by inversion, aliquoted, and stored in protein low bind polypropylene tubes at –80 °C within 2 hours of harvesting. Only CSF samples without visible blood were processed by centrifugation. Hemoglobin levels in all final CSF samples were measured by ELISA to eliminate those with evidence of significant levels of hemoglobin, denoting blood contamination[364].

2.3.2 CSF Preparation and Digestion

To enhance the detection of low-abundance CSF proteins, abundant proteins were depleted using the Multi-Affinity Removal System spin cartridge (Agilent; Santa Clara, CA, USA) that removes the 6 most abundant human CSF proteins (albumin, IgG, IgA, haptoglobin, transferrin, and α-1-antitrypsin) according to the manufacturer's protocol. Depleted samples were buffer exchanged into 50 mM ammonium bicarbonate (NH_4HCO_3) by centrifugation using Amicon Ultra3K columns (Millipore; Darmstadt, Germany) to a final volume of 300 µL.

The samples were reduced with addition of 10 mM DTT at 56 ºC for 30 minutes. Samples were then alkylated in 55 mM iodoaceteamide in the dark at room temperature for 30 minutes. Next, 3 µL of 1% ProteaseMAX and Trypsin Gold (Promega; Madison, WI, USA) were added to the samples at a 1:20 ratio and digested at 37 ºC for 9 hours. All samples were then de-salted using Pepclean C-18 spin columns (Pierce; Rockford, IL, USA). Peptide digests were eluted with 20 µL 0.1% TFA and 60% ACN by spinning at 1500 *g* for 1 minute twice. Finally, samples were dried by vacuum centrifugation.

2.3.3 Liquid Chromatography Tandem Mass Spectrometry

Peptide digests were re-suspended in 0.1% TFA and analyzed in triplicate by nanoflow reversed-phase liquid chromatography tandem mass spectrometry (LC-MS/MS) using a Dionex Ultimate 3000 LC system (Dionex Corporation; Sunnyvale, CA, USA) coupled online to a linear ion trap (LIT) mass spectrometer (LTQ, ThermoFisher Scientific; San Jose, CA, USA). Run orders for each experiment were randomly determined. Separations were performed using 75 μm i.d. x 360 o.d. x 10 cm long fused silica capillary columns (Polymicro Technologies; Phoenix, AZ ,USA) that were slurry packed in house with 5 μm, 300 Å pore size C-18 silica-bonded stationary phase (Jupiter, Phenomenex; Torrance, CA, USA). Approximately 1 μg of total peptide digest, as determined by BCA assay, was injected onto a C-18 trap column (Dionex, ThermoFisher Scientific; San Jose, CA, USA), the column was washed for 3 min with mobile phase A (2% acetonitrile, 0.1% formic acid in water) at a flow rate of 30 μL/min. Peptides were eluted using a linear gradient of 0.3% mobile phase B (0.1% formic acid in acetonitrile)/min for 130 minutes, then to 95% B in an additional 10 min, all at a constant flow rate of 0.20 μL/min. Column washing was performed at 95% B for 20 minutes, after which the column was re-equilibrated in mobile phase A prior to subsequent injections. The LIT-MS was operated in a data dependent MS/MS mode in which each full MS scan was followed by five MS/MS scans where the five most abundant peptide molecular ions are selected for collision-induced dissociation (CID), using a normalized collision energy of 30%. Data were collected over a broad mass to charge (*m/z*) precursor ion selection scan range of *m/z* 375-1800 with an isolation window of 3 *m/z*. Dynamic exclusion was used to minimize redundant selection of peptides previously selected for CID with the following settings: repeat count = 1, repeat duration = 30 s, exclusion list size = 500, exclusion duration = 90 s and expiration S/N threshold = 3.

2.3.4 Spectral Counting

Tandem mass spectra were searched against a combined UniProt human protein database from the European Bioinformatics Institute (http://www.ebi.ac.uk/integr8, downloaded 10-05-2010, 58,769 sequences) using the SEQUEST algorithm in BioworksBrowser (v3.31, ThermoFisher Scientific; Waltham, MA, USA). For a fully tryptic peptide to be considered legitimately identified, it had to achieve charge state and proteolytic cleavage-dependent cross correlation (Xcorr) scores of 1.9 for [M+H]1+, 2.2 for [M+2H]2+ and 3.5 for [M+3H]3+, and a minimum delta correlation ΔCn of 0.08. Additionally, peptides were searched for methionine oxidation with a mass addition of 15.9949 and serine, threonine and tyrosine phosphorylation with a mass addition of 79.9663. A false peptide discovery rate less than 2% was determined by searching the primary tandem MS data using the same criteria against a decoy database wherein the protein sequences are reversed[365]. Results were further filtered using software developed in-house, and differences in protein abundance between the samples were derived by summing the total CID events that resulted in a positively identified peptide for a given protein in accession across all samples (spectral counting)[349-351]. We further filtered our data by specifying that for a protein to be considered for subsequent statistical analysis, at least 2 unique peptides of the protein had to be detected in at least one pooled sample, in keeping with recent guidelines designed to improve reproducibility in spectral count data analyses[366].

2.3.5 Statistical Analysis of Relative Protein Abundance

We used the beta binomial test for spectral count data[367] together with normalization to total spectral counts[27] to assess relative levels of identified proteins between groups. To control the false discovery rate (FDR)[368] of the test, we imputed obtained *p* values into the R package "Q Value" to generate *q*

values from the associated *p* values. Bootstrap-based resampling of *p* values[369-373] was used to correct for multiple testing, with the FDR set at 0.05. To provide further insight into the relative differences in protein abundance between groups, we computed log2 fold difference values for each 2 group comparison (sALS/HC, sALS/OND, OND/HC). A value of "1" was added to each protein's spectral count value to account for proteins with a zero spectral count before computing the fold difference[374]. To further control false positives in our analysis, we used a joint *q* value and fold change criteria to assign statistical significance to a given protein identified in our analysis. Previous work has shown that proteins with high spectral count values tend to produce low fold differences and vice versa[350,366]. Accordingly, we used a minimum log2 fold difference of 0.26 for proteins with an average spectral count of 100 or more, a 0.58 log2 fold difference for proteins with an average spectral count of 1 to 100, and a 0.77 log2 fold difference for proteins with an average count of less than 1 to filter our list of proteins with a *q* value of less than 0.05.

2.3.6 Ontological Enrichment Analysis

After filtering our dataset, we used the program STRAP (version 1.5)[375] to characterize the CSF proteome based on the annotations of each identified protein in the Gene Ontology (GO) domains "Biological Process", "Cellular Complex", and "Molecular Function". We next visualized our list of statistically significant proteins in a network layout using Cytoscape[376]. Proteins were visualized first by log2 fold difference values using a red (decreased in x for the x/y fold difference) to green (increased in x for the x/y fold difference) gradient above each protein's name.

To identify biological pathways associated with our list of differentially abundant proteins, we performed enrichment analysis using ClueGO[377]. The hypergeometric test (with Benjamini-Hochberg multiple testing correction[368]) was used to assess enrichment of categories in the GO

domain "Biological Process"[378]. Consistent with recent guidelines for the selection of a reference set[379,380], we used our list of all identified proteins across groups as the reference set for enrichment analysis. In the resultant graph, the proportion of shared proteins associated with a pair of given GO terms was evaluated using the kappa statistic. Pairs of terms (nodes) with a kappa value of at least 0.4 were connected with edges in the network, with the edge thickness reflecting the kappa score value.

Following the identification of over-represented GO Biological Processes, we used Cluepedia[381] to enrich the networks created from these terms. First, we visualized leading terms (GO Biological Process terms with the highest number of statistically significant proteins) together with the proteins associated with that term and the respective fold difference. In the second phase of enrichment, we sought to provide a functional context to the alterations in relative protein levels we identified. To that end, we selected an over-represented GO Biological Process ("Regulation of Extracellular Matrix" [ECM]) and visualized known STRING[382,383] actions (activation, inhibition, expression, and post-translational modification) for statistically significant ECM proteins, other ECM proteins detected in our CSF samples, and several ECM proteins not found in our CSF samples. STRING action scores were used to connect nodes (proteins) in the network. All final figures were made in Adobe Illustrator CS5 (Adobe Systems, Mountain View, CA, USA).

2.3.7 Feature Selection, Classifier Construction, and Validation

In the second phase of the study, we used our CSF proteomic profiles to construct a classifier capable of separating ALS CSF samples from HC and OND CSF samples. The data mining software package Weka[384] was used for this purpose. The classification task was the binary separation of ALS

samples (ALS) from HC and OND (collectively, NON) samples. The training set included all of our pooled sALS and HC CSF proteomic profiles and 3 of the 6 OND proteomic profiles. An independent test set comprised of the remaining 3 OND samples, 9 individual sALS samples, 2 pooled fALS samples, 7 individual fALS samples, and 4 individual HC samples was used for subsequent validation of the classifier. The assignment of samples to the training or test set is indicated in Table 1.

To develop a model resilient to overfitting of the training set, we used a support vector machines algorithm for classification and performed filtering and feature selection on our list of proteins in the training set samples. Filtering was performed by removing any protein from our list if the mean spectral count of any of the classes was zero. Golub's index (GI), a feature selection method previously used for both disease classification[385] and feature selection[386] of spectral count data, was used to select proteins for the classifier. The GI for a protein, *i*, was calculated as follows:

$$GI_i = (\mu_i^{ALS} - \mu_i^{NON}) / (\sigma_i^{ALS} + \sigma_i^{NON})$$

where μ_i^{CLASS} is the mean normalized spectral count for protein *i* for the indicated class and σ_i^{CLASS} is the standard deviation for protein *i* for the indicated class. Proteins with a $GI \geq 1.5$ were included in the classifier. Weka's linear support vector machine (SVM) learning algorithm was used to build the classifier. Consistent with prior studies[386,387], we used a complexity parameter, C, of 100 for classifier training and test set evaluation. To evaluate the performance of the classifier on the training set, we used stratified 10-fold cross validation. We then validated our classifier on the test set described above and in Table 1. To evaluate the performance of the classifier on the test set, we used common measures of predictive performance (ROC curve, sensitivity, specificity, ROC AUC, and F-measure).

2.3.8 Validation of Selected Proteins

To validate our LC-MS/MS results, we used several complementary techniques. Proteins selected for our SVM classifier were validated using Western blotting (WB). Polyacrylamide gel electrophoresis (PAGE), electrophoretic transfer to PVDF membrane, and WB were performed as previously described[388]. Briefly, equal volumes of CSF were loaded in each SDS-PAGE gel lane and total protein by reversible PVDF membrane stain (G-Biosciences; St. Louis, MO, USA) was used as a loading control. For WB experiments, the following antibodies were used: rabbit-anti-WDR63 (Abcam; Cambridge, MA, USA), rabbit-anti-APLP1 (Proteintech; Chicago, IL, USA), rabbit-anti-SPARCL1 (Lifespan Biosciences; Seattle, WA, USA), rabbit-anti-CADM3 (Sigma Aldrich; St. Louis, MO, USA), and rabbit-anti-secretogranin I (Proteintech; Chicago, IL, USA). To permit blot to blot comparisons, Western blot data were normalized using sum total normalization[389].

ELISAs for complement C3 and cystatin C were performed as previously described[390,391]. Immunohistochemistry and light microscopy of spinal cord tissues for tenascin R were performed as previously described[392]. Immunohistochemistry, immunofluorescence, light microscopy, and confocal microscopy of spinal cord tissues for eIF 4e-transporter (4e-T) were performed as previously described[392].

2.4 RESULTS

2.4.1 Global CSF Analysis

Our experimental work flow is illustrated in Figure 2.1. The demographics of each of our pooled samples are shown in Table 2.1. Within each of these pooled CSF samples, we identified an average of 6,137 peptides, corresponding to an average of 1,234 unique proteins per sample. Collectively, we identified 1,712 unique proteins across all groups after filtering. (Supplemental Table 1). To further understand the composition of the obtained CSF proteome, we grouped these proteins based on their annotations in the Gene Ontology (GO) domains "Biological Process", "Cellular Complex", and "Molecular Function". Figure 2.2 shows the proportional representation of the various sub-categories in each GO domain with each value expressed as a percentage of the total. Sub-category proportions did not differ substantially between sporadic ALS (sALS), healthy control (HC), and other neurological disease (OND) groups (data not shown). Our results indicate that proteins associated with diverse biological processes, cellular complexes, and molecular functions are found in the CSF proteome. Notably, we detect proteins from numerous intracellular organelles, including the nucleus, mitochondria, ribosomes, and ER in the CSF, consistent with previous work[320,321].

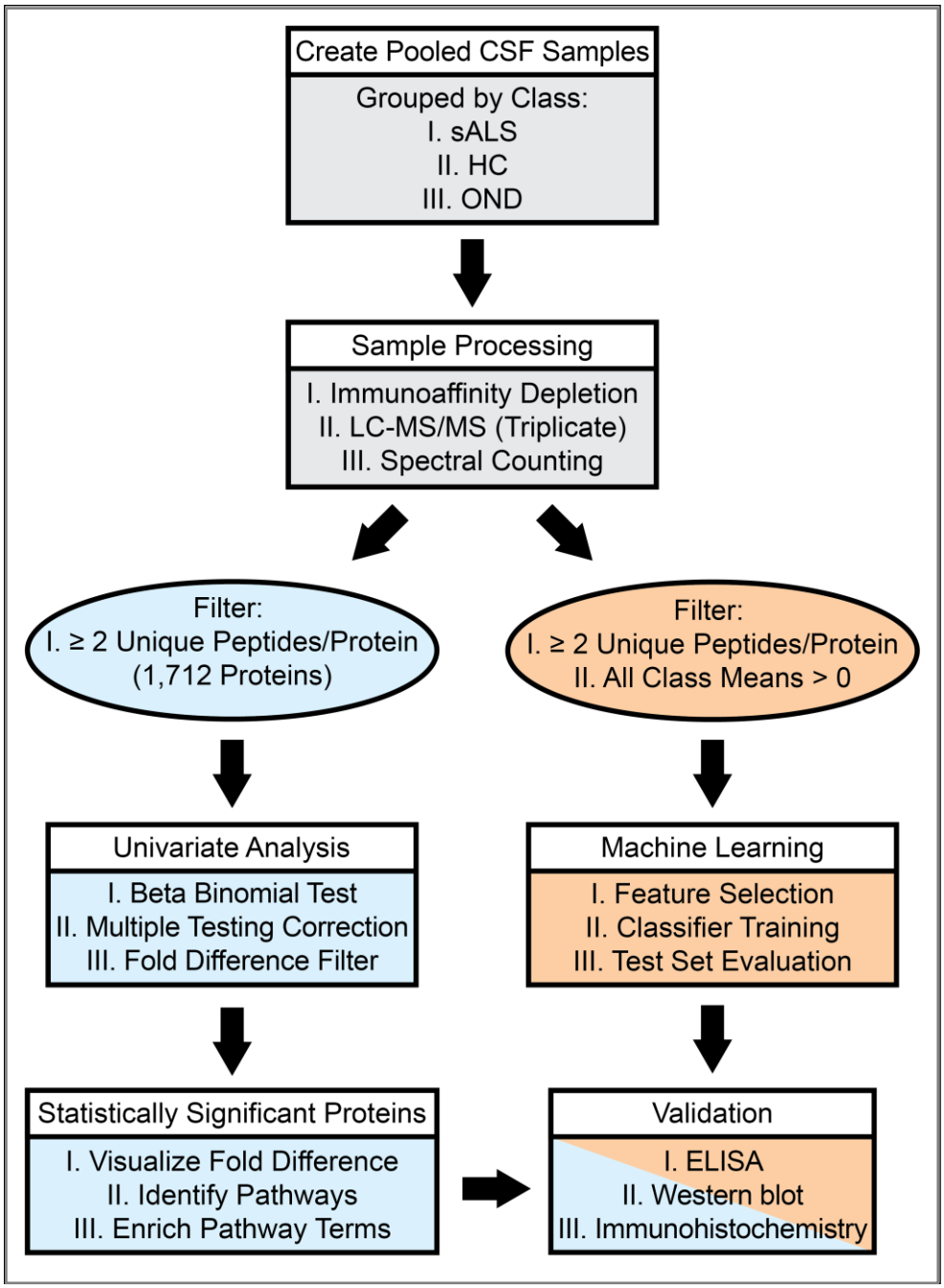

Figure 2.1 Experimental workflow. The process of sample preparation, data acquisition, and data analysis are shown in a flowchart. sALS = sporadic amyotrophic lateral sclerosis, HC = healthy control, OND = other neurological disease.

Table 2.1 Subject demographics. Patient group, diagnosis, class, and age range (years) are shown. For ALS samples, the site of disease onset and use of riluzole are indicated. The set column indicates the classifier evaluation set a sample was assigned to. Samples are ordered by class then age. HC = healthy control, MS = multiple sclerosis, LMND = lower motor neuron disease, UMND = upper motor neuron disease, AD = Alzheimer's disease, OND = other neurological disease.

POOLED SAMPLES						
Group	**Diagnosis**	**Class**	**Age Range**	**Site of Onset**	**Riluzole**	**Set**
1	sALS	ALS	< 40	Limb	No	Train
2	sALS	ALS	< 40	Limb	No	Train
3	sALS	ALS	40-60	Limb	No	Train
4	sALS	ALS	40-60	Limb	Yes	Train
5	sALS	ALS	40-60	Limb	Yes	Train
6	sALS	ALS	40-60	Bulbar	No	Train
7	sALS	ALS	> 60	Limb	No	Train
8	sALS	ALS	> 60	Limb	Yes	Train
9	sALS	ALS	> 60	Bulbar	No	Train
10	HC	HC	< 40	n/a	n/a	Train
11	HC	HC	< 40	n/a	n/a	Train
12	HC	HC	< 40	n/a	n/a	Train
13	HC	HC	30-60	n/a	n/a	Train
14	HC	HC	40-60	n/a	n/a	Train
15	HC	HC	40-60	n/a	n/a	Train
16	HC	HC	> 60	n/a	n/a	Train
17	HC	HC	> 60	n/a	n/a	Train
18	MS	OND	< 40	n/a	n/a	Test
19	MS	OND	40-70	n/a	n/a	Train
20	LMND	OND	40-65	n/a	n/a	Test
21	UMND	OND	40-65	n/a	n/a	Train
22	AD	OND	> 60	n/a	n/a	Test
23	AD	OND	> 60	n/a	n/a	Train
24	fALS	ALS	30-60	Limb	No	Test
25	fALS	ALS	> 40	Limb	No	Test

INDIVIDUAL SAMPLES						
Subject	**Diagnosis**	**Class**	**Age**	**Site of Onset**	**Riluzole**	**Set**
1	sALS	ALS	42	Limb	Yes	Test
2	sALS	ALS	44	Limb	Yes	Test
3	sALS	ALS	44	Limb	Yes	Test
4	sALS	ALS	53	Limb	Yes	Test
5	sALS	ALS	54	Limb	Yes	Test
6	sALS	ALS	55	Limb	Yes	Test
7	sALS	ALS	75	Limb	Yes	Test
8	sALS	ALS	76	Limb	Yes	Test
9	sALS	ALS	77	Limb	Yes	Test
10	fALS	ALS	50	Limb	No	Test
11	fALS	ALS	52	Limb	Yes	Test
12	fALS	ALS	52	Limb	Yes	Test
13	fALS	ALS	53	Limb	No	Test
14	fALS	ALS	60	Limb	No	Test
15	fALS	ALS	62	Limb	No	Test
16	fALS	ALS	62	Limb	Yes	Test
17	HC	HC	33	n/a	n/a	Test
18	HC	HC	50	n/a	n/a	Test
19	HC	HC	51	n/a	n/a	Test
20	HC	HC	65	n/a	n/a	Test

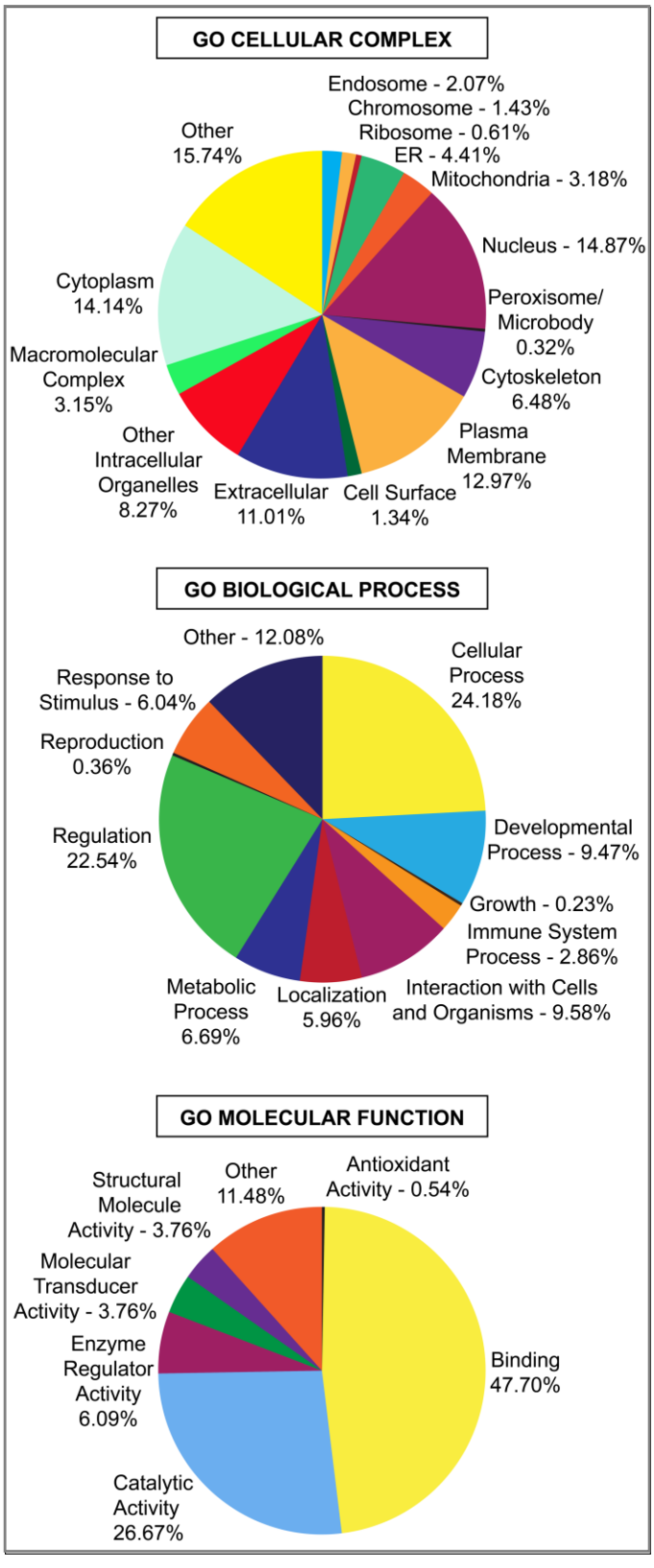
GO CELLULAR COMPLEX
Endosome - 2.07%
Chromosome - 1.43%
Ribosome - 0.61%
ER - 4.41%
Mitochondria - 3.18%
Nucleus - 14.87%
Peroxisome/ Microbody 0.32%
Cytoskeleton 6.48%
Plasma Membrane 12.97%
Cell Surface 1.34%
Extracellular 11.01%
Other Intracellular Organelles 8.27%
Macromolecular Complex 3.15%
Cytoplasm 14.14%
Other 15.74%
GO BIOLOGICAL PROCESS
Other - 12.08%
Cellular Process 24.18%
Developmental Process - 9.47%
Growth - 0.23%
Immune System Process - 2.86%
Interaction with Cells and Organisms - 9.58%
Localization 5.96%
Metabolic Process 6.69%
Regulation 22.54%
Reproduction 0.36%
Response to Stimulus - 6.04%
GO MOLECULAR FUNCTION
Antioxidant Activity - 0.54%
Other 11.48%
Structural Molecule Activity - 3.76%
Molecular Transducer Activity - 3.76%
Enzyme Regulator Activity 6.09%
Catalytic Activity 26.67%
Binding 47.70%

Figure 2.2 Gene Ontology (GO) domain overview of all identified proteins. All identified proteins were input into the three GO domains – Biological Process, Cellular Complex, and Molecular Function – and the resultant terms and percentage of proteins associated with these terms are visualized as pie charts. Term names and percentages are located next to their position on the chart. Percentages correspond to all 1,712 proteins identified across all classes (sALS, HC, and OND).

2.4.2 Statistical Analysis of Relative Protein Abundance

To identify proteins of differential abundance in the CSF between sALS, HC, and OND groups, we performed univariate statistical analysis. Filtering the list of statistically significant proteins from this analysis using a fold difference criteria (see Experimental Section) predominantly had the effect of removing several proteins for which the class average spectral count was less than 1. In total, we identified 123 proteins that met our FDR and fold difference significance criteria (Supplemental Table 2). The top 20 proteins of increased and decreased abundance are shown in Table 2.2. Several proteins with documented associations with ALS were identified in the top 20 protein list, including complement C3, cystatin C, neurofilament medium polypeptide, ephrin type-A receptor 4, and secretogranin 2. Another consistent theme in the top 20 protein list was a decrease in relative levels of extracellular matrix (ECM)-associated proteins in sALS, including tenascin R, semaphorins 7A and 3G, cell adhesion molecule 3, neurexin-3-alpha, agrin, and oligodendrocyte-myelin glycoprotein (Table 2.2).

Table 2.2 Top 20 increased and decreased CSF proteins. The top 20 proteins with statistically significant increased or decreased relative abundance in sALS samples are shown by q value rank (lowest to highest). Protein name, gene name, and Uniprot accession number is shown and protein isoform is indicated in the accession number. The log2 fold difference (FD) for each two group comparison is shown.

INCREASED ABUNDANCE

Protein	**Gene Name**	**Accession**	***q***	**FD sALS/HC**	**FD sALS/OND**	**FD OND/HC**
Neurofilament medium polypeptide	NEFM	P07197	<0.0001	2.3	2.4	-0.1
WD repeat-containing protein 63	WDR63	Q8IWG1	<0.0001	1.8	2.3	-0.5
Complement C3	C3	P01024	<0.0001	0.3	0.1	0.2
Very large A-kinase anchor protein	CRYBG3	Q68DQ2	0.0004	1.5	1.3	0.2
Acid phosphatase-like protein 2	ACPL2	Q8TE99	0.0010	0.9	2.0	-1.1
Serine/threonine-protein kinase PLK1	PLK1	P53350	0.0010	1.2	1.4	-0.2
Protein phosphatase 1J	PPM1J	Q5JR12	0.0013	1.4	1.3	0.1
AF4/FMR2 family member 4	AFF4	Q9UHB7	0.0041	0.6	1.5	-0.8
PDZDC RING finger protein 4	PDZRN4	Q6ZMN7	0.0044	2.1	1.6	0.5
Actin	ACTB	P60709	0.0044	1.5	0.4	1.1
Disks large-associated protein 1	DLGAP1	O14490	0.0050	1.3	0.3	0.9
Tripartite motif-containing protein 43B	TRIM43B	A6NCK2	0.0050	1.2	0.8	0.5
ALK tyrosine kinase receptor	ALK	Q9UM73	0.0056	1.4	1.2	0.2
Protein Daple	CCDC88C	Q9P219	0.0056	1.1	0.7	0.5
SMG5	SMG5	Q9UPR3	0.0056	1.0	0.8	0.2
V-set and IG domain protein 4	VSIG4	Q9Y279	0.0066	1.2	0.7	0.5
Tafazzin	TAZ	Q16635	0.0066	0.9	0.7	0.2
Protein XXbac-BCX360G3.2-001	BCX360G3.2	B0V386	0.0088	1.1	0.9	0.2
OTU domain-containing protein 7A	OTUD7A	Q8TE49	0.0105	0.8	1.2	-0.3
Hyaluronan-binding protein 2	HABP2	Q14520	0.0107	1.1	0.9	0.2

DECREASED ABUNDANCE

Protein	Gene Name	Accession	*q*	FD sALS/HC	FD sALS/OND	FD OND/HC
Multiple EGF-like domains protein 8	MEGF8	Q7Z7M0	0.0004	-1.1	-0.3	-0.8
Cystatin-C	CST3	P01034	0.0004	-0.1	-0.3	0.1
Golgi membrane protein 1	GOLM1	Q8NBJ4	0.0005	-1.4	-0.1	-1.2
Cell adhesion molecule 3	CADM3	Q8N126	0.0013	-0.9	-0.9	0.0
Semaphorin-7A	SEMA7A	O75326	0.0038	-0.8	-0.5	-0.3
Semaphorin-3G	SEMA3G	Q9NS98	0.0040	-0.6	1.0	-1.6
Secretogranin-2	SCG2	P13521	0.0040	-0.6	-0.2	-0.4
Neurexin-3-alpha	NRXN3	Q9Y4C0	0.0044	-0.7	0.2	-1.0
Putative PRAME family member 24	PRAMEF24	A6NMC2	0.0050	-1.5	-1.1	-0.4
Cartilage acidic protein 1	CRTAC1	Q9NQ79	0.0050	-0.3	0.6	-0.9
Oligodendrocyte-myelin glycoprotein	OMG	P23515	0.0058	-0.9	-0.8	-0.2
Disks large homolog 5	DLG5	Q8TDM6	0.0064	-1.4	-0.8	-0.6
Testican-2	SPOCK2	Q92563	0.0114	-0.9	0.2	-1.2
Cathepsin D	CTSD	P07339	0.0142	-0.2	-0.7	0.5
Agrin	AGRN	O00468	0.0158	-0.7	-0.4	-0.3
Gelsolin	GSN	P06396	0.0165	-0.1	-0.2	0.1
Follistatin-related protein 4	FSTL4	Q6MZW2	0.0176	-0.6	0.9	-1.5
Di-N-acetylchitobiase	CTBS	Q01459	0.0183	-1.3	-1.2	-0.1
Delta/Notch-like EGFR receptor	DNER	Q8NFT8	0.0194	-1.4	-0.6	-0.8
Ephrin type-A receptor 4	EPHA4	P54764	0.0202	-0.6	-0.1	-0.5

To identify biological pathways associated with our list of differentially abundant CSF proteins, we performed enrichment analysis in the Gene Ontology (GO) Biological Process domain. We found 27 enriched GO terms that were over-represented in our list of statistically significant proteins. These results are shown in Figure 2.3. Several themes emerged from our analysis of over-represented biological processes. We identified many neuron-specific processes, including "synapse

organization", "regulation of axonogenesis", "regulation of synaptic plasticity", and "fasciculation of sensory neuron axon". Of note, all proteins comprising the term "fasciculation of sensory neuron axon" (ephrin type A receptors 3 and 4 and multiple epidermal growth factor-like domains protein) were significantly altered in sALS samples compared to healthy control samples. Other major processes identified from the analysis included "regulation of extracellular matrix", "acute inflammatory response", and "glial cell differentiation", each of which has clear relevance to ALS.

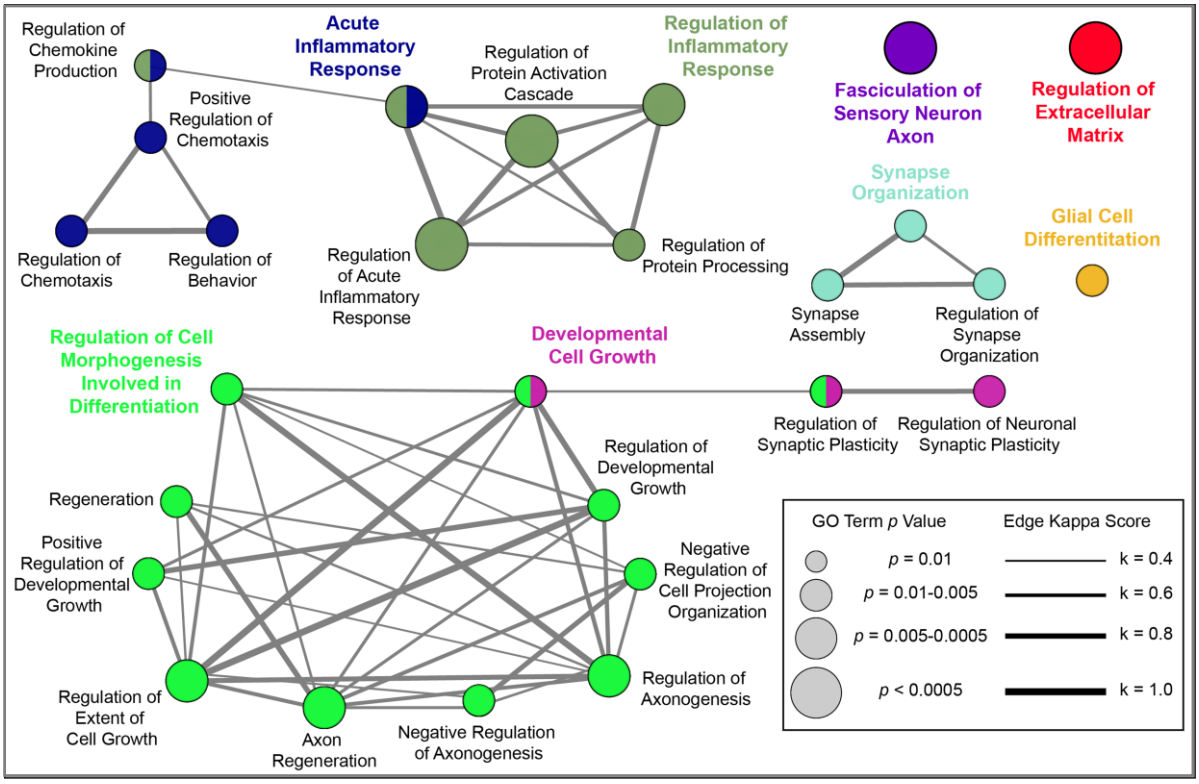

Figure 2.3 GO Biological process enrichment. Proteins whose levels were significantly different between sALS, HC, and OND groups were used to identify over-represented GO Biological Process terms. The results are shown in a network view where node size corresponds to the term's *p* value and edge thickness corresponds to kappa score value as indicated in the legend at right. Nodes are positioned for ease of interpretation and edge length is arbitrary. Leading terms, GO terms with the highest number of included proteins, are shown in a larger, colored font.

Taking those biological processes with the highest number of associated proteins, we next visualized these terms and their associated proteins together in a network view (Figure 2.4). A protein's association with a term is indicated by an edge connecting the two. The relative contributions of proteins of increased and decreased abundance in sALS can be seen in this view. For example, the identification of the terms "acute inflammatory response" and "regulation of inflammatory response" is mainly due to increased levels of proteins associated with these terms in sALS CSF samples, particularly those proteins of the complement pathway. Likewise, the enrichment of the terms "synapse organization" and "extracellular matrix organization" stems primarily from the decreased levels of proteins associated with these terms in sALS samples. Collectively, this network view underscores the notion that the ALS disease process is associated with a concomitant decrease in synaptic and ECM proteins and increase in inflammation-related proteins within the CSF. We also note that proteins with a high degree of connectivity in the network of Figure 2.4 (i.e., those associated with several terms) tended to be ECM-associated proteins, such as tenascin R and laminin subunit alpha 2 (LAMA2), providing further evidence that ECM alterations are a preponderant pathological phenomenon in sALS (Figure 2.4).

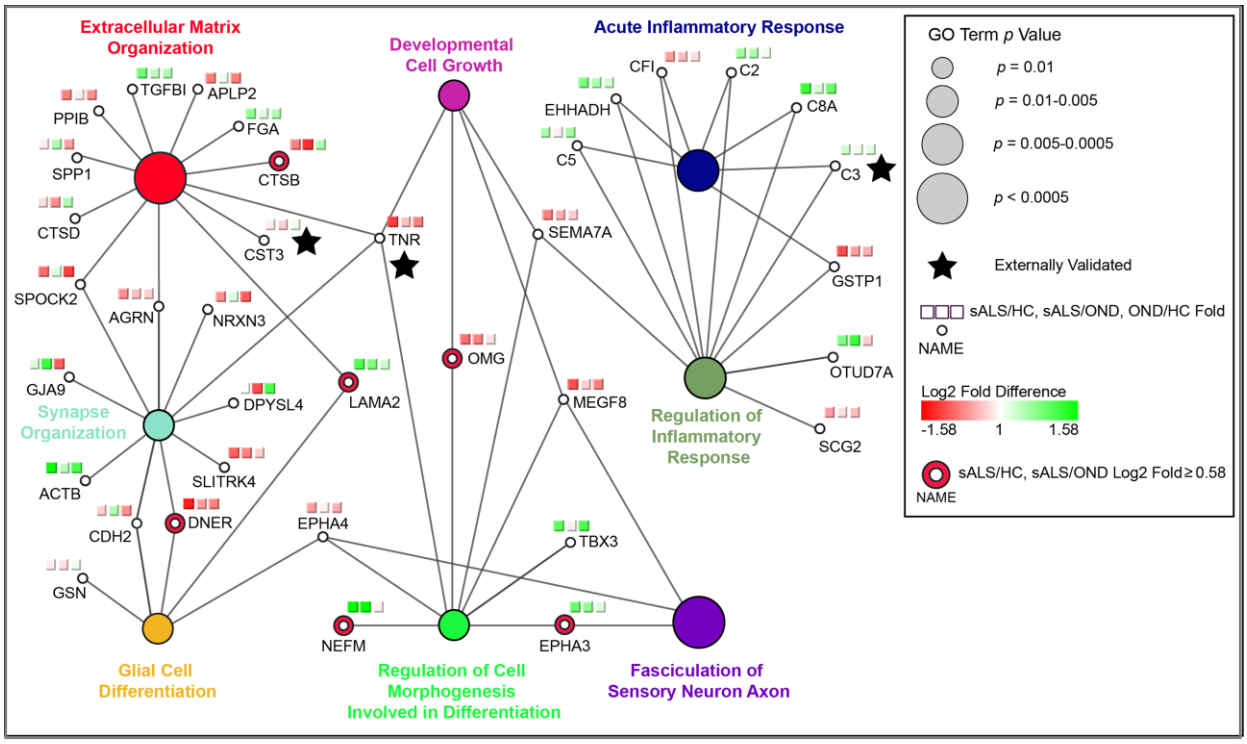

Figure 2.4 GO leading terms with associated proteins. Leading terms from Figure 2.3 are shown with their associated proteins. Each two-group log2 fold difference (sALS/HC, sALS/OND, OND/HC) is visualized using a red to green gradient. Proteins with a log2 fold difference > 0.58 for sALS relative to both HC and OND groups are emphasized as indicated, as are externally validated proteins.

To provide functional context and a pathway-level understanding of the observed ECM alterations, we linked ECM proteins using STRING action scores to create a network of the "regulation of extracellular matrix" GO term. We note that not all proteins from the term are shown to enhance the interpretability of the figure. The final network is shown in Figure 2.5. Several findings emerge from this analysis. First, we provide clear evidence of the power of LC-MS/MS CSF proteomic profiling to identify ECM-associated proteins. Of the 102 proteins shown in Figure 2.5, 85 could be detected in at least one of our pooled CSF samples (those that could not are

bracketed with parentheses in Figure 2.5). Second, proteins whose levels are significantly altered in sALS CSF converge on few common targets, suggesting that pathological ECM protein and signaling alterations are widespread in ALS. Lastly, we again note that the majority of altered ECM proteins are decreased in sALS samples. The network view thus emphasizes that these decrements may have widespread signaling effects, particularly for proteins such as gelsolin (GSN) that act on numerous ECM proteins.

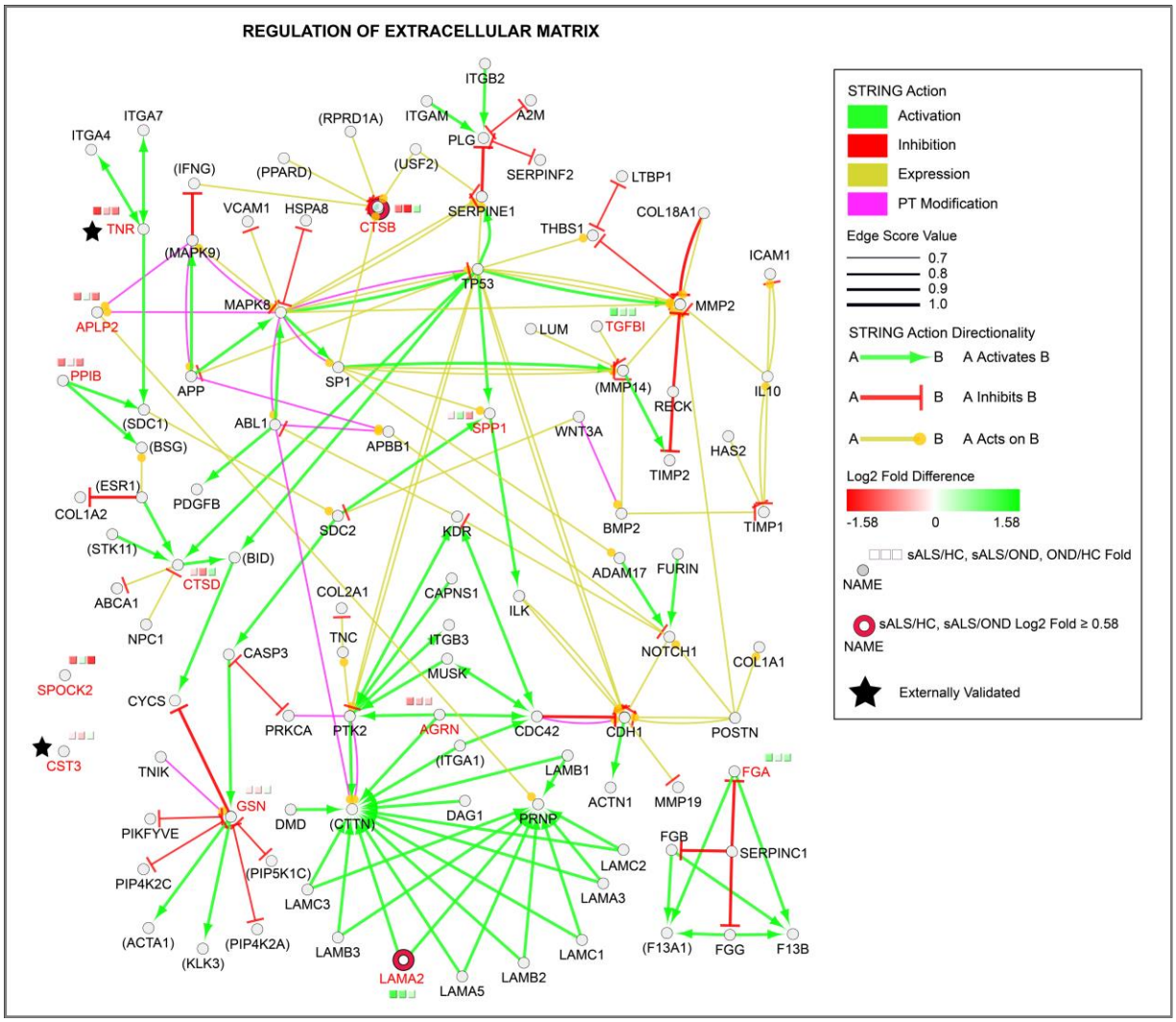

Figure 2.5 Enrichment of "Regulation of Extracellular Matrix" GO term. Statistically significant proteins from the GO Biological Process term "Regulation of Extracellular Matrix" were visualized as circular nodes, with log2 fold difference (on a red to green gradient) shown in the three squares above each node. Proteins with a log2 fold difference > 0.58 for sALS relative to both HC and OND groups are emphasized as indicated, as are externally validated proteins. The network was enriched using STRING action scores (activation, inhibition, expression, and post-translational modification; colored as indicated) to add associated proteins to the network. Statistically significant protein names from the LC-MS/MS data are shown in red font for emphasis. Names of proteins not

detected in our LC-MS/MS analysis are bracketed by parentheses. Edge width reflects the strength of the STRING action score as indicated in the legend and edge length is arbitrary.

2.4.3 Validation of Known ALS Biomarkers

We observed significant differences in a number of proteins previously identified as candidate ALS CSF biomarkers by LC-MS/MS. To further evaluate the utility of these proteins as CSF biomarkers, we performed ELISAs and Western blots on individual CSF samples from subjects comprising our ALS, HC, and OND pooled samples. The results of these experiments are shown in Figure 2.6. Complement C3 levels were measured by ELISA in 23 sALS, 26 HC, and 12 OND CSF samples. Statistically significant increases in CSF C3 levels were observed when comparing sALS or OND samples to HC samples (mean sALS = 3.42 ± 0.29 µg/mL, mean OND = 3.40 ± 0.37 µg/mL, and mean HC = 2.22 ± 0.12 µg/mL, $p < 0.001$ for the sALS/HC comparison, $p < 0.01$ for the OND/HC comparison). We measured cystatin C levels by ELISA in 20 sALS samples, 8 HC samples, and 11 OND samples. A statistically significant decrease in cystatin c levels was observed in sALS CSF relative to HC (means = 3.27 ± 0.34 µg/mL and 4.98 ± 0.36 µg/mL, respectively, $p < 0.01$). A non-significant decrease in cystatin C levels was seen when comparing sALS samples to OND samples (means = 3.27 ± 0.34 µg/mL and 4.26 ± 0.35 µg/mL, respectively, $p > 0.05$). Levels of secretogranin I were measured by Western blotting of 14 sALS, 10 HC, and 10 OND CSF samples. Secretogranin I was significantly decreased in sALS compared to HC ($p < 0.01$) and OND ($p < 0.01$) samples.

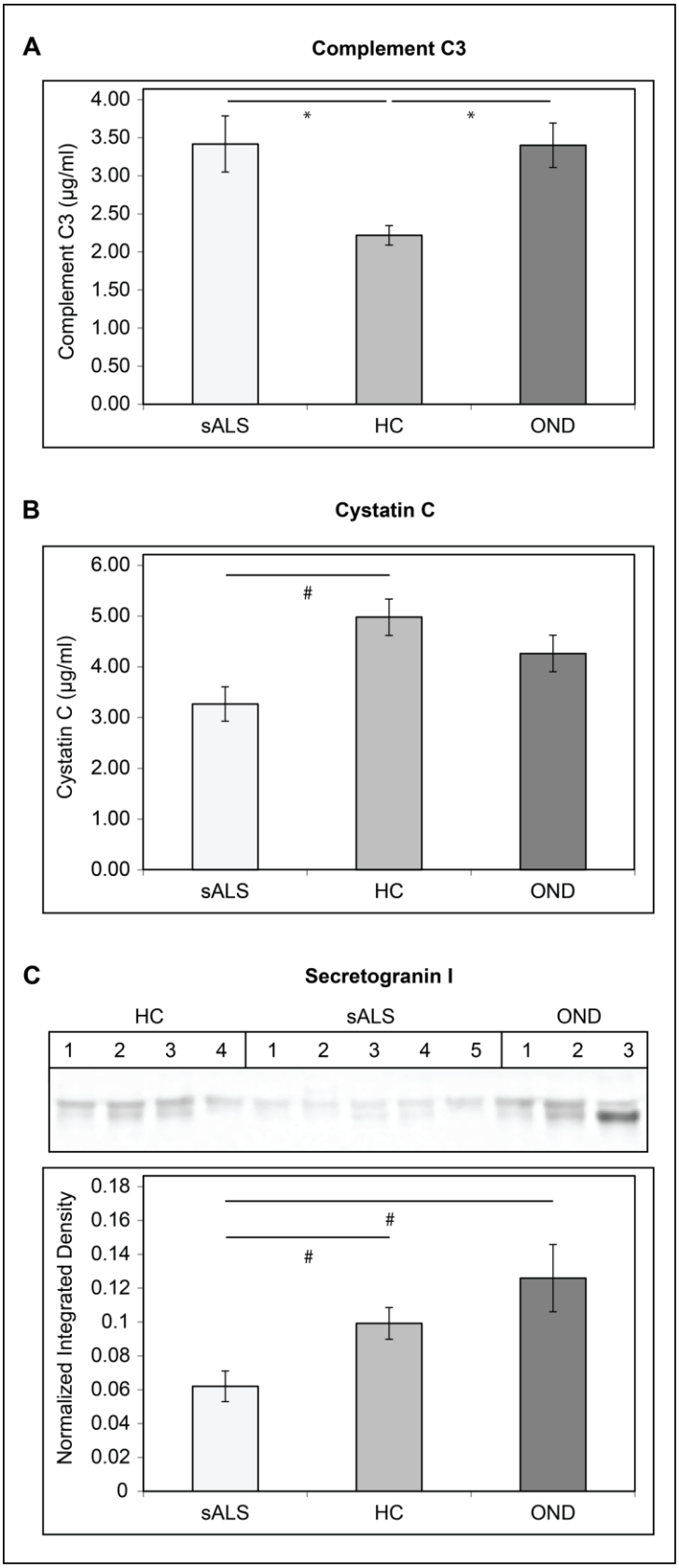
A
Complement C3
Complement C3 (µg/ml)
4.00
3.50
3.00
2.50
2.00
1.50
1.00
0.50
0.00
*
*
sALS
HC
OND
B
Cystatin C
Cystatin C (µg/ml)
6.00
5.00
4.00
3.00
2.00
1.00
0.00
#
sALS
HC
OND
C
Secretogranin I
HC
sALS
OND
1 2 3 4 1 2 3 4 5 1 2 3
Normalized Integrated Density
0.18
0.16
0.14
0.12
0.1
0.08
0.06
0.04
0.02
0
#
#
sALS
HC
OND

Figure 2.6 Validation of known ALS biomarkers. A. Complement C3 levels in CSF from sALS, HC, and OND subjects were measured by ELISA in triplicate. The concentration of Complement C3 (µg/mL ± SEM) is indicated on the y axis. **B.** Cystatin C levels in CSF from sALS, HC, and OND subjects were measured by ELISA. The concentration of cystatin C (µg/mL ± SEM) is indicated on the y axis. **C.** Relative levels of secretogranin I in CSF from sALS, HC, and OND subjects were measured by Western blot. The mean normalized integrated density value ± SEM is indicated on the y axis. For **A-C**. * = $p < 0.001$ for the indicated comparison, # = $p < 0.01$ for the indicated comparison.

2.4.4 Validation of Protein Alterations in ALS Spinal Cord Tissue

Selected proteins from our list of differentially abundant proteins were validated using immunohistochemistry and immmunofluorescence. Because decreases in ECM proteins were a consistent theme in our results, we stained 4 sALS and 4 HC lumbar spinal cord tissue sections with anti-tenascin R antibody. Tenascin R is a component of perineuronal nets, the densely organized extracellular matrix surrounding neurons. We observed a clear loss of tenascin R immunoreactivity surrounding motor neurons in sALS lumbar spinal cord that was not seen in HC subjects (Figure 2.7). Thus, the ECM of the ALS-afflicted motor neurons shows perturbations consistent with the results of LC-MS/MS proteomic profiling of CSF.

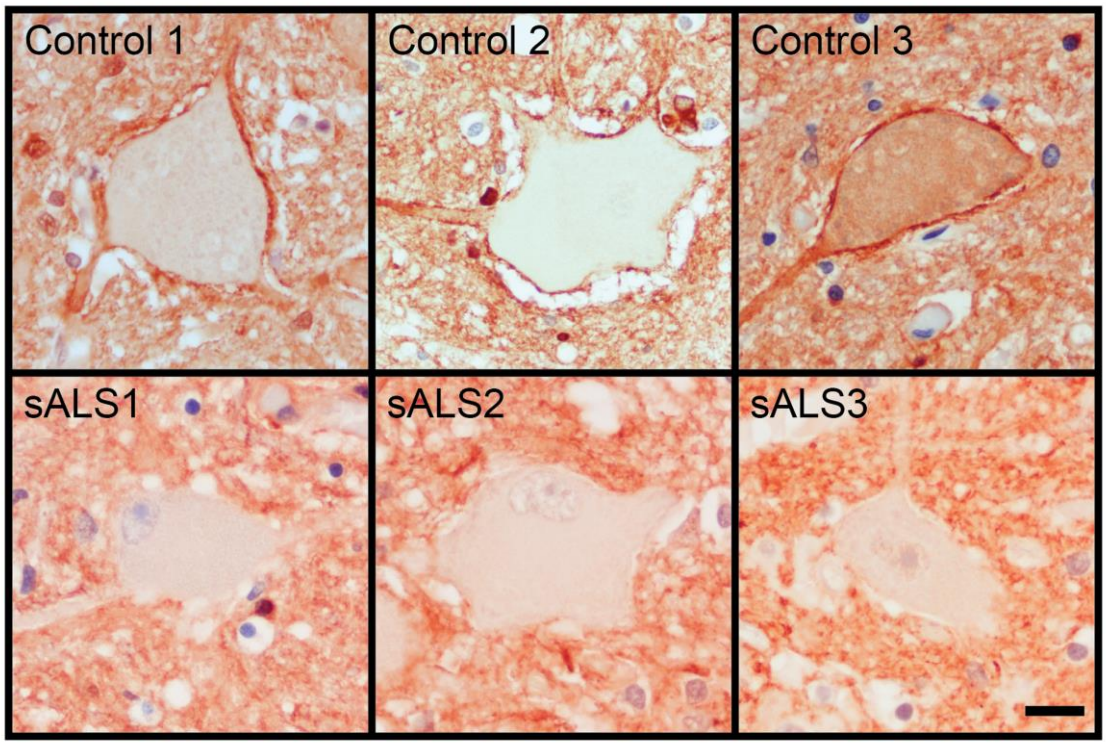

Figure 2.7 Tenascin R validation. Lumbar spinal cord sections from sALS and HC patients were stained using a polyclonal anti-tenascin R antibody. Top Panel. Motor neurons from HC subjects show strong tenascin R immunoreactivity around the cell body. Bottom panel. Motor neurons from sALS cases show an absence of this staining pattern. All images were acquired with a 40x objective and the scale bar = 10 µm.

LC-MS/MS also identified a significant increase in levels of the eIF 4e transporter (4e-T) in the CSF of sALS patients when compared to HC. 4e-T is a component of stress granules[393] and we therefore performed tissue staining to determine if 4e-T is a component of inclusions in sALS spinal cord motor neurons, as has been observed for other stress granule-associated proteins[394]. We observed filamentous and granular nuclear 4e-T staining and cytoplasmic 4e-T-positive inclusions in lumbar spinal cord motor neurons in the 4 sALS cases examined (Figure 2.8. By contrast, the 4e-T staining in motor neurons of all 4 HC subjects was diffuse, non-filamentous, and nuclear.

Immunofluorescence microscopy was then used to determine if 4e-T inclusions were p62 positive. We observed considerable accumulation of autofluorescent cytoplasmic lipofuscin in motor neurons (Figure 2.8; arrowheads) that obfuscated the detection of cytoplasmic 4e-T. This accumulation was not present in the nucleus, however, and numerous nuclear, p62-positive 4e-T granules in sALS spinal cord motor neurons not seen in motor neurons of HC subjects are evident (Figure 2.8; arrows).

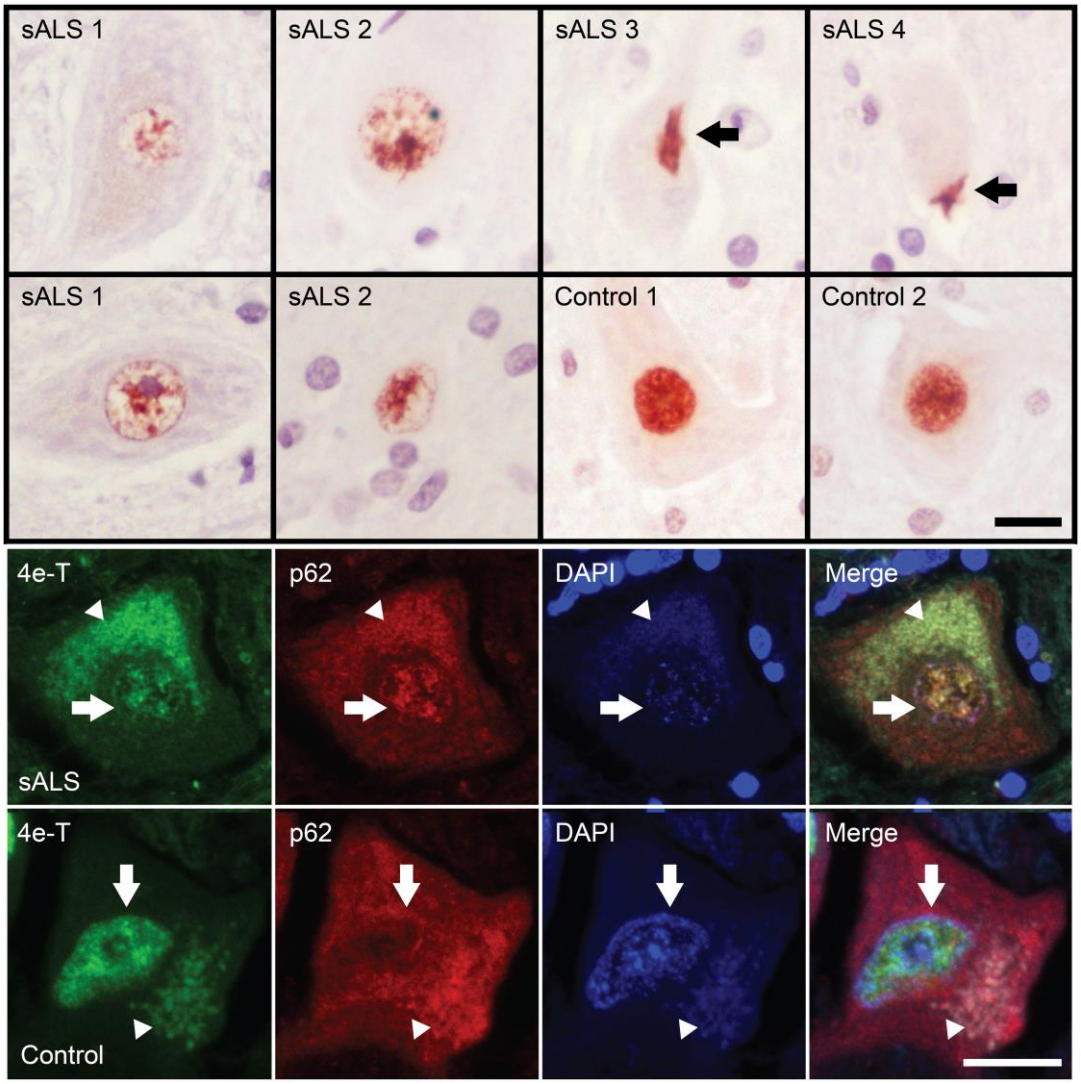

Figure 2.8 eIF 4e Transporter (4e-T) validation data. Lumbar spinal cord sections from sALS and HC patients were stained using a polyclonal 4e-T antibody. Top panels. Light microscopy was used to visualize 4e-T staining in the lumbar spinal cord of sALS and HC subjects. Staining in HC subjects is diffuse throughout the nucleus. In contrast, sALS cases show nuclear and cytoplasmic (arrows) 4e-T inclusions and a loss of diffuse staining. All images were acquired with a 40x objective and the scale bar = 10 µm. Bottom panels. Immunofluorescence was used to further characterize 4e-T alterations in sALS. sALS 4e-T nuclear inclusion staining overlaps with p62 staining (arrows). Nuclear 4e-T staining in HC is diffuse and no nuclear p62 is observed (arrows).

The presence of cytoplasmic autofluorescent lipofuscin is prominent in both cases and is indicated by arrowheads. All images were acquired with a 63x objective and the scale bar = 10 µm.

2.4.5 Classifier Construction and Machine Learning

In the final phase of the study, we used our pooled sample CSF proteomic profiles from the training set to build a support vector machine (SVM) classifier capable of distinguishing ALS samples from non-ALS samples in an independent test set. We first used filtering to remove proteins for which any class mean spectral count was 0, as such proteins could lead to an overfitted classifier and, consequently, poor validation performance on separate test sets. Moreover, low CSF peptide counts may reflect low protein levels that can lead to an inability to validate protein levels via other methodologies.

Feature selection was used to identify proteins that exhibited large alterations between ALS and HC/OND (collectively, NON) samples. Four proteins were selected for training of the classifier: WD repeat-containing protein 63 (WDR63), amyloid-like protein 1 (APLP1), SPARC-like protein 1 (SPARCL1), and cell adhesion molecule 3 (CADM3). WDR63 was increased in the CSF of ALS samples, while the remaining three proteins were decreased in sALS samples relative to NON samples.

These four proteins were used as features for building a linear SVM classifier using the training set samples. For the initial evaluation of the classifier, we used stratified 10-fold cross validation. All training set samples were correctly classified in the cross validation. An independent test set consisting of individual CSF samples analyzed by LC-MS/MS was used to further validate the classifier. Several familial ALS (fALS) samples were included to increase the size of the test set, as indicated in Table 1. While etiologically distinct from sALS subjects, we postulated that motor

neuron death may nevertheless produce changes in CSF protein levels that are common to both sALS and fALS. The performance metrics of the test set evaluation and an ROC curve are shown in Figure 2.9. The 4 protein classifier achieved 83% sensitivity and 100% specificity with the test set, misclassifying one sALS sample and two fALS samples. Inspection of the misclassified samples showed that relative levels of WDR63 were lower and relative levels of APLP1 were higher in these samples than in the other ALS test set samples.

We then validated the levels of our four classifier proteins by Western blot (WB) in select individual CSF samples from the training set samples. The results of these experiments are shown in Figure 2.10. WB experiments were performed on sALS (n=15) samples, HC samples (n=12), and OND (n=10) samples. Relative levels of WDR63 were increased in sALS CSF compared to HC and OND samples ($p < 0.001$ for both comparisons). Two adjacent bands for WDR63 were observed and the results reflect levels of total WDR63 in the CSF. Relative levels of APLP1 were decreased in the CSF of sALS patients relative to HC ($p < 0.001$) and OND ($p < 0.01$) samples. Relative levels of SPARCL1 were decreased in the CSF of sALS patients relative to HC ($p < 0.01$) and OND ($p < 0.05$) samples. Relative levels of CADM3 were decreased in the CSF of sALS patients relative to HC and OND samples ($p < 0.001$ for both comparisons).

A

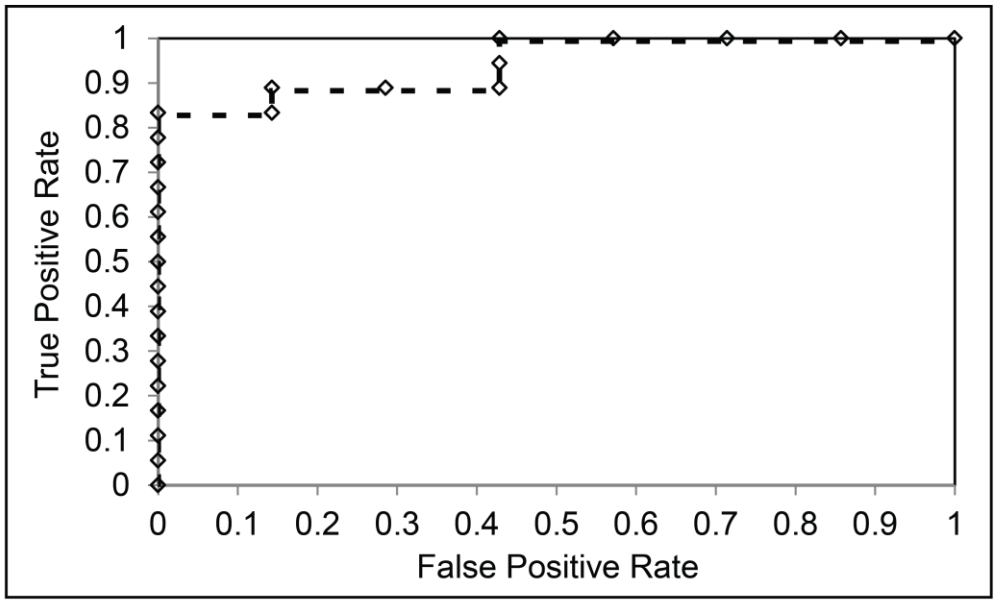

B

Confusion Matrix			**Classification Errors**	
Predicted Class			*Samples Misclassified*	
ALS	Non	*True Class*	1 sALS	
15	3	ALS (n=18)	2 fALS	
0	7	Non (n=7)		
Performance Metrics				
Sensitivity	*Specificity*	*Accuracy*	*ROC AUC*	*F Measure*
83%	100%	88%	0.94	0.90

Figure 2.9 Classifier performance. A. ROC curve showing the performance of the support vector machines classifier on an independent test set. The various levels of the decision threshold are shown as diamonds along the curve. **B.** Confusion matrix, classifier errors, and the indicated performance metrics are shown for the application of the classifier to an independent test set.

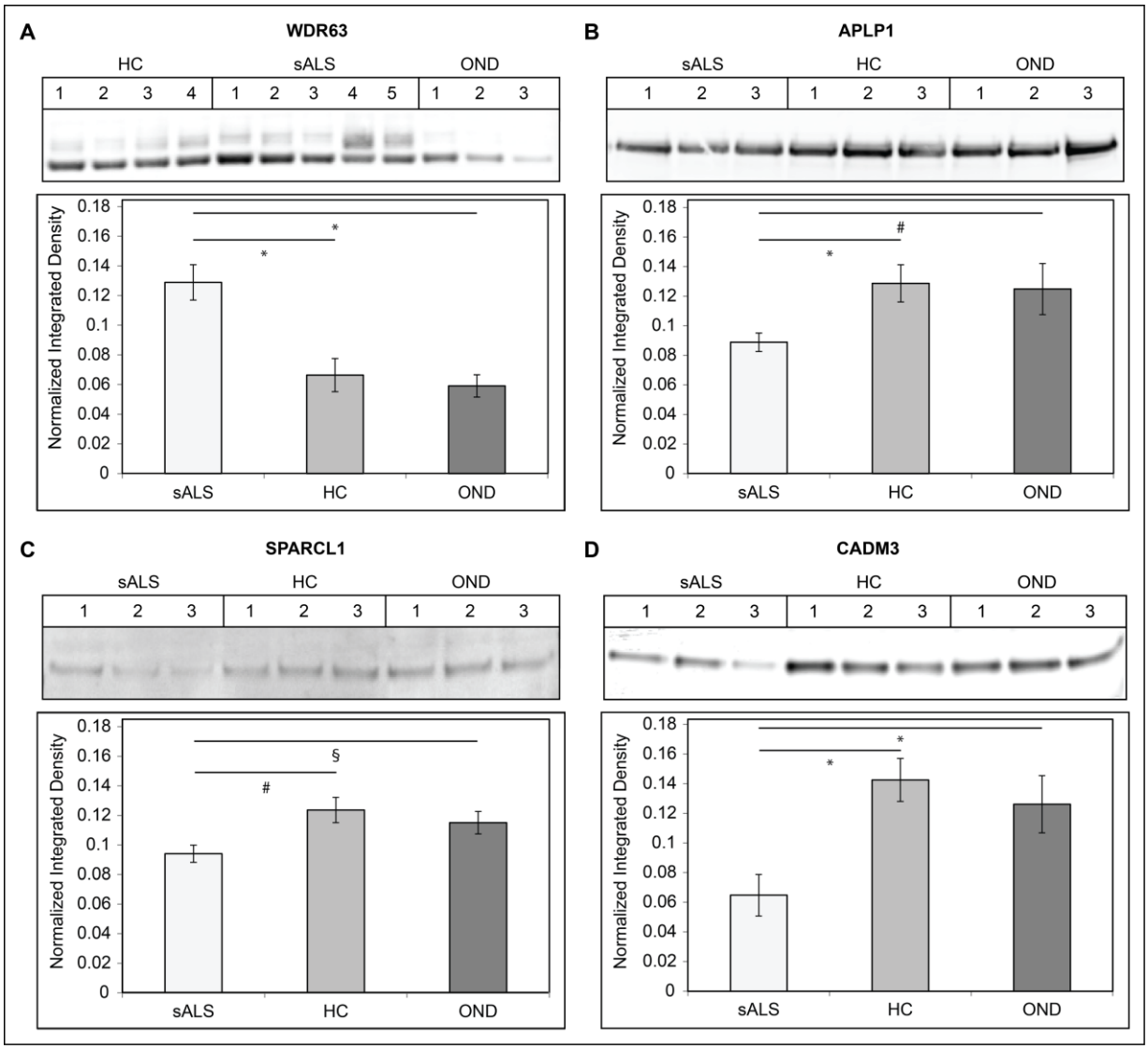

Figure 2.10 Validation of classifier proteins. Validation of Classifier Proteins. Relative levels of classifier proteins in CSF from training set sALS, HC, and OND subjects were measured by Western blot. The mean normalized integrated density value ± SEM is indicated on the y axis. **A.** WDR63. **B.** APLP1. **C.** SPARCL1. **D.** CADM3. For **A**-**D**, * = $p < 0.001$ for the indicated comparison, # = $p < 0.01$ for the indicated comparison, and § = $p < 0.05$ for the indicated comparison.

2.5 DISCUSSION

The goals of this study were two-fold. First, we sought to use LC-MS/MS to construct comprehensive CSF proteomic profiles of sALS, HC, and OND samples to identify ALS protein/pathway alterations. Second, we sought to build a classifier capable of distinguishing ALS from HC and OND samples using our CSF proteomic profiles. With regard to our first aim, we identified 1,712 proteins in the CSF across all groups. This number is consistent with recent studies characterizing the normal CSF proteome[320,321]. Similarly, our data sets show strong concordance in the proportion of all identified proteins assigned to the various Biological Process, Cellular Complex, and Molecular Function Gene Ontology domains, suggesting that the overall composition of the CSF proteome is relatively stable, despite multiple daily turnovers of the total CSF volume[395,396]. This, together with CSF's proximity to the CNS tissue microenvironment, makes it an ideal biomarker source for neurological disorders such as ALS. The results also illustrate the considerable sensitivity that is achieved by pooling samples and using label-free relative quantitation, a finding that has been shown in other studies characterizing the CSF proteome[320,321].

The sensitivity of our LC-MS/MS method enabled the detection of differences in relative levels of many proteins between sALS and non-sALS samples. Several of these proteins have documented associations with ALS. For example, we detected and validated alterations in the previously described candidate ALS CSF biomarkers complement C3[390], cystatin C[391,397] and secretogranin I[398]. We also demonstrate decreases in the known ALS disease modifier[399], ephrin type A receptor 4 (EphA4) in the CSF of ALS subjects. Reducing EphA4 expression or signaling prolongs survival in ALS model systems[399], so the decrease we observe in ALS CSF may reflect a compensatory response by the CNS to the ALS disease process.

We used enrichment analysis to identify biological processes and pathways altered in ALS. The majority of over-represented processes were related to inflammation, synaptic activity, cell growth, or extracellular matrix (ECM) regulation. The latter three processes are similar to those recently identified using microarray analysis of gene expression in oculomotor and spinal motor neurons[400], while elevations in inflammation-associated proteins, specifically those of the complement pathway, have been previously associated with human ALS[390,401-403] and ALS model systems[404,405]. We detect elevations in several proteins of the complement pathway, confirming previously-described elevations of CSF C3[390,401] and providing new evidence for an increase in C5 (which is upregulated in animal models of ALS[405,406]) and C2, as well as decreased complement factor I. Our results support a role of elevated complement pathway activation as a contributing factor to motor neuron death and a potential therapeutic target. These complement pathway proteins may also be useful biomarkers to evaluate the effectiveness of drugs that target this pathway.

Aberrant synaptic changes are also well-described in human ALS and ALS model systems. Axonal dying-back is recognized both as a pathologic feature and hypothesized causal mechanism in ALS[407,408] and degenerative structural changes are observed at synapses of motor neurons and neuromuscular junctions (NMJ) in ALS spinal cord tissue[409,410]. We now identify candidate synaptic proteins that contribute to these pathological changes. For example, decreases in semaphorins 7A and 3G were observed in sALS CSF. The semaphorins act as axonal guidance molecules and have previously been linked to ALS[411,412]. They are expressed in a variety of cell types, including neurons, glia, regulatory T-cells, and vascular epithelial cells. Probing these cell types for altered levels of semaphorins and other synaptic proteins in ALS tissues or model systems may provide insights into how cell type-specific altered synaptic protein expression leads to changes in synapse structure and function that lead to or contribute to motor neuron degeneration in ALS.

Many of the synaptic proteins that were altered in sALS samples are also components of the extracellular matrix (ECM). Pathological ECM alterations have been described for ALS[413] and ALS model systems[414]. Our results showed consistent decreases in levels of ECM proteins, including tenascin R, agrin, and cell adhesion molecule 3. These observations point to a loss of integrity of perineuronal nets (PNN), the highly specialized ECM surrounding neurons. The functions of PNNs are diverse and include physically surrounding neurons, protecting against harmful external agents[415], influencing synaptic transmission[416], and buffering against oxidative stress[417]. Validation of the decrease in tenascin R seen in CSF by immunohistochemistry of spinal cord tissues further establishes altered morphology and protein composition of PNNs as a pathological phenomenon in ALS, consistent with findings on TNR in ALS animal models[414]. As the alterations we observed were localized to motor neurons, we propose that pathological PNN alterations contribute to selective MN vulnerability in ALS.

An implicit and overarching assumption of CSF proteomic profiling is the idea that protein alterations detected in CSF can provide evidence of intracellular changes resulting from the ALS disease process[363]. We showed previously that RBM45, an RNA binding protein whose levels are increased in the CSF of ALS patients[392], forms cytoplasmic inclusions in motor neurons and glia of ALS patients. Similarly, we now show that increased levels of the stress-granule associated[393] eIF4E transporter protein (4e-T) in the CSF of sALS patients correlate with its presence in p62-positive nuclear granules and cytoplasmic inclusions (Figure 2.8). Intranuclear inclusions are a pathological feature of sALS[418,419] and we demonstrate the presence of a transport protein, 4e-T, in these inclusions. Moreover, while p62-positive intranuclear inclusions have been described in *C9ORF72*-linked familial ALS tissue[419], we demonstrate the presence of such inclusions for the first time in sporadic ALS patients.

Our second major objective was to build a discriminant classifier capable of distinguishing ALS patients from healthy controls and other neurodegenerative disease patients on the basis of the CSF proteomic profiles of each group. We[390] and others[420] have shown that the CSF protein levels and machine learning can be used to distinguish sALS and healthy control subjects. Whether this approach is also feasible for the simultaneous separation of sALS from HC and OND samples was unclear. As is typical for high-dimensional –omics data sets, we were able to build a classifier capable of correctly classifying all training set samples. Validation on an independent test set composed of sALS, fALS, HC, and OND samples demonstrated that the classifier generalized well, achieving 83% sensitivity and 100% specificity.

Given the considerable clinical and pathological heterogeneity of ALS[332-335], no biomarker (or panel of biomarkers) is likely to achieve 100% sensitivity and specificity when separating ALS from both HC and OND samples. Because ALS is a relatively rare disorder, the specificity of a classifier is of paramount importance. In this regard, our set of classifier proteins shows considerable promise, correctly classifying all HC and OND samples. The misclassified ALS samples had lower WDR63 and higher APLP1 levels than the other ALS samples profiled. Determining the relationship between WDR63 and APLP1 CSF levels and ALS disease mechanisms and clinical parameters, thus, is an important area of future research. Similar to other LC-MS/MS studies[386], the sample size of both the training and test sets is small relative to the number of proteins identified. Future studies are thus needed to confirm the predictive ability of this biomarker panel with a larger set of samples.

Previously identified CSF protein biomarkers for ALS have often been of increased abundance in ALS, such as complement C3 and neurofilament proteins[390]. Markers of inflammation or neuronal injury will correctly separate ALS from HC samples. They are, however, less likely to correctly distinguish ALS from OND samples (Figure 6a), which is also important for biomarker-

based disease classification. To account for this, we grouped HC and OND samples together as NON (i.e., non-ALS) samples prior to feature selection. Proteins identified by this approach may include more specific markers of ALS-associated loss of motor neuron synaptic integrity or degeneration. The roles of APLP1 and CADM3 in neuromuscular junction (NMJ) function discussed below provide support for this notion.

Classification based on decreased protein abundance creates the potential for misclassification in subsequent studies due to protein instability or differences in analytical sensitivity. For this reason, future studies are required to evaluate the longitudinal stability of the decreases we observed in our classifier proteins. Likewise, evaluating the clinical stage at which these alterations become apparent has considerable implications for the diagnostic/prognostic value of these markers. From an analytical perspective, our ability to detect all proteins of the classifier in all of our individual samples profiled by Western blot suggests that these markers are readily detectable in CSF. They are thus likely amenable to future measurement by quantitative approaches, such as ELISA, which may further enhance measurement sensitivity and classification accuracy.

The four proteins used in our classifier have plausible connections to motor neuron degeneration. Three of the proteins used in the classifier, amyloid-like protein 1 (APLP1), SPARC-like protein 1 (SPARCL1), and cell adhesion molecule 3 (CADM3) were decreased in the CSF of ALS patients. Each protein has documented associations with neurons and synaptic activity, making them promising candidate biomarkers for ALS. APLP1 associates with NMDA receptors and regulates surface expression of this family of glutamatergic receptors[421]. This regulation is crucial for maintaining cellular homeostasis and synaptic activity. Knockout of APLP1 and APLP2 (also significantly reduced in our ALS samples) results in reduced pre- and post-synaptic compartment

size at the NMJ[422]. Reduced levels of APLP1 in ALS, therefore, may contribute to muscle de-innervation and axonal die-back by altering the integrity of the NMJ.

SPARCL1 belongs to the BL-40 family of ECM proteins[423]. The protein is secreted by astrocytes and promotes synapse formation[424]. Knockout of the SPARCL1 gene in mice resulted in a decrease in the number of excitatory synapses in the superior colliculus[425]. In addition to synapse formation, the protein may also be essential for synaptic maintenance. If so, reduced levels of SPARCL1 could result in decreases in synaptic activity that ultimately contributes to motor neuron degeneration. SPARCL1 also binds extracellular calcium[423]. Reduced astrocytic or neuronal SPARCL1 may then also promote calcium dyshomeostasis, which could likewise contribute to motor neuron vulnerability.

CADM3 (or nectin-like molecule 1 or synCAM3) is a cell junction protein that localizes to synapses[425]. The protein is an immunoglobulin-like molecule that is enriched in the nervous system and regulates cell-cell contacts and synapse formation[426]. In keeping with this role, developmental patterns of CADM3 expression are observed in the nervous system of multiple organisms[427.] The protein also has a role in the formation of functional NMJs[428.] Decreased levels of CADM3, thus, are predicted to impair synaptic maintenance, produce neuromuscular junction impairments, and reduce ECM integrity. Cumulatively, CADM3-induced alteration of any or all of these processes could make motor neurons susceptible to degeneration.

At present, studies characterizing the function of WDR63, the last of our classifier proteins, have not been performed. Unlike APLP1, SPARCL1, and CADM3, levels of WDR63 were elevated in ALS samples relative to HC and OND. This specificity for ALS makes it a promising biomarker though a hypothesized role in motor neuron degeneration or ALS more generally is difficult to predict. The WD-repeat is a common structural motif and many diverse functions, including signal

transduction, mRNA synthesis, and cytoskeletal assembly, among others, can be assigned to proteins containing WD repeats[429,430]. Thus, further research is necessary to determine a functional connection between WDR63 and ALS.

In conclusion, we constructed LC-MS/MS proteomic profiles of sALS, HC, and OND CSF samples. We used these profiles to identify proteins whose levels are significantly altered in sALS samples relative to HC and OND samples. In doing so, we identified several proteins with documented associations with ALS, as well as several new candidate biomarkers with clear biological relevance to motor neuron degeneration. Using ontological analysis, we described several biological pathways that are altered in ALS. Lastly, we used an SVM learning algorithm to build a classifier capable of separating ALS samples from HC and OND samples. Collectively, our results illustrate the utility of label-free LC-MS/MS proteomic methods, the promise of CSF as a biomarker source, and the applicability of machine learning methods to classifying samples based on mass spectrometric-based proteomic profiles.

3.0 TOTAL PROTEIN IS AN EFFECTIVE LOADING CONTROL FOR CEREBROSPINAL FLUID WESTERN BLOTS

3.1 CHAPTER SUMMARY

Cerebrospinal fluid (CSF) has been used to identify biomarkers of neurological disease. CSF protein biomarkers identified by high-throughput methods, however, require further validation. While Western blotting (WB) is well-suited to this task, the lack of a validated loading control for CSF WB limits the method's accuracy. We investigated the use of total protein (TP) as a CSF WB loading control. Using iodine-based reversible membrane staining, we determined the linear range and consistency of the CSF TP signal. We then spiked green fluorescent protein (GFP) into CSF to create defined sample-to-sample differences in GFP levels that were measured by WB before and after TP loading correction. Levels of CSF complement C3 and cystatin C measured by WB with TP loading correction and ELISA in amyotrophic lateral sclerosis and healthy control CSF samples were then compared. CSF WB with the TP loading control accurately detected defined differences in GFP levels and corrected for simulated loading errors. Individual CSF sample Western blot and ELISA measurements of complement C3 and cystatin C were significantly correlated and the methods showed a comparable ability to detect between-groups differences. CSF TP staining has a greater linear dynamic range and sample-to-sample consistency than albumin, a commonly used CSF loading control. The method accurately corrects for simulated errors in loading and improves the

sensitivity of CSF WB compared to using no loading control. The TP staining loading control improves the sensitivity and accuracy of CSF WB results.

3.2 INTRODUCTION

Western blotting (WB) is an antibody-based technique for the identification of protein targets transferred to a membrane following separation by polyacrylamide gel electrophoresis (PAGE). Refinements to the technique, including the use of fluorescently labeled antibodies[431,432], imaging with high dynamic range detectors such as CCDs and photodiode arrays, and the application of morphological image processing to gels and blots[433,434] allow multiplexed detection and quantitative measurement of proteins in biological samples.

These advances make WB a valuable tool for protein quantification and the validation of biomarkers obtained via high-throughput methods such as mass-spectrometry. While these high-throughput methods are a sensitive, unbiased means of identifying protein biomarkers, validation of putative markers by a complementary technique is imperative, as inadequate validation can lead to poor biomarker performance in a clinical setting[435-437]. The enzyme linked immunosorbent assay (ELISA) remains the "gold standard" for biomarker validation and is one of the most-widely used techniques for this purpose[438,439]. Frequently, however, high-quality ELISA kits for newly defined candidate markers are not commercially available and developing and validating an ELISA "in-house" is time-consuming, expensive, technically challenging, and dependent on the availability of at least two highly sensitive and specific antibodies to the protein of interest. By contrast, PAGE/WB is a simple, relatively inexpensive method capable of detecting multiple forms of a given protein target, such as multimeric forms or cleavage products. These advantages, combined with the

aforementioned refinements to the sensitivity and quantitative performance of the method make it a useful approach for the study of CSF proteins and the initial validation of candidate protein biomarkers.

To ensure accurate, reproducible WB results, proper correction for technical error, normalization, and processing of the data is essential. Traditionally, WB experiments have used expression levels of so-called "housekeeping genes" as loading controls to correct for differences in protein concentration or errors in loading. The assumption of this method is that the housekeeping genes (often, beta-actin, beta-tubulin, or GAPDH) are highly expressed at relatively constant levels across cells, tissues, and disease/injury types. Increasingly, however, the validity of this assumption in the analysis of cultured cells[440-442], tissue types [441,443-445], and disease/injury states[441,443,444,446,447] has been criticized. As none of the above housekeeping proteins are considered secreted proteins, their validity as loading controls for WB of biological fluids can likewise be questioned. In place of the housekeeping proteins, normalization to total protein (TP) has emerged as a reliable loading control[434,443,445,448-453]. Following PAGE, TP stains can be used directly on the gel or following transfer to a PVDF or nitrocellulose membrane. In general, these stains are linear over several orders of magnitude, correlate well with total protein levels obtained by the BCA or Bradford assays, accurately correct for errors in loading, and are reversible[434,443,445,448-453].

The aforementioned methods have been largely applied to WB experiments measuring protein levels in cultured cells or tissue homogenates. Whether they apply equally well to biological fluids used for biomarker discovery and validation, which typically have individual protein abundances spanning several orders of magnitude and high levels of proteins such as albumin, is unclear. One biological fluid of particular interest in the study of biomarkers of neurological disease is cerebrospinal fluid (CSF). CSF is a clear fluid that surrounds the brain and spinal cord. It arises

from the secretory epithelium of the choroid plexus in the brain's 3rd and 4th ventricles. A normal, adult human carries approximately 150 ml of CSF and this volume is turned over 3-4 times per day. The protein content of CSF varies from approximately 0.3 to 1.3 µg/µl and the most abundant CSF protein is albumin[396,454,455]. CSF has been used to define protein biomarkers for a host of neurological disorders, including Alzheimer's disease (AD)[456], frontotemporal lobar degeneration (FTLD)[457], Parkinson's disease[458], amyotrophic lateral sclerosis (ALS)[359], multiple sclerosis[459], various forms of CNS tumors[460], and schizophrenia[461], among others.

Despite its obvious utility to neurological disease biomarker research, a validated methodology and loading control for CSF biomarker validation by PAGE/WB does not exist. Previous studies using PAGE/WB of CSF samples have used a variety of loading controls, including albumin[462], transthyretin[463], and transferrin[464]. Others have used no loading control or equal CSF volume loading[465,466]. A validated loading control for CSF WB would improve the accuracy of the obtained results. An ideal CSF loading control should be able to correct for individual differences in total protein concentration, which can be large when examining CSF from healthy and diseased individuals. Moreover, because CSF samples are obtained by invasive lumbar puncture and are often scarce in quantity, an ideal loading control should also be amenable to multiplexed PAGE/WB analysis. With these considerations in mind, we investigated the utility of TP as a loading control for CSF WB. We first defined the linear range of detection for CSF TP by gel and membrane stain. Subsequently, we used simulated experiments in which the amounts of CSF total protein and spiked green fluorescent protein (GFP) were varied individually and in tandem to evaluate total protein loading's corrective performance. Lastly, we extend the method to the validation of two candidate biomarkers of ALS, cystatin C and complement C3 (C3). Collectively, the results demonstrate that

iodine-based TP membrane staining is a reliable, reversible loading control that improves the accuracy of CSF WB.

3.3 MATERIALS AND METHODS

3.3.1 Cerebrospinal Fluid (CSF) Samples

Lumbar puncture was used to obtain CSF samples from subjects at the University of Pittsburgh Medical Center (UPMC) upon informed patient consent. This study was approved by the UPMC institutional review board. After collection, samples were spun at 3000 rpm at 4° C for 10 minutes to remove any cells or debris. Samples were then aliquoted in small volumes and stored in low protein binding polypropylene tubes at -80° C within 2 hours of collection. Only CSF samples without visible blood were centrifuged and hemoglobin levels in all final CSF samples were measured by ELISA to eliminate those with evidence of significant levels of hemoglobin (> 200 ng/ml), reflecting blood contamination[364,467].

The protein concentration of all samples was measured using the BCA assay (Thermo Scientific; Rockford, IL). To minimize inter-sample variability for the evaluation of total protein staining as a loading control, we pooled CSF samples for our initial experiments. Eight pooled samples comprised of CSF from healthy, ALS, and AD subjects were created. The protein content of the pooled CSF samples ranged from 0.46 µg/µl to 0.78 µg/µl. To assess the linearity of CSF total protein, we concentrated selected pooled CSF samples using Amicon Ultra 3K cutoff columns (Millipore; Darmstadt, Germany) to permit loading higher amounts of total protein on PAGE mini gels. In some experiments, recombinant, purified GFP (Abcam; Cambridge, MA) was spiked into

pooled CSF samples in nanogram amounts. For experiments measuring levels of the ALS candidate biomarkers cystatin C and C3, ten individual healthy and ten ALS subject samples were used. The protein content of these samples ranged from 0.45 µg/µl to 1.3 µg/µl and a total of 5 µg was loaded per lane for each sample.

3.3.2 Polyacrylamide Gel Electrophoresis (PAGE) and Electrophoretic Transfer

Prior to PAGE, CSF samples were added to a mixture containing 4x LDS sample loading buffer (2% lithium dodecyl sulfate, 10% glycerol, 200 mM Tris; pH 8.4) and DTT (50 mM final concentration). The samples were diluted with PBS to ensure equal loading volumes and heated at 70° C for 10 minutes. Samples were run on 4-12% NuPAGE Bis-Tris gradient mini gels (Life Technologies; Grand Island, NY) at 150 V using MOPS buffer (50 mM MOPS, 50 mM Tris, 0.1% SDS, 1 mM EDTA; pH 7.7). Following completion of the PAGE run, samples were transferred to Immobilon FL PVDF membrane (Millipore; Darmstadt, Germany) using Towbin buffer (192 mM glycine, 25 mM Tris). To optimize the transfer of CSF high and low molecular weight proteins, we used a ramped overnight transfer strategy, previously shown to result in improved transfer of diverse molecular weight protein mixtures to membranes[468]. Membranes were transferred at a constant 8 V for 6 hours, then a constant 16 V for 6 hours. This ramped approach improved the transfer of CSF proteins as compared to common transfer strategies (e.g., 100 V for 1 hour, or 20 V for 12-16 hours; data not shown).

3.3.3 Total Protein Staining

Total protein (TP) staining was performed on PAGE gels and PVDF membranes following transfer. For TP gel staining, gels were stained with Bio-Safe Coomassie (Bio-Rad; Hercules, CA) overnight at room temperature. PVDF membranes were stained for 30 minutes at 4° C with Blot FastStain (G-Biosciences; St. Louis, MO), a proprietary, reversible TP stain for PVDF membranes, according to the manufacturer's instructions. Blot FastStain is a reversible total protein stain based on iodine binding that produces purple bands. Stained gels and membranes were scanned on an Odyssey CLx imager (Licor; Lincoln, NE) at 169 µm resolution. All processed images were free of pixel saturation. PVDF membranes were de-stained in ultrapure water until no bands could be detected at the highest intensity setting of the Odyssey CLx imager.

3.3.4 Western Blot

PVDF membranes were blotted using the Benchpro automated Western blot (WB) processing system (Life Technologies; Grand Island, NY). Membranes were blocked for 1 hour in Licor blocking buffer (Licor; Lincoln, NE), incubated in primary antibodies overnight, washed with PBS, incubated in secondary antibodies for 1 hour, washed with PBS, and imaged on the Odyssey Clx. The following primary antibodies were used: rabbit-anti-GFP (1:2,000; Life Technologies; Grand Island, NY; RRID: AB_221569), chicken-anti-GFP (1:2,500; Aves Labs; Tigard, OR; RRID: AB_10000240), mouse-anti-albumin (1: 5,000; Proteintech Labs; Chicago, IL; RRID: AB_11042320), rabbit-anti-cystatin C (1:2,000; Proteintech Labs; Chicago, IL; RRID: AB_2088058), and chicken-anti-C3 (1:3,000; Encor Biotechnology; Gainesville, FL). Secondary antibodies (1:10,000) were produced in goat to the species of the primary antibody and were

conjugated with IRdye fluorophores visible in the 700 and 800 channels of the CLx imager. Images were acquired on the CLx imager at 169 µm resolution and all processed images were free of pixel saturation.

3.3.5 Enzyme Linked Immunosorbent Assay (ELISA)

Sandwich ELISAs were used to quantitate levels of cystatin C and C3. Cystatin C ELISAs (Biovendor; Asheville, NC) were performed according to the manufacturer's instructions. C3 ELISAs were performed as previously described[390].

3.3.6 Image Processing and Data Analysis

All gel and membrane images were processed in ImageJ (National Institutes of Health; Bethesda, MD). Images were background subtracted using a rolling ball algorithm[434,469]. Relative quantitation was performed to obtain integrated density values according to published guidelines[389,470]. Individual values were relatively scaled to allow membrane to membrane comparisons by summing all values from a membrane and dividing each individual value by this total[389]. Quantitative protein measurements from ELISAs were obtained by fitting a linear equation to the standard curve and using this equation to calculate unknown values. Between-groups comparisons were made using the independent samples T-test with Sidak correction for multiple comparisons[471]. Correlation between values obtained by ELISA and WB were made by Pearson correlation. Data were analyzed using Excel 2010 (Microsoft; Tacoma, WA). Final figures were constructed in Illustrator CS5 (Adobe Systems; Mountainview, CA).

3.4 RESULTS

3.4.1 CSF Total Protein Signal Linearity and Consistency

To characterize the CSF total protein (TP) stain signal, we first determined the signal linearity, detection limit, and saturation limit of CSF TP by gel and membrane stain. These signals were compared to that obtained by Western blot (WB) for albumin, a previously used loading control for CSF WB[462] and the most abundant CSF protein. The results of these experiments are shown in Figure 3.1. The CSF TP staining signal is linear ($R^2 > 0.99$) from 0.25 µg of total CSF protein to 20 µg by Coomassie gel stain and from 0.25 µg to 16 µg for PVDF membrane stain. By contrast, several points in total protein-albumin WB signal relationship showed clear departures from linearity ($R^2 = 0.97$), and a higher degree of error. Following statistical analysis of the untransformed data, we used a square root transformation of values along both axes to visualize all points on the graphs in Figure 3.1A-C clearly. For comparison, the range of 0.25 µg to 20 µg is shown with the untransformed values for the three methods (Figure 3.1D). The detection limits (approximately 10 and 35 ng for gel and membrane stain, respectively) and saturation range (between 40 and 50 µg total protein for both) of each method are shown in Figure 3.2.

Coomassie Gel Stain

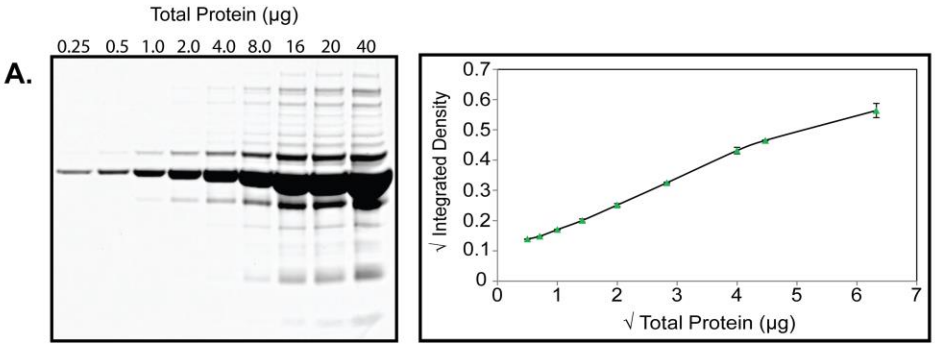

PVDF Membrane Stain

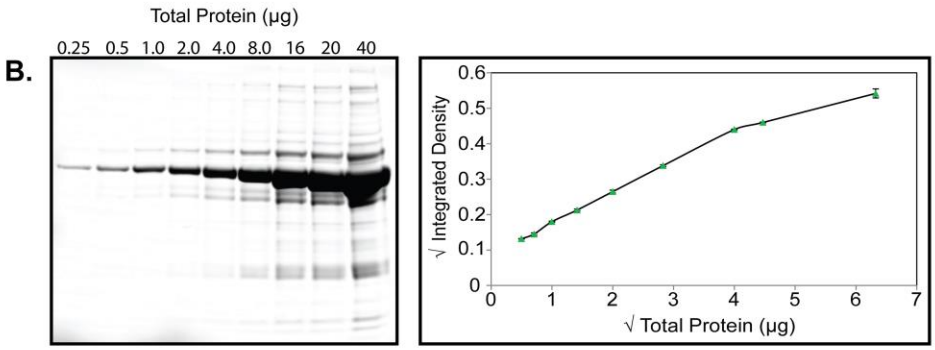

Albumin Western Blot

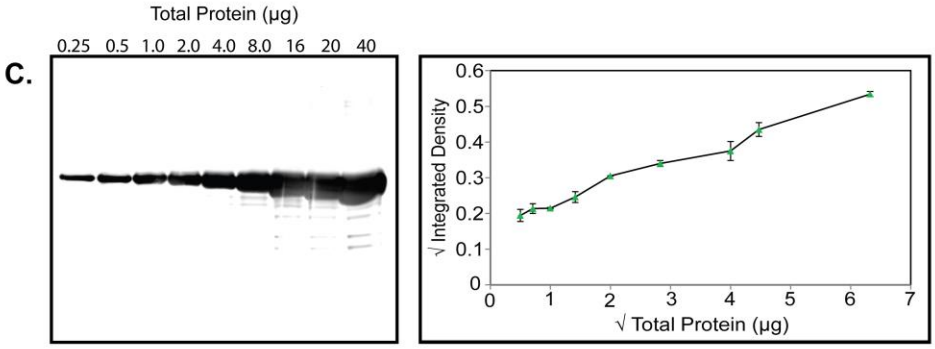

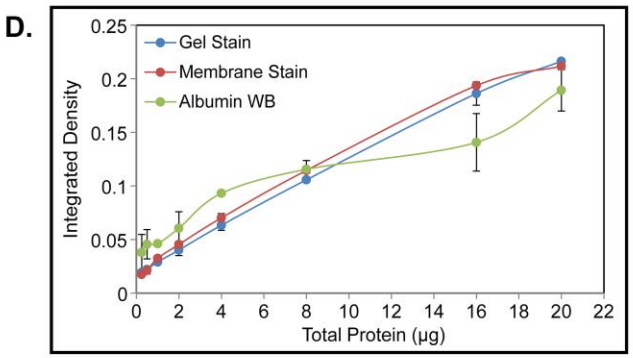

Figure 3.1 CSF total protein linearity. A. Left, Representative Coomassie stained gel of a serial dilution of increasing amounts of CSF TP ranging from 0.25 µg to 40 µg from the same sample. Right, quantification of the TP signal. Square root transformed TP amount (x axis) and sum total normalized, square root transformed integrated density (y axis) are plotted in a line-connected XY scatter graph. Data are shown as the mean ± SD for triplicate experiments using separate pooled samples. **B.** Same as (**A**), but for PVDF membrane stain. **C.** Same as (**A** and **B**), but for albumin Western blot. **D.** Comparison of the untransformed values obtained by each method over the range of 0.25-20 µg total protein loading. Data are shown as the mean ± SD for triplicate experiments using separate pooled samples.

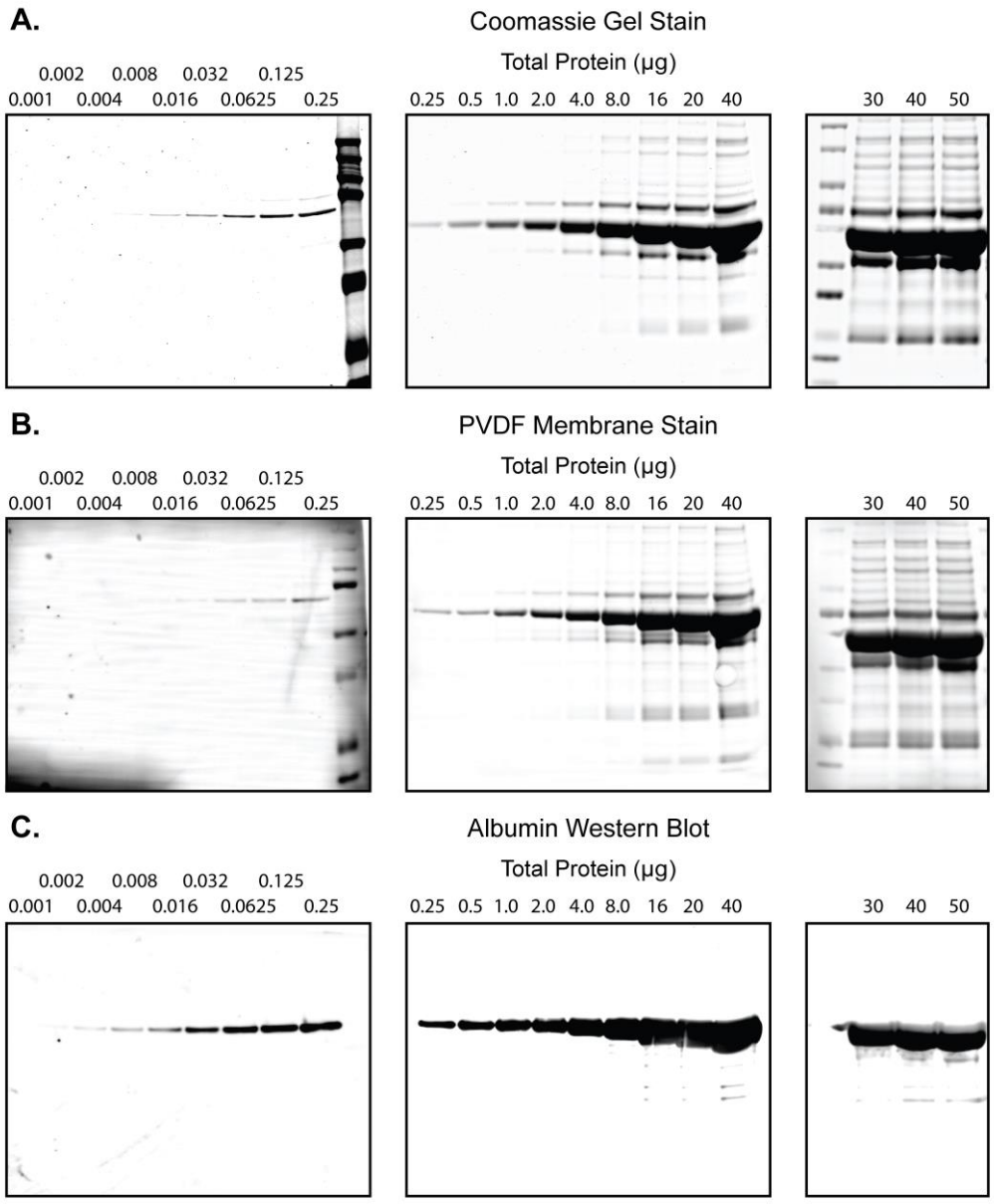

Figure 3.2 Full characterization of CSF total protein staining and albumin Western blot. A. A range of CSF total protein amounts were loaded and the resultant gel Coomassie stained. The leftmost image shows the detection limits of CSF total protein, while the rightmost image shows the point at which the stain signal begins to saturate. The center image shows a series of CSF total protein amounts between the detection and saturation limits. **B.** Same as (A) but for PVDF membrane stain. **C.** Same as (**A** and **B**) but for albumin Western blot.

We also evaluated the sample to sample consistency of the CSF TP signal by loading identical protein amounts from each of our 8 pooled CSF samples. The results of quadruplicate experiments are shown in Figure 3.3. The coefficient of variation (CV; calculated as [standard deviation/mean] x 100) was used as a measure of consistency. By gel and membrane stain, CSF TP signal shows a low degree of variability, with a CV of approximately 5% by either method. The consistency of the albumin signal by WB was considerably lower, with a CV of 15.08%. This result was consistent with the data of Figure 3.1, where TP by gel or membrane stain showed a low degree of error, even when loading large amounts of protein (compare error bars in Figure 3.1D).

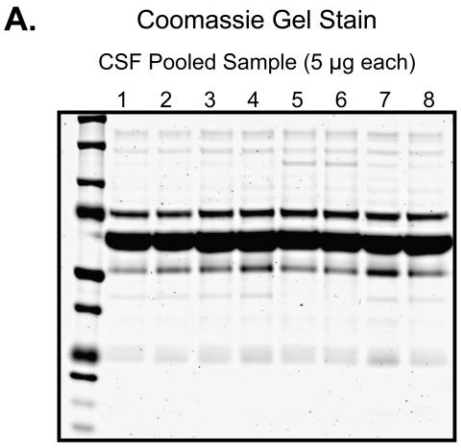

D.

Loading Control	CV (%)
Total Protein (Gel Stain)	5.05
Total Protein (Membrane Stain)	4.65
Albumin (Western Blot)	15.08

Figure 3.3 CSF total protein consistency. The consistency of the CSF total protein signal was evaluated by loading 5 µg of CSF total protein from 8 separate pooled samples and measuring the resultant integrated density. **A.** Representative Coomassie stained gel. **B.** Same as (**A**), but for PVDF

membrane stain. **C.** Same as (**A** and **B**), but for albumin WB. **D.** Summary of results. The CV ([standard deviation/mean] x 100) of quadruplicate experiments was determined.

3.4.2 CSF Total Protein is an Effective Loading Control

To evaluate the performance of CSF TP staining as a loading control, we performed simulated experiments in which CSF TP and spiked-in GFP were varied in tandem and then individually. Because GFP is not found in human CSF, we could control the amount of the protein present in our pooled samples and the sample-to-sample differences in TP and GFP. We compared our measurements of individual sample TP and GFP levels to the defined, "true" values as an evaluation of the performance of TP loading correction. As gel and PVDF membrane total protein staining performed comparably (Figure 3.1D), results from GFP spiking experiments are shown only with the PVDF membrane stain as a loading control. This allowed for reversible detection of total protein, multiplexed blotting using two anti-GFP antibodies, and accounts for variability introduced by the electrophoretic transfer process.

The results of these experiments are presented in Figure 3.4. For the first experiment, we simulated extreme error in loading by varying the amount of CSF TP and GFP in tandem. In this experiment the ratio of GFP to total protein was constant across an 8 fold change in TP and GFP (1.25-10 µg total protein; 25-200 ng GFP; Figure 3.4A). The TP and GFP signal was linear across this range of values (R^2 > 0.99 for both). Correction with an ideal loading control in this example should produce identical values for all samples when the data are normalized by sum total. As shown in Figure 3.4A, correction by TP signal is able to correct for the loading error (m = 0.0002 in the y = mx + b equation, where m expected = 0) and produced relatively consistent values (range = 0.19 to

0.22 for the expected 0.2 corrected value). The corrective performance is inversely related to the amount of TP, with the worst performance occurring at the highest amount of TP.

In the second simulation experiment, we varied the amount of TP (2.5-10 µg), but kept the amount of GFP constant (100 ng). This experiment simulates a WB experiment where different concentrations of a protein are found across samples. Loading by total protein followed by correction with an appropriate loading control should, therefore, lead to observable differences in measured values across samples. As shown in Figure 3.4B, TP loading correction results in values that approximate the true observed differences. By contrast, the uncorrected values are similar (range = 0.24-0.27 for the expected uncorrected value of 0.25). We observed declining performance of the loading control at the upper range of TP, consistent with the previous experiment.

For the final simulation experiment, we loaded constant amounts of TP (5 µg; CSF TP plus GFP) and created a two-fold difference in GFP across samples (100-200 ng). Figure 3.4C shows that the uncorrected values obtained from this experiment underestimate the true fold difference (1.64, 36% error). TP loading correction, however, allows more accurate determination of fold differences across samples (1.93, 7% error). Collectively, these experiments show that CSF TP can correct for errors in loading and permits accurate detection of true differences in protein abundance.

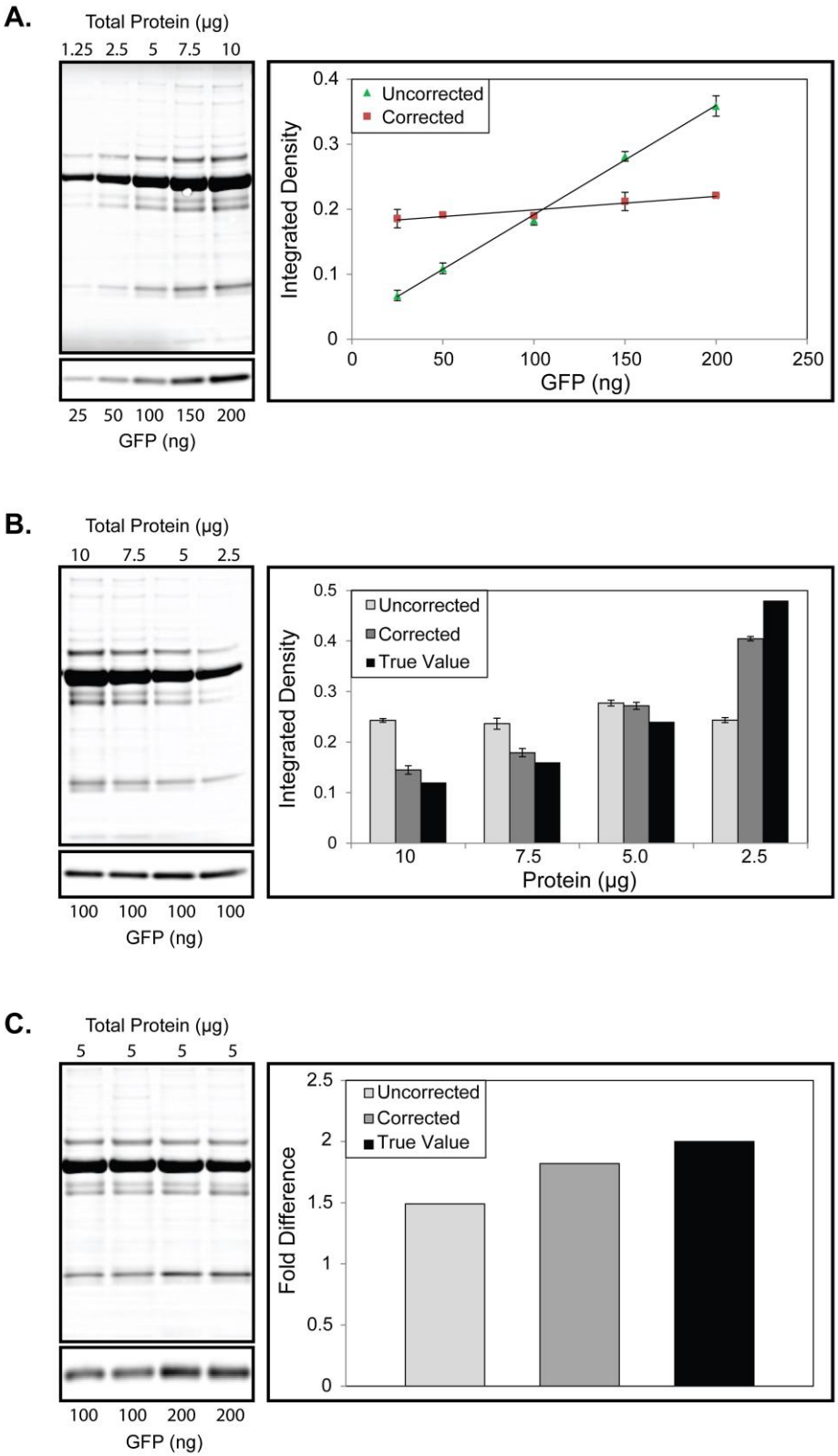
A.
Total Protein (µg)
1.25 2.5 5 7.5 10
25 50 100 150 200
GFP (ng)
Uncorrected
Corrected
Integrated Density
0.4
0.3
0.2
0.1
0
0 50 100 150 200 250
GFP (ng)
B.
Total Protein (µg)
10 7.5 5 2.5
100 100 100 100
GFP (ng)
Uncorrected
Corrected
True Value
Integrated Density
0.5
0.4
0.3
0.2
0.1
0
10 7.5 5.0 2.5
Protein (µg)
C.
Total Protein (µg)
5 5 5 5
100 100 200 200
GFP (ng)
Uncorrected
Corrected
True Value
Fold Difference
2.5
2
1.5
1
0.5
0

Figure 3.4 Corrective performance of CSF total protein (TP) loading control. **A.** Left, Representative images of in-tandem varying spiked GFP and CSF TP. Right, quantification of the corrected (red squares) and uncorrected (green triangles) normalized integrated density values obtained for each band. **B.** Left, representative images of a serially diluted CSF TP stained membrane and equal loading GFP WB are shown. Right, quantification of the resultant uncorrected and corrected normalized integrated density values against the true value based on GFP concentration. **C.** Left, representative images of a constant TP stained membrane and two-fold difference loaded GFP WB are shown. Right, the resultant fold-difference obtained from the uncorrected and corrected values is plotted against the true two-fold difference for triplicate experiments. Plots in **A.** and **B.** represent the mean ± SD of triplicate experiments.

3.4.3 Application to the Study of Candidate ALS CSF Biomarkers

In the final phase of this study, we compared the performance of WB and TP staining to ELISA in the measurement of levels of two candidate ALS biomarkers, complement C3 (C3) and cystatin C[359,390,391,397,403], in CSF from five ALS and five healthy control subjects for each protein. To permit comparisons across blots and platforms, we first multiplied the concentration of C3 or cystatin C obtained by ELISA by the volume of CSF loaded for each sample (5 μg TP) to generate "true" values for each subject. Next, these values and obtained WB values were normalized by sum total normalization[389]. To do so, all values for a given blot or ELISA were summed and each data point divided by this value. This scales all values from 0-1, with the number corresponding to each data point's proportion of the total signal. The resultant values were used to compare individual CSF sample measurements and relative between-groups differences of total protein, C3, and cystatin C obtained by each method.

For C3, we performed WB in triplicate and ELISAs in quadruplicate for five ALS and five healthy control CSF samples. The results of these experiments are shown in Figure 3.5. Using TP staining of the PVDF membrane, we did not detect significant differences between-groups (p = .13; Figure 3.5A, D). By WB corrected by TP loading and ELISA, we detected a significant increase in total C3 levels in the CSF of ALS patients compared to controls (p = 0.01 by WB; p = 0.03 by ELISA; Figure 3.5B, D). We then assessed the correlation of the ELISA and WB results on a sample to sample basis. In general, there was a high degree of agreement between the two methodologies (Pearson r = 0.90; average error = 14.39%; Figure 3.5C) and the total protein corrected values showed a greater degree of correlation than the uncorrected values (r = 0.90 and 0.673, respectively; Table 3.1). C3 is extensively proteolytically cleaved to generate fragments with cell signaling functions. Electrophoretic separation via PAGE permits examination of the individual C3 fragments, in addition to total C3 levels. Using this information, we also found that levels of C3α were not significantly different between-groups (p = 0.07), while levels of C3β were statistically significant between-groups (p = 0.028; Figure 3.5B, D).

Cystatin C ELISAs and WBs were performed in quadruplicate for a second set of five ALS and five healthy control CSF samples. These results are shown in Figure 3.5E-H. By PVDF membrane stain, we did not detect significant differences in TP signal between-groups (p = 0.79; Figure 3.5E, H). A significant decrease in cystatin C was, however, observed in the ALS group compared to the control group by ELISA (p = .013) and TP corrected WB (p = 0.038; Figure 3.5F, H). While the agreement between platforms was not as strong as that obtained for C3, we still observed significant correspondence between the two methods (Pearson r = 0.654, p = 0.040); average error = 31.24%). As with C3, correction of the WB signal by total protein staining improved the correlation of WB and ELISA results ($r_{corrected}$ = 0.654, $r_{uncorrected}$ = 0.507; Table 3.1). Removing

ALS sample 2, which had unexpectedly high WB signal and error (161%) reduces the overall average error to 15.06% (Figure 3.5G). The data from these and the C3 experiments are summarized in Table 3.1.

Table 3.1 Summary of complement C3 and cystatin C data. A summary of group data obtained by ELISA and WB is shown. ELISA/WB Proportion = the mean indicated group proportion of the total signal, *p* ELISA/WB = the Sidak-corrected, independent samples t-test *p* value for the between-groups healthy control-ALS comparison, % WB error = the average percentage error for the WB-ELISA comparison of each sample, ELISA-WB r = the Pearson correlation coefficient of the ELISA-WB values obtained for each sample, TPLC = total protein loading control corrected value, No TPLC = value obtained with no total protein loading control correction, *p* r = the *p* value of the correlation coefficient indicated in the ELISA-WB r column.

	ELISA Proportion		**WB Proportion**		***p* ELISA**	***p* WB**	**% WB Error**	**ELISA-WB r**	***p* r**
Complement C3	*Control*	*ALS*	*Control*	*ALS*				*TPLC*	*TPLC*
Total C3	0.0751	0.125	0.0772	0.123	0.03	0.01	14.39	0.9	> 0.001
C3α	n/a	n/a	0.0827	0.117	n/a	0.07		*No TPLC*	*No TPLC*
C3β	n/a	n/a	0.0405	0.159	n/a	0.028		0.673	0.0329
Total Protein	0.1	0.1	0.109	0.0903	0	0.13			
	ELISA Proportion		**WB Proportion**		***p* ELISA**	***p* WB**	**% WB Error**	**ELISA-WB r**	***p* r**
Cystatin C	*Control*	*ALS*	*Control*	*ALS*				*TPLC*	*TPLC*
Total Cystatin C	0.134	0.659	0.118	0.0817	0.013	0.038	31.24	0.654	0.04
Total Protein	0.1	0.1	0.0982	0.101	0	0.79		*No TPLC*	*No TPLC*
								0.507	0.134

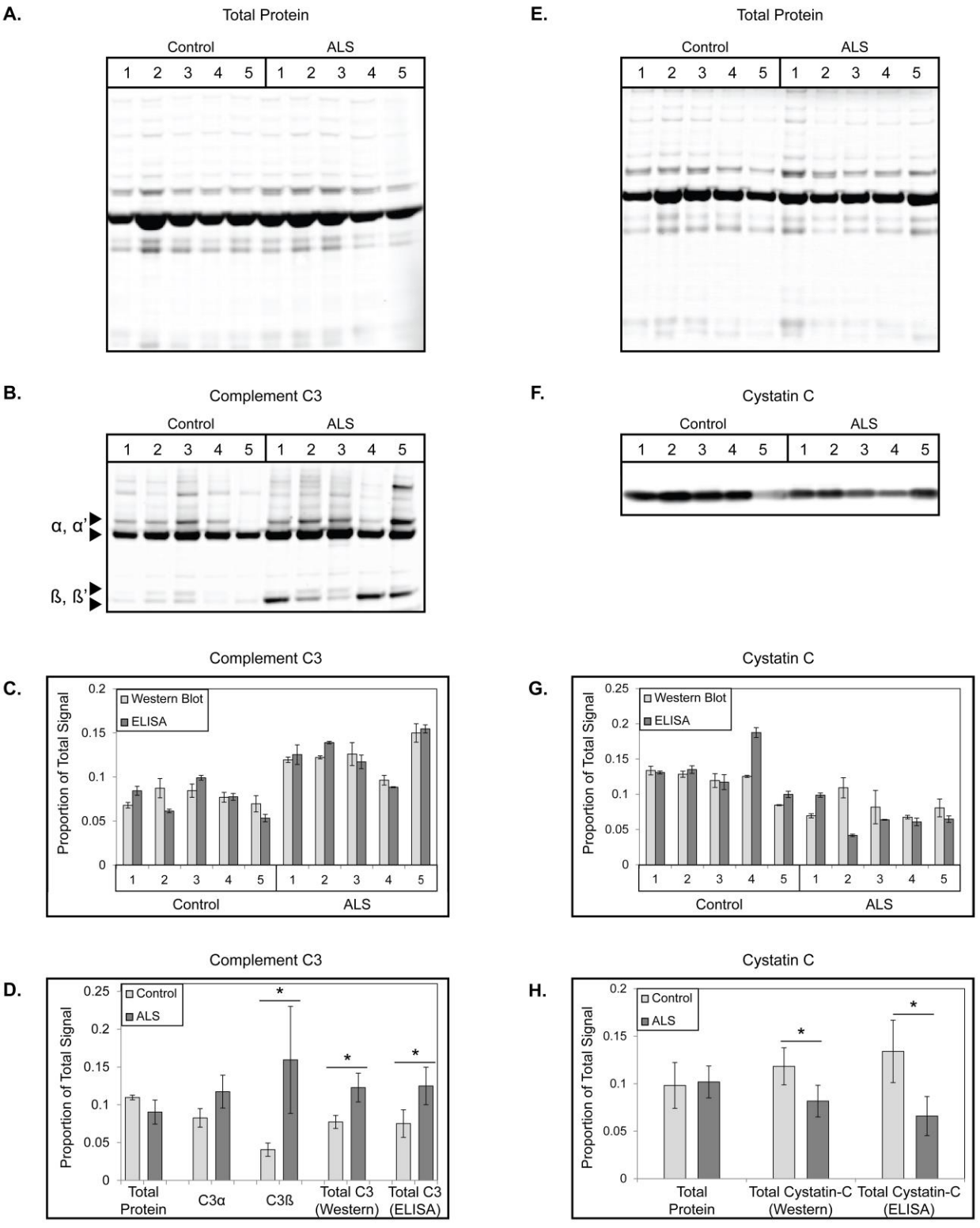

Figure 3.5 Application of total protein loading correction to candidate ALS CSF biomarkers.

A. Representative TP stained membrane of 5 µg total loading for 5 healthy control and 5 ALS CSF

samples. **B.** Representative WB of complement C3 in the CSF of above healthy control and ALS CSF samples. **C.** Plot comparing normalized, relative individual subject C3 levels obtained by ELISA and TP corrected WB from the above CSF samples. **D.** Plot comparing normalized, relative between-groups differences for TP, C3α, C3β, total C3 WB, and total C3 ELISA. * = corrected $p < 0.05$. **E.-H.** Same as (**A-D**), respectively, but for cystatin C in a second set of 5 ALS and 5 healthy control CSF samples. Plots **A-D** represent the mean ± SD of triplicate WB experiments, **E-H** quadruplicate WB experiments, and all plots show quadruplicate ELISA results.

3.5 DISCUSSION

Total protein (TP) staining has emerged as a reliable and accurate loading control for Western blots (WB) of cell and tissue lysates[434,443,445,449-453]. Whether it is similarly useful for the blotting of cerebrospinal fluid (CSF) has not been investigated. Moreover, while a variety of CSF WB loading controls have been used previously[462-466], their linearity, consistency, and corrective performance have not been evaluated directly. Here, we define the linearity and consistency of CSF TP gel and membrane staining, assess its corrective performance as a loading control in simulated experiments, and compare its performance to results obtained by ELISA for the validation of two candidate ALS biomarkers.

Previous studies have demonstrated an extensive linear range of TP staining, often spanning several orders of magnitude, using a variety of reagents[434,443,445,449-453]. In the present study, we observe a lower saturation range (between 40-50 µg; Figure 3.2) and upper limit to the linear range (16 µg by PVDF membrane stain and up to 20 µg by Coomassie gel stain versus between 4-8 µg by albumin; Figure 1D). This result is not surprising, however, as albumin is estimated to comprise at

least 60% of the protein content of CSF[472,473]. Thus, saturation of the albumin signal occurs rapidly, limiting the overall linearity of the CSF TP signal. Nevertheless, it should be noted that the linear range we observe extends from volumes of less than 1 µl of CSF to the maximum permissible on a mini-gel for typical CSF TP concentrations by either PVDF membrane or gel stain. Staining a duplicated Coomassie gel has been suggested as a corrective control for Western blots previously[443] and we demonstrate the larger dynamic range of this method relative to PVDF membrane staining, consistent with prior reports[434]. We, however, recommend using the membrane stain as a loading control. Membrane staining accounts for inconsistencies and loss of protein caused by the transfer of proteins from the gel to the membrane. Moreover, using a reversible membrane stain obviates the need to run a duplicate gel.

The sample to sample consistency is also an important consideration when choosing a loading control for WB. Using pooled samples, we found that the consistency of CSF TP signal by gel or membrane stain was high (approximately 5% CV by either method; Figure 3.3D). Likewise, we observed very low variability from gel to gel by either method while assessing the linearity of CSF TP (Figure 3.1A, B). By contrast, the TP staining pattern for our individual ALS and healthy control samples was more variable (Figure 3.5A, E). Several factors could account for this. First, our pooled CSF samples were largely homogenous in terms of their TP content, spanning less than a two-fold range, unlike the individual ALS and healthy control samples, which spanned a three-fold range. Thus, technical errors and instrument imprecision would be expected to produce larger variability in our individual samples as compared to the pooled samples. Second, our individual samples comprised ALS and healthy control subjects. Large differences in protein content (including albumin levels) between disease and control CSF samples are well documented[474-477]. These differences are likely averaged out in the pooled samples, which comprise ALS, AD, and healthy

control subjects. Importantly then, the results from our pooled samples likely reflect the true consistency of the method, as they are relatively unaffected by pre-analytical factors.

While albumin is the most abundant protein in CSF by several orders of magnitude, and thus a likely candidate for use as a loading control[463], we provide several compelling reasons to avoid using it for this purpose in CSF WB. First, by WB, the linear range and consistency of albumin is considerably less than that observed for CSF TP gel or membrane stain (Figures 3.1 and 3.3). This is likely due to saturating amounts of albumin on the surface of the membrane, resulting in a signal that is not reflective of the true protein content. In addition, using a TP stained gel or reversible membrane stain allows the user to analyze total protein and then examine multiple individual protein targets on the same membrane. This is a relevant consideration given that CSF sample volumes are often limited due to the nature of the collection procedure. CSF albumin levels have also been shown to change in response to various diseases [320,477-480], making its utility as a loading control questionable. Lastly, while the albumin band alone can be used for normalization following gel or membrane TP staining, its corrective performance and linear range is less than that of the TP signal collectively (data not shown).

The corrective performance of a loading control is a consideration of equal importance to its linearity and consistency. We evaluated the corrective performance of CSF TP as a loading control using simulated experiments in which known amounts of GFP were spiked into CSF. The amount of GFP and CSF TP were varied, first in tandem, and then separately (Figure 3.4A-C, respectively). The results of these experiments indicate that the CSF TP loading control is capable of correcting for large errors in sample loading (Figure 3.4A) and permits accurate detection of true differences in protein concentration and abundance (Figure 3.4B, C). The corrective performance of the total protein loading control began to deteriorate at the highest levels of CSF total protein (10 µg).

Nevertheless, the range of corrective ability (8 fold; Figure 3.4A) vastly exceeds what would be expected by individual sample variability, technical error, or instrument variability when loading by TP amount or CSF volume.

After testing the ability of the TP stain to correct for errors in simulated experiments, we extended the approach to the study of candidate CSF biomarkers for ALS by blotting for C3 and cystatin C. Using sum total normalization, we converted values obtained by WB and ELISA to their corresponding relative proportions. While this results in the loss of quantitative information from the ELISAs, it permits a cross-platform comparison of the ability of each method to detect relative differences in protein abundance. Using the TP loading control, we observed significant correlation between the normalized ELISA and WB data and comparable sensitivity in detecting differences in target protein abundance (Figure 3.5; Table 3.1). Further, we highlight the utility of PAGE-based protein separation by showing a significant elevation of the C3β, but not C3α, fragment in ALS samples relative to controls. The performance of the TP corrected WB method was not as high when blotting for cystatin C, although much of the increased error was a result of an unexpectedly high value from a single ALS sample. Nevertheless, we still detected a significant reduction in cystatin C levels between-groups, consistent with previous studies[359,391,397]. While ELISA, by virtue of its greater dynamic range, sensitivity, and quantitative accuracy, will remain the preferred method for validating CSF biomarkers, our results demonstrate that WB can be a useful and economical method for the assessment of relative protein levels in CSF samples.

A variety of total protein stains have been used as loading controls for WB[435,443,445,448-453]. We predict that many of these will be suitable for CSF WB. The choice of stain will be predicated on study goals and available resources. Given the unique protein composition of CSF, which is at least 60% albumin[472,481] and typically has a total protein concentration of at least 0.4 µg/µl, sensitivity and

signal saturation are unlikely to be primary concerns. For a study seeking to probe low-abundance proteins in CSF by WB at typical linear detection levels (nanogram range), a microgram amount of CSF total protein will almost certainly be required, which is far greater than the nanogram amount detection limits of the stains characterized here and elsewhere [435,443,448-453]. Likewise, the saturation limit of the stains characterized here was only reached following concentration of CSF samples. Reversibility, conversely, is an important consideration, especially with human CSF samples, which are often of limited volume. The iodine-based stain used for this study was completely reversible within 10 minutes using distilled water washes, providing fast and mild destaining conditions. By contrast destaining is longer and harsher with stains such as Coomassie and Ponceau, and the more recently characterized Direct Blue 71[449]. We observed a greater sensitivity of Coomassie gel staining of CSF total protein than PVDF membrane staining (Figure 3.2). This is likely due to the difficulty of electrophoretically transferring small amounts of CSF to PVDF membrane, however, as we observe a sensitivity of 2 ng by dot blot with the iodine-based stain used here (data not shown). This is comparable to the sensitivity of epicocconone based stains[445], which for their reversibility, sensitivity, and linear range are also useful total protein stains for TP loading control. Trihalo-based tryptophan fluorescence (stain-free)[434] has emerged as another promising means of using total protein as a loading control. The signal is linear over a range comparable to that observed here, although with lower sensitivity. The main drawback of the method appears to be the cost of the required gels and imaging system. The novel loading control evaluation method we present (Figure 3.4) will allow researchers to determine which total protein stain works best with their protein of interest, sample and membrane type, and image acquisition system. The method as presented could easily be adapted to cell or tissue lysates and GFP substituted for another protein known not to occur in the sample tested, if needed.

CSF has proven to be useful for the discovery of neurological disease biomarkers and basic research on the CNS. As recent efforts at defining the CSF proteome have illustrated, there is a diverse array of proteins found in both healthy and diseased CSF[320,464,482]. WB remains an indispensable technique for the study of protein mass, modifications, and relative abundance in the CSF. Recent studies have emphasized, however, that levels of CSF proteins can be relatively unstable and influenced by a variety of pre-analytical factors[432,483]. These observations and the range of total protein concentrations observed across diseases makes clear the need for a corrective loading control for CSF WB. We have demonstrated that CSF TP is a linear, consistent, and accurate loading control well-suited to this purpose.

4.0 THE RNA BINDING MOTIF 45 (RBM45) PROTEIN ACCUMULATES IN INCLUSION BODIES IN AMYOTROPHIC LATERAL SCLEROSIS (ALS) AND FRONTOTEMPORAL LOBAR DEGENERATION WITH TDP-43 INCLUSIONS (FTLD-TDP) PATIENTS

4.1 CHAPTER SUMMARY

RNA binding protein pathology represents one of the best characterized pathologic features of amyotrophic lateral sclerosis (ALS) and frontotemporal lobar degeneration patients with TDP-43 or FUS pathology (FTLD-TDP and FTLD-FUS). Using liquid chromatography tandem mass spectrometry, we identified altered levels of the RNA binding motif 45 (RBM45) protein in the cerebrospinal fluid (CSF) of ALS patients. This protein contains sequence similarities to TAR DNA binding protein 43 (TDP-43) and Fused-In-Sarcoma (FUS) that are contained in cytoplasmic inclusions of ALS and FTLD-TDP or FTLD-FUS patients. To further characterize RBM45, we first verified the presence of RBM45 in CSF and spinal cord tissue extracts of ALS patients by immunoblot. We next used immunohistochemistry to examine the subcellular distribution of RBM45 and observed in a punctate staining pattern within nuclei of neurons and glia in the brain and spinal cord. We also detected RBM45 cytoplasmic inclusions in 91% of ALS, 100% of FTLD-TDP, and 75% of Alzheimer's disease (AD) cases. The most extensive RBM45 pathology was observed in patients that harbor the *C9ORF72* hexanucleotide repeat expansion. These RBM45 inclusions were

observed in spinal cord motor neurons, glia and neurons of the dentate gyrus. By confocal microscopy, RBM45 colocalizes with ubiquitin and TDP-43 in inclusion bodies. In neurons containing RBM45 cytoplasmic inclusions we often detected the protein in a punctate pattern within the nucleus that lacked either TDP-43 or ubiquitin. In conclusion, we identified RBM45 using a proteomic screen of CSF from ALS and control subjects for candidate biomarkers, and link this RNA binding protein to inclusion pathology in ALS, FTLD-TDP and AD.

4.2 INTRODUCTION

Amyotrophic lateral sclerosis (ALS) is the most frequent adult-onset motor neuron disease and is characterized by a degeneration of motor neurons, leading to progressive muscle weakening and a typical life expectancy of 2 to 5 years after disease onset[484]. Frontotemporal lobar degeneration (FTLD) is the second most frequent cause of dementia and is a clinically diverse syndrome, with phenotypes including behavioral changes, semantic dementia, and progressive non-fluent aphasia and characterized by cellular inclusions containing tau (FTLD-tau), TAR DNA binding protein 43 (TDP-43: FTLD-TDP) or Fused-In-Sarcoma (FUS: FTLD-FUS)[485,486].

The presence of cytoplasmic inclusions positive for ubiquitin in degenerating neurons is a pathological hallmark of ALS and FTLD[487,488]. The observation that some ALS patients develop cognitive deficits with prominent frontal lobe features, and that the associated neuropathology resembles that of FTLD led to the idea that ALS and FTLD might be related[489,490]. An intronic hexanucleotide repeat expansion in the *C9ORF72* gene (GGGGCC) has recently been shown to be the genetic cause of chromosome 9p21-linked ALS-FTLD, and accounts for 30-40% of familial ALS and a similar portion of familial FTLD, further linking these two neurodegenerative disorders [190,191].

RNA generated from genomic non-coding repeat expansions may disrupt normal RNA metabolism by sequestering RNAs and proteins involved in other transcription/translation events[491].

TDP-43 and FUS have been identified as components of ubiquitinated inclusions occurring in ALS patients without Cu/Zn superoxide dismutase mutations and in FTLD patients[485,492]. Both TDP-43 and FUS are primarily located in the nucleus of cells, but mislocalize and form neuronal and glial inclusions in ALS, FTLD-TDP and FTLD-FUS[493-495]. Mutations in *TDP-43* and *FUS* have been identified as a genetic cause in approximately 4% of familial ALS and in rare cases of FTLD[496]. Both TDP-43 and FUS bind numerous RNAs (reviewed in [495,497]) and are abnormally processed in ALS[169], linking altered RNA metabolism to ALS, FTLD-TDP and FTLD-FUS[497].

During an unbiased mass spectrometry based proteomic analysis of cerebrospinal fluid (CSF) from ALS and control subjects, we detected an increase in the RNA binding motif 45 (RBM45) protein in the CSF of ALS patients. This protein is expressed at highest levels in the brain[498], and has been suggested to be up-regulated in animal models of spinal cord injury and nerve degeneration[499]. Furthermore, RNA recognition motifs are conserved between RBM45, TDP-43 and FUS. Therefore we sought to further characterize RBM45 expression and distribution in the brain and spinal cord of ALS, FTLD-TDP and control subjects.

RBM45 protein was detected in the CSF and central nervous tissue of ALS and control subjects. We observed RBM45 in a punctate pattern predominately in the nucleus of neurons and glia in the hippocampus and spinal cord of control subjects. In ALS patients, RBM45 was also contained in cytoplasmic inclusions in motor neurons that were immunoreactive for TDP-43 and ubiquitin. RBM45 was evident within cytoplasmic inclusions in 100% of FTLD-TDP and 75% of AD patients. In contrast to TDP-43, we also detected RBM45 in the nucleus of neurons containing cytoplasmic inclusions. Finally, the most abundant RBM45 pathology was observed in ALS patients

that harbor the hexanucleotide repeat expansion of the *C9ORF72* gene. Thus, RBM45 represents a new RNA binding protein located in cytoplasmic inclusions typical of ALS and FTLD-TDP patients.

4.3 MATERIALS AND METHODS

4.3.1 Tissue and CSF Samples

ALS and control post-mortem fixed and frozen tissue was obtained from the University of Pittsburgh Brain Bank and the Center for ALS Research. Clinical diagnoses were made by board certified neuropathologists according to consensus criteria for each disease. All human tissues were obtained through a process that included written informed consent by the subjects' next of kin. The acquisition process was evaluated by the University of Pittsburgh Institutional Review Board/University of Pittsburgh Committee for Oversight of Research Involving the Dead and determined to be exempt from review by the full committee. Subject demographics are listed in Table 4.1. The average age for each subject category was 59.7 +/- 11.2 years for ALS, 60.2 +/- 11.2 years for Controls, 76.7 +/- 9.9 years for frontotemporal lobar degeneration with TDP-43 inclusions (FTLD-TDP), and 78.2 +/- 7.3 years for Alzheimer's disease (AD) patients. The post-mortem interval for each subject group was 7.3 +/- 4.6 hours for ALS, 6.6 +/- 5.0 hours for Controls, 9.0 +/- 7.5 hours for FTLD-TDP, and 4.5 +/- 1.0 hours for AD patients. While there was a statistically significant difference in age across the subject groups due to the more advanced age of the FTLD-TDP and AD cases ($p = 0.01$), there was no significant difference of post-mortem interval ($p = 0.6$). All FTLD-TDP cases either presented with motor neuron disease or developed motor neuron deficits and best fit neuropathologic criteria for FTLD-TDP type B with TDP-43 inclusions in spinal cord motor neurons and frontal and/or

temporal cortex[500]. All AD cases were Braak stage VI with frequent plaque pathology by CERAD criteria[501,502]. Two of four AD cases had additional TDP-43 pathology in the hippocampus, as noted in Table 2. CSF samples were collected as described in Chapter 2.3.

4.3.2 Immunohistochemistry

Paraffin-embedded tissue sections of spinal cord from ALS (n=23), FTLD-TDP (n=2), and non-neurologic disease control (n=7), and hippocampus from ALS (n=9), FTLD-TDP (n=6), Alzheimer's disease (n=4) and non-neurologic disease control (n=5) cases were used for immunohistochemistry. All sections were deparaffinized, rehydrated, and antigen retrieval performed using Target Antigen Retrieval Solution, pH 9.0 (DAKO) for 20 minutes in a steamer. After cooling to room temperature, non-specific binding sites were blocked using Super Block (Scytek) for 1 hour. The following primary antibodies were used for immunohistochemistry: affinity purified rabbit polyclonal anti-RBM45 generated to amino acids 1-130 (1:75; Sigma-Aldrich Prestige antibody HPA020448), custom made affinity purified rabbit monoclonal antibody to the C-terminal 15 amino acids of RBM45 (1:200 dilution; PI462476), affinity purified rabbit polyclonal anti-RBM45 antibody AV41154 (Sigma-Aldrich), rabbit polyclonal anti-TDP43 (1:10,000; Proteintech), and mouse monoclonal anti-Ubiquitin antibody (1:1,000; Cell Signaling) with overnight incubation. After three washes, tissue sections were incubated for 1 hour in the appropriate biotinylated IgG secondary antibodies (1:200; Vector Labs) diluted in Super Block (Scytek). Slides were washed in PBS for 15 minutes and immunostaining visualized using the Vectastain Elite ABC reagent (Vector Labs) and Vector NovaRED peroxidase substrate kit (Vector Labs). Slides were counterstained with hematoxylin (Sigma Aldrich). Sections were visualized using an Olympus BX40 light microscope and images acquired using a Nikon DS L2 digital camera.

A semi-quantitative assessment of RBM45 and TDP-43 cytoplasmic inclusion pathology was performed on all coded sections of the lumbar spinal cord and hippocampus by three independent investigators. The following scoring system was used: (-) = none; (+) = 1 – 3 inclusions per section; (++) = 4 – 9 inclusions per section; (+++) = 10 or more inclusions per section. A quantitative assessment of RBM45 and TDP43 pathology was performed on select spinal cord sections. The gray matter was morphologically identified for each lumbar spinal cord section on pictures at 1.25X magnification using a Leica microscope and outlined using NIH ImageJ software. The area of the gray matter was calculated via the ROI (region of interest) tool of NIH ImageJ software (1 pixel= 1.276 microns). Then, counts of total motor neurons, neuronal and glia inclusions for both RBM45 and TDP-43 were established per slide and results reported as a proportion of gray matter area density for RBM45 and TDP-43 inclusions.

4.3.3 Repeat-Primed PCR

100 ng of genomic DNA was used as template in a final volume of 28 µl containing 14 µl of FastStart PCR Master Mix (Roche Applied Science, Indianapolis, IN) and a final concentration of 0.18 mM 7-deaza-dGTP (New England Biolabs, Ipswich, MA), 1X Q-Solution (Qiagen), 0.7 µM reverse primer consisting of ~four GGGGCC repeats with an anchor tail, 1.4 µM 6FAM-fluorescent labeled forward primer located 280 bp telomeric to the repeat sequence, and 1.4 µM anchor primer corresponding to the anchor tail of the reverse primer. A touchdown PCR cycling program was used where the annealing temperature was gradually lowered from 70°C to 56°C in 2°C increments with a 3 minute extension time for each cycle. Fragment length analysis was performed on an AB 3730xl genetic analyzer (Applied Biosystems, Foster City, CA) and data analyzed using GeneScan software (version 4, ABI). The repeat-primed PCR is designed so that the reverse primer binds at different

points within the repeat expansion to produce multiple amplicons of incrementally larger size, producing a characteristic sawtooth pattern with a 6 bp periodicity.

4.4 RESULTS

4.4.1 Proteomic Analysis of CSF and Identification of RBM45

We performed an unbiased mass spectrometry based proteomic analysis of CSF samples from ALS, healthy controls, multiple sclerosis, Alzheimer's disease, upper motor neuron disease and lower motor neuron disease patients to discover candidate biomarkers for ALS. The subject demographics of this proteomics profiling are shown in Table 4.1 A complete and detailed description of all the proteins and cellular pathways that appeared altered in ALS versus the various controls groups is found in Chapter 2.4. From the top 400 proteins identified in the CSF, we detected peptides from 13 nucleic acid binding proteins in the CSF, with many of them altered in ALS patients. Several exhibited statistically significant increased relative abundance in the CSF of ALS subjects when compared across all other groups (healthy control and other neurological diseases). Of these, the RNA binding protein motif 45 (RBM45) appeared in almost all ALS groups but only a few of the control groups and exhibited the largest difference between ALS and all other groups. Peptides to both TAR DNA binding protein 43 (TDP-43) and Fused-in-Sarcoma (FUS) were only detected in a few of the subject groups using this mass spectrometry based proteomic method and therefore were not in the top 400 proteins detected in CSF.

RBM45 is a 476 amino acid protein that exhibits structural similarities with TDP-43 and FUS (Figure 4.1), two RNA binding proteins contained in cytoplasmic inclusions of neurons and glia in

ALS and FTLD patients. RBM45 contains three RNA recognition motifs (RRMs) whereas TDP-43 has two and FUS has one RRM. RBM45 contains a C-terminal nuclear localization sequence, similar to FUS, but lacks both the glycine rich domain contained in both TDP-43 and FUS and a defined nuclear export sequence (Figure 4.1). RNA-binding protein 40 (Table 4.2) contains two RRM domains and will be further characterized in a future study. However the gene is located on the Y chromosome and is believed to participate in spermatogenesis[503], thus making a direct link to ALS less obvious.

Table 4.1 Subject demographics. Patient subject case number and disease group, age, gender, PMT (post-mortem interval), and presence or absence of *C9ORF72* repeat expansion. ALS = amyotrophic lateral sclerosis; FALS = familial amyotrophic lateral sclerosis; FTLD-TDP = frontotemporal lobar degeneration with TDP-43 inclusions; AD = Alzheimer's disease; CT = non-neurological disease control. All AD cases were Braak stage VI.

Case ID	Group	Age	Gender	PMT	C9ORF72
1	ALS	40	M	6	No
2	ALS	68	M	4	Yes
3	ALS	43	M	6	Yes
4	ALS	45	M	7	No
5	ALS	62	M	7	No
6	ALS	72	F	9	No
7	ALS	69	M	5	No
8	ALS	50	F	7	No
9	ALS	60	F	4	No
10	ALS	59	M	4	No
11	ALS	77	F	4	No
12	ALS	79	F	4	No
13	ALS	52	F	21	No
14	ALS	45	M	7	No
15	ALS	65	M	5	No
16	ALS	66	M	18	No
17	ALS	53	F	12	No
18	ALS	73	F	6	No
19	ALS	59	M	5	No
20	ALS	70	F	4.5	No
21	FALS	55	M	14	No
22	FALS	63	F	4	Yes
23	FALS	48	F	5	No
24	FTLD-TDP	69	M	6	No
25	FTLD-TDP	67	M	24	No
26	FTLD-TDP	69	M	6	No
27	FTLD-TDP	85	M	3	No
28	FTLD-TDP	91	F	8	No
29	FTLD-TDP	79	M	7	No
30	AD	73	F	4	No
31	AD	71	M	4	No
32	AD	85	M	5	No
33	AD	84	F	5	No
34	CT	54	M	6	No
35	CT	53	F	4	No
36	CT	76	M	13	No
37	CT	57	M	2	No
38	CT	48	M	2	No
39	CT	58	F	5	No
40	CT	76	M	14	No

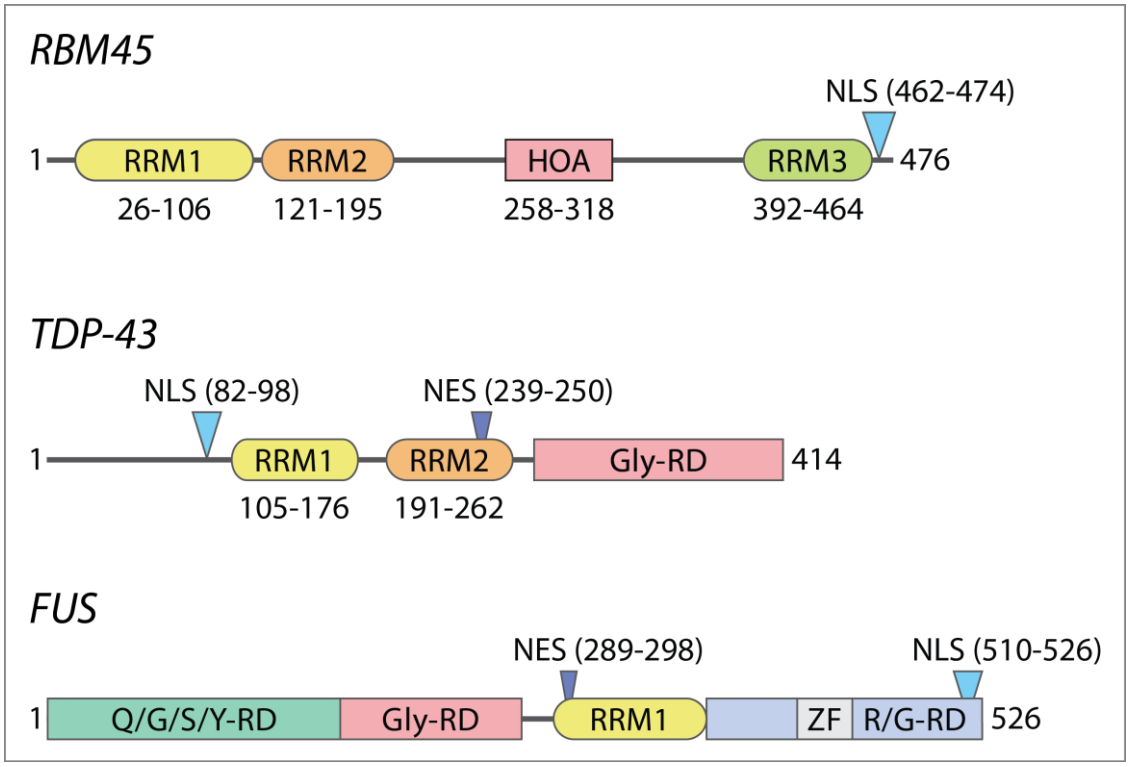

Figure 4.1 RBM45, TDP-43, and FUS domain structures. Amino acid domain analysis of TDP-43, FUS, and RBM45 are shown in a schematic diagram. Each protein has one or more RNA recognition motifs (RRMs). TDP-43 and FUS share a common glycine-rich-domain (Gly-RD) that is absent from RBM45. A nuclear localization signal (NLS) is present in each protein, with a C-terminal location in both FUS and RBM45. RBM45 lacks a defined nuclear export signal (NES) present in both TDP-43 and FUS. FUS also contains a glutamine/glycine/serine/tyrosine-rich domain (Q/G/S/Y-RD), a zinc finger binding motif (ZF), and an arginine/glycine-rich domain (R/G-RD) that spans the ZF domain. RBM45 amino acid domains were defined according to http://www.uniprot.org, and the location of each RRM is defined in the figure.

Table 4.2 RNA binding proteins identified by CSF proteomics. The name and accession number for all RNA binding proteins identified by proteomic profiling of cerebrospinal fluid of ALS, healthy control, and other neurological disease subjects are shown. The full analysis of the relative abundance of these proteins in each group is found in Chapter 2.

Protein	Accession
RNA-binding protein 45	Q8IUH3
Ribonuclease T2	O00584
Transcription factor jun-B	P17275
RNA polymerase I	P17480
Transcription factor TBX3	O15119
RNA helicase DDX59	Q5T1V6
RNA-binding protein 40	Q96LT9
Nucleolar RNA helicase 2	Q9NR30
RNA-binding protein Raly	Q9UKM9
ZFR2	Q9UPR6
MLXIPL	Q9NP71
RAD54-like protein	Q92698
SPO11	Q9Y5K1

4.4.2 Distribution of RBM45 in Control and ALS Spinal Cord

We next examined the cell type-specific expression patterns and subcellular localization of RBM45 in ALS and control subjects using immunohistochemistry. Non-neurologic disease control subjects exhibited a punctate staining pattern for RBM45 in the nucleus and cytoplasm of motor neurons in the lumbar spinal cord, with limited staining of nuclei within glial cells (Figure 4.2A and B). Examination of sporadic and non-SOD1 familial ALS spinal cord tissue revealed RBM45-positive inclusion pathology bearing a striking resemblance to that seen with TDP-43 or FUS in ALS motor neurons (Figure 4.2C-E). Several distinct morphologies were observed, including skein-like (Fig. 4.2D), globular (Figure 4.2C and E), and neuritic (Figure 4.2D and E) inclusions. Prior studies have

demonstrated a clearance of TDP-43 from the nucleus of neurons that harbor cytoplasmic inclusions[153,492]. However, we observed motor neurons with cytoplasmic RBM45 inclusions that retained RBM45 in a speckled or diffuse staining pattern in the nucleus (Figure 4.2D). In addition, we were able to detect glial inclusions that stained positive for RBM45 (Figure 4.2E and F). We also detected RBM45 inclusions in the spinal cord of familial ALS and FTLD-TDP cases (Figure 4.2G–I). A quantitative assessment of RBM45 and TDP-43 pathology is shown in Figure 4.3 and Supplemental Table 3. Within the spinal cord, we observed cytoplasmic RBM45 motor neuron inclusions in 78% of ALS patients (n = 18 of 23 cases). RBM45 glial cytoplasmic inclusions were observed in the spinal cord from 74% of ALS patients (n = 17 of 23 cases). Two cases displayed RBM45 glial inclusions but no motor neuron inclusions (cases 18 and 21). Conversely, no RBM45 containing inclusions were observed in either cell type in the spinal cord of control subjects. From this data there appeared to be a relationship between the RBM45 and TDP-43 pathology that was further examined by double-label confocal microscopy as described below.

The anti-RBM45 antibody used above recognizes amino acids 1-50 that contains a small region of the first RRM and therefore potential cross-reactivity with other proteins such as TDP-43 and FUS that contain these domains. However a blocking peptide to this epitope completely eliminates immunoreactivity (Figure 4.4), suggesting that this antibody is not also recognizing similar epitopes in TDP-43 or FUS. In addition, RBM45 amino acids 1-50 exhibit little sequence identity to either TDP-43 or FUS. However we also used another commercial antibody to RBM45 that recognizes amino acids 216-257 (lacks any RRM domain sequences) and a custom affinity purified rabbit monoclonal antibody to the terminal 15 amino acids of RBM45 for immunohistochemistry. Both of these antibodies could detect RBM45 inclusions in either the spinal cord or hippocampus (Figure 4.4).

Using a repeat-primed polymerase chain reaction (PCR) method [191], we determined that three ALS patients harbored c*9ORF72* repeat expansions, defined as having greater than 30 repeats (Table 4.1). This represented 10% of our sporadic ALS and 33% of our familial ALS population. Interestingly, these subjects exhibited the highest number of neuronal and glial cytoplasmic RBM45 inclusions (Figure 4.3, Supplemental Table 3). This is similar to a recent study indicating that individuals with the c*9ORF72* repeat expansion had the highest number of p62 positive cytoplasmic inclusions in the lumbar spinal cord and hippocampus[504]. Within the lumbar spinal cord, ALS patients with the c*9ORF72* repeat expansion also exhibited the highest amount of TDP-43 inclusions (Figure 4.3, Supplemental Table 3). We quantified the amount of RBM45 and TDP-43 inclusions within the lumbar spinal cord gray matter for 2 – 4 sections of each ALS case (see Methods). c*9ORF72* positive cases contained on average 12.6 RBM45 neuronal inclusions per mm^2 of gray matter whereas all other ALS cases contained 3.4 RBM45 neuronal inclusions per mm^2 of gray matter. There was no difference in the number of RBM45 inclusions within glia in *c9ORF72* repeat expansion cases.

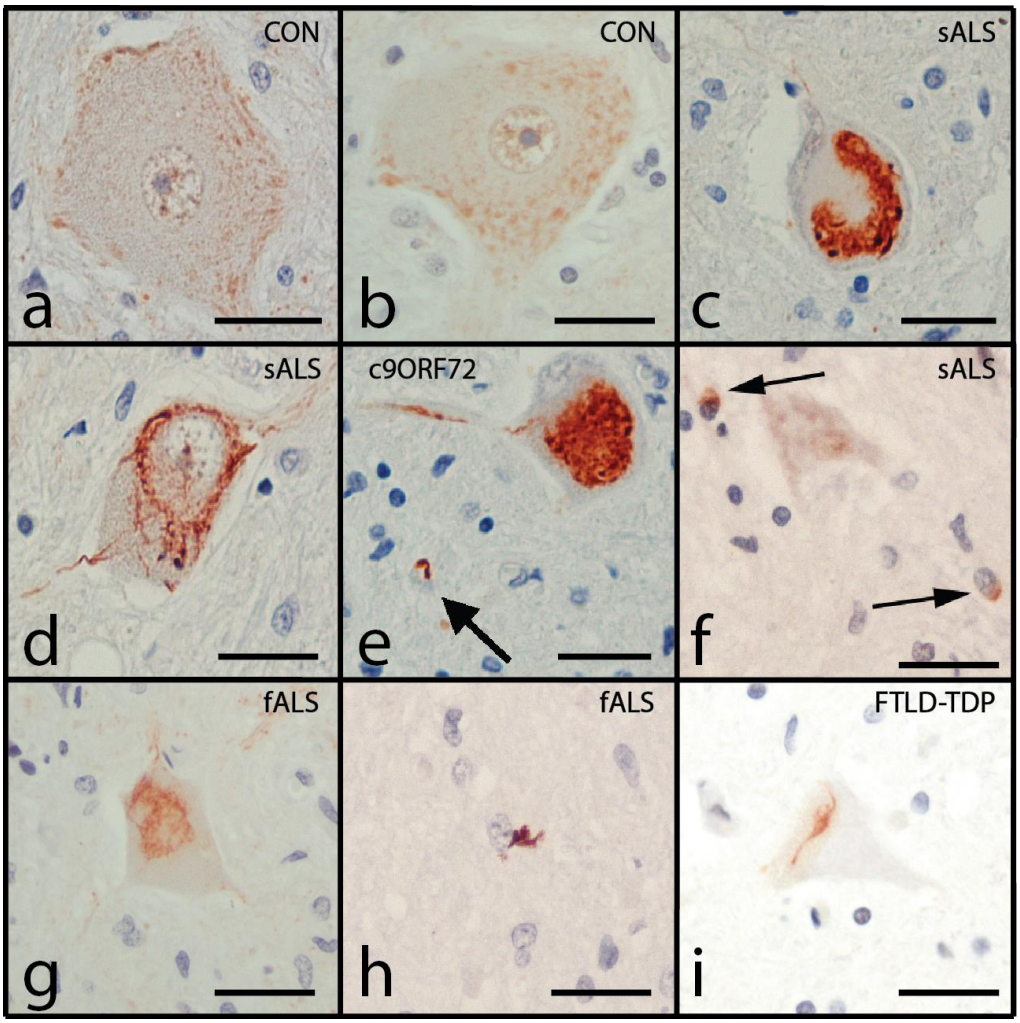

Figure 4.2 RBM45 distribution in spinal cord by light microscopy. Representative sections are shown from lumbar spinal cord sections from control, ALS and FTLD-TDP patients stained for RBM45 and counterstained with hematoxylin. **A.**, **B.** Motor neurons from control subjects show a punctate staining of the nucleus and cytoplasm. **C.** – **E.** Motor neurons from ALS patients, including a *C9ORF72* case in (**E**), contain RBM45-positive inclusions with globular, skein-like, and neuritic morphology. Arrow in (**E**) indicates a glial inclusion. **F.** Two glial inclusions from a sporadic ALS patient are shown (arrows). **G.** RBM45 positive inclusions were also detected in the motor neurons of non-SOD1, non-*C9ORF72* fALS cases. **H.** Glial inclusions are also observed in fALS. **I.** Spinal

cord motor neuron of FTLD-TDP case containing skein-like RBM45 inclusion. All images are taken at 40X magnification. Scale bars equal 30 μm. Panels represent the following case numbers in Table 4.1: (**A**) = 37; (**B**) = 39; (**C**) = 2; (**D**) = 2; (**E**) = 3; (**F**) = 13; (**G**) = 23; (**H**) = 21; (**I**) = 24.

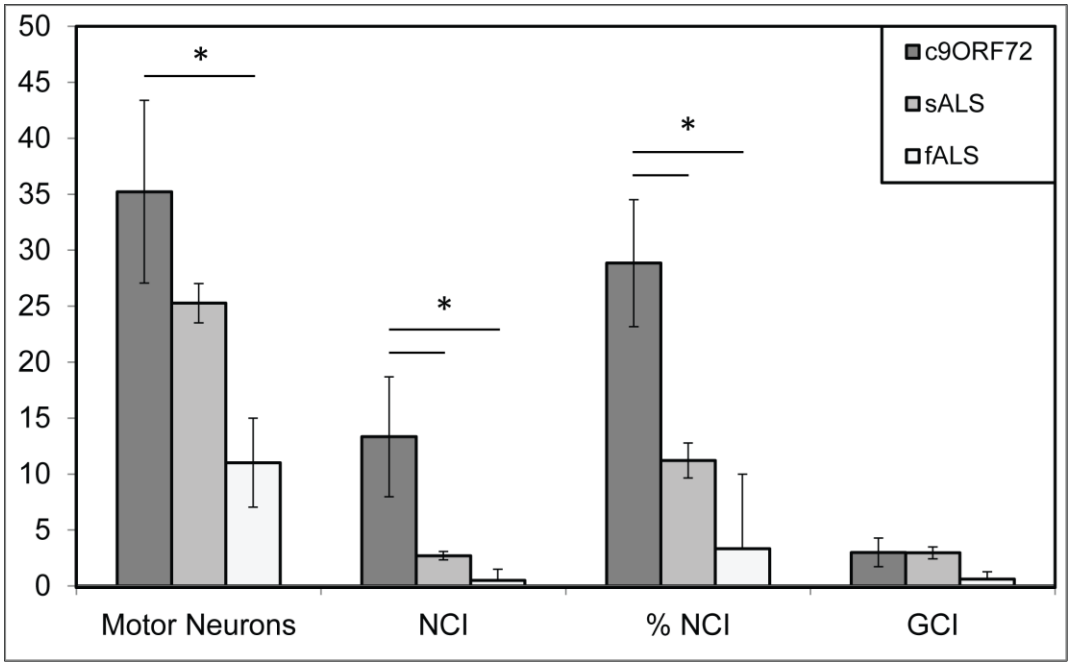

Figure 4.3 Assessment of RBM45 pathology in various forms of ALS. RBM45 pathology was scored by three separate investigators. The results represent the mean ± SEM for each metric reported. Sections of lumbar spinal cord from c9ORF72-linked ALS, sALS, and fALS cases were scored for the number of remaining anterior horn motor neurons, neuronal cytoplasmic inclusions (NCIs), the percentage of motor neurons harboring NCIs (% NCI), and the number of glial inclusions. Each ALS group was compared using the independent samples T-test. * = $p < 0.01$.

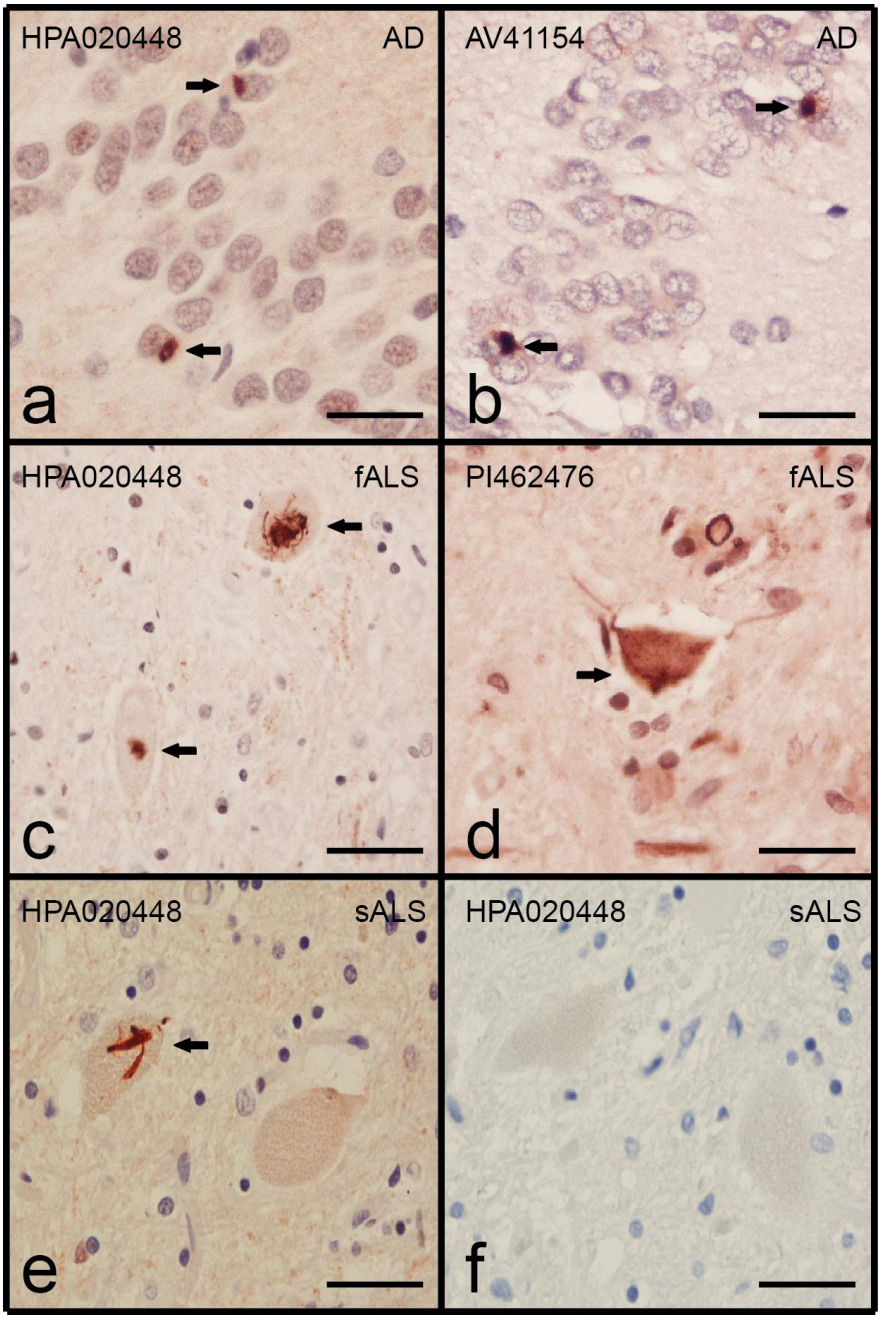

Figure 4.4 RBM45 antibody specificity and inclusion recognition. RBM45 pathology is recognized by multiple antibodies to RBM45. **A.**, **B.** Hippocampal RBM45 pathology is seen in adjacent sections of an AD case. RBM45 positive inclusions are marked with arrows. Antibodies used were HPA020448 generated to amino acids 1-50, AV41154 generated to amino acids 216-257,

and PI462476 to amino acids 452-467. RBM45 inclusions are detected by affinity purified rabbit polyclonal anti-RBM45 antibodies HPA020448 and AV41154 as indicated by arrows in (A) and (B), respectively. Scale bar = 20 µm. **C.**, **D.**. Multiple antibodies detect RBM45 pathology in lumbar spinal cord motor neurons in ALS cases. Adjacent sections of lumbar spinal cord from an ALS case were stained with anti-RBM45 antibodies HPA020448 (**C**) or affinity purified rabbit monoclonal antibody PI462476 (**D**). Inclusions are marked by arrows. Scale bar = 30 µm. **E.**, **F.** Anti-RBM45 antibody HPA020448 does not detect inclusions when pre-incubated with blocking peptide. Adjacent sections of a sALS case were incubated with anti-RBM45 antibody HPA020448 in the absence (**E**) or presence (**F**) of RBM45 blocking peptide (aa's 1-50). In the absence of blocking peptide, the antibody detects RBM45 positive inclusions in motor neurons. When incubated with blocking peptide, however, all immunostaining is eliminated. An inclusion in (**E**) is marked with an arrow. Scale bar = 30 µm. Panels represent the following case numbers in Table 4.1: (**A** and **B**) = 30; (**C** and **D**) = 22; (**E** and **F**) = 10.

4.4.3 RBM45 Distribution in the Hippocampus

Since TDP-43 pathology is also evident in the dentate of FTLD-TDP cases, we next evaluated the distribution of RBM45 in the hippocampus from FTLD-TDP, ALS and control subjects. Control subjects, including both non-neurologic controls and Alzheimer's disease, exhibited a punctate or speckled RBM45 pattern within the nucleus of dentate granule cells (Figure 4.5A-C). In FTLD-TDP patients there were RBM45 positive cytoplasmic inclusions within dentate granule cells (Figure 4.5D-F). A speckled RBM45 immunoreactivity was still evident in the nucleus of dentate granule cells in FTLD-TDP cases. RBM45 inclusions were also detected in dentate granule neurons of ALS cases (Figure 4.5G), as well as some hippocampal pyramidal neurons in ALS and FTLD-TDP

patients (Figure 4.5H and I). RBM45 dystrophic neurites were not detected in the hippocampus. Of the available hippocampal tissue, we observed RBM45 neuronal inclusions in 63% of ALS cases (n = 5 of 8), with no glial inclusions in any case. While only six FTLD-TDP cases were available for this study, RBM45 pathology occurred in 83% of FTLD-TDP hippocampi (n = 5 of 6) and in both available FTLD-TDP spinal cord sections. Collectively, RBM45 pathology was present in some form/region in all FTLD-TDP cases examined. RBM45 inclusions were also observed in the dentate gyrus and pyramidal neurons for 3 of 4 AD cases (Supplemental Table 3). We used confocal microscopy to determine association of RBM45 with tau pathology in AD cases. RBM45 did not co-localize with phosphorylated tau (pTau) in the hippocampus of AD cases (Figure 4.6). A speckled RBM45 pattern was also detected within the nuclei of dentate cells in AD cases (Figure 4.6A and B). Finally, we detected no RBM45 pathology in the hippocampus of any non-neurologic disease control case.

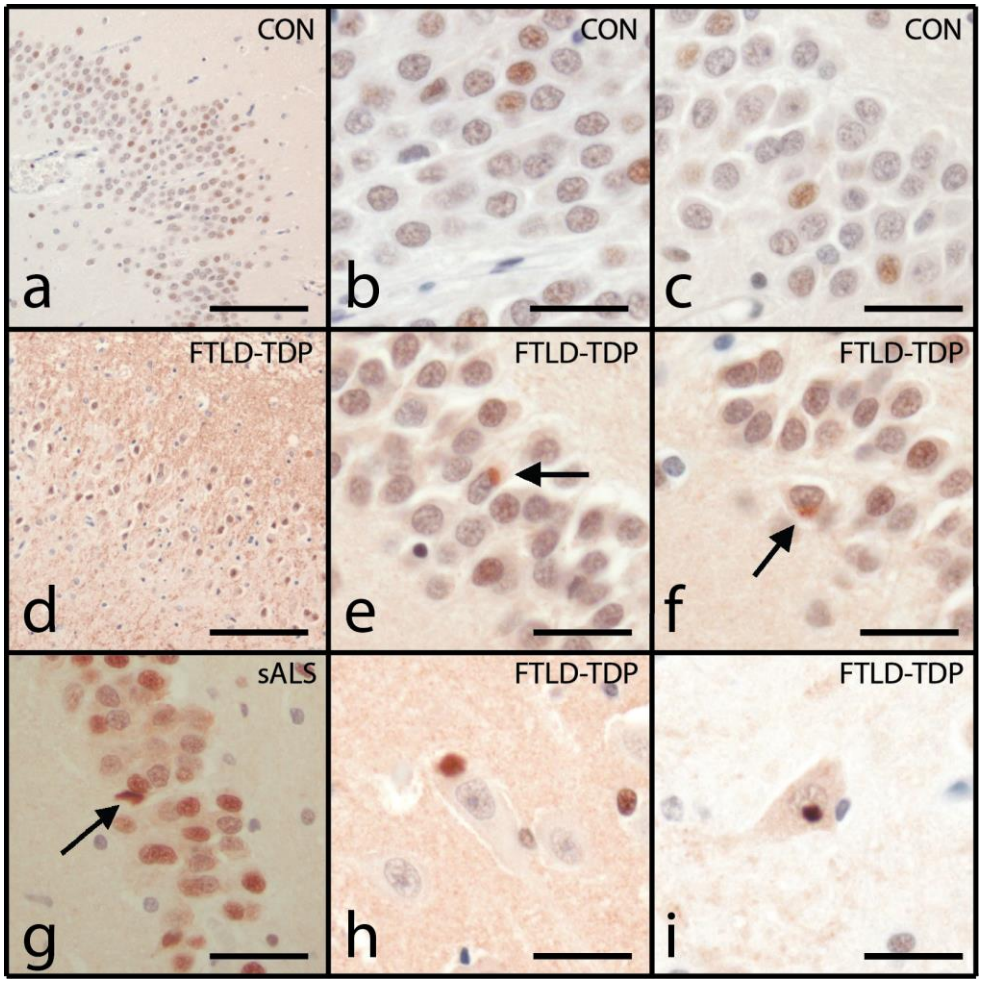

Figure 4.5 RBM45 localization in the hippocampus. Representative hippocampal sections from ALS, FTLD-TDP and control subjects immunostained for RBM45 and counterstained with hematoxylin. **A.** – **C.**: RBM45 immunoreactivity in non-neurologic disease controls. RBM45 is located in the nucleus of dentate granule cells. **D.** – **F.**: RBM45 cytoplasmic inclusions are observed in dentate granule cells in FTLD-TDP cases (arrows in **E** and **F**). **G.** RBM45 pathology in the hippocampus of sporadic ALS. **H.**, **I.** Rare CA3 pyramidal neurons in FTLD-TDP cases contained RBM45 inclusions. For panels **A** and **D**, the magnification is 10X and the scale bars denote 60 μm, while in all other panels the magnification is 40X and scale bars indicate 20 μm. Panels represent the

following case numbers in Table 4.1: (**A**) = 38; (**B**) = 40; (**C**) = 39; (**D**) = 29; (**E**) = 27; (**F**) = 26; (**G**) = 17; (**H**) = 29; (**I**) = 24.

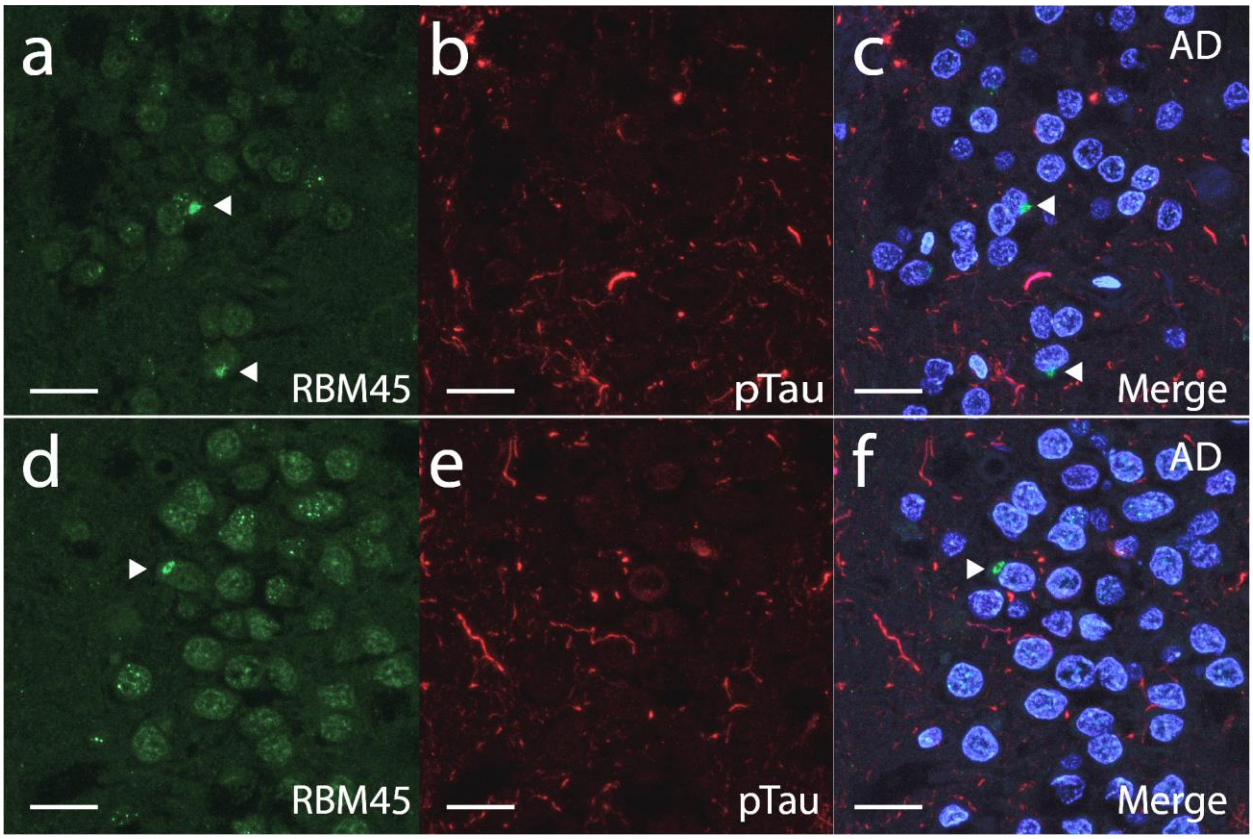

Figure 4.6 RBM45 and tau pathology do not overlap in AD cases. Hippocampal sections from two AD cases stained for RBM45 (green) and phosphorylated tau (red) with nuclei (DAPI-blue) in the merged image. Abundant pTau pathology is seen in both cases, as well as RBM45 inclusions marked with arrows. No overlap of pTau pathology with RBM45 inclusions or speckled RBM45 nuclear staining is seen. Scale bar = 20 µm. Panels represent the following case numbers in Table 4.1: (**A-C**) = 30; (**D-F**) = 33.

4.4.4 Co-localization of RBM45 and TDP-43

We next examined the co-localization of RBM45 and TDP-43 pathology in ALS, FTLD-TDP and AD by double-label confocal microscopy, with DAPI to identify nuclei. We detected co-localization of RBM45 and TDP-43 within cytoplasmic inclusions of spinal cord motor neurons in ALS (Figure 4.7A-C). We also noted ALS motor neurons with both nuclear RBM45 and co-localization in cytoplasmic TDP-43 inclusions (Figure 4.7C). Interestingly, Figure 4.7A, B represent ALS cases with the *C9ORF72* repeat expansion and exhibit reduced RBM45 nuclear staining when compared to ALS cases without the repeat expansion.

In the hippocampus of FTLD-TDP and AD patients, RBM45 co-localized with TDP-43 in cytosolic and rare intranuclear inclusions of dentate granule cells (arrows in Figure 4.7D, E). We also observed co-localization of RBM45 to TDP-43 inclusions in the dentate of AD patients (Figure 4.7F). A speckled RBM45 nuclear staining pattern was evident in many dentate granule cells that are distinct from the more diffuse TDP-43 nuclear immunostaining. Using multiple images from 10 ALS, 4 FTLD-TDP, and 5 AD cases, we determined that RBM45 was present in 64% of the TDP-43 inclusions in the spinal cord of ALS cases and 70% of the TDP-43 inclusions in the hippocampus of FTLD-TDP and AD cases. Examples of TDP-43 inclusions that lack RBM45 are shown in Figure 4.8. We observed ALS spinal cord motor neurons with nuclear RBM45 and weak or absent co-localization to TDP-43 cytoplasmic inclusions (Figure 4.8A). In subjects with the *C9ORF72* repeat expansion, we also observed spinal cord motor neurons devoid of nuclear RBM45 and lacking RBM45 positive cytoplasmic inclusions (Figure 4.8B). Finally, the hippocampus of ALS, FTLD-TDP and AD subjects contained TDP-43 inclusions without RBM45 (arrowheads in Figure 4.8C). We did not detect RBM45 inclusions that completely lack TDP-43 immunoreactivity.

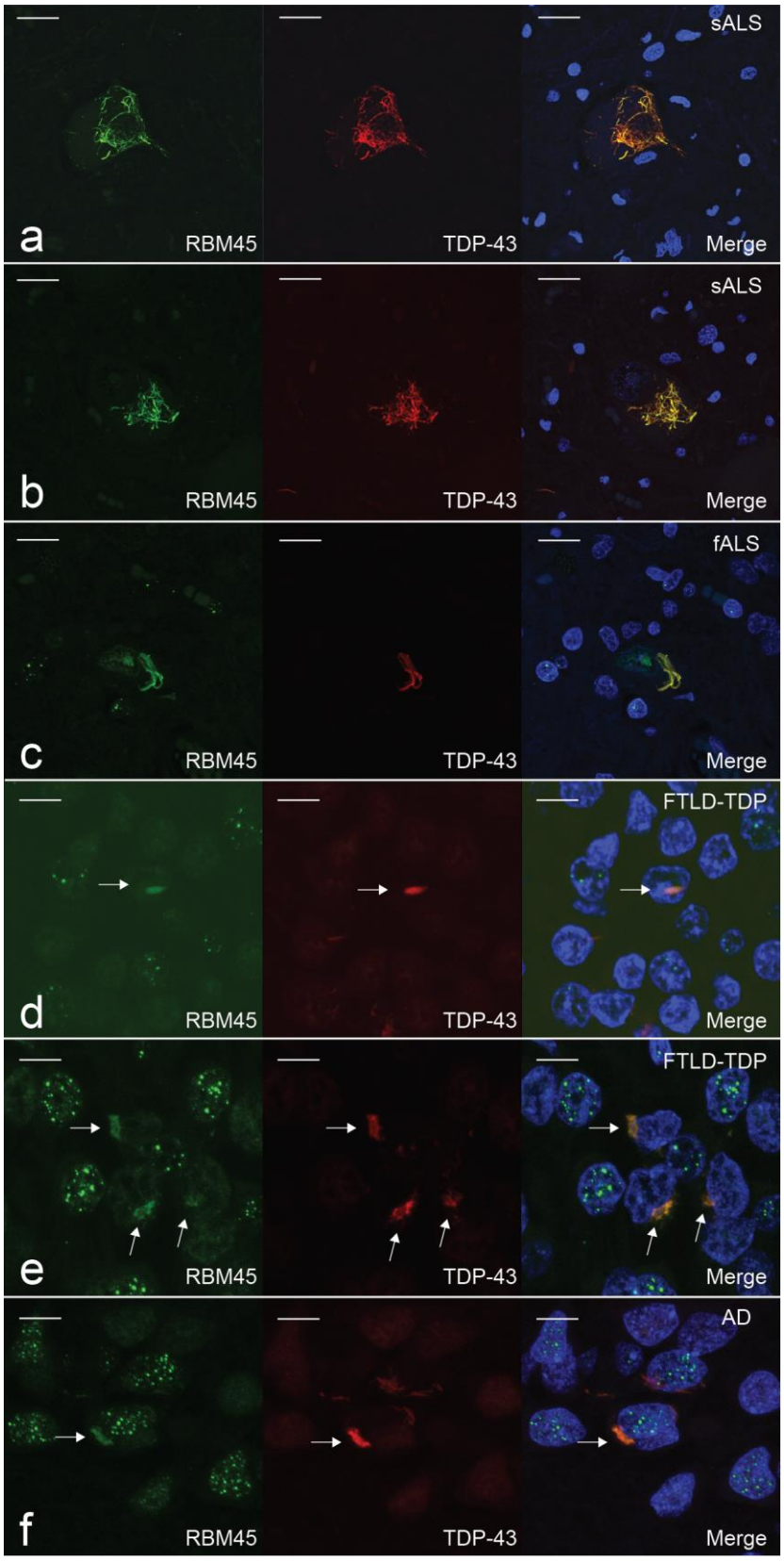
a
RBM45
TDP-43
sALS
Merge
b
RBM45
TDP-43
sALS
Merge
c
RBM45
TDP-43
fALS
Merge
d
RBM45
TDP-43
FTLD-TDP
Merge
e
RBM45
TDP-43
FTLD-TDP
Merge
f
RBM45
TDP-43
AD
Merge

Figure 4.7 Double-label immunofluorescence for RBM45 and TDP-43. A. – C. RBM45 (green) colocalization with TDP-43 (red) positive inclusions in ALS spinal cord motor neurons is shown. DAPI visualizes nuclei (blue) in the merged images. RBM45 also remained in the nucleus of a motor neuron with cytoplasmic TDP-43 inclusions (**C**). **D. – F.** RBM45 colocalization with TDP-43 inclusions in the dentate gyrus of FTLD-TDP (**D** and **E**) and AD (**F**) cases. Arrows denote co-localization in intranuclear (**D**) and cytoplasmic (**E** and **F**) inclusions. Speckled RBM45 nuclear stain is observed in all panels and is devoid of TDP-43. Scale bars denote 20 μm in panels A-C and 30 μm in panels D-F. Each panel represents the following case numbers in Table 4.1: (**A**) = 2; (**B**) = 3; (**C**) = 7; (**D**) = 24; (**E**) = 28; (**F**) = 30.

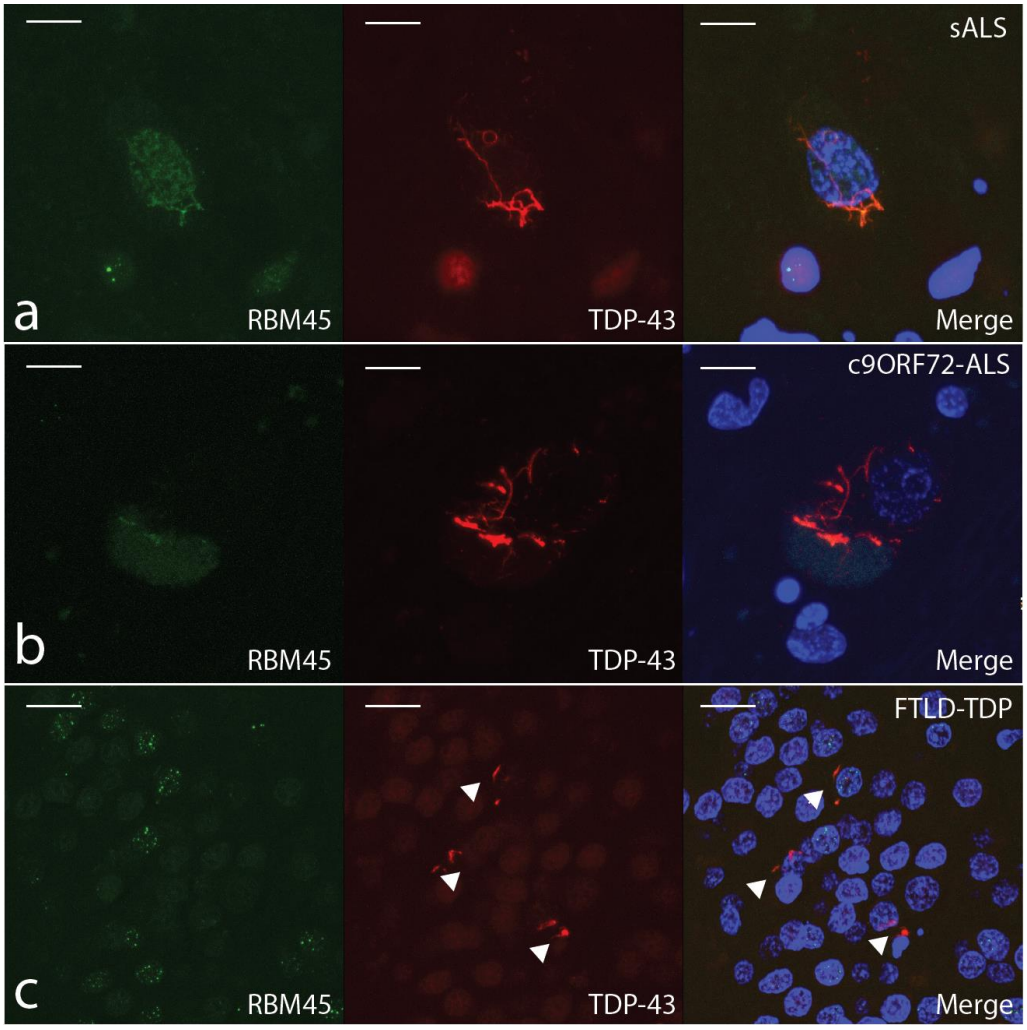

Figure 4.8 TDP-43 pathology independent of RBM45 pathology. TDP-43 pathology can occur independently of RBM45 pathology in ALS and FTLD cases. RBM45 is labeled in green, TDP-43 denoted in red and DAPI (blue) visualizes nuclei in the merged images. **A.** Motor neuron with nuclear RBM45 and a TDP-43 positive inclusion that labels poorly for RBM45. Several such inclusions were found throughout the lumbar spinal cord of sALS and fALS cases. **B.** Motor neurons from *C9ORF72* ALS cases exhibited nuclear depletion of RBM45. RBM45 was not contained in the TDP-43 inclusions in this motor neuron. **C.** Several TDP-43 positive, RBM45 negative inclusions are indicated by arrowheads in the dentate gyrus of an FTLD case. While no RBM45 positive inclusions were seen, the speckled nuclear staining pattern was observed in several adjacent cells.

Scale bar = 20 μm. Panels represent the following case numbers in Table 4.1: (**A**) = 7; (**B**) = 2; (**C**) = 27.

4.4.5 Co-localization of RBM45 and ubiquitin

As ubiquitin-positive inclusions are a pathologic hallmark of both ALS and FTLD-TDP[505,506], we examined the co-localization of RBM45 and ubiquitin-containing inclusions in ALS and FTLD-TDP. RBM45 containing cytoplasmic inclusions in lumbar spinal cord motor neurons of sporadic and familial ALS cases were frequently co-labeled with ubiquitin (Figure 4.9A-C). RBM45 nuclear immunoreactivity in neurons or glia lacked ubiquitin staining (Figure 4.9A, C). These results suggest that RBM45 pathology is highly coincident with ubiquitin in cytoplasmic inclusions, but nuclear RBM45 lacks ubiquitin.

Ubiquitin also labeled RBM45 cytoplasmic inclusions within dentate granule cells of FTLD-TDP patients (Figure 4.9D, E). In addition, we also observed punctate RBM45 nuclear staining in cells that contained cytoplasmic ubiquitin-containing inclusions (Figure 4.9D, E). However we did not detect RBM45 within ubiquitin labeled dystrophic neurites in the dentate of FTLD-TDP subjects (Figure 4.9D), and ubiquitin did not label the speckled nuclear RBM45 immunoreactivity (Figure 4.9D, E).

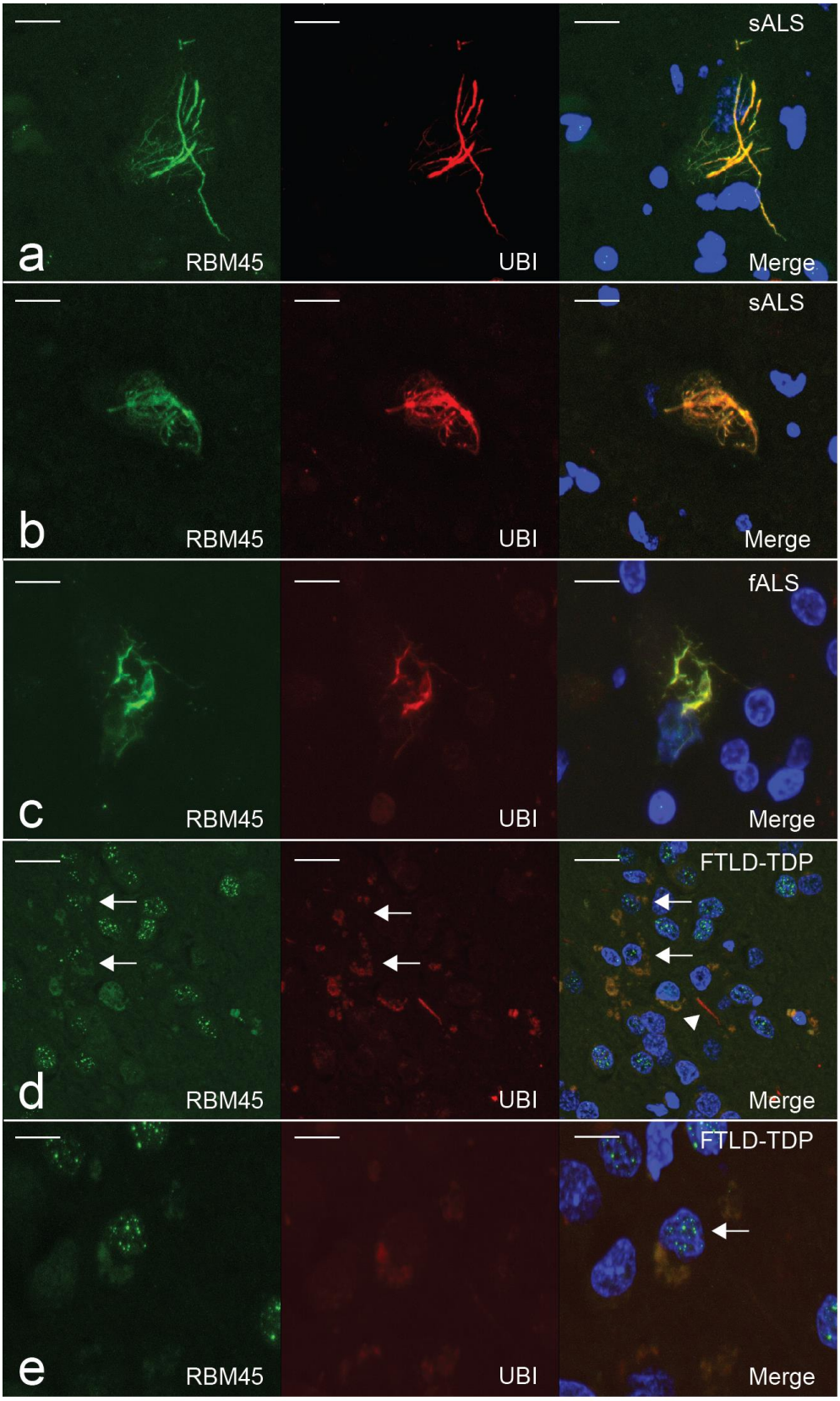
a
RBM45
UBI
sALS
Merge
b
RBM45
UBI
sALS
Merge
c
RBM45
UBI
fALS
Merge
d
RBM45
UBI
FTLD-TDP
Merge
e
RBM45
UBI
FTLD-TDP
Merge

Figure 4.9 Double-label immunofluorescence for RBM45 and Ubiquitin. Double-label immunofluorescence for RBM45 (green) and ubiquitin (red) in the spinal cord and hippocampus is shown. **A.** – **C.** RBM45 co-localization with ubiquitin in ALS spinal cord motor neurons. DAPI visualizes nuclei (blue) in the merged images. Cytoplasmic ubiquitin inclusions are positive for RBM45; however, nuclear RBM45 is not labeled by ubiquitin (**C**). **D.**, **E.** Co-localization of RBM45 to ubiquitin cytoplasmic inclusions in the dentate gyrus. Arrows denote cells that exhibit co-localization of RBM45 and ubiquitin within an inclusion but retaining a speckled RBM45 nuclear immunostaining. Note the lack of RBM45 labeling of an ubiquitin positive dystrophic neurite in the dentate gyrus as indicated by arrowhead (**D**). Scale bars denote 20 μm in panels **A-D** and 30 μm in panel E. Each panel represents the following case numbers in Table 4.1: (**A**) = 10; (**B**) = 7; (**C**) = 22; (**D**) = 27; (**E**) = 26.

4.5 DISCUSSION

We report a new RNA binding protein that exhibits cytoplasmic inclusions in spinal motor neurons and dentate granule cells in ALS and FTLD-TDP patients. This protein, RBM45, was identified by an unbiased mass spectrometry based proteomic screen of CSF and verified by immunoblot analysis. Additional RNA and DNA binding proteins were also observed in our CSF based proteomics analyses that warrant further investigation (Table 4.2). We focused efforts in this study to RBM45 since it exhibited the most statistically significant *q* value and highest effect size between the ALS and control groups, was known to be developmentally regulated in the nervous system, contained structural similarities to TDP-43 and FUS, and commercial antibodies were available. RBM45 was detected in a punctate or speckled immunostaining pattern in the nucleus of neurons and glia. We

observed RBM45-positive inclusions in motor neurons and glia in sporadic and familial ALS cases, as well as in hippocampal neurons of FTLD-TDP and AD patients. The most abundant RBM45 spinal cord pathology was detected in patients that harbor the *C9ORF72* hexanucleotide repeat expansion, with approximately 3 times as many inclusions observed in these cases. This was not due to increased numbers of remaining motor neurons in the *C9ORF72* cases but an increased percentage of the remaining motor neurons containing inclusions. There were no differences in the amount of glial RBM45 inclusions in *C9ORF72* repeat expansion cases versus ALS cases without the repeat expansion. We did not detect any intranuclear RBM45 inclusions in the spinal cord. Importantly, no RBM45 inclusions were detected in any region or cell type examined in control subjects. Significant co-localization of RBM45 with TDP-43 or ubiquitin was detected within inclusions of both ALS and FTLD-TDP patients, but RBM45 did not co-localize with tau pathology in AD cases. RBM45 within the nucleus was not labeled by ubiquitin and did not co-localize with TDP-43.

Few prior studies have investigated RBM45, and our study is the first to report on the distribution and expression of RBM45 in the human brain and spinal cord. In control subjects, we saw punctate staining of the nucleus and cytoplasm of motor neurons of the lumbar spinal cord, along with speckled nuclear staining of adjacent glia (Fig. 4.2A, B). This is consistent with the initial characterization of the protein in rodents, which suggested that the protein is capable of shuttling between the nucleus and cytoplasm[507]. Moreover, we detected limited, predominantly nuclear RBM45 in a speckled staining pattern within dentate granule cells of control subjects (Fig. 4.5A-C). Nuclear speckles were commonly observed in a variety of cell types, including neurons and glia. In mammalian cells, they occur in interchromatin regions of the nucleus and contain RNA[508,509], and are dynamic structures most commonly observed using antibodies to splicing factors that function as

regulators of pre-mRNA splicing[510,511]. The speckled staining pattern seen for RBM45 is consistent with a role as an RNA binding protein involved in pre-mRNA splicing.

The abundant level of RBM45 in the CSF of control subjects suggests that this RNA binding protein may also have an extracellular function. Numerous RNA species are contained within biofluids and many have been reported as biomarker candidates for human diseases[512,513], and while speculative, RNA binding proteins such as RBM45 may modulate extracellular RNA signaling between cells. Recent evidence indicates that cultured cells stimulated to release microRNAs also release numerous RNA binding proteins that may contribute to the protection of extracellular micoRNAs[514].

We established a connection between RBM45 and neurodegenerative disease by virtue of the cytoplasmic inclusion pathology observed in a total of 91% of ALS, 100% of FTLD-TDP and 75% of AD cases. We did not identify any clinical attributes (age, gender, site of disease onset, disease duration) that would provide insight into why some ALS cases fail to exhibit RBM45 pathology. Further studies are necessary to explore the mechanisms of RBM45 inclusion formation and to characterize RBM45 in other neurodegenerative disorders. The pattern of RBM45 inclusion pathology strongly resembles that observed for TDP-43 (Figure 4.7). Namely, we identified numerous cytoplasmic neuronal and glial inclusions in the lumbar spinal cord of sporadic and non-SOD1 familial ALS patients (Figure 4.2), as well as neuronal inclusions in the hippocampus in FTLD-TDP and AD patients (Figure 4.5). This pattern is similar to that seen for the related proteins TDP-43 and FUS in sporadic and non-SOD1 familial ALS cases [492,515]. Indeed, we saw considerable overlap of RBM45 and TDP-43 pathology by confocal microscopy in ALS, FTLD-TDP and AD patients. However, we did not detect RBM45 in TDP-43 or ubiquitin-positive dystrophic neurites in the dentate gyrus of FTLD-TDP patients (Figure 4.9). We also did not observe RBM45 in tau

pathology in the hippocampus of AD patients (Figure 4.6). Co-localization with FUS will be assessed in future studies.

Overall, RBM45 co-localized with 64% of cytoplasmic TDP-43 inclusions in ALS spinal cord and 70% of TDP-43 inclusions in the hippocampus of FTLD-TDP and AD cases. By confocal microscopy we did not detect any RBM45 inclusions that were completely devoid of TDP43 immunoreactivity, suggesting that RBM45 inclusion formation is always associated with TDP-43 inclusions in these brain and spinal cord regions (Figure 4.8). By confocal microscopy we also noted a punctate or speckled RBM45 nuclear staining in neurons containing RBM45, TDP-43 or ubiquitin inclusions (Figures 4.7, 4.8, and 4.9). Retention of FUS in the nuclei of cells harboring cytoplasmic inclusions has been noted in ALS cases that do not harbor mutations in FUS[516]. TDP-43 inclusions may temporally occur earlier in the pathobiology of ALS and RBM45 may be later sequestered into these inclusions. Future cell culture studies are necessary to determine the temporal pattern of TDP-43 and RBM45 deposition within inclusions and if RBM45 containing inclusions are cytotoxic. Since many neurons were observed that had both cytoplasmic RBM45 and speckled nuclear RBM45, the formation of RBM45 inclusions does not preclude its normal distribution, and hence function, in the nucleus. It is possible that the loss of RBM45 from the nucleus is cytotoxic and future studies will explore this possibility.

Aside from RBM45's affinity for poly(C) and poly (G) RNA[507], little is known about RBM45-mediated regulation of gene expression, and continued studies of RBM45 function in splicing may provide insight into disease associated dysregulation of gene expression. Interestingly, the most abundant RBM45 pathology occurred in the spinal cord of subjects containing the *C9ORF72* repeat expansion. Recently, ubiquitin or p62 positive and TDP-43 negative inclusions were noted in non-motor regions including the hippocampus and cerebellum of subjects with the

C9ORF72 repeat expansion[193,504,517,518], and it is possible that RBM45 may be contained within these inclusions in the cerebellum. We did not have access to cerebellar tissue from these cases to explore this question. We also noted reduced nuclear immunostaining for RBM45 in cases that harbor the *C9ORF72* repeat expansion (Figure 4.2), though studies using a larger number of subjects containing the repeat expansion is necessary to confirm this observation.

The presence of RBM45 pathology in a majority of ALS and all FTLD-TDP cases suggests that RBM45 inclusions occur via a pathway common to familial and non-familial forms of neurodegeneration. Prior studies have linked mutations or gene variations in a number of RNA processing proteins to ALS and FTLD-TDP, including TDP-43, FUS, senataxin, the survival motor neuron protein, and ataxin-2 (reviewed in [519]). This raises the possibility that RBM45 mutations may also occur in familial forms of ALS or FTLD. However the chromosomal location of the RBM45 gene, 2q31.2, has not been linked to ALS or FTLD in any prior genetic linkage study. Nevertheless, our data strengthens the link between ALS and FTLD-TDP to RNA metabolism (reviewed in [495,497]). It is also important to note that TDP-43 has been shown to interact with the RNA for FUS and RBM45 in neurons, suggesting a functional role for TDP-43 in the expression of both FUS and RBM45[520].

In summary, we have identified a novel RNA binding protein in cytoplasmic inclusions of motor neurons and glia in sporadic and familial ALS, as well as in hippocampal neurons in FTLD-TDP and AD. RBM45 inclusions readily co-localize with both TDP-43 and ubiquitin, but RBM45 can be distinguished from these proteins through its speckled nuclear immunostaining and lack of incorporation into hippocampal dystrophic neurites. The most abundant RBM45 pathology typically occurred in patients that harbor the *C9ORF72* repeat expansion. Additional work is needed to understand how this protein contributes to both the normal RNA metabolism as well as to

neurodegenerative disorders. Nevertheless, the identification of a new RNA binding protein associated with these disorders holds promise for further mechanistic insights into disease pathogenesis and strengthens the role of RNA metabolism in these disorders.

5.0 IMMUNOPRECIPITATION AND MASS SPECTROMETRY DEFINES AN EXTENSIVE RBM45 PROTEIN-PROTEIN INTERACTION NETWORK

5.1 CHAPTER SUMMARY

The pathological accumulation of RNA-binding proteins (RBPs) within inclusion bodies is a hallmark of amyotrophic lateral sclerosis (ALS) and frontotemporal lobar degeneration (FTLD). RBP aggregation results in both toxic gain and loss of normal function. Determining the protein binding partners and normal functions of disease-associated RBPs is necessary to fully understand molecular mechanisms of RBPs in disease. Herein, we characterized the protein-protein interactions (PPIs) of RBM45, a RBP that localizes to inclusions in ALS/FTLD. Using immunoprecipitation coupled to mass spectrometry (IP-MS), we identified 132 proteins that specifically interact with RBM45. Select PPIs were validated by immunocytochemistry, demonstrating that RBM45 associates with a number of other RBPs primarily via RNA-dependent interaction in the nucleus. Analysis of the biological processes and pathways associated with RBM45-interacting proteins indicates enrichment for nuclear RNA processing/splicing via association with hnRNP proteins and cytoplasmic RNA translation via eiF2 and eiF4 pathways. Moreover, several other ALS-linked RBPs, including TDP-43, FUS, Matrin-3, and hnRNP-A1, physically associate with RBM45, consistent with the observation of these proteins together in intracellular inclusions in ALS/FTLD. Taken together, our results define a PPI network for RBM45, suggest novel functions for this

protein, and provide new insights into the contributions of RBM45 to neurodegeneration in ALS/FTLD.

5.2 INTRODUCTION

The aggregation of RNA-binding proteins (RBPs) into inclusion bodies is one of the most prevalent and well-characterized pathological findings in amyotrophic lateral sclerosis (ALS) and frontotemporal lobar degeneration (FTLD). The identification of cytoplasmic mis-localized TDP-43[33], and later FUS[68,69], as primary components of ubiquitinated inclusions in motor neurons and glia in these disorders led to the "two-hit" hypothesis of RBP-mediated neurodegeneration. This model proposes that the pathological aggregation of RBPs confers toxicity by simultaneous gain of toxic function of the aggregates and the loss of normal functions served by these proteins in regulating gene expression. Ample experimental evidence now exists in support of this model, with studies consistently finding that under- or overexpression of numerous RBPs is sufficient to induce neuronal cell death in a variety of model systems (reviewed in [70]).

This model of RBP-mediated neurodegeneration depends, in part, on the ability of RBPs to self-associate and interact with other RBPs within protein aggregates. Many ALS-linked RBPs, including TDP-43, FUS, hnRNP-A1, and TAF15 are aggregation prone as a result of prion-like domains contained within their protein sequence[50,521]. Mutations in the prion-like domain lead to familial forms of ALS/FTLD marked by the pathological aggregation of the mutant protein (reviewed in [522]). In addition to self-aggregation, these proteins are capable of sequestering other proteins into aggregates/inclusions as a consequence of the normal functional associations between these proteins. For example, proteomic analysis of TDP-43 aggregates showed deposition of stress

granule proteins G3BP and PABPC1 as well as paraspeckle proteins PSF and NONO[523]. Similar observations of paraspeckle proteins p54nrb and NONO in FUS-positive inclusions[524] provide additional evidence in support of this concept. Thus, understanding the protein-protein interactions (PPIs) of ALS-linked RBPs is a necessary step towards defining the protein composition of inclusions in ALS/FTLD and new insight into mechanisms of disease.

Determining RBP PPIs is also essential for understanding the normal functions of RBPs, and how these functions may be compromised as a result of RBP aggregation in ALS/FTLD. Numerous RBP functions depend on the association of RBPs with protein/nucleic acid complexes. For example, FUS is a component of both nuclear gems, which participate in snRNP biogenesis, and paraspeckles, which are involved in cellular stress responses[524,525]. The expression of mutant FUS reduces levels of these nuclear sub-structures, suggesting mechanisms by which loss of normal FUS function contributes to cell death in ALS/FTLD. In addition, many ALS/FTLD-linked RBPs also associate with cytoplasmic stress granules[95], and disease-associated mutations tend to promote the excess formation of these structures[103]. While stress granules normally aid in the response to cellular stress by protecting mRNAs and shifting gene expression towards a stress response, excessive stress granule formation promotes the formation of insoluble RBP aggregates that may be precursors to inclusion bodies[95,103,526]. This can lead to loss of other normal functions, such as impaired P-body formation that occurs in response to mutant FUS sequestration in stress granules[527]. PPIs can be used to predict these and similar functional associations[523]. Defining RBP PPIs, therefore, helps uncover novel functions and candidate disease mechanisms related to these multifunctional proteins.

Given the diversity of RBP functions, which includes regulating transcription, RNA splicing/export, and miRNA biogenesis[70], a relatively high-throughput approach is preferable to identify candidate functions/binding partners for targeted validation. Immunoprecipitation coupled to

mass spectrometry (IP-MS) offers tremendous promise towards identifying large sets of RBP protein-protein interactions (PPIs) and associated biological processes/pathways. The sensitivity of this approach can be further enhanced by the use of cross-linking methods, such as treatment with small cross-linking agents or formaldehyde, to detect low-affinity protein interactions[528,529]. This approach has previously been used to identify proteins interacting with the ALS-linked Ewing Sarcoma (EWS) RBP[530], where interactions with hnRNPs and FUS are consistent with roles of EWS in mRNA splicing[531] and inclusion formation in ALS/FTLD[532], respectively. Thus, IP-MS can identify multiple protein binding partners of a given target and this information can be used to predict novel functions and roles in disease.

Here, we applied this approach to RBM45, a recently characterized RNA-binding protein found in inclusions in ALS, FTLD, and Alzheimer's disease (AD)[533]. These inclusions are positive for TDP-43, and RBM45 physically interacts with TDP-43 and FUS *in vitro*[528]. RBM45 contains three RNA-recognition motifs (RRMs), a nuclear localization sequence (NLS), and a homo-oligomerization (HOA) domain that mediates self-association of the protein, and can localize to cytoplasmic stress granules[528,534]. The expression of RBM45 is developmentally regulated and the highest expression levels occur in the brain[535]. These properties make RBM45 a promising target for continued studies of ALS/FTLD, though at present little is known about the function of RBM45. To delineate protein binding partners of RBM45 and putative biological functions of the protein, we used an IP-MS approach to comprehensively characterize RBM45 protein-protein interactions (PPIs). We identified 132 RBM45 PPIs by IP-MS, including PPIs with many RBPs. Our results were used to associate RBM45 with biological processes and pathways. These were primarily related to nuclear mRNA processing and cytoplasmic RNA translation. Our IP-MS findings also indicate that RBM45 interacts with a number of ALS-linked proteins, including TDP-43, FUS, Matrin-3, hnRNP-

A1, and hnRNP-A2/B1. Selected PPIs were externally validated via complementary techniques. Collectively, our results shed new light on RBM45 PPIs, biological functions, and contributions to neurodegeneration in ALS/FTLD.

5.3 MATERIALS AND METHODS

5.3.1 Cell Culture and Plasmid Construction

HEK293 (FreeStyle™ 293-F Cells, Invitrogen) cells were cultured in DMEM medium with 10% FBS and 1% Pen-Strep at 37˚C with 5% CO_2. Transfection was performed using the Lipofectamine 2000 (Life technologies) and stable cell lines were selected in the presence of 500 μg/ml G418 (Life Technologies) 48 hours post-transfection. The RBM45 cDNA clone plasmid, cGST-hRBM45 (HsCD00356971), was obtained from the DNASU Plasmid Repository at Arizona State University, Tempe. The cDNA was amplified by PCR using Phusion High-Fidelity DNA Polymerase (NEB) and sub-cloned into the pcDNA3 vector (Invitrogen). The 3xFLAG tag (DYKDHDGDYKDHDIDYKDDDDK) or 2xHA tag (DYPYDVPDYAGGAAYPYDVPDYA) was appended to the N-terminus of specific proteins to generate the 3xFLAG- or 2xHA-tagged construct.

5.3.2 Immunoprecipitation

Each immunoprecipitation (IP) was carried out in triplicate. Stable cell lines expressing FLAG-RBM45, HA-RBM45, or pcDNA3 vector were grown on 10cm plates till 90% confluent and harvested. For regular IP, cells from one 10cm plate were lysed with 500 μl of 0.5% NP40 lysis

buffer (50 mM HEPES pH 7.6, 150 mM KCl, 2 mM EDTA, 0.5% NP40, 0.5 mM DTT and protease (Sigma P8340)/phosphatase (Calbiochem 524629)/RNase inhibitors (Ambion AM2694)) at 4˚C for 15 min. For formaldehyde crosslinking-IP, formaldehyde in-cell crosslinking was performed prior to IP as previously reported[528]. Cells from one 10cm plate were suspended in 1 ml PBS containing 0.1% formaldehyde and incubated at room temperature for 7 min with gentle agitation. The suspension was spun for 3 min at 1,800 g at room temperature and the supernatant was discarded. The pellet was washed with 1 ml 1.25 M glycine in cold PBS twice to quench the crosslinking reaction. The pellet was further washed in PBS, lysed with 500 µl of 1% NP40 lysis buffer (50 mM HEPES pH 7.6, 150 mM KCl, 2 mM EDTA, 1% NP-40, 0.5 mM DTT and protease/phosphatase inhibitors) at 4˚C and sonicated in a water bath sonicator (Misonix Sonicator 3000) at level 2 for 4 cycles (15 sec on/30 sec off).

The lysates were first cleared by spinning at 16,000 g at 4˚C for 15 min to remove cell debris, pre-cleared using IgG-Agarose (Sigma A0919) for 1 hour and further centrifugated. The resulting supernatants were immunoprecipitated with appropriate amounts of agarose beads corresponding to 50 µg of either pre-crosslinked antibody or IgG. FLAG-IP was performed using anti-FLAG M2 Affinity Gel (Sigma A2220), HA-IP was performed using anti-HA Agarose (Sigma A2095), and IgG-IP control was performed using Mouse IgG-Agarose (Sigma A0919). IPs were performed at 4˚C for 2 hr and the beads were washed six times in IP buffer. The proteins were eluted with SDS sample buffer and heated at 95˚C for 5 min for regular IP samples and heated for 20 min for formaldehyde crosslinking IP samples. The samples were then run on the Bolt 4-12% Bis-Tris Plus Gel (Life Technologies), and stained using Bio-Safe Coomassie Stain (BioRad).

5.3.3 Protein Digestion

Gel lanes in the molecular weight range between 10 kDa and greater than 250 kDa were excised into individual fractions, excluding the stained IgG-H (52kDa) and IgG-L (25kDa) bands. Bands fractions were then further reduced into cubes of 1-2mm^3, destained, washed, dried and further processed using an established method[536]. Briefly, each fraction was reduced using 10mM DTT (6˚C for 30 min) and alkylated using 55mM iodoacetamide (room temperature for 30 min, in the dark), using multiple hydration and dehydration cycles of the acrylamide gel. Fractions were then digested using 20 ng/mL of Trypsin Gold (Promega) (37°C, overnight). Finally, peptides were extracted, concentrated to dryness under vacuum and stored at -20°C until LC-MS analysis.

5.3.4 LC-MS Analysis and Protein Identification

Each fraction was reconstituted in 0.1% formic acid and analyzed using online liquid chromatography on a nanoAcquity-UPLC coupled to a Thermo LTQ Orbitrap Velos mass-spectrometry. Samples were loaded onto a 100-µm diameter column (length 100 mm) packed with 3 µm Reprosil Pur C18 AQ resin. Solvent A and B were 0.1% formic acid in water and acetonitrile, respectively. The gradient was 3% B to 40% B in 17 min followed by 40% B to 90% B in 0.5 min, then 90% B for 2 min and final re-equilibration for 10.5 min. The flow rate was set to 500 nL/min The mass spectrometer was operated in positive ion mode using a spray voltage of 1.8 kV, and a capillary temperature of 200°C. Data were acquired in top-15, data-dependent acquisition mode using a collision voltage of 30 V.

Mass spectra were extracted, deconvolved and deisotoped using Proteome Discoverer 1.4.1.14 (Thermo Fisher Scientific, Waltham, MA) and searched against a concatenated database

(*Homo sapiens*, *Mus musculus*, UniprotKB/Swissprot) using Mascot (Matrix Science, London, UK; version 1.4.1.14). Oxidation (Met), carbamidomethylation (Cys) were specified as variable modifications. Peptides were allowed maximum two trypsin missed cleavages with a mass tolerance of ±10 ppm, and a fragment ion mass tolerance of ±0.8 Da. Search results were imported into Scaffold (Proteome Sofgtware Inc., Portland, OR), and identifications were confirmed by X!Tandem (The GPM, v2010.12.01.1). Only proteins with probabilities equal or higher than 99.0% were retained for analysis (one or more peptide per protein contributing to a positive match). Computation of putative PPIs (manual and SAINTexpress) were based on exclusive spectrum counts, as determined by Scaffold.

5.3.5 Gene Ontology Analysis of Protein-Protein Interactions

A combination of an unsupervised probabilistic approach (SAINTexpress[537]) and a manual approach was used to identify proteins potentially interacting with RBM45. For each protein-protein interaction, SAINTexpress predicted an individual probability based on spectral counts and reported average probabilities across all replicates (AvgP), average fold-change, average spectral counts and a Bayesian False Discovery Rate (BFDR)[538]. Empty vector IPs were used as experimental controls to provide a background list of proteins binding non-specifically to the construct. The interactions provided by SAINTexpress were filtered for protein fold change equal or greater than 2, for proteins observed in at least 2 out of 3 replicates and with an AvgP equal or greater than 0.7, as recommended[537].For manual elucidation of candidate PPIs, only proteins observed in at least 2 out of 3 replicates were retained in RBM45 IPs. Fold-change was calculated as the sum of exclusive spectral counts across RBM45 replicates divided by the sum of the exclusive spectral counts of that

protein in the vector control replicates. Any protein with a fold-change smaller than 2 was filtered out.

To identify biological processes associated with the list of RBM45 interacting proteins, we performed enrichment analysis in the Gene Ontology (GO) Biological Process domain using Cytoscape[539] together with the ClueGo plugin[377]. We performed enrichment analysis using the right-sided hypergeometric test with Benjamini-Hochberg post-hoc correction. GO terms were considered significant at the $p < 0.001$ level and the resultant significant terms were visualized in a network layout where GO Biological Process terms were visualized as color-coded circular nodes, with node size corresponding to enrichment *p* value. The overlap of proteins associated with any two Biological Process terms was evaluated using the kappa statistic and nodes were connected where the κ value was ≥ 0.4 using edges, with edge thickness corresponding to kappa score. We then took leading terms, those GO Biological Process terms with the highest number of associated proteins, and visualized these in a network layout where Biological Process terms were connected by edges to their associated proteins. All final figures were assembled using Adobe Illustrator CS5 (Adobe Systems; San Jose, CA, USA).

5.3.6 Immunocytochemistry

For immunocytochemistry, HEK293 cells were grown on number 1.5 glass coverslips. Cells were washed with 1X PBS and fixed in 4% paraformaldehyde for 10 min. After fixation and further washing, cells were permeabilized by immersion in 1X PBS containing 0.1% Triton X-100 for 15 min. After further washing, cells were blocked by incubation in SuperBlock (Scytek) for 1 hr. Subsequently, primary antibody solutions were applied and allowed to incubate for 2 hr. Following primary antibody incubations, coverslips were washed four times in a 1:10 mixture of

SuperBlock:1X PBS. Secondary antibodies were applied following these washes, allowed to incubate for 1 hr, and washed four times as above. Cell nuclei were visualized by staining with a 300 nM DAPI solution for 10 min followed by washing with 1X PBS. Coverslips were mounted on glass slides using 2,2'-thiodiethanol (TDE) according to the method of [540]. In brief, coverslips were immersed in a series of increasing concentrations of TDE (10%, 25%, 50%, 97%). The final TDE solution has a refractive index of 1.518 to match that of the immersion oil used in imaging the slides.

The primary antibodies used for immunofluorescence were as follows: rabbit monoclonal RBM45 C-terminal antibody (custom-made, 1:250), rabbit monoclonal hnRNP-A1 antibody (Cell Signaling 8443S, 1:800), mouse monoclonal hnRNP-A2B1 antibody (Santa Cruz sc-32316, 1:250), rabbit polyclonal hnRNP-A3 antibody (Sigma AV41195, 1:200), mouse monoclonal hnRNP-L antibody (Novus Biological NB120-6106, 1:1000), rabbit monoclonal Matrin-3 antibody (Abcam ab151714, 1:500), mouse monoclonal G3BP antibody (BD Transduction Laboratories, 1:250), mouse monoclonal SMN antibody (Sigma S2944, 1:400), and mouse monoclonal FLAG M2 antibody (Sigma F3165, 1:1000). The secondary antibodies used for immunofluorescence were goat-anti-Cy2 (rabbit) and goat-anti-Cy5 (Mouse) (Millipore, 1:1000 for both).

5.3.7 Microscopy, Digital Deconvolution, and Co-localization Analysis

An Observer Z1 microscope (Zeiss) was used for all image acquisitions using a 63x (1.4 NA) objective and LED light source. Images were acquired as three-dimensional stacks with a Z sampling interval of 0.240 µm. Images were shading corrected and background subtracted. Following acquisition, images were deconvolved using Huygens Essential deconvolution software (SVI). Deconvolution and chromatic shift correction were performed using a measured PSF obtained by volume imaging of 200 µm fluorescent beads (Life Technologies) together with the Huygens

Essential PSF Distiller application. Deconvolution was performed using the software's classic maximum likelihood estimation algorithm. Deconvolved images were used to analyze the co-localization of RBM45 and selected RBM45 interacting proteins identified by IP-MS. Co-localization analysis was performed using ImageJ[541] in conjunction with the JaCoP plugin[542]. Images were automatically thresholded for analysis using the method of [543] and the M1 and M2 overlap coefficients[542] and intensity correlation quotient (ICQ)[544] were calculated. Statistical significance of the ICQ was evaluated using the normal approximation of the sign test as in [544].

5.4 RESULTS

5.4.1 Identification of the RBM45 Interacting Proteins in HEK-293 Cells

A schematic outline of the immunoprecipitation-mass spectrometry procedure used in this study is shown in Figure 5.1. FLAG-RBM45 or empty vector was overexpressed in HEK293 cells and immunoprecipitated using whole cell lysates in triplicate. HA-tagged RBM45 was also included and used as a reference for the data analysis. HEK293 cells expressing empty vector alone served as negative controls. Regular IP and formaldehyde crosslinking IP were performed in parallel to identify strongly and weakly RBM45-associated proteins separately. Immunoblot analysis of the immunoprecipated fractions showed that tagged-RBM45 was enriched in the pulldown. In contrast, no RBM45 was detected in the pulldown in the vector control or IgG pulldown. These data demonstrate that tagged-RBM45 can be efficiently and specifically immunoprecipitated from cell extracts. Co-immunoprecipitated proteins were then separated using SDS-PAGE and stained.

Coomassie staining of the gels loaded with RBM45-IP identified several bands that were not present in vector (sample 2 and 4) or IgG controls (data not shown).

Immunoprecipitated proteins were gel extracted, trypsin digested, and identified by liquid chromatography tandem mass spectroscopy (LC-MS/MS) (Figure 5.1A, see Methods). In total, 235 unique proteins were identified using a protein false discovery rate equal or lower than 1%. We then applied a manual thresholding approach and a probabilistic PPI prediction algorithm (SAINTexpress) to compute the most likely associations between each of these 235 proteins and RBM45, yielding 132 high-confidence candidates (Figure 5.1). These 132 candidate proteins were found in at least 2 out of the 3 FLAG-IP triplicates and were at least 2-fold more abundant compared to vector control, suggesting that they specifically associate with RBM45 (Supplemental Table 4). Of these 132 proteins, 28 were found exclusively by regular-IP, 68 were found exclusively by crosslinking-IP, and 36 were found in both regular-IP and crosslinking-IP groups. Analysis of the average number of total spectrum counts by different immunoprecipitation group showed that in both regular IP and crosslinking IP, the proteins identified from empty vector groups were significantly lower than the proteins identified from FLAG-/HA-IP groups, providing further evidence of the specificity of the approach (Supplemental Table 4).

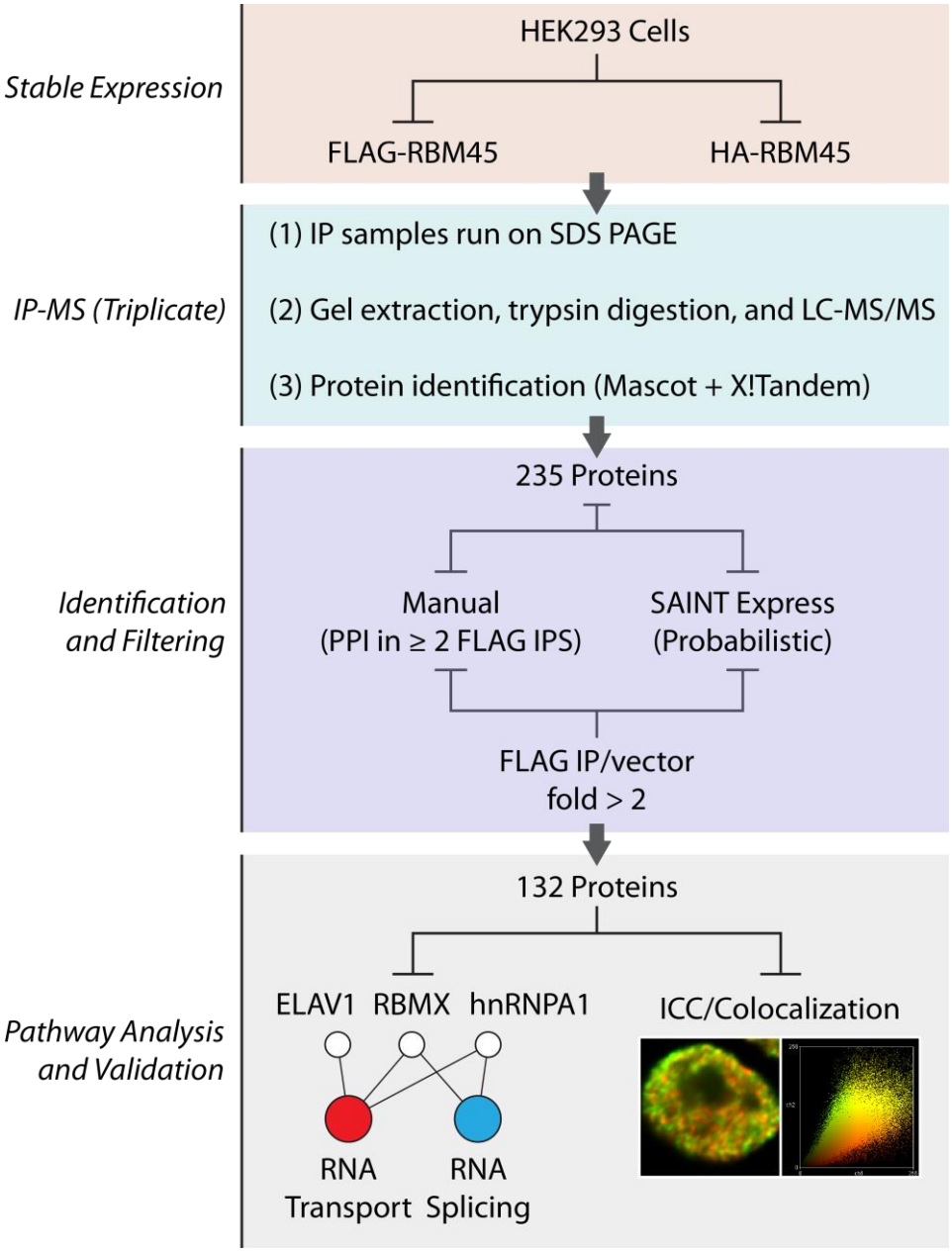

Figure 5.1 Workflow. A schematic of the workflow used to determine RBM45 PPIs is shown. IP-MS = immunoprecipitation/mass spectrometry (MS), LC-MS/MS = liquid chromatography tandem MS.

Table 5.1 Top 20 RBM45 interacting proteins. The top 20 of 132 identified RBM45 interacting proteins is shown. Proteins are arranged in descending order of relative abundance measured by LC-MS/MS (spectral count). Entries in bold were externally validated. The full list of RBM45 interacting proteins with spectral count values for regular and cross-linking IPs, as well as fold change values and associated pathways is found in Supplemental Table 4.

Accession	*Gene Name*	*Protein*
Q8IUH3	RBM45	RNA-binding protein 45
P14866	**HNRNPL**	**Heterogeneous nuclear ribonucleoprotein L**
P22626	**HNRNPA2B1**	**Heterogeneous nuclear ribonucleoproteins A2/B1**
P43243	**MATR3**	**Matrin-3**
Q00839	HNRNPU	Heterogeneous nuclear ribonucleoprotein U
P61978	HNRNPK	Heterogeneous nuclear ribonucleoprotein K
P09651	**HNRNPA1**	**Heterogeneous nuclear ribonucleoprotein A1**
Q93008	USP9X	Probable ubiquitin carboxyl-terminal hydrolase FAF-X
Q9NZI8	IGF2BP1	Insulin-like growth factor 2 mRNA-binding protein 1
Q8N163	CCAR2	Cell cycle and apoptosis regulator protein 2
P52272	HNRNPM	Heterogeneous nuclear ribonucleoprotein M
Q08211	DHX9	ATP-dependent RNA helicase A
P08107	HSPA1A	Heat shock 70 kDa protein 1A/1B
Q13263	TRIM28	Transcription intermediary factor 1-beta
P11940	PABPC1	Polyadenylate-binding protein 1
P51991	**HNRNPA3**	**Heterogeneous nuclear ribonucleoprotein A3**
P07910	HNRNPC	Heterogeneous nuclear ribonucleoproteins C1/C2
P38159	RBMX	RNA-binding motif protein, X chromosome
O43390	HNRNPR	Heterogeneous nuclear ribonucleoprotein R
Q13148	**TARDBP**	**TAR DNA-binding protein 43**

5.4.2 Gene Ontology and Pathway Analysis

To identify putative biological processes associated with RBM45-interacting proteins, we performed enrichment analysis in the Gene Ontology (GO) domain "Biological Process" (Figure 5.2). The results of this analysis identified two predominant themes: (1) nuclear RNA processing and (2)

cytoplasmic RNA translation. RNA processing terms were chiefly related to splicing (e.g., "regulation of RNA splicing", "alternative mRNA splicing"). Other nuclear RNA-associated terms included "mRNA transport", "regulation of mRNA stability", and "nuclear export". Cytoplasmic translational themes were more diverse and included events directly to mRNA translation ("translation initiation", "translation termination"), as well as downstream processing events ("protein targeting to ER", "nonsense mediated mRNA decay"). Finally, terms unrelated to these phenomena and unconnected to any nodes included "apoptotic nuclear changes" and "telomere maintenance" (Figure 5.2).

To provide further insights into the biological processes identified by this approach, we took leading terms, those terms with the highest number of associated proteins, from our results and visualized these terms with their associated proteins in a network layout where edges connect proteins to an associated biological process (Figure 5.3). The results show the individual proteins that result in the identification of an enriched biological process. For example, the identification of the "mRNA metabolic process" and "regulation of RNA splicing" terms results in large part from the many hnRNP proteins in our list of RBM45-interacting proteins. Conversely, the enrichment for "regulation of translation" results from the presence of initiation and elongation factors (e.g., eIF proteins) in our list of RBM45-interacting proteins (Figure 5.3).

Major canonical pathways associated with RBM45-interacting proteins were identified using Ingenuity Pathway Analysis (IPA®, QIAGEN Redwood City). Out of a total of 103 pathways, 28 were significantly enriched (p-value lower than 0.05). The top 5 pathways, ranked by significance and percent overlap are "EIF2 Signaling", "Regulation of eIF4 and p70S6K Signaling", "mTOR Signaling", "Telomere Extension by Telomerase", and "RAN Signaling" (Supplemental Table 4). These results were consistent with associations found in the gene ontology analysis. Collectively,

this view emphasizes the diverse array of biological functions served by RBM45-interacting proteins.

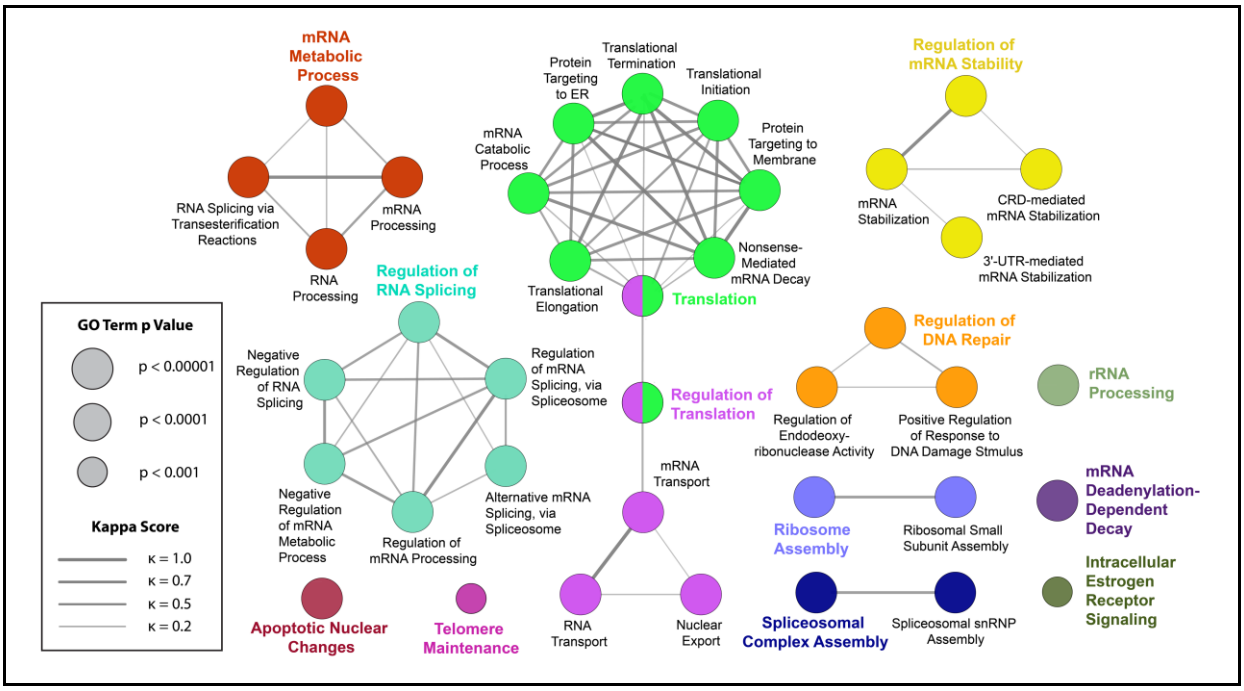

Figure 5.2 Enriched GO Biological Process terms. RBM45-interacting proteins were tested for GO Biological Process enrichment using the right-sided hypergeometric test with Benjamini-Hochberg post-hoc p value correction. Terms with a p value of 0.001 or less were visualized in a network layout, where node size corresponds to term p value. The proportion of shared proteins between terms was evaluated using the kappa statistic and nodes with a kappa score (κ) of at least 0.4 were connected with edges on the graph, with edge width proportional to kappa score. Leading terms, those terms with the highest number of proteins, are colored for emphasis.

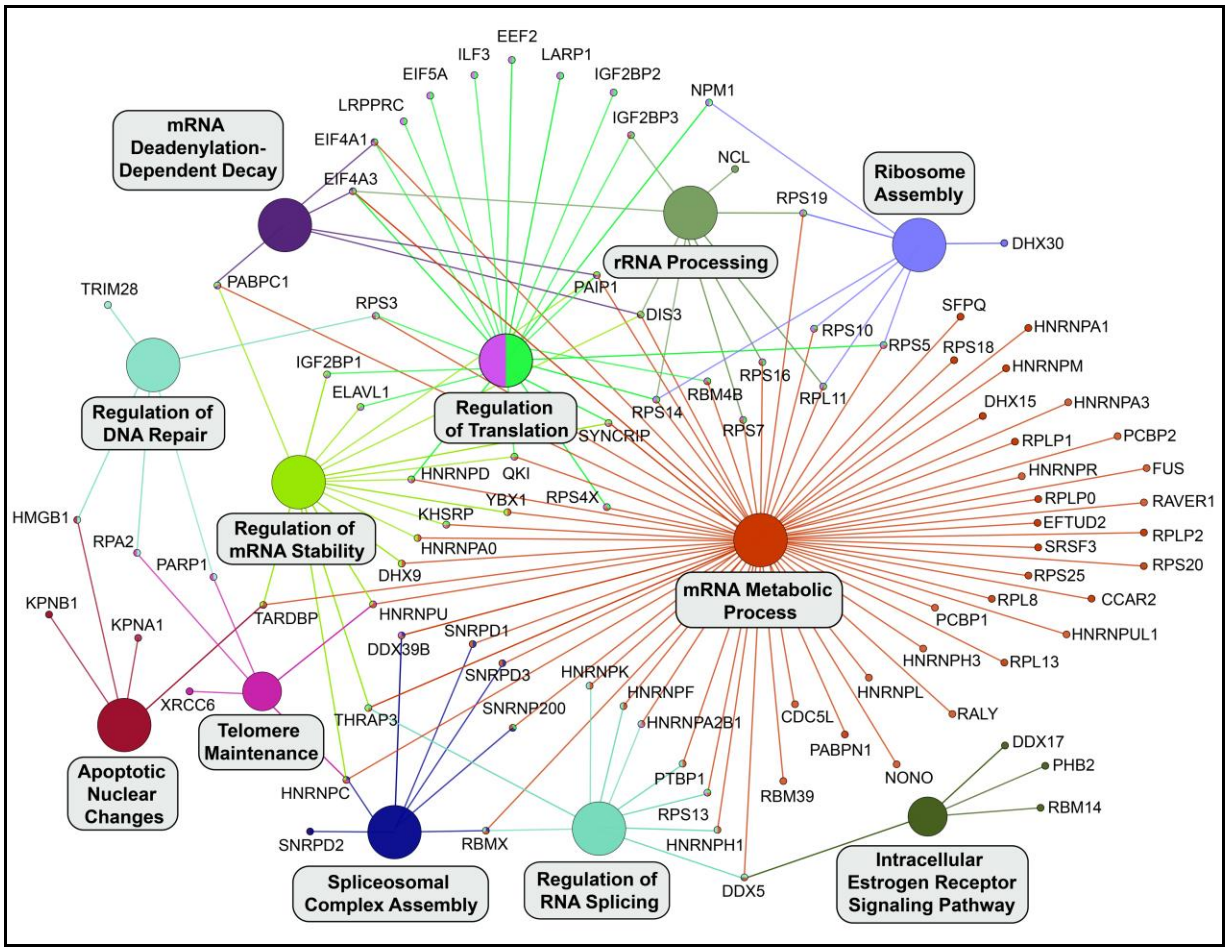

Figure 5.3 Leading terms with associated proteins. Leading terms from Figure 3 were placed into a separate network and all associated proteins from the list of RBM45-interacting proteins were visualized as nodes and connected to the appropriate term. Where a protein is associated with multiple terms, multiple edges emanate from that protein and edges are color-matched to their associated terms.

5.4.3 Co-localization Analysis

To assess the association of RBM45 and selected interacting proteins in cells, we used immunocytochemistry of our FLAG-RBM45 stable HEK293 cells together with digital

deconvolution and co-localization analysis. The results of this analysis are shown in Figure 5.4. Because the staining we observe for the majority of the proteins analyzed is predominantly nuclear, multiple methods were used to provide a quantitative measure of the extent of co-localization. We thus analyzed the co-localization of FLAG-RBM45 and selected proteins using Manders coefficients[542] and the intensity correlation quotient (ICQ)[544], together with pixel intensity scatter plots. The ICQ evaluates the co-variation of pixel intensities for each protein and provides a correlation-based metric (the ICQ, range -0.5 to 0.5) that reflects the degree to which protein staining intensities vary in synchrony and associated statistical significance. If staining intensities vary in synchrony (co-localization), the ICQ is large and positive. For proteins with subcellular segregation, the ICQ is large and negative, while for random variations in intensity, the ICQ = ~0.

The results of this analysis are shown in Figure 5.4H. We used SMN as a negative control, as the staining for this protein is predominantly cytoplasmic. As shown in Figure 5.4G, by either measure of co-localization, the association between RBM45 and SMN is low, reflecting subcellular segregation, as anticipated. We then evaluated the extent of co-localization between RBM45 and several RBM45-interacting proteins. FLAG-RBM45 staining was exclusively nuclear and we evaluated the co-localization of RBM45 with several nuclear hnRNP proteins. By both methods, the highest degree of co-localization was observed between RBM45 and hnRNP-A1 (Figure 5.4A,H). RBM45 also exhibited statistically significant co-localization with hnRNP-A3, hnRNP-L, and Matrin 3, in descending order of extent of co-localization (Fig. 5.4C,D,F,H). By contrast, RBM45 co-localization with hnRNP-A2/B1 by either approach was lesser and did not reach statistical significance, despite a nuclear localization for both proteins (Fig. 5.4B). This finding highlights the utility of digital deconvolution and quantitative co-localization measures for assessing the true extent of association between proteins by immunocytochemistry. We also observed a lack of co-

localization between RBM45 and G3BP, the latter of which was predominantly cytoplasmic (Figure 5.4E). The absence of statistically significant co-localization between RBM45 and hnRNP-A2/B1 and G3BP may reflect the absence of required stimuli/signaling events necessary for the interaction of these proteins. The association of RBM45 and G3BP, for example, most likely occurs in cytoplasmic stress granules not observed under basal conditions[528].

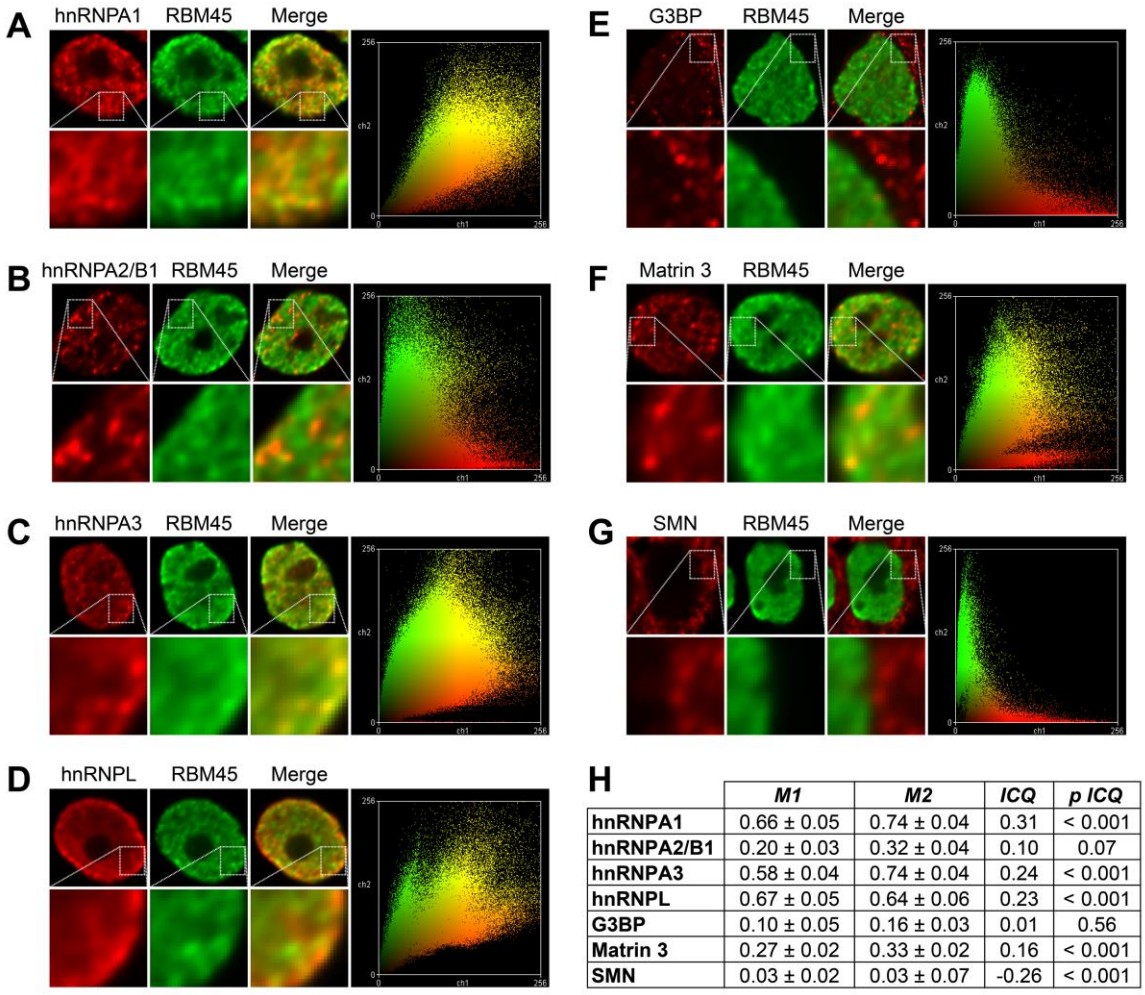

H

	M1	*M2*	*ICQ*	*p ICQ*
hnRNPA1	0.66 ± 0.05	0.74 ± 0.04	0.31	< 0.001
hnRNPA2/B1	0.20 ± 0.03	0.32 ± 0.04	0.10	0.07
hnRNPA3	0.58 ± 0.04	0.74 ± 0.04	0.24	< 0.001
hnRNPL	0.67 ± 0.05	0.64 ± 0.06	0.23	< 0.001
G3BP	0.10 ± 0.05	0.16 ± 0.03	0.01	0.56
Matrin 3	0.27 ± 0.02	0.33 ± 0.02	0.16	< 0.001
SMN	0.03 ± 0.02	0.03 ± 0.07	-0.26	< 0.001

Figure 5.4 Colocalization analysis of RBM45 and selected proteins. A-G. The co-localization of RBM45 and the indicated proteins were evaluated using immunocytochemistry together with co-localization analysis. Representative images and pixel intensity scatter plots are shown with cutouts at higher magnification to highlight detail. **H.** Results of Co-localization analysis. M1 = RBM45

overlap with indicated protein. M2 = indicated protein overlap with RBM45. ICQ = intensity correlation quotient. p ICQ = p value of ICQ. Manders coefficients (M1 and M2) measure the proportion of co-localizing proteins in each channel of a two-channel image and are shown as mean ± SEM. The intensity correlation quotient (ICQ) has a range of -0.5 (perfect segregation) to 0.5 (perfect co-localization), with random intensity variation resulting in a value ~0. The statistical significance of each ICQ value is shown at far right. SMN staining was used as a negative control.

5.5 DISCUSSION

We used IP-MS to identify RBM45 PPIs and gain insight into the biological functions of this ALS/FTLD-associated RNA-binding protein (RBP) in HEK293 cells. By employing two complementary IP methods, regular IP and formaldehyde crosslinking-IP, we detected 132 RBM45 PPIs with high confidence. Our ability to identify numerous RBM45 PPIs with high confidence was a result of our stringent IP-MS approach. We identified 132 "true" interactors along with another 6 proteins matched to putative contaminants in the CRAPome database[545]. Triplicate IPs were analyzed by mass spectrometry. Identified proteins were subjected to a manual thresholding approach (resulting in 132 hits) and a probabilistic approach (resulting in 131 hits) to remove non-specifically bound proteins and predict putative PPIs. The resulting candidate proteins overlapped at 98.9%, highlighting the robustness of the analytical method. RBPs were the most prominent protein family identified by our analytical approach, both in overall number of proteins and individual protein spectral counts. Taking the list of RBM45 PPIs, we next used enrichment and pathway analysis to link RBM45 PPIs to putative biological functions and pathways. The results showed enrichment for nuclear RNA processing via hnRNPs and cytoplasmic translation functions via eiF2

and eiF4 pathways. Taken together, these results provide new insights into the PPIs, biological functions, and roles in ALS/FTLD of RBM45.

These insights are necessary to further understand the role of RBM45 (and RBPs more generally) in ALS/FTLD. RBM45 is a component of ubiquitinated inclusions in neurons and glial cells in ALS, FTLD, and AD patients[533]. The mechanisms mediating the protein's incorporation into inclusions are poorly understood, however. RBM45 is distinct from other inclusion forming RBPs, such as TDP-43, FUS, TAF15, and hnRNP-A1, in that it does not possess a prion-like domain[521]. RBM45 does, however, contain a homo-oligomerization (HOA) domain that mediates RBM45 self-association and association with other RBPs, including TDP-43 and FUS, suggesting a role for this domain in RBM45 inclusion formation[528]. Consistent with this notion, we identify numerous inclusion-forming RBPs that bind to RBM45 via our IP-MS approach, including hnRNP-A1, hnRNP-A2/B1, TDP-43 and FUS (reviewed in [546]). For several of these proteins, the homo-oligomerization (HOA) domain is requisite for interaction. Thus, while the HOA domain is likely necessary for normal RBM45 functions, its role in mediating RBM45 oligomerization and association with other RBPs suggests this domain also contributes to the pathological aggregation of RBM45 and other RBPs in ALS/FTLD. The presence of prion-like domains in many RBM45 interacting proteins and the lack of a prion domain in RBM45 also suggests that RBM45 aggregation may be driven by its association with other aggregation-prone RBPs, as has been observed for RBPs such as PSF and NONO found in TDP-43/FUS positive aggregates[523,524]. The identification of numerous ALS-associated proteins within our RBM45 PPI list suggests that RBM45 can directly contribute to disease by virtue of its association with these proteins.

The aggregation of RBPs in ALS/FTLD confers toxicity both by aggregation-induced toxic gain of function as well as aggregation-induced loss of normal RBP function. Thus, understanding

the normal functions of RBPs is critical to identifying molecular mechanisms of disease and potential therapeutic targets. RBPs are typically multifunctional and act in both the nucleus and cytoplasm, influencing transcription, RNA splicing, RNA export, translation, and transport of mRNAs[547]. RBM45 associates with many its binding proteins via RNA-mediated interaction, suggesting that RBM45 and its binding proteins share the regulation of specific RNA targets. We used our list of RBM45-interacting proteins to generate a list of putative RBM45 biological functions and associated pathways using Gene Ontology and pathway analysis. Two major themes emerged: nuclear RNA processing/splicing via hnRNPs and cytoplasmic translation via the eiF2 and eiF4 pathways (Figures 5.2, 5.3; Supplemental Table 4). The many splicing-associated proteins in our list (Table 5.1, Supplemental Table 4) suggest a role for RBM45 in the regulation of splicing events. Dysregulation of RNA splicing is a well-characterized phenomenon in ALS/FTLD and can result from RBP cytoplasmic mis-localization, aggregation, or both[548]. Loss of individual RBP function due to these phenomena can have profound effects on transcriptional regulation. For example, TDP-43 and FUS bind to more than 50% of the human transcriptome and the loss of these proteins results in substantial global alterations in transcription and splicing[51,167,549]. We anticipate that future studies directly examining the role of RBM45 in the regulation of transcription and RNA splicing will likewise reveal widespread RBM45 binding across the transcriptome and substantial influence on mRNA splicing decisions.

In further support of this notion, the identification of RBM45 PPIs with 19 members of the hnRNP family suggests considerable functional overlap between RBM45 and this diverse class of proteins. Spectral count values for many of these proteins were among the highest observed in our study (Supplemental Table 4) and we accordingly predict considerable functional overlap between RBM45 and the hnRNP family. hnRNPs participate in a variety of mRNA processing/maturation

processes, including mRNA maturation, splicing, nuclear export, and 3'-end processing[550]. Abnormalities in the expression/function of hnRNPs are associated with a number of human diseases, including ALS by virtue of the recent demonstration that mutations in the prion domains of hnRNP-A2/B1 and hnRNP-A1 cause familial forms of ALS[103]. Our analysis of the co-localization of RBM45 and these proteins demonstrates that RBM45 co-localizes most highly with hnRNP-A1, followed by hnRNP-A3 and hnRNP-L, with low, non-significant co-localization observed with hnRNP-A2/B1 (Figure 5.4).

The association of RBM45 with hnRNP-A1, together with the aggregation-prone prion-like domain of hnRNP-A1, may thus mediate both the function and aggregation of RBM45. We observe a high degree of nuclear co-localization between these proteins (Figure 5.4A). hnRNP-A1 serves many purposes in the nucleus, including regulating the transcription of numerous genes[551]. Transcriptional regulation by hnRNP-A1 is, in part, conferred by its ability to bind and relax G-quadruplex nucleic acid structures, including the fALS-linked c9ORF72 GGGGCC hexanucleotide repeat expansion[552,553]. RBM45 may thus be sequestered to c9ORF72 repeat expansion G-quadruplex structures in c9-linked fALS cases, causing a loss of normal RBM45 functions. Indeed, we identify numerous c9ORF72 repeat expansion binding proteins, including FUS, ELAVL1, hnRNP-K, hnRNP-L, hnRNP-Q, and hnRNP-U, as RBM45 PPIs (Supplemental Table 4)[553,554]. Despite its high affinity for poly(G)/(C) RNA[535], RBM45 binding to c9ORF72 has not been shown, although discrepancies between experimental approaches and results suggest that additional c9-binding RBPs remain as yet unidentified[553,554].

We also found significant co-localization of RBM45 with hnRNP-A3 and hnRNP-L in the nucleus (Figure 5.4C,D). hnRNP-L is a multifunctional protein that regulates transcript splicing[555], stability[556], and translation[557]. The protein affects splice site decisions for a large number of

transcripts and is capable of inhibiting spliceosome assembly via coordinated action with hnRNP-A1[558,559]. These results, together with their RNA-dependent physical interaction and co-localization of RBM45 with these proteins, provides further evidence of a role for RBM45 in mRNA splicing decisions. hnRNP-A3 is involved in the nucleocytoplasmic trafficking of mRNA[560] and is involved in telomere maintenance and protection by virtue of its direct binding to telomeres[561,562]. The protein is also a component of p62 positive/TDP-43 negative inclusions in c9ORF72-linked fALS motor neurons[554]. hnRNP-A3 is a component mRNP complexes that act to stabilize mRNA[563]. The co-localization of RBM45 and hnRNP-A3 within distinct nuclear foci (Figure 5.4C) suggests a possible role for RBM45 in this process as well.

A variety of cytoplasmic RBP functions also contribute to cellular function and studies have repeatedly shown that loss of these functions negatively impact cellular viability. TDP-43, for example, associates with cytoplasmic stress granules[46], regulates local mRNA translation[564], and participates in RNA transport[565]. Our results likewise suggest important cytoplasmic functions for RBM45 in both normal cellular homeostasis and disease. A direct role for RBM45 in translation is predicted from the identification of numerous elongation and initiation factors (e.g., eiF4a, eiF5A, EEF2, … [Figure 5.3]) as RBM45 interactors. Twelve percent of the eiF2 signaling pathway responsible for charged tRNA delivery to the ribosome and start site recognition is mapped by PPIs with RBM45, highlighting a possible role of RBM45 in early translational events (Supplemental Table 4). Indirect contributions to translation included the GO biological process "Protein Targeting to ER" (Figure 5.2). ER stress is a well-characterized phenomenon in ALS[566] and RNA-binding proteins may directly associate with ER to modulate its functions in certain cell/tissue types[567]. Despite these findings, immunocytochemical analysis shows an exclusively nuclear staining pattern

for RBM45 in HEK293 cells (Figure 5.4). Future studies are, therefore, necessary to determine the factors influencing the subcellular distribution of RBM45.

One limitation of the current approach is that our analyses were performed exclusively in HEK293 cells. HEK293 cells are rapidly dividing, have a unique gene expression profile, unstable karyotype, and are tumorigenic[568]. Each of these properties could influence the list of RBM45 PPIs detected in the present work. Future studies are necessary to determine cell-type and phenotype-specific RBM45 PPIs and how these contribute to cellular physiology. One area of particular interest is the role of RBM45 in cell division and cell type specification. The initial characterization of RBM45 demonstrated developmental regulation and neuronal enrichment of RBM45 expression[498], suggesting that RBM45 and, by extension, RBM45 PPIs contribute to cell division and organismal development. Delineating which RBM45 PPIs occur in differentiated cell population, such as neurons, may likewise yield insight into RBM45 PPIs and cellular functions that lead to its incorporation into inclusions in ALS/FTLD. In addition, stronger formation of RNA binding protein complexes is typically seen under prolonged periods of stress[569]. Further studies examining the RBM45 protein complexes under stress and basal conditions may similarly help identify biological pathways relevant to RBM45 aggregation.

Finally, we used multiple immunoprecipitation methods coupled with mass spectrometry to increase the confidence of our results. Two different tagged RBM45 constructs as well as the presence or absence of a formaldehyde crosslinker were used for immunoprecipitation. We used a combination of cross-linking and regular IP to distinguish weak and strong interactions, respectively. While commonly used to identify PPIs, regular IP may also yield non-physiological protein associations resulting from artefactual, non-specific binding after cell lysis[570]. Formaldehyde is a mild, cell-permeable and reversible crosslinker with very short spacer length (2.3–2.7 Å) and cross-

links only closely associated proteins[571]. *In vivo* formaldehyde crosslinking-IP can preserve transient and weak physiological protein-protein interactions and has been used for discovering novel protein-protein interactions[571-575]. Crosslinking-IP also facilitates stringent immunoprecipitations via increased detergent concentration, sonication and extensive washes. Identification of a protein only in crosslinking-IP experiments suggests that the interaction with RBM45 is weak. However, one cannot predict the biologic significance of the interaction with RBM45 based solely in whether the interaction is strong or weak. Of the identified 132 proteins, 68 proteins were found solely in crosslinking-IP, while only 28 proteins were found exclusively in regular IP. It is possible that the protein-binding sites in these 28 proteins were masked by the crosslinking reaction and thus not detected by crosslinking-IP.

Collectively, our results demonstrate that RBM45 associates with a large and functionally diverse set of protein binding partners. Functions served by these proteins, particularly the hnRNPs, suggest plausible and previously unknown biological functions for RBM45. The identification of these functions and the association of RBM45 with numerous ALS-associated RBPs points to RBM45-mediated mechanisms of disease in ALS/FTLD and provides further insight into the pathological aggregation of RBM45 occurring in neurodegenerative disease. The association of RBM45 with the set of proteins identified herein provides new directions for future studies of RBM45's role in neuronal development, the regulation of gene expression, and neurodegeneration.

6.0 RBM45 ASSOCIATION WITH NUCLEAR STRESS BODIES DEFINES AN ALTERED STRESS RESPONSE IN ALS/FTLD

6.1 CHAPTER SUMMARY

RNA binding protein (RBP) dysregulation by aggregation and loss of normal function in neurons and glia is a prevalent pathological finding in amyotrophic lateral sclerosis (ALS) and frontotemporal lobar degeneration (FTLD). The persistent association of these proteins in protein-RNA complexes, such as stress granules, can initiate RBP dysregulation by promoting aggregation and removing RBPs from their normal cellular milieu. We describe the association of RBM45, an ALS/FTLD-linked RBP, with nuclear stress bodies (NSBs), a stress-induced protein-RNA complex driven by the transcription of pericentromeric Satellite III DNA. Endogenous RBM45 associates with NSBs in response to a variety of stressors, including heat shock, genotoxic stress, and oxidative stress. This association is dependent on intact RNA binding as removal of RRMs 2 or 3 from the protein is sufficient to abrogate RBM45 NSB association. The persistent association of RBM45 with NSBs is sufficient to induce RBM45 aggregation and does not induce the aggregation of the NSB proteins SAFB and HSF1. FTLD dentate gyrus granule cells show upregulation of the NSB response that is not seen in control subjects. Collectively, these results define a new stress-response pathway altered in ALS/FTLD and provide further evidence of the preponderant role of RNA binding proteins in these disorders.

6.2 INTRODUCTION

RNA binding protein (RBP) pathology is common to many forms of neurodegenerative disease, including amyotrophic lateral sclerosis (ALS), frontotemporal lobar degeneration (FTLD), Alzheimer's disease, and Parkinson's disease[576]. These disorders are frequently marked by the deposition of RBP inclusions in affected brain regions, for example in motor neurons in ALS and in hippocampal dentate granule cells in FTLD, as well as in glial cells in both disorders. RBP inclusion pathology is common to many forms of these disorders, including sporadic ALS/FTLD[8], familial ALS/FTLD caused by mutations in RBP genes (e.g., *TARDBP*, *FUS*)[8], and *C9ORF72*-linked familial ALS/FTLD[190,203]. The common occurrence of RBP pathology together with the intrinsic propensity of some RBPs to aggregate[50,71] suggests that RBP dysfunction is a key susceptibility factor for neurodegeneration in ALS/FTLD. Current disease models implicate both the aggregation (gain of toxic function) and attendant loss of normal RBP function in the degenerative process. RBP aggregates are frequently directly toxic to cells and disrupt numerous cellular processes, such as ER function and nucleocytoplasmic transport[57,71,577,578]. Similarly, knockdown or knockout of ALS-linked RBP genes, such as *TARDBP* or *FUS* (or their orthologs), results in developmental abnormalities, reduced lifespan, motor deficits, and substantial global alterations in gene expression in several model systems (reviewed in [579-581]).

Chronic self-association of RBPs in protein-RNA complexes may lead to both aggregation and loss of normal RBP function. RBP association with stress granules (SGs), cytoplasmic stress-induced protein-mRNA complexes, is a well-described example of this phenomenon. During cellular stress, SGs form to protect mRNAs from a harmful cellular environment and stall the translation of associated mRNAs, resulting in prioritization of translation of stress response-associated mRNAs (reviewed in Anderson et al.[96]). SGs normally dissipate following stressor removal, however, the

persistent association of RBPs in SGs during chronic stress is sufficient to induce the aggregation of RBPs, especially those containing low complexity (LC), prion-like domains. The presence of LC domains facilitates aggregation and can lead to the formation of several forms of amyloid or amyloid-like structures, including amyloidogenic oligomers, fibrils, and hydrogels[49,50,95,582,583]. ALS-linked RBPs with LC domains, including TDP-43 and FUS, associate with SGs and SG marker proteins are found in neuronal cytoplasmic inclusions in ALS patients[49,394]. SG-mediated RBP aggregation is also sufficient to induce loss of normal RBP functions. The sequestration of RBPs in SGs removes RBPs from their normal cellular milieu. TDP-43 and FUS are frequently found mis-localized in cytoplasmic SGs and depleted from the nucleus in ALS/FTLD[33,264]. Substantial alterations in gene expression result from the loss of nuclear TDP-43 or FUS and underscore the preponderant role of RBPs in regulating this process[169,584].

Collectively, these findings illustrate how the persistent association of RBPs in protein-RNA complexes is sufficient to induce toxic gain and loss of normal RBP function, particularly when aggregation-competent RBPs are present. While SGs have been the predominant complex studied in the context of ALS, emerging evidence points to dysregulation of other RNP granules and protein-RNA nuclear bodies, including paraspeckles[170,172] and gems[527,585], in ALS. The persistent association of ALS-linked RBPs with these complexes, together with a stressful cellular environment or maladaptive genetic background, may be sufficient to induce their aggregation as well as to sequester other RBPs in oligomeric aggregates. The observation of impaired paraspeckle formation in cells expressing mutant FUS and paraspeckle proteins in FUS-positive inclusions in ALS underscores this possibility[172]. As with SGs, understanding how the dysregulation of other RNP complexes contributes to both the toxic gain and loss of normal RBP function is of considerable

importance to understanding the role of RBPs in neurodegeneration and may help define new therapeutic targets for ALS/FTLD.

While RNP granules and nuclear bodies are, thus, of general interest in the study of ALS, one nuclear substructure that may be of particular relevance is the nuclear stress body (NSB). NSBs are intranuclear RNP granules that form following the onset of cellular stress and dissociate following stressor removal. NSBs form in response to a variety of stressors, including heat shock, oxidative insult, genotoxic stress, UV irradiation, proteasomal inhibition, and exposure to heavy metals (reviewed in Biamonti et al.[586]). NSB formation is a component of the cellular response to stress regulated by the heat shock transcription factor (HSF) family of proteins. During cellular stress, HSF1 undergoes reversible modification to form a DNA-binding trimer that induces the transcription of pericentromeric satellite III (sat III) DNA sequences[586,587]. Pericentromeric sat III sequences are normally transcriptionally silent and stress-induced sat III transcripts remain in close proximity to their genomic locus of origin, acting as a scaffold for RBP binding that forms the NSB[586-588]. The protein composition of NSBs is not fully defined, though NSBs are known to be enriched in pre-mRNA processing proteins, including splicing factors (e.g., SF2/ASF, SAM68) and contain HSF1 and scaffold attachment factor B (SAFB)[586]. Given the generality of the NSB response and the structural similarity of NSBs and SGs, NSBs may represent another protein-RNA complex capable of inducing RBP aggregation under conditions of chronic stress.

Persistent activation of the NSB response may also explain the pathology of RBM45 in ALS/FTLD. RBM45 is a neuron-enriched RBP whose expression is developmentally regulated[507]. RBM45 is found in TDP-43 positive cytoplasmic inclusions in neurons and glia in ALS/FTLD[164]. The protein lacks an LC domain, but is capable of self-association via a homo-oligomerization (HOA) domain[528]. In addition to its presence in cytoplasmic inclusions, RBM45 is also exhibits a

speckled nuclear staining pattern in ALS/FTLD patient tissue[164]. While this pattern is suggestive of incorporation into a nuclear body such as speckles or Cajal bodies, subsequent characterization of the protein showed a diffuse, non-speckled staining pattern under basal conditions[589]. Moreover, RBM45 physically interacts with a variety of splicing factors[589]. We, therefore, hypothesized that RBM45 is a component of NSBs and that the persistent association of RBM45 with NSBs would be sufficient to induce the aggregation of the protein. To address these hypotheses, we examined the properties of RBM45 during conditions of acute and chronic stress, mapped the domains of RBM45 necessary for it stress-associated functions, and examined ALS/FTLD patient tissue for the presence of NSBs. Our results demonstrate that RBM45 is a component of NSBs, that nucleic acid binding domains in the protein mediate this response, and that NSBs are enriched in ALS/FTLD patient tissue. Together, our results define a new aspect of RBP dysregulation in these disorders and provide new insight into the mechanisms of RBP aggregation.

6.3 MATERIALS AND METHODS

6.3.1 Cell Culture, Treatments, and Plasmid Construction

HEK293 cells were grown in DMEM with 10% fetal bovine serum and 1% penicillin/streptomycin at 37 °C in a 5% CO_2 environment. To induce nuclear stress bodies (NSBs) cells were stressed using a variety of reagents. Heat shock was performed by incubating the cells in a 42 °C environment for 1 hour followed by 1 hour of recovery[590]. Serum starvation was performed by placing cells in serum-free media for 1 hour. Cells were also treated with the following reagents to induce nuclear stress bodies: 20 µM $CDSO_4$ (2-24 hours), 400 µM H_2O_2 (2-24 hours), 1 mM sodium arsenite (0.25-1

hours), or 20 μM mitoxantrone (MTX; 2-24 hours)[590-592]. For expression of WT and domain deletion RBM45, the cDNA clone plasmid, cGST-hRBM45 (HsCD00356971; DNASU Respository, Arizona) was used. cDNA was PCR amplified using Phusion High-Fidelity DNA Polymerase (New England Biosciences) and sub-cloned into a pcDNA3 vector (Invitrogen). To provide specific tags to identify RBM45 the 3xFLAG tag (DYKDHDGDYKDHDIDYKDDDDK) or 2xHA tag (DYPYDVPDYAGGAAYPYDVPDYA), were N-terminally appended to specific proteins to generate 3xFLAG- or 2xHA-tagged constructs. Site-directed mutagenesis using overlap extension PCR was used to generate domain deletion constructs. Sequences of all constructs were confirmed with DNA sequencing and sizes of the expressed proteins were validated by SDS-PAGE and immunoblot[528].

6.3.2 Cell Immunofluorescence, Microscopy, and Digital Deconvolution

Indirect immunofluorescence was performed as in Li et al.[589]. In brief, cells were grown on 20 mM #1.5 coverslips. When cells reached 70% confluence, they were treated as indicated above, washed with 1X PBS, fixed in 4% paraformaldehyde, and permeabilized using 0.1% Triton X-100 in PBS. Following washing with 1X PBS, cells were blocked with Superblock (Scytek) for 1 hour and immersed in primary antibody solutions for 2 hours. Subsequently, they were washed 4 times (10 minutes each) with IF wash buffer (1:10 Superblock/1X PBS), and immersed in secondary antibody solutions for 1 hour. Secondary antibodies used were goat-anti-rabbit Cy2 (Abcam) and goat-anti-mouse Cy5 (Abcam). Following secondary antibody incubations, coverslips were wash 4 times as above, washed 4 times with 1X PBS, incubated in a 300 nM DAPI solution for 10 minutes, and washed 4 times with 1X PBS. Coverslips were immersed in increasing concentrations of 2,2-

thiodiethanol (TDE) as in [540], and mounted in a 97% TDE solution with a refractive index of 1.518 to match that of the immersion oil used for imaging.

The following antibodies were used for immunofluorescence and immunohistochemistry: rabbit-anti-RBM45 (Sigma), rabbit-anti-RBM45 (custom; Pacific Immunology), mouse-anti-SAFB (Lifespan Biosciences), rabbit-anti-SAFB (Proteintech), mouse-anti-HSF1 (Abcam), rabbit-anti-HSF1 (Proteintech), mouse-anti-SC35 (Abcam), mouse-anti-coilin (Abcam), mouse-anti-SMN (Sigma), mouse-anti-G3BP (Genetech), and mouse-anti-HA (Sigma). Secondary antibodies for immunofluorescence were conjugated to Cy2 and Cy5. Goat-anti-rabbit Cy2 and goat-anti-mouse Cy5 (Abcam) were used for immunofluorescence. Goat-anti-rabbit Alexafluor 488 and goat-anti-mouse Alexafluor 594 (Life Technologies) were used for fluorescence immunohistochemistry.

For image acquisition, slides were imaged on a Zeiss Observer Z1 microscope with a 1.4 NA 63x objective and LED light source. All images were acquired as three dimensional Z-stacks with a Z sampling range of 12 µM, X/Y sampling interval of 0.102 µM, and a Z sampling interval of 0.240 µM. Images were corrected for CCD shading and background subtracted. Following image acquisition, images were deconvolved using Huygens digital deconvolution software (SVI). A measured PSF was generated by imaging fluorescent 200 nm diameter Tetraspeck beads (Life Technologies) mounted in 97% TDE and inputting the obtained images into the Huygens software's PSF distiller application. All images were then deconvolved using the measured PSF together with a maximum likelihood deconvolution algorithm.

6.3.3 Tissue Immunofluorescence and Image Analysis

Tissue immunohistochemistry was performed as described in Collins et al.[164]. Tissue sections (6 µm thick) were deparaffinized, rehydrated by successive immersion increasing concentrations of

ultrapure water in ethanol, and subjected to antigen retrieval. Antigen retrieval was performed in citra buffer (pH 6.0; Biogenex) with steam heating for 30 minutes. Sections were washed in PBS, blocked using Superblock (Scytek), and immersed in primary antibody solutions overnight. The next day, the slides were washed 4 times in PBS and incubated in secondary antibody solutions for 1 hour. Subsequently, slides were again washed 4 times in PBS, and immersed in a 300 nM DAPI solution to permit visualization of nuclei. Following washing, slides were immersed in autofluorescence eliminator reagent (Millipore) to quench endogenous lipofuscin autofluorescence. Slides were mounted using #1.5 glass coverslips, with gelvatol mounting media.

6.3.4 Data Analysis, Statistics, and Figure Construction

All images were processed using NIH ImageJ[469]. The number of RBM45-positive puncta in tissue quantified by automatic thresholding of tissue immunofluorescence images and morphometric counting of puncta meeting size (0.25-2 µM) requirements. Differences in the number of puncta between groups were evaluated using the Student's t test with a *p* value of 0.01 considered statistically significant. All figures were constructed using Adobe Illustrator CS5 (Adobe).

6.4 RESULTS

6.4.1 RBM45 is a Component of Nuclear Stress Bodies

To determine the function(s) of RBM45 and relate the speckled nuclear staining pattern for the protein observed in ALS/FTLD patients (Figure 4.7) to biological function, we used

immunofluorescence in HEK293 cells. Consistent with prior results (Figure 5.4), we observed a diffuse nuclear immunoreactivity of RBM45 under basal conditions, with no speckled staining evident. Consequently, RBM45 immunofluorescence against proteins marking subnuclear structures showed no incorporation of the protein into nuclear speckles, Cajal bodies, or nuclear gems (Figure 6.1A-C). Similarly, RBM45 did not associate with cytoplasmic stress granules (SGs) following the induction of oxidative stress via administration of 0.5 mM sodium arsenite (Figure 6.1D). Following sodium arsenite treatment, however, we noted the incorporation of RBM45 into intranuclear punctate structures that resembled those seen in ALS/FTLD patient tissue (Figure 6.1D). Subsequent analysis showed that these foci correspond to the incorporation of RBM45 into nuclear stress bodies (NSBs). In stressed cells, RBM45 colocalizes with the NSB marker protein scaffold attachment factor B (SAFB) in NSBs (Figure 6.1E) and HSF1 (Figure 6.4).

Further analysis demonstrated that this incorporation into NSBs is a general stress response. As previously demonstrated, treatment of cells with H_2O_2 (400 µM), mitoxantrone (20 µM), cadmium sulfate ($CDSO_4$ [30 µM]), heat shock (1 hour at 42 °C followed by 1 hour recovery), and serum starvation (1 hour) all induced the formation of SAFB/HSF1-positive NSBs[586,591]. We demonstrate now that these same treatments induce a re-distribution of RBM45 to NSBs as well (Figure 6.1E, 6.2). In unstressed cells, both RBM45 and SAFB are diffusely localized throughout the nucleus (Figure 6.2A), while stressor treatments induce the formation of large foci with high levels of RBM45, SAFB, and HSF1 (Figure 6.2B-E).

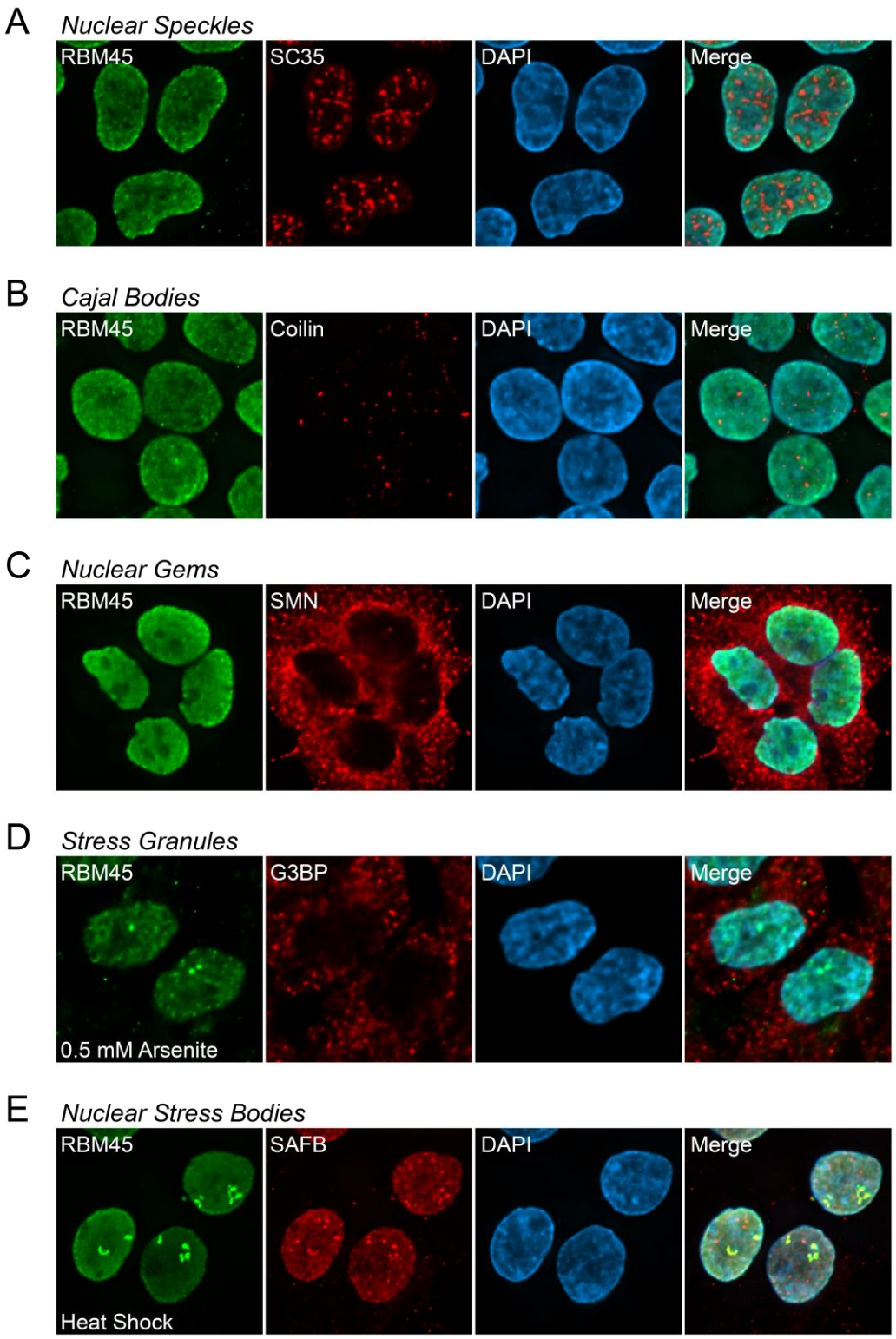

Figure 6.1 RBM45 association with nuclear stress bodies (NSBs). HEK293 cells were stained for endogenous RBM45 and marker proteins of the indicated protein-RNA complexes. Under basal

conditions, RBM45 is diffusely localized throughout the nucleus and does not associate with nuclear speckles, Cajal bodies, or nuclear gems (**A**-**C**, respectively). Following the onset of cellular stress (**D**, **E**), RBM45 redistributes to nuclear foci corresponding to NSBs. Despite stress-associated functions, RBM45 does not associate with G3BP-positive cytoplasmic stress granules (**D**). All images were acquired using a 63x, 1.4 NA objective.

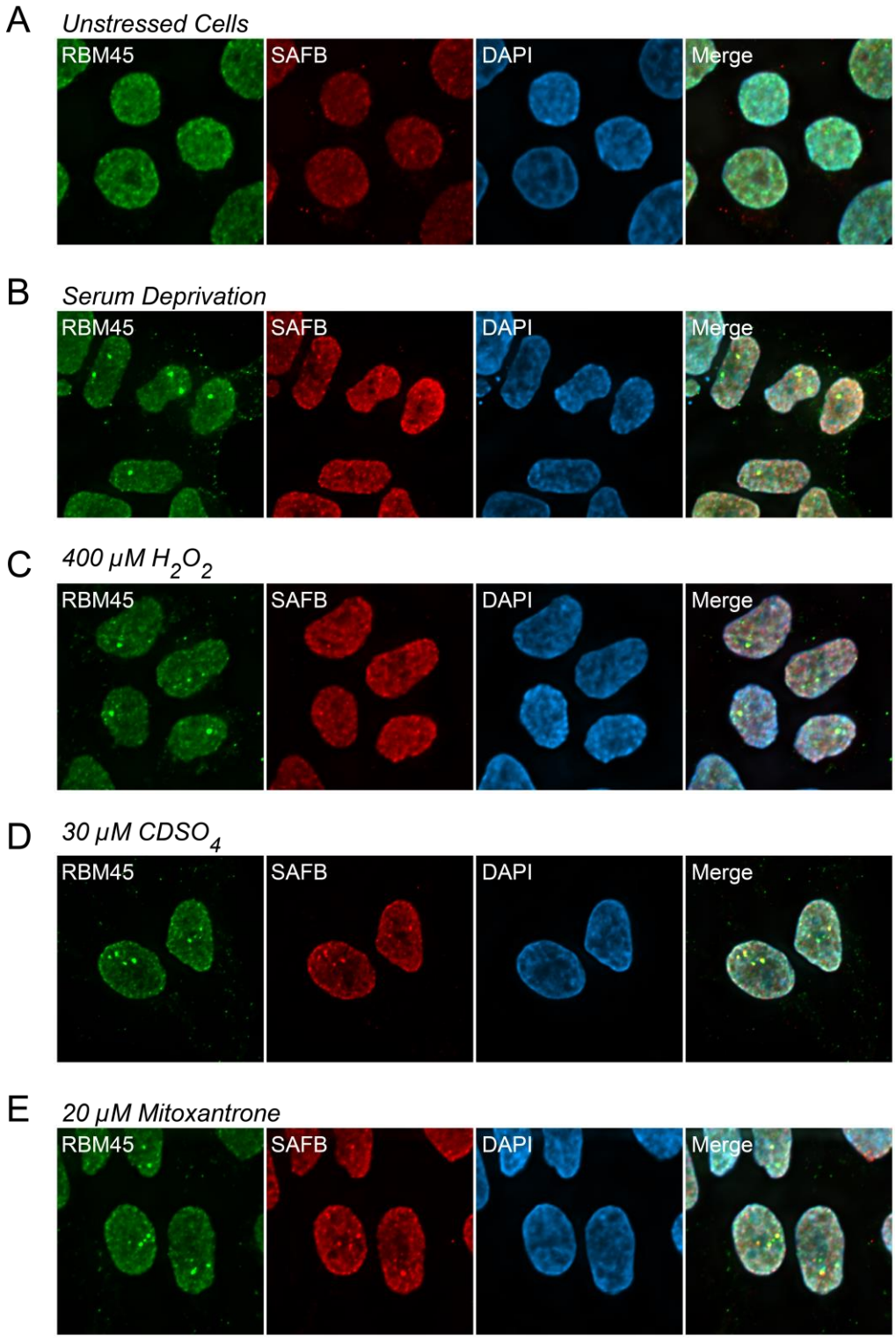

Figure 6.2 RBM45 association with NSBs is a general stress response. HEK293 cells were treated as indicated and stained for RBM45 and the NSB marker SAFB. The results show that a

variety of cellular stressors can induce NSB formation and RBM45 recruitment to NSBs. By contrast, in control cells, RBM45 and SAFB are diffusely localized throughout the nucleus, with no NSBs evident. All images were acquired using a 63x, 1.4 NA objective.

6.4.2 RBM45 RNA Binding Domains are Required for NSB Recruitment

To understand the domain elements necessary for the recruitment of RBM45 to NSBs, we used overexpression of domain deletion forms of HA-tagged RBM45, as in Li et al.[528] The domain structure of RBM45 is shown in Figure 6.3.The results of these experiments are shown in Figure 6.4. Consistent with prior studies[591], overexpression of NSB protein components resulted in a larger average size and overall number of granules in cells subjected to heat shock (Figure 6.4). In contrast, no NSBs were evident in unstressed cells (Figure 6.4A), despite the overexpression of RBM45. The results also demonstrate that several domains in the RBM45 protein are required for its association with NSBs. Removal of the nuclear localization sequence (NLS) resulted in cytoplasmic sequestration of RBM45 that prevented its incorporation into NSBs. RRMs 2 and 3 were also required for the incorporation of RBM45 into NSBs. This is consistent with recent work showing that many RBM45 protein-protein interactions are RNA-dependent[589]. By contrast, the homo-oligomerization (HOA) domain that is necessary for RBM45 self-association, was not requisite for NSB recruitment. This finding argues that the association of RBM45 with NSBs is driven by RRM2/3 binding to sat III transcripts, as has been proposed for other NSB proteins[586].

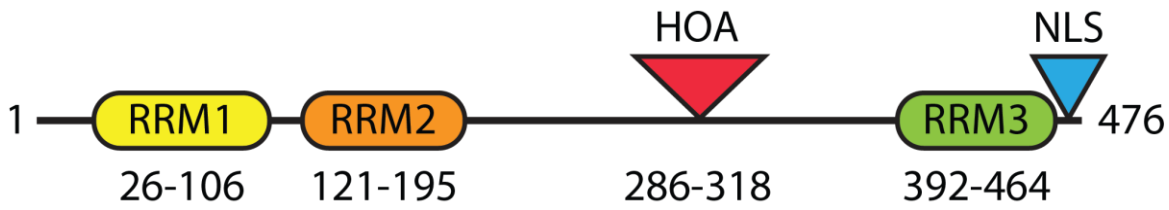

Figure 6.3 RBM45 Domain Structure. A schematic of the domains in the RBM45 full length protein is shown. RRM = RNA recognition motif, HOA = homo-oligomerization domain, NLS = nuclear localization sequence.

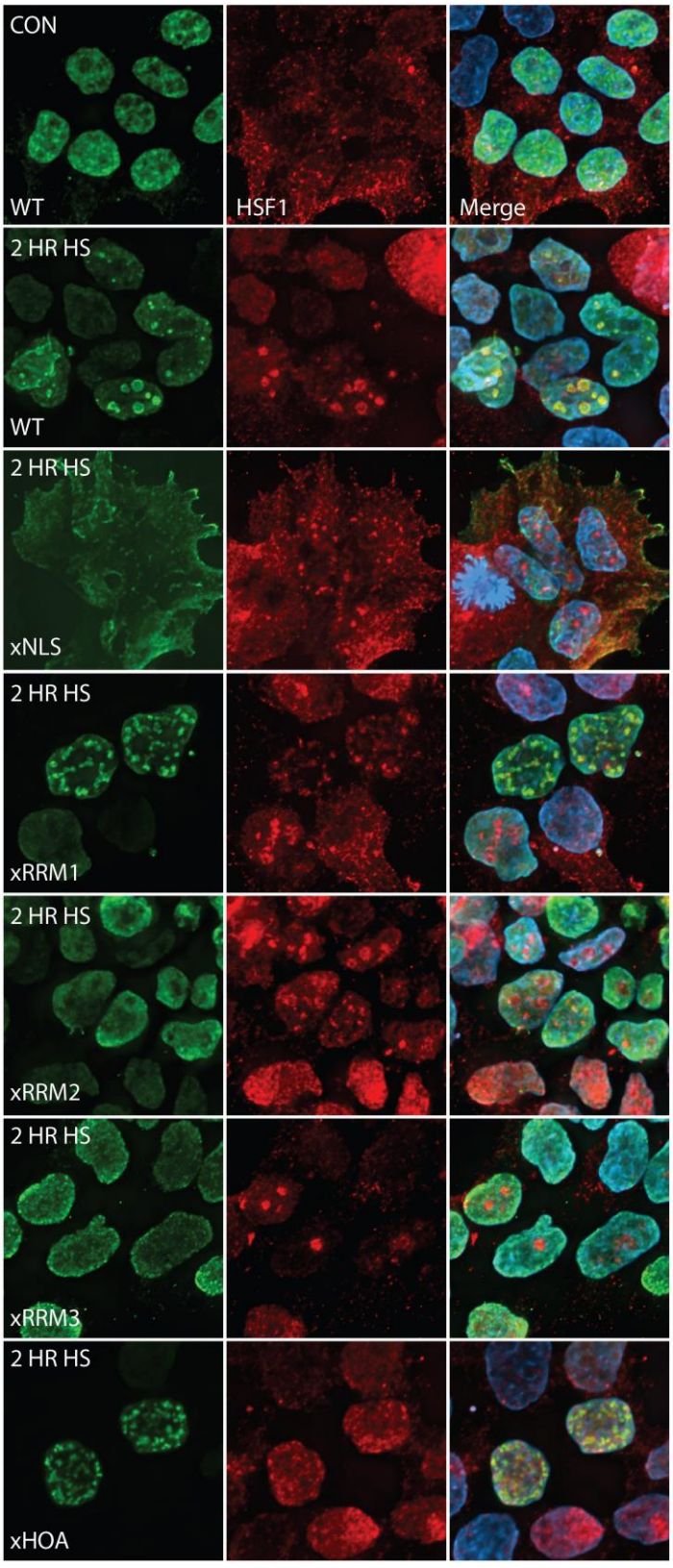
CON
WT
HSF1
Merge
2 HR HS
WT
2 HR HS
xNLS
2 HR HS
xRRM1
2 HR HS
xRRM2
2 HR HS
xRRM3
2 HR HS
xHOA

Figure 6.4 RBM45 domain deletion experiments. HEK293 cells were transiently transfected to express domain deletion constructs of RBM45 as indicated in the figure. Following the transfection, cells were treated as indicated and stained for the HA tag and the NSB marker HSF1 to evaluate the incorporation of the tagged construct into NSBs. As shown, the NLS, RRM2, and RRM3 are necessary for RBM45 incorporation into NSBs. All images were taken with a 63x 1.4 NA objective.

6.4.3 Relationship of TDP-43 and FUS to NSBs

RBM45 has been shown to physically interact with TDP-43 and FUS[528,589] and is found in TDP-43 positive cytoplasmic inclusions in ALS/FTLD[392]. We, therefore, sought to determine whether TDP-43 and FUS are also components of NSBs and whether disturbing physiological TDP-43/FUS levels would induce NSBs. For the first aim, cells were heat shocked as above and stained for RBM45, TDP-43, and FUS. As shown in Figure 6.5A, TDP-43 and FUS do not associate with RBM45-positive NSBs. This is in keeping with studies in ALS/FTLD tissue, in which RBM45 nuclear puncta were distinct from TDP-43 (Figure 4.7). Next, we asked whether disrupting TDP-43 or FUS levels would cause the formation of NSBs (Figure 6.5B). Cells are highly susceptible to alterations in physiological TDP-43/FUS levels, either by knockout/down or overexpression[497]. We used overexpression of TDP-43, FUS, and a vector control to simultaneously disrupt physiological RBP levels and further evaluate whether TDP-43 and FUS are components of NSBs. As shown in Figure 6.5, the overexpression of TDP-43 was sufficient to induce the formation of NSBs, though TDP-43 is not a component of these structures. FUS overexpression induced nuclear translocation of HSF1, but did not result in the formation of NSBs, and the vector control also did not exhibit NSBs following transfection.

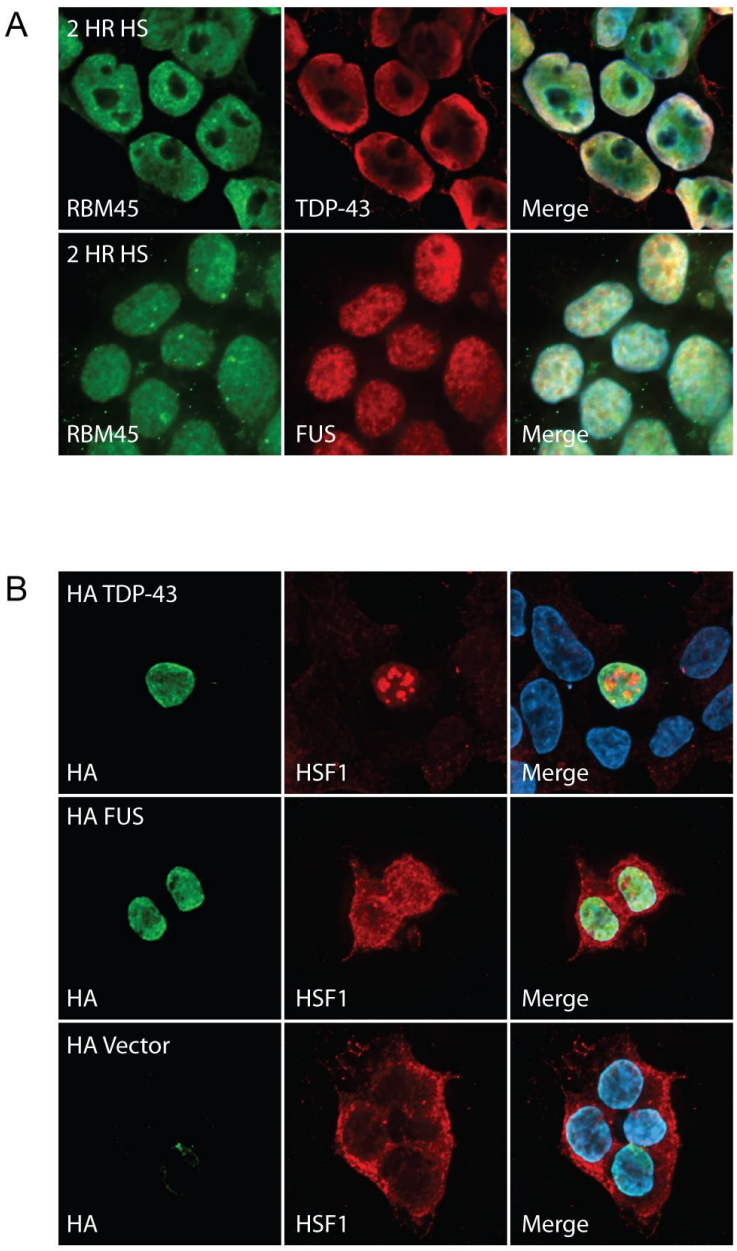

Figure 6.5 TDP-43, FUS, and nuclear stress bodies. A. HEK293 cells were heat-shocked for 2 hours at 42 °C and evaluated for the presence of TDP-43 and FUS in RBM45-positive NSBs. Neither protein redistributes to the nuclear RBM45 foci following heat shock. **B.** TDP-43 and FUS were then overexpressed in HEK293 cells to determine how disruption of the levels of these proteins affects the formation of NSBs. As shown, TDP-43 overexpression was sufficient to drive NSB

formation, while FUS and vector expression did not result in NSB formation. All images were taken with a 63x, 1.4 NA objective.

6.4.4 Persistent RBM45 NSB Association Leads to Nuclear Inclusion Formation

To test whether the persistent association of RBM45 with NSBs is capable of inducing aggregation of the protein, we treated cells with 20 μM mitoxantrone (MTX) or 30 μM cadmium sulfate ($CDSO_4$) for varying amounts of time. We also sought to determine whether other NSB proteins, specifically SAFB and HSF1, are also incorporated into potential NSB-derived protein aggregates. The results of these experiments are shown in Figure 6.6. As shown, under basal conditions, NSBs are not observed, while either stressor treatment induces a robust NSB response. Transient NSBs were induced by 6 hour MTX or 2 hour $CDSO_4$ treatment. We hypothesized that chronic stress would be sufficient to induce RBM45 inclusion formation as has been suggested for TDP-43/FUS aggregation following persistent association with stress granules[95]. Thus, cells were treated for 24 hours and allowed to recover for 4 hours. As shown, in either treatment, RBM45 nuclear foci persist, while NSB marker proteins SAFB and HSF1 dissipate from NSBs following recovery. These results suggest that the persistent association of RBM45 with NSBs is sufficient to induce its aggregation.

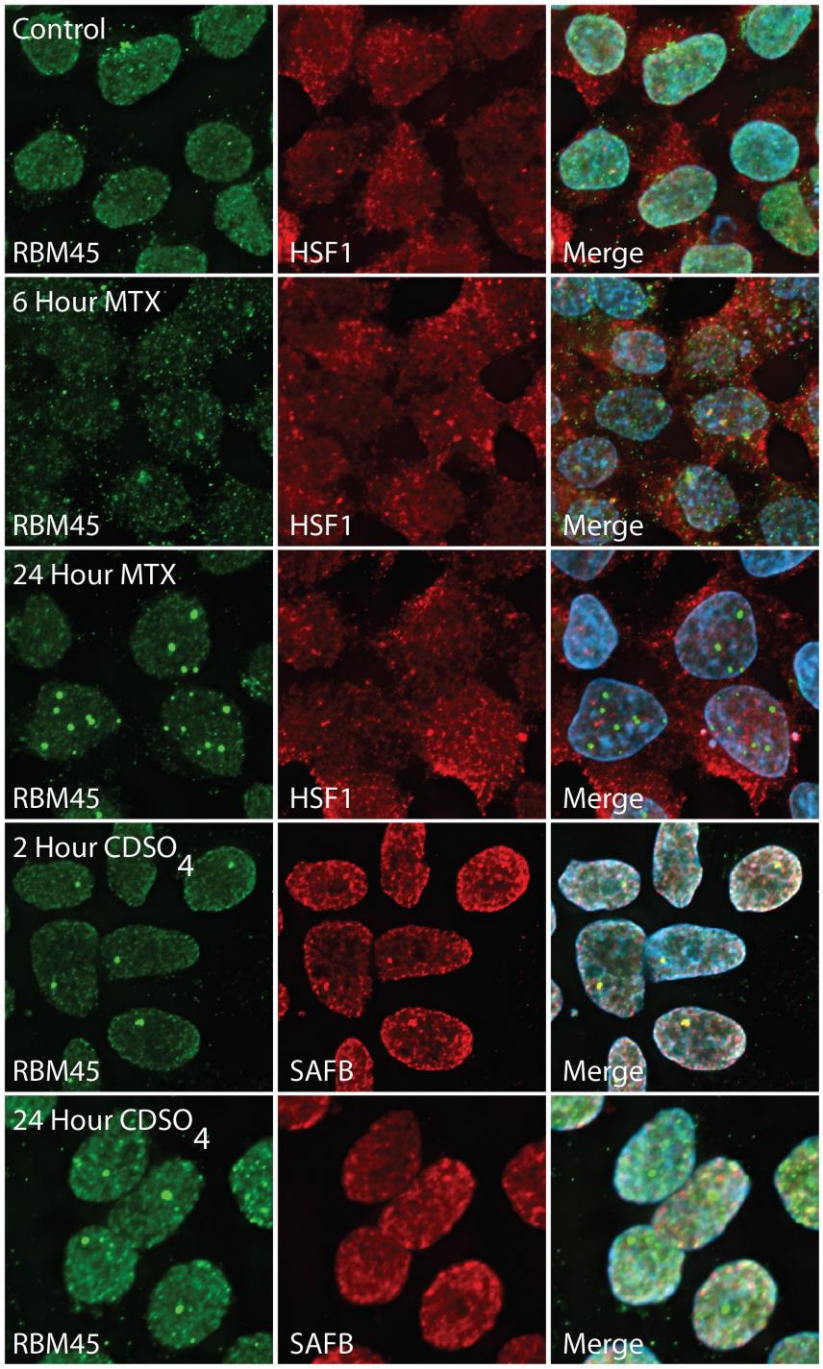

Figure 6.6 Persistent NSB association drives RBM45 inclusion formation. HEK293 cells were treated as indicated to examine the potential aggregation of NSB proteins under chronic stress. Shorter duration treatments (6 hour MTX; 2 hour $CDSO_4$) induce the NSB response. Chronic (24 hour treatment) stress followed by recovery shows dissipation of NSB marker proteins from NSBs

and reveals persistent RBM45-positive nuclear inclusions. All images were taken with a 63x 1.4 NA objective.

6.4.5 Observation and Quantification of RBM45-Positive NSBs in FTLD

For the final phase of the study, we quantified the number of RBM45-positive NSBs in dentate gyrus granule cells of FTLD and healthy control subjects. The results of these experiments are shown in Figure 6.7. As shown, the number of RBM45-positive NSBs was significantly increased in FTLD patients as compared to controls. We also sought to determine whether HSF1 and SAFB positive NSBs could be detected in human tissue. To that end, we stained healthy control and FTLD tissue sections with antibodies against these proteins. The results of these experiments are shown in Figure 6.8. As shown, NSBs were not detectable in the hippocampus of healthy control subjects. In contrast, numerous NSBs and enhanced nuclear HSF1 reactivity were seen in multiple hippocampal cell types, including dentate gyrus granule cells and cells from the CA1 region of the hippocampus.

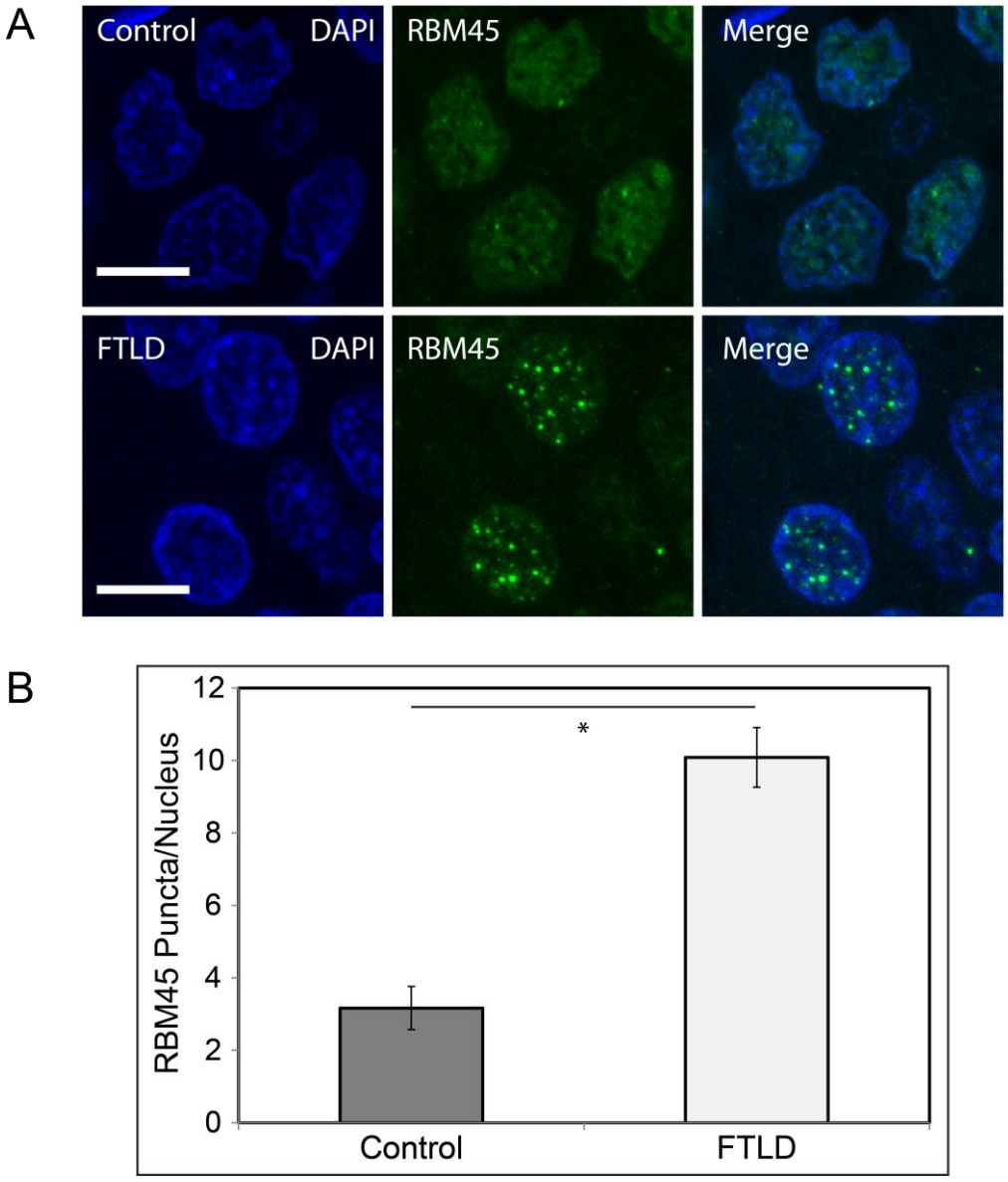

Figure 6.7 RBM45 NSB quantification in FTLD. The number of RBM45 positive puncta in dentate gyrus granule cells was quantified using immunofluorescence and image processing. A. Representative immunofluorescence images of a healthy control and FTLD subject. All images were taken with a 63x 1.4 NA objective and the scale bars = 10 µm. B. Resultant quantification. A total of n = 5 controls and n = 5 FTLD tissue sections were stained and n = 50 dentate granule cells were counted for each section. The results show the mean ± SEM. * = $p < 0.01$.

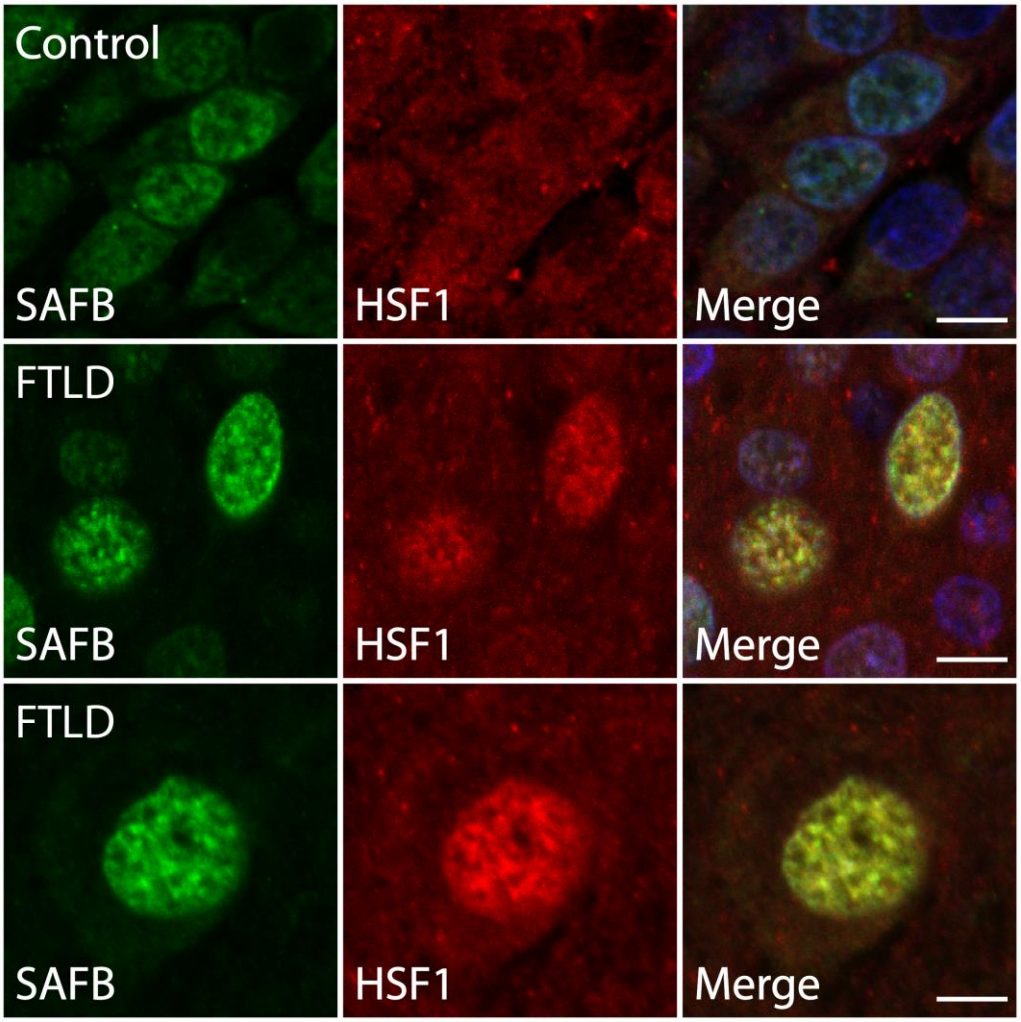

Figure 6.8 Nuclear Stress Bodies (NSBs) in FTLD Patient Tissue. NSBs were visualized in human FTLD tissue using antibodies against the NSB marker proteins SAFB and HSF1. In the top series of panels, staining for SAFB and HSF1 is diffuse in hippocampal dentate gyrus cells and no NSBs are evident. In the middle and bottom panels, SAFB and HSF1-positive NSBs are seen in hippocampal dentate granule cells (middle) and CA1 neurons (bottom). All images were taken with a 63x 1.4 NA objective and the scale bar = 10 µm.

6.5 DISCUSSION

The purpose of the present study was to characterize the biological functions of the RNA binding protein (RBP) RBM45 as they relate to the incorporation of the protein into speckled nuclear foci in ALS/FTLD. To that end, we identified RBM45 as a component of nuclear stress bodies (NSBs), a stress-induced nuclear protein-RNA complex templated on pericentromeric satellite III DNA transcripts. The association of RBM45 and NSBs is part of the general cellular response to stress and occurs following the onset of a variety of stressors (Figures 6.1, 6.2). Other studies have shown that the formation of NSBs occurs in response to several distinct forms of cellular stress, including oxidative, genotoxic, heat shock, and hyperosmotic stress[586-592]. Our results extend these findings by further demonstrating the generality of the NSB response and identifying RBM45, an ALS/FTLD-linked RNA binding protein, as a component of NSBs. The generality of the NSB response (Figure 6.2), the numerous forms of intracellular stress that occur in ALS/FTLD[40], and the increased numbers of NSBs in FTLD patient tissue (Figures 6.7, 6.8) observed here collectively provide compelling evidence for contributions of NSBs to the RBP pathology of ALS/FTLD and further underscores the contribution of RBP dysfunction to disease.

NSBs were discovered in the 1980's[586] and since that time, considerable progress has been made in understanding the mechanisms of the formation of these structures. The onset of cellular stress results in the trimerization of heat shock factor 1 (HSF1). The DNA binding competent HSF1 trimer induces the transcription of pericentromeric satellite III (sat III) repeat sequences[586]. These sequences act as a scaffold for the binding of the protein constituents of NSBs. The genomic origins of sat III transcripts are primarily in region 9q12, with other regions in chromosomes 12 and 15 also containing sat III repeats. Sat III transcripts from the 9q12 region are the most-well studied non-coding RNAs involved in the NSB response, however[586,590,591]. Sat III repeats originating from the

9q12 locus are G-rich strands and the association of RBM45 with NSBs likely derives from sat III binding, as RBM45 preferentially binds G-rich RNA[507]. This hypothesis is in keeping with previous data showing the necessity of RNA binding for RBM45 interaction with other RBPs[589] and incorporation into NSBs (Figure 6.4).

Despite advances in our understanding of the formation of NSBs, their function(s) remain elusive. One hypothesis suggests that NSBs act to repurpose gene expression in a manner favoring the cellular response to stress by sequestering selected RBPs in NSBs[586]. This view would suggest that the aggregation of RBM45 resulting from its persistent association with NSBs is a by-product of the over-activation of the NSB response. Similar hypotheses have been proposed for the aggregation of TDP-43 and FUS by virtue of their sustained incorporation into stress granules (SGs)[95]. TDP-43 and FUS are distinct from RBM45, however, in that they possess prion-like, low-complexity domains that facilitate their aggregation[102]. RBM45 does possess a homo-oligomerization (HOA) domain that permits the protein to self-associate and bind other proteins. While this domain is inessential for RBM45 incorporation into NSBs (Figure 6.4), it may nevertheless facilitate the aggregation of the protein following chronic stress (Figure 6.6). This would make RBM45 similar to FUS, whose LC domain is not required for SG association, but does mediate the extent of incorporation into SGs[49].

We also asked whether TDP-43 and FUS participate in the NSB response and found that neither protein is a component of NSBs (Figure 6.5). This is consistent with the lack of TDP-43 positivity for RBM45 nuclear foci in FTLD patient tissue (Figure 4.7). Nevertheless, disruption of homeostatic TDP-43 levels was sufficient to induce NSB formation in HEK293 cells, further underscoring the importance of homeostatic RBP levels to cellular viability[52,54,56]. The absence of TDP-43 from NSBs does, however, raise the question of how RBM45 is incorporated into

cytoplasmic inclusions in neurons and glial cells in ALS/FTLD (Figure 4.7). One possibility is that RBM45 undergoes nucleocytoplasmic transport as part of its normal functions. Evidence in favor of this concept comes from the identification of RBM45 protein-protein interactions with RNA transport proteins, nucleocytoplasmic shuttling proteins, and cytoplasmic-translation associated proteins (Supplemental Table 4). Moreover, while RBM45 is predominantly nuclear by immunocytochemistry, we nevertheless detect low levels of the protein in cytoplasmic fractions by Western blot[528]. This together with the presence of a classical NLS in the protein's domain structure argues that RBM45 possesses cytoplasmic functions. The performance of these functions together with nucleocytoplasmic transport defects in ALS/FTLD patients[203,204] could lead to the accumulation of excessive levels of cytoplasmic RBM45 that are then incorporated into TDP-43 inclusions. The greater extent of RBM45 pathology in nucleocytoplasmic transport-deficient *C9ORF72* fALS patients (Supplemental Table 3) provides evidence in support of this concept.

The NSB response is found only in primate cells, which contain sat III DNA sequences not found in lower vertebrates, such as rodents[586]. We provide evidence of upregulation of the NSB response in FTLD patients (Figures 6.7, 6.8) and the sufficiency of this upregulation to induce the aggregation of RBM45 (Figure 6.6). Removal of RBPs from their normal cellular milieu is sufficient to induce substantial alterations in gene expression[51,165] and disruption of TDP-43 levels can induce the NSB response (Figure 6.5). Both of these observations suggest that non-primate animal models of ALS/FTLD may insufficiently capture the full extent of RBP aggregation, loss of function, and dysregulation of gene expression, particularly as related to the contributions of RBM45 to these phenomena in ALS/FTLD. Future studies examining the NSB response in patient-derived IPSC motor neurons may provide a useful means to more accurately assess the contributions of RBM45 to neurodegeneration in ALS/FTLD. Moreover, comparisons of gene expression changes found in these

cell lines to those observed in transgenic rodent lines (e.g., TDP-43, *C9ORF72*-repeat expansion, etc....) may provide useful information about the strengths and weaknesses of transgenic animal lines in the modeling of disease. One such study has suggested that rodent models fare poorly in modeling transcriptomic changes associated with human ALS/FTLD[593]. Thus, further comparisons are warranted and have considerable implications for the design of therapeutic interventions and clinical trials for these diseases.

In summary, we sought to characterize the biological function(s) of RBM45 related to its incorporation into nuclear foci. We found that these foci derive from RBM45's RNA binding-dependent incorporation into NSBs and that the persistent association of RBM45 with NSBs is sufficient to induce its aggregation. This provides a plausible explanation for the increased presence of RBM45 foci in the nucleus of FTLD patients, foci that are not typically observed in healthy control subjects. Collectively, these results define a new stress-response pathway altered in ALS/FTLD, provide further evidence of the role of protein-RNA complexes in RBP aggregation, and suggest new therapeutic targets for these disorders.

7.0 GENERAL DISCUSSION

7.1 GLOBAL PROFILING STRATEGIES IN THE STUDY OF ALS

The ability of global profiling approaches to identify novel mechanisms of disease/pathology makes it of value for further stratification of the ALS/FTLD patient population. The recognition that ALS/FTLD exist as a spectrum of disorders has led to the designation of subtypes of disease. While classification schemes for ALS are not as developed as those for FTLD[594], improved genomic, transcriptomic, proteomic, and pathological profiling of patients should lead to improvements in the stratification of ALS and creation of sub-types of disease. This, consequently, should lead to improved clinical trial design and implementation for ALS[595]. The accurate and reliable delineation of subtypes of disease will require large-scale, multi-center efforts directed towards the genomic, transcriptomic, and proteomic global profiling of ALS patients and model organisms.

7.1.1 CSF Biomarkers for ALS

Studies of proteomic alterations to the cerebrospinal fluid (CSF) in ALS began several decades ago, when isoelectric focusing and electrophoresis were used to define blood brain barrier disruption in ALS by virtue of altered protein composition of the CSF[596]. Since that time, the utility of CSF protein levels to the study of ALS has been demonstrated via many approaches. Given the inherent difficulty in accurately diagnosing ALS[327,334], the number of motor neurons typically lost by the time

of symptom presentation[327], the increasing recognition that ALS is likely a spectrum of disorders with numerous distinct etiologies[336,337], and the low success rate of ALS clinical trials[595], CSF protein biomarkers (diagnostic, prognostic, and therapeutic) have received increasing focus in the study of ALS. At present, the best-studied fluid biomarkers of ALS are the heavy and light chains of the neurofilament protein. Phosphorylated neurofilament heavy chain (pNFH), is a sensitive and reliable biomarker of disease[323,597]. Neurofilament phosphorylation influences axonal diameter, axonal conduction velocity, and the rate of axonal transport, and hyperphosphorylated, aggregated neurofilament is a common pathological finding in axons in various forms of ALS[78]. Thus, aggregated, hyperphosphorylated neurofilament heavy chain is hypothesized to be released from injured, dying axons during the ALS disease process. Consistent with this notion, pNFH is often not detectable in control CSF, while it may reach ng/ml levels in ALS patients[323]. Similar results have been obtained by measuring CSF neurofilament light chain (NFL)[598] and results presented herein also suggest that neurofilament medium (NFM) levels are substantially increased in CSF as well (Table 2.2). Given the necessity of the co-polymerization of NFH, NFL, and NFM for neurofilament function, it is perhaps unsurprising that all three subunits can be detected in the CSF following motor neuron death in ALS.

While neurofilament alone performs well as a diagnostic and prognostic biomarker of ALS[597,598], more recent studies have demonstrated improved performance when panels of protein markers are used. This finding has been shown for panels with[323] and without pNFH[359]. The development of protein biomarker panels has traditionally relied upon existing knowledge of proteomic alterations associated with disease. For example, multiplex profiling of inflammatory molecules, such as cytokines, has been performed to determine the diagnostic value of CSF cytokines and the time course of cytokine elevations in ALS[599]. Previous implementations of this

strategy have had several limitations. First, the number of proteins evaluated has typically been low. This owes, in part, to the methods used, which tend to employ targeted profiling of a known subset of proteins or an unbiased approach with limited detection capabilities, such as SELD-TOF MS[359]. Global, unbiased profiling yields a larger number of identified proteins, and consequently, is likely to identify biomarkers with better predictive ability. This latter point is related to a second issue of targeting protein subsets for biomarker panels, which is their reliance on existing knowledge of disease, as in the case of pNFH. Unbiased approaches that provide complete proteomic profiles of disease, control, and disease control subjects are likely to not only yield more robust markers/marker panels, but also provide new insights into mechanisms of disease. We have demonstrated the plausibility of this idea, showing that CSF levels of extracellular matrix (ECM) and synaptic proteins are decreased in CSF (Table 2.2, Figure 2.5), that these alterations can reliably separate ALS from control/disease control subjects (Figure 2.9), and that they correspond to changes occurring in motor neurons in ALS patients (Figure 2.7). The application of feature selection and machine learning to proteomic profiles and spectral count data is still relatively inchoate[386], but the continued application of these methods together with large-scale efforts to profile disease populations should ultimately lead to diagnostic and prognostic markers of disease with high sensitivity and specificity.

The identification of candidate biomarkers of disease necessitates an evaluation of their longitudinal stability. In the field of ALS, unfortunately, such studies are relatively rare. Many prior studies in ALS used a cross-sectional approach to examine correlations between candidate biomarkers and clinical markers of disease progression and survival, with few studies measuring changes in biomarker levels in longitudinal biofluids collected within individual patients. Those studies using a longitudinal approach have tended to shown that CSF markers are stable throughout the course of disease. NFL levels in CSF, for example, remain relatively constant over the

progression of disease in ALS patients[598]. Longitudinal analyses of NFL and patient survival indicated that NFL levels in CSF were inversely correlated with patient survival, providing further support for the hypothesis of these proteins being released from dying motor neurons. Cystatin C was one of the first CSF protein biomarkers suggested for ALS as part of a SELD-TOF MS screen[359], which identified decreases in CSF levels of the protein of ALS patients. Subsequent longitudinal validation of this finding by ELISA demonstrated that cystatin C levels decline within ALS patients over the course of disease and that initial cystatin C levels were predictive of survival, with lower levels corresponding to a shorter duration of disease[391]. Despite promising results from these two biomarkers, considerable additional work is needed to validate many other candidate markers of disease, including those identified here. Preliminary evidence does indicate longitudinal decreases in APLP1 (Figure 2.10) in ALS patients (unpublished observation). In part, the lack of longitudinal validation of other markers can be attributed to the difficulties associated with the collection and storage of CSF samples. ALS patients may experience increasing difficulty in traveling to clinical sites and undergoing lumbar puncture for CSF collection. This has led to studies designed to extend CSF biomarkers to plasma, which have met with positive results[598], though plasma markers typically have poorer specificity/sensitivity than their CSF counterparts[317].

An equally important and relatively unexplored aspect of CSF biomarkers in ALS is identifying biomarkers that can reliably signal the onset of pathological processes in ALS in advance of substantive motor neuron degeneration (predictive biomarkers). Such markers would be of vital importance in designing and testing preventative therapeutic interventions. Naturally, such approaches are not applicable to sporadic patients, as the unknown etiology makes determining a priori who will develop disease impossible. Studies using fALS patients and model systems may hold promise in this regard, however, and may lead to the identification of proteins that reliably

indicate the onset of general degenerative processes in motor neurons or inflammatory activity in surrounding glial cells. CSF pNFH and NFL are increased in fALS and sALS patients at symptom onset, however, increased levels of either subunit could not be detected at pre-symptomatic stages in fALS subjects in a recent study[600]. This provides further evidence in the support of the hypothesis of neurofilament release from dying neuron in ALS. Thus, while CSF neurofilament proteins may be excellent biomarkers for the diagnosis of ALS and prognostic markers of disease progression, they are unlikely to serve as pre-symptomatic markers of disease initiation. Similar results are to be expected for other markers of pathology, such as CSF TDP-43[601]. Indeed, the very notion that CSF biomarkers arise from dying motor neurons may make CSF proteomic profiling unsuited to the detection of pre-symptomatic disease onset. Instead, a combination of genetic sequencing to identify susceptibility[316], assessment of contributing lifestyle risks, and neurophysiological testing[602] may be better suited to early detection, though determining the point in disease at which known CSF biomarkers become detectable remains an open and relevant question.

Despite negative results from analyses of neurofilament in pre-symptomatic fALS subjects, this patient population will, nevertheless, provide a unique opportunity to investigate biomarkers in a human population prior to disease onset. At present, two clinical research studies are enrolling pre-symptomatic subjects with SOD1 mutations or *C9ORF72* repeat expansions. The samples and clinical information collected from these individuals will provide a substantially larger set of samples (both in overall number and per patient longitudinal number). Global profiling of CSF, tissue, and other sample types will provide a more extensive cataloging of molecular characteristics of pre-symptomatic patients that will yield insight into the composition of CSF prior to symptom onset. Moreover, retrospective correlation of CSF proteomic alterations with changes in clinical parameters should aid in determining which markers serve as reliable indicators of the onset of

disease. This approach, together with the development of animal models that accurately recapitulate the genetic and pathological aspects of these forms of ALS should facilitate the development of therapeutic interventions designed to slow or prevent the onset of disease. In the case of SOD1 and *C9ORF72*, these approaches are particularly applicable, as misfolded SOD1 and *C9ORF72* DPRs can be detected in the CSF[205,603]. Misfolded SOD1 has been hypothesized to facilitate the cell-to-cell spread of disease via prion-like induction of aggregation of mutant SOD1 from soluble monomers to insoluble aggregates[604]. Thus, determining the point at which mutant SOD1 and oligomeric SOD1 are present in CSF has considerable implications for understanding the time course of disease onset and progression in *SOD1* fALS patients. Similarly, the presence of DPRs in CSF suggests the possibility of a similar phenomenon occurring in *C9ORF72* patients, though this has not been directly demonstrated. Nevertheless, the toxicity of DPRs in neuronal cell culture models[605] implies that DPRs in the CSF would have deleterious consequences for motor neurons. The results from these studies and others examining pre-symptomatic changes will thus have considerable implications for models of disease spread and our understanding of how extracellular factors contribute to motor neuron death in ALS.

A final use for CSF protein biomarkers of ALS is in the monitoring of response of patients to therapeutic interventions. The poor track record of ALS clinical trials[595] has led to calls for the inclusion of biomarkers of target engagement in all future trials[606]. CSF protein biomarkers can serve this purpose to the extent that they reflect the ongoing injury and death of motor neurons and therapeutic interventions target the process resulting in the proteomic alterations seen in CSF. Inflammation is a finding common to many forms of ALS and increased levels of pro-inflammatory factors are thought to drive non-cell autonomous mechanisms of disease. While therapeutics designed to target inflammation have performed poorly in clinical trials[280-282], these studies did not

use CSF protein biomarkers of inflammation to assess whether target engagement was actually achieved during the trial. A more recent study did achieve this, showing that tocilizumab reduced transcription of pro-inflammatory factors in circulating monocytes and that this transcriptional decrease resulted in decreased circulating levels of inflammatory factors in CSF[607]. Our results (Table 2.2, Figure 2.6, Table 3.1, Figure 3.5) likewise suggest readily detectable markers of inflammation in the CSF that could be used for this purpose. Beyond the utility of such markers as measures of therapeutic response, they may also prove useful for settling the, at times, contentious[608] issue of the contribution of inflammation to neurodegeneration in ALS. While the diagnosis of fALS will continue to necessarily rely on clinical assessment and genetic testing, CSF levels of mutant proteins may be useful measures of the effectiveness of therapies targeting these forms of ALS. The detection and quantification of misfolded SOD1 and *C9ORF72* DPRs in CSF[603,605] may therefore be a useful readout of the effectiveness of therapies, such as anti-sense oligonucleotides, targeting the production of these proteins. SOD1 antisense oligonucleotides have recently been used in a human clinical trial[609]. This phase I safety study did not use CSF SOD1 as pharmacodynamic biomarker, so the effects of the treatment on CSF SOD1 levels are unclear. Given the absence of serious adverse events, however, future Phase II/III trials using this compound will likely determine CSF SOD1 levels. The use of CSF SOD1 in this manner is particularly illustrative of the utility of CSF therapeutic response biomarkers, because the relationship between disease and production of the mutant protein is relatively direct. While measuring CSF DPR levels may likewise provide insight into therapies targeting the production of this species, the causes of neurodegeneration in *C9ORF72* ALS are less well-defined and likely multifactorial. Proposed mechanisms include DPRs, RNA foci, haploinsufficiency, and impaired nucleocytoplasmic transport[610]. Thus, in this and other forms of ALS where multiple factors contribute to motor neuron degeneration, multiple markers of

therapeutic response via targeted or global profiling may be necessary to accurately assess the potential of a therapeutic intervention.

7.1.2 Genomic Studies in ALS

The last decade has seen remarkable advances in our understanding of the genetics of fALS, with approximately 70% of fALS accounted for by known mutations in fALS-linked genes[316,334]. This represents a gain of approximately 50% in the last ten years. This rapid growth is a result of two factors: (1) the substantial portion of fALS attributable to the *C9ORF72* repeat expansion (40% of fALS) and (2) the continued advancement of genetic sequencing technologies. The sheer number and diversity of genes whose mutations leads to familial forms of ALS makes evident the idea that dysfunction in several cellular pathways is sufficient to cause the cell-type specific degeneration seen in ALS and FTLD. Having established this, the more daunting challenge is for researchers to delineate how fALS-linked mutations exert their deleterious effects and to what extent these unique and rare forms of ALS share pathomechamisms with the more common sporadic form of disease. RNA binding protein pathology seems to be a unifying aspect of almost all forms of ALS, with the notable exception of *SOD1* fALS. More specifically, sporadic, *TARDBP* fALS, *C9ORF72* fALS, and familial forms linked to genes apparently unrelated to TDP-43 such as *CHMP2B* and *OPTN* fALS all exhibit TDP-43 pathology in motor neurons. Our results extend this finding by demonstrating that RBM45 pathology is likewise common to several forms of ALS (Figure 4.3, Supplemental Table 3). Moreover, our proteomics results demonstrate that these changes extend to the CSF proteome and can be used to separate both sALS and fALS from healthy and disease control subjects (Figure 2.9). Thus, it seems likely that CSF proteomic changes reflect downstream events resulting from motor neuron degeneration. Similar reasoning has been used in the interpretation genome-wide association

studies (GWAS) in ALS. Variation in loci in the *KIFAP3* and *EphA4* genes have been found to significantly impact survival in ALS patients[308,399]. The *KIFAP3* protein is a kinesin-associated motor protein and reduced expression of the protein is associated with reduced survival. Conversely, SNPs conferring reduced expression (or pharmacological inhibition in model organisms) of EphA4, an axonal repellent molecule, results in enhanced survival in ALS patients[399]. Thus, one interpretation of these results has been that variability in the expression of these genes conferred by SNPs influences the rate of motor neuron degeneration, but likely does not, in and of itself, initiate the degenerative process[316].

The identification of risk or causative genetic factors in apparently sporadic ALS is a related field of inquiry with implications for the classification of disease. The estimated heritability of ALS is 21%[312], though the confidence interval for this value is large and substantially larger estimates of disease heritability have been reported[611]. One group proposed an oligogenic basis of sALS and used screening of multiple fALS-linked genes in sALS patients to test this hypothesis. The results showed that variability in multiple fALS-linked genes is found in apparently sporadic ALS patients[612]. While this finding provides support for both an oligogenic basis of disease and important genetic contributions to sporadic ALS, it also suggests considerable complexity in the genetics of the disease. Because this study used only screening for mutations in a subset of known fALS-linked genes, it is likely that additional, unknown combinations of *de novo* mutations of known fALS genes, unknown fALS genes, and other genes are sufficient to produce the sporadic form of disease. The potential combinatorial complexity of this situation is daunting and may make a truly complete understanding of the genetics of ALS unattainable. Nevertheless, continued genomic sequencing of fALS kindreds to identify genes sufficient to cause disease in an autosomal-dominant manner is warranted[316]. Currently, approximately 70% of fALS is explained by mutations in known ALS

genes; however, given the small proportion of fALS explained by most genes (often 1-2%[316,613]), there are likely many fALS genes left to identify. Further complicating matters is the fact that this does not take into account environmental factors that contribute to the development of disease, which are estimated at 0.39[611]. Aside from rare geographical clusters, environmental risk factors have been hard to define for ALS, but may include smoking, exposure to heavy metals, military service, and agricultural chemical exposure[614]. The contributions of non-chemical environmental factors have been difficult to replicate and their mechanism(s) of action remain uncertain to the extent that they are true contributors to the development of disease. Collaborative efforts are presently underway to perform whole genome sequencing for large numbers of ALS patients in worldwide project to sequence and generate iPS cells from large numbers of ALS patients. These efforts will likely lead to the identification of new causative genes for ALS and genetic polymorphisms that influence rate of disease progression.

7.1.3 Transcriptomic Profiling in ALS

The common occurrence of RBP pathology in several forms of ALS suggests that these forms of disease may also share deficits in RNA processing. TDP-43 and FUS have numerous roles in both the nuclear and cytoplasmic processing and transport of RNAs and RBM45 interacts extensively with RNA splicing factors, including many members of the hnRNP family (Table 5.1 Figure 5.3). Since aggregation of RBPs is common to several forms of ALS, several groups have attempted to address whether these forms of ALS likewise share common deficits in RNA transcript levels, processing, and localization owing to RBP dysfunction. Brain transcriptomic profiling of cerebellar tissue in control, sALS, and *C9ORF72* fALS showed large numbers of RNA processing alterations in both forms of ALS, including extensive alternative splicing and alternative polyadenylation

defects. These defects differed between sALS and *C9ORF72* fALS, with the latter showing a considerably larger number of both type of defects (approximately four-fold greater splicing and two-fold greater polyadenylation)[615]. The *C9ORF72* repeat expansion produces nuclear RNA foci, which are hypothesized to sequester RNA binding proteins[553,554]. Thus, *C9ORF72* RNA transcripts may induce altered RNA processing in ALS motor neurons independently of the transcriptional/processing alterations conferred by TDP-43 nuclear depletion and cytoplasmic aggregation (which are also present in *C9ORF72* fALS). Given the nuclear location of the foci and larger number of reported processing defects in *C9ORF72* fALS brain tissue than sALS[615], *C9ORF72* repeat transcripts seem to be particularly disruptive to RNA processing. To the extent that the RNA processing defects are directly related to the presence of these transcripts (and not, e.g., nucleocytoplasmic transport defects, DPR pathology, etc...) some have suggested that these defects should be therapeutically tractable by approaches such as anti-sense oligonucleotides targeting the foci. Our results suggest this may be an oversimplification, as *C9ORF72* fALS patients consistently showed the greatest amount of motor neuron RBP pathology (Figure 4.3, Supplemental Table 3), which itself is sufficient to induce RNA processing defects[169]. Thus, by collective virtue of (i) *C9ORF72* transcript-mediated sequestration of RBPs, (ii) nucleocytoplasmic transport defects in *C9ORF72* fALS, and (iii) the greater extent of RBP aggregation in this form of disease, we expect that RNA processing defects are greatest for this form of ALS (Figure 1.2).

This view would reciprocally argue that forms of ALS in which RBP pathology and loss of function are not present should exhibit the fewest RNA transcription/processing defects. Evidence in support of this view comes from studies of the SOD1 mouse model of fALS. As noted above, SOD1 fALS patients (and transgenic mice) are unique in that they do not typically exhibit RBP pathology[8]. Using an approach similar to that performed in human patients, whole transcriptome profiling of

SOD1 transgenic mouse brain tissue revealed alterations in only a small number of transcripts and splicing events[616]. Similar results were obtained using whole transcriptome profiling of NSC34 motor-neuron like cells following exposure to mutant SOD1[617] and in a separate SOD1 mouse model using whole spinal cord tissue[618]. While in the former study, exposure to SOD1 did upregulate transcription of antioxidant response element genes, the small overall number of transcriptomic changes, especially relative to that observed for, e.g., TDP-43 depletion[168], for all of these studies argues that changes in RNA transcription and processing observed in ALS relate directly to the dysfunction of RBPs, and not to downstream events related to the death of motor neurons or presence of inflammatory/pro-apoptotic factors. While this implies a relatively straightforward relationship between RNA processing defects and RBPs in disease, it also suggests that therapeutic approaches to will need to directly target RBP homeostasis, not ongoing degenerative processes (e.g., inflammation), to ameliorate these defects. Given the multitude of RBP functions and localization to SGs and NSBs in ALS (Figures 1.2, 6.7), this may prove challenging, if not impossible, to do in a palliative fashion. Approaches that can reliably signal the onset of RBP dysfunction, such as proteomic profiling, may thus be necessary to prevent the onset of degenerative processes related RBP processing functions and aggregation.

Additional approaches to the study of transcriptomic changes in ALS have taken advantage of methods capable of selectively isolating motor neurons for RNA extraction. One such study characterized the transcriptomic profile of spinal motor neurons and oculomotor neurons (which are relatively spared from degeneration in ALS) using laser capture microdissection from neurologically normal human subjects. These two populations of neurons showed distinct transcriptomic profiles, with differential expression of approximately 1,700 genes observed between neuron populations[400]. These results show how distinct transcriptomic profiles can arise in different motor neuronal

populations, even from a common genetic background. These differences are likely due to differences in size, metabolic requirements, and synaptic activity. Consistent with results presented here (Figures 2.5, 2.7), extracellular matrix (ECM) and synaptic structure-related biological processes were identified via enrichment analysis of differentially regulated transcripts[400], underscoring the idea that ECM alterations are a key susceptibility factor in the selective degeneration of spinal motor neurons in ALS. This analysis also identified oxidative phosphorylation, synaptic activity, and ubiquitin-mediated protein degradation pathways as significant contributors to differences in motor neuron sub-population transcriptomic differences. This latter pathway is likely general to many forms of ALS given the preponderant role of protein aggregation in all forms of ALS[8].

Collectively, the preceding observations on transcriptional/splicing changes in ALS and spinal motor neurons highlights the responsive nature of gene expression. The ability of cells to regulate gene expression in response to internal and external stimuli confers benefits to cell survival, particularly during periods of stress, development, or other changes. Cells are known to change gene expression profiles following a variety of environmental signals[619]. Failure to properly regulate gene expression following adverse stimuli may underlie the transcriptomic changes seen in ALS. In this context, the transcriptome can be seen as a bridge linking the environmental and genetic aspects of ALS. For example, one study examined the transcriptomic changes associated with TDP-43 overexpression or depletion. These manipulations were found to produce distinct transcriptomic alterations in drosophila[620]. Thus, the pathological aggregation (by virtue of e.g., overwhelmed autophagy) and loss of normal function accompanying RBP dysfunction in ALS are each capable of inducing alterations in gene expression and the regulation thereof. When the (at present unknown) totality of RBPs aggregated and improperly subcellularly sequestered is considered, the potential

extent of transcriptional dysregulation is extensive. At present, no studies have examined whether therapeutic interventions targeting RBPs or protein aggregates mitigate transcriptional alterations, though the ability of high-throughput sequencing technologies to rapidly and relatively inexpensively generate this information makes transcriptional profiling a potentially appealing readout of therapeutic effectiveness.

7.1.4 Proteomic Profiling in ALS

Proteomic analyses are less standardized and more technically challenging than genomic and transcriptomic technologies. Consequently, the application of proteomics to the study of ALS/FTLD is relatively immature when compared to nucleic acid sequencing and quantification studies. Proteomic characterization of biofluids, chiefly CSF and plasma represent the vast majority studies applying proteomic profiling to the study of ALS. These studies have yielded useful insights into the biology of ALS, as described above. As our results here suggest (Chapter 2), the continued application of mass-spectrometric global biofluid profiling approaches can be expected to yield considerable information with regards to mechanisms of disease, therapeutic efficacy, and disease progression. Ongoing longitudinal proteomic profiling of CSF through large multi-center efforts will provide considerable insight into the nature of the CSF proteomic landscape over the course of disease and in various forms of disease. All of this information has considerable implications for the diagnosis, treatment, and design of clinical trials for ALS.

Outside of biofluid proteomic profiling, other research groups have used proteomics to comprehensively categorize alterations resulting from various ALS/FTLD disease mechanisms. One such study attempted to characterize proteins that co-aggregate with a particularly aggregation-prone mutant form of TDP-43[523]. In identifying a diverse set of co-aggregating proteins, the results

indicated that TDP-43 aggregation is sufficient to induce dysfunction in a host of subcellular processes and structures, including ubiquitin proteasome system function and paraspeckle composition. Subsequent proteomic analysis of FTLD brain tissue confirmed alterations in paraspeckle proteins and underscored the value of proteomic profiling for identifying downstream proteomic changes resulting from ALS/FTLD disease mechanisms[621]. Direct application of technologies such as MALDI-TOF MS imaging to ALS/FTLD tissue[622] may yield even greater insight into proteomic alterations accompanying disease.

7.2 MODELING ALS/FTLD

One of the great challenges in the field of ALS/FTLD research is to develop model systems that accurately recapitulate the mechanisms of disease leading to ALS/FTLD. The past 10 years have seen remarkable progress made in this endeavor, with numerous transgenic mouse lines representing a host of fALS-linked mutations being created and characterized and the development of IPSC motor neuron cultures creating the potential to bring personalized medicine into the realm of ALS/FTLD. As each model system has distinct advantages and limitations, the continued characterization of each model and comparison to the human form of disease is necessary to objectively determine which models are appropriate for which research goals.

7.2.1 Transgenic Mouse Models of ALS

The first transgenic mouse models of ALS were based on the identification of mutations in the *SOD1* genes as the cause of approximately 20% of fALS. These mice proved extremely useful for

disentangling whether loss of SOD1 function, gain of toxic function, or both were responsible for motor neuron degeneration. By virtue of SOD1 pathology, progressive motor impairments, and motor neuron degeneration, mice overexpressing the mutant human protein were deemed to be the proper model system for the human form of disease. Mice lacking the murine SOD1 gene lacked these characteristics and were phenotypically normal, ruling out loss of normal SOD1 function as a primary cause of disease in *SOD1* fALS patients[623,624]. In subsequent years, the SOD1 mouse models based on several fALS causing *SOD1* mutations have continued to be widely used in research on mechanisms of and treatments for ALS. Over-reliance on the model for the latter objective has been one factor suggested to account for the poor record of ALS clinical trials[595]. Given the genetic and molecular complexity of non-SOD1 forms of ALS, this is perhaps not surprising. Nevertheless, the SOD1 transgenic mouse model remains one of the best models of the pathology and progressive motor phenotype accompanying the human form of the disease. The SOD1 mouse model will thus likely remain a prominent model system, both for studies of SOD1 fALS and as a basis of comparison with other forms of ALS to determine the generality of a proposed mechanism of disease or effectiveness of a therapeutic intervention.

The discovery of TDP-43 inclusions and fALS-causing mutations spurred the creation of several lines of TDP-43 transgenic mice. Modeling TDP-43 proteinopathy in mice proved immediately more challenging than modeling SOD1 mutations, as mice either lacking the *TARDBP* gene or overexpressing the mutant human protein suffered from early lethality[625]. Moreover, the creation of multiple lines overexpressing either the wild-type human protein or the mutant A315T mutant protein revealed a variety of behavioral phenotypes, pathologies, and mutant protein expression levels. Mice rarely had comparable motor abnormalities to SOD1 mice and in some cases exhibited other disease phenotypes with unclear relevance to human disease, such as gut

pathology[625]. The difficulties in modeling familial or sporadic TDP-43 proteinopathy are immediately apparent when one considers that, unlike SOD1, toxicity is conferred by both toxic gain and loss of normal function. While modeling one of these phenomena in mice has proven relatively straightforward, understanding the additive/synergistic effects conferred by both has proven challenging and limitations in TDP-43 mouse models reflect this difficulty.

Several attempts have been made to create transgenic mouse models of *C9ORF72* repeat expansion-linked fALS. As the mechanisms of toxicity of the repeat expansion and function of the *C9ORF72* protein are not known, the relevance of transgenic mouse lines based on this genetic abnormality to human disease is not known. As with TDP-43 and SOD1, the development of transgenic lines has used knockout and insertional approaches separately. Removal of the murine *C9ORF72* ortholog does not result in neurodegeneration or a motor phenotype[626]. While this argues against haploinsufficiency as a mechanism of disease, it is worth noting that mice with repeat expansion insertions also do not exhibit neurodegeneration, motor abnormalities, or reduced lifespan, despite the presence of histopathological features found in human *C9ORF72* ALS/FTLD patients[627,628]. More recent evidence suggests that the *C9ORF72* protein is required for proper immune function[629,630], though the relevance of these findings to human *C9ORF72* ALS/FTLD is unknown.

Our results suggest that a fundamental limitation of all transgenic mouse models of ALS/FTLD is their inability to capture the full complement of cellular dysregulation in these diseases. Specifically, our results show activation of the NSB response in FTLD patients (Figure 6.7), a finding that will not be replicable in any transgenic mouse line by virtue of its lack of pericentromeric satellite III sequences[586]. Similarly, these models are unable to adequately model the inherent genetic variability that occurs from one individual to another. At present, the effect of such

variability on the regulation of gene expression and the development and progression of ALS are unknown. Consequently, these factors cannot be modeled in mice and other lower organisms and may hinder the development of effective therapies for disease. While lower organisms such as yeast, drosophila, and *C. elegans* have each provided important insights into ALS/FTLD[101,103,583], the comparatively simple nervous system and genetic complexity of these organisms limits their utility as true models of disease, despite their utility for rapidly screening the phenotypic effects of mutations and modifiers of disease toxicity.

7.2.2 Induced Pluripotent Stem Cell (IPSC) Models of ALS/FTLD

Induced pluripotent stem cell (IPSC) models of disease offer a promising alternative to lower organism model systems for capturing the genetic variability and complexity that contributes to ALS/FTLD. Worldwide efforts are underway to obtain and biobank cells from familial and sporadic ALS patients, as well as healthy control subjects and relatives of fALS patients. Culturing of skin fibroblasts from these individuals creates a self-renewing pool of cells that accurately represent the individual's underlying genetic makeup. While studies of these fibroblasts may, themselves, provide insights into the contributions of genotype to the development of disease-associated pathology[631], the reprogramming of fibroblasts into motor neurons to delineate the exact genetic contributions to the selective cell-type vulnerability that is a hallmark of ALS[632]. Characterization of SOD1 fibroblasts showed abnormalities consistent with those observed in transgenic mouse models, however, the subsequent demonstration that these defects could be corrected via genetic targeting demonstrated the remarkable promise of IPSCs both as models of disease and as a new model system for the evaluation of therapeutic interventions[633]. IPSCs offer perhaps even greater promise towards the modeling of more complex forms of ALS, such as sporadic, *TARDBP* fALS, and *C9ORF72* fALS.

One study used reprogramming of fibroblasts from sALS patients to generate motor neurons. Subsequent characterization showed that these motor neurons were prone to developing TDP-43 pathology[634]. Future studies using larger populations of sporadic cell lines together with genomic information will help determine how genetic variation contributes to motor neuron death in sporadic ALS. Similar results can be expected from studies modeling *TARDBP* fALS and *C9ORF72* fALS, which are beginning to be reported. These studies show that neurons derived from patients tend be more vulnerable to the development of a host of pathological processes associated with disease[632]. Given the identical environmental conditions, these results strongly support a genetic basis for susceptibility to ALS, even in sporadic patients. Thus, IPSC models may be an ideal system for determining the genetic contributions to disease phenotype. The amenability of these systems to targeted genomic manipulation through, e.g., CRISPR-cas9 or TALEN, will allow the mechanisms of these genetic contributions to disease to be directly evaluated as well[635]. A final use of IPSC models is in the screening of drugs for future clinical trials. Several such studies are underway and have shown that IPSCs can identify compounds that ameliorate or prevent the development of a disease-like phenotype in patient-derived motor neurons[632-634]. Similarly, culturing of patient neurons may also be used to select patient subsets most likely to benefit from a particular therapeutic compound being tested in clinical trials. Thus, IPSC models of disease seem poised to become the predominant model system in the field of ALS/FTLD research. While cell culture models are necessarily limited in their generalizability to complex organisms, the power to therapeutically target mechanisms of disease based on individual's genome offers tremendous promise towards the development of therapeutics that effectively target the underlying cause(s) of neurodegeneration for heterogeneous disorders such as ALS/FTLD.

7.3 RNA BINDING PROTEINS IN ALS/FTLD

Work presented herein builds on the well-established concept of RNA binding protein (RBP) mediated neurodegeneration in ALS/FTLD. The number of RBPs whose mutation is sufficient to cause ALS/FTLD[613], the number of aggregation competent RBPs with LC domains[102], and the number of co-aggregating RBPs[523] in models of ALS/FTLD all highlight the potential of dysregulation of these proteins' functions to adversely affect neuronal health and homeostasis. The well-supported "two-hit" hypothesis suggests that these proteins confer loss of normal function and toxic gain of function in disease. Our results provide evidence of both concepts contributing mechanisms of disease related to RBM45. RBM45, like many RBPs, appears to serve many functions related RNA processing and cytoplasmic translation by virtue of its protein binding partners (Supplemental Table 4). Moreover, we show that RBM45 inclusions are common to ALS, FTLD, and Alzheimer's disease (Supplemental Table 3). This latter phenomenon is related to the protein's incorporation into nuclear stress bodies (NSBs). No link between neurological disease and NSBs has previously been made, despite the presence of numerous RBPs in NSBs. Our results thus provide further evidence of dysregulation of protein-RNA complexes in ALS/FTLD and establish new mechanisms by which the persistent association of RBPs can lead to their aggregation.

The first description of TDP-43 association with stress granules paved the way for the concept of impaired protein-RNA granule function as a primary cause of protein aggregation and cellular dysfunction in models of ALS/FTLD[46]. Since that time, emerging evidence points to the dysregulation of numerous types of protein-RNA complexes in ALS FTLD, including gems[585], paraspeckles[523], and, now, NSBs (Figures 6.7, 6.8). An imperative task for the field of ALS/FTLD research is to more fully characterize the functions and protein/RNA composition of these granules, many of which (such as NSBs) are poorly understood/defined. Given these limitations in our

understanding of these structures, it is difficult to predict how their dysregulation contributes to neurodegeneration. Similarly, the incomplete characterization of the protein composition of these granules makes ascertaining which RBPs are in aggregates, and therefore, hypofunctioning challenging. The observation that many RBPs are multifunctional[558] (Figure 5.3) also suggests that understanding their role in disease requires a cataloguing of these functions to determine which are essential, especially to neurons, and which have redundancies that may be compensated for by other proteins.

Understanding how RBP aggregates contribute to cellular toxicity is an equally important task in the study of ALS/FTLD. There seems to be general agreement in models suggesting toxicity of oligomers, as has been proposed for amyloid beta[8], however, the exact means by which these oligomers are toxic remains uncertain. The presence of ubiquitinated inclusions in ALS/FTLD (Figure 4.9) and work in cell culture models strongly implicates impaired protein clearance and ER stress in the degenerative process[33,63]. Prolonged activation of ER stress can induce apoptotic signaling and TDP-43 likewise affects the regulation of apoptotic proteins[63]. TDP-43 and other RBPs in aggregates may be post-translationally modified and determining the function(s) of these modifications and their contribution to aggregation is likewise an important step towards understanding the toxic properties of RBP aggregates.

As is clear from the preceding paragraphs, the complexity of RBP-mediated neurodegeneration is considerable. This complexity makes the design and implementation of therapeutic approaches challenging. With SOD1 and *C9ORF72* fALS, anti-sense oligonucleotides represent a promising approach to mitigate the presence of the neurotoxic mutant gene product. This approach is more likely to be of harm to patients than of help in the case of RBPs[625]. Therapeutics targeting RBPs must target several aspects of their dysfunction, including aggregation, loss of

regulatory functions, and subcellular mis-localization. While studies have used drug screens to find modifiers of toxicity[634] such approaches are unlikely to identify compounds that fully restore neuron RBP homeostasis. Finding therapeutic approaches that do so will require a more refined understanding of the functions and potential for toxicity of RBPs.

7.4 FUTURE PERSPECTIVES

We have provided herein comprehensive proteomic profiles of CSF from ALS, healthy control, and other neurological disease subjects and shown how this can be leveraged to yield robust biomarkers and new insights into mechanisms of disease in ALS/FTLD. Continued proteomic, transcriptomic, and genomic profiling of the ALS population remains the most reasonable approach to fully characterize the disorders comprising the spectrum of ALS to FTLD. Tremendous strides in our understanding of these disorders have been made by genome sequencing efforts towards the identification of causal variants and variants influencing the susceptibility to disease and rate of progression. This is perhaps best exemplified by the approximately 40% of fALS cases now known to originate from the *C9ORF72* repeat expansion. There is still a substantial proportion of familial ALS unexplained by known mutations and this number will likely decrease rapidly as sequencing technologies continue to improve and decrease in cost, while large-scale collaborative efforts towards the sequencing of ALS patients continue. The larger challenge, as has been proven with studies of *C9ORF72*, will be defining the causal mechanisms of cellular toxicity. Our results argue that IPSC model systems will be an increasingly important part of the solution to these challenges. Specifically, we have shown that NSB pathology is a common finding in FTLD and know from previous work on NSBs that such pathology will not be observed in animal models. Thus, the

creation of IPSC lines may be necessary to fully delineate the causes of disease. The effects of genetic variation on susceptibility to and progression of disease will likely also yield many insights into neuronal physiology in the years ahead. Several such variants are currently known, and as with disease causing mutations, this number should grow rapidly in the years ahead.

This work also underscores the vital role of RBPs in both neuronal health/homeostasis and neurodegeneration. Increasingly, the toxic effects of RBPs are linked to their association with various forms of protein-RNA granules, such as SGs or NSBs. Continued efforts towards understanding the function of these structures and how these may ultimately lead to maladaptive changes such as aggregation have implications for our understanding of both human disease and the normal regulation of gene expression. Ultimately, the presence of RBPs in protein-RNA complexes seems to center on the regulation of gene expression. A more thorough understanding of the mechanisms by which such structures, and RBPs themselves, regulate gene expression would also likely provide insight into the mechanisms of ALS/FTLD. Moreover, this would also provide new insights into developmental processes, for which several ALS-linked RBPs are implicated.

Molecular profiling of disease, as presented here, is a valuable approach for defining disease on a biological basis, rather than a clinical one. As these results have illustrated, this has implications for practically all aspects of disease research, from the development of disease-specific biomarkers to the treatment of associated pathologies. As profiling approaches grow more sophisticated and comprehensive, so too will our ability to understand, treat, and prevent these debilitating disorders.

BIBLIOGRAPHY

1. Logroscino G, Traynor BJ, Hardiman O, Chio A, Mitchell D, Swingler RJ, Millul A, Benn E, Beghi E, Eurals. Incidence of amyotrophic lateral sclerosis in Europe. J Neurol Neurosurg Psychiatry 2010;81(4):385-90.

2. Uenal H, Rosenbohm A, Kufeldt J, Weydt P, Goder K, Ludolph A, Rothenbacher D, Nagel G, Group ALSrS. Incidence and geographical variation of amyotrophic lateral sclerosis (ALS) in Southern Germany--completeness of the ALS registry Swabia. PLoS One 2014;9(4):e93932.

3. Vazquez MC, Ketzoian C, Legnani C, Rega I, Sanchez N, Perna A, Penela M, Aguirrezabal X, Druet-Cabanac M, Medici M. Incidence and prevalence of amyotrophic lateral sclerosis in Uruguay: a population-based study. Neuroepidemiology 2008;30(2):105-11.

4. Logroscino G, Beghi E, Zoccolella S, Palagano R, Fraddosio A, Simone IL, Lamberti P, Lepore V, Serlenga L, Registry S. Incidence of amyotrophic lateral sclerosis in southern Italy: a population based study. J Neurol Neurosurg Psychiatry 2005;76(8):1094-8.

5. Wolfson C, Kilborn S, Oskoui M, Genge A. Incidence and prevalence of amyotrophic lateral sclerosis in Canada: a systematic review of the literature. Neuroepidemiology 2009;33(2):79-88.

6. Sun CN, Araoz C, Lucas G, Morgan PN, White HJ. Amyotrophic lateral sclerosis. Inclusion bodies in a case of the classic sporadic form. Ann Clin Lab Sci 1975;5(1):38-44.

7. Takahashi K, Nakamura H, Okada E. Hereditary amyotrophic lateral sclerosis. Histochemical and electron microscopic study of hyaline inclusions in motor neurons. Arch Neurol 1972;27(4):292-9.

8. Blokhuis AM, Groen EJ, Koppers M, van den Berg LH, Pasterkamp RJ. Protein aggregation in amyotrophic lateral sclerosis. Acta Neuropathol 2013;125(6):777-94.

9. Rosen DR, Siddique T, Patterson D, Figlewicz DA, Sapp P, Hentati A, Donaldson D, Goto J, O'Regan JP, Deng HX and others. Mutations in Cu/Zn superoxide dismutase gene are associated with familial amyotrophic lateral sclerosis. Nature 1993;362(6415):59-62.

10. de Belleroche J, Orrell R, King A. Familial amyotrophic lateral sclerosis/motor neurone disease (FALS): a review of current developments. J Med Genet 1995;32(11):841-7.

11. Rotunno MS, Bosco DA. An emerging role for misfolded wild-type SOD1 in sporadic ALS pathogenesis. Front Cell Neurosci 2013;7:253.

12. Chattopadhyay M, Valentine JS. Aggregation of copper-zinc superoxide dismutase in familial and sporadic ALS. Antioxid Redox Signal 2009;11(7):1603-14.

13. Fridovich I. Superoxide dismutases. Annu Rev Biochem 1975;44:147-59.

14. Rotilio G, Calabrese L, Bossa F, Barra D, Agro AF, Mondovi B. Properties of the apoprotein and role of copper and zinc in protein conformation and enzyme activity of bovine superoxide dismutase. Biochemistry 1972;11(11):2182-7.

15. Andersen PM, Nilsson P, Keranen ML, Forsgren L, Hagglund J, Karlsborg M, Ronnevi LO, Gredal O, Marklund SL. Phenotypic heterogeneity in motor neuron disease patients with CuZn-superoxide dismutase mutations in Scandinavia. Brain 1997;120 (Pt 10):1723-37.

16. Radunovic A, Delves HT, Robberecht W, Tilkin P, Enayat ZE, Shaw CE, Stevic Z, Apostolski S, Powell JF, Leigh PN. Copper and zinc levels in familial amyotrophic lateral sclerosis patients with CuZnSOD gene mutations. Ann Neurol 1997;42(1):130-1.

17. Reaume AG, Elliott JL, Hoffman EK, Kowall NW, Ferrante RJ, Siwek DF, Wilcox HM, Flood DG, Beal MF, Brown RH, Jr. and others. Motor neurons in Cu/Zn superoxide dismutase-deficient mice develop normally but exhibit enhanced cell death after axonal injury. Nat Genet 1996;13(1):43-7.

18. Bruijn LI, Houseweart MK, Kato S, Anderson KL, Anderson SD, Ohama E, Reaume AG, Scott RW, Cleveland DW. Aggregation and motor neuron toxicity of an ALS-linked SOD1 mutant independent from wild-type SOD1. Science 1998;281(5384):1851-4.

19. Wang J, Xu G, Gonzales V, Coonfield M, Fromholt D, Copeland NG, Jenkins NA, Borchelt DR. Fibrillar inclusions and motor neuron degeneration in transgenic mice expressing superoxide dismutase 1 with a disrupted copper-binding site. Neurobiol Dis 2002;10(2):128-38.

20. Elam JS, Taylor AB, Strange R, Antonyuk S, Doucette PA, Rodriguez JA, Hasnain SS, Hayward LJ, Valentine JS, Yeates TO and others. Amyloid-like filaments and water-filled nanotubes formed by SOD1 mutant proteins linked to familial ALS. Nat Struct Biol 2003;10(6):461-7.

21. Furukawa Y, Kaneko K, Yamanaka K, O'Halloran TV, Nukina N. Complete loss of post-translational modifications triggers fibrillar aggregation of SOD1 in the familial form of amyotrophic lateral sclerosis. J Biol Chem 2008;283(35):24167-76.

22. Banci L, Bertini I, Durazo A, Girotto S, Gralla EB, Martinelli M, Valentine JS, Vieru M, Whitelegge JP. Metal-free superoxide dismutase forms soluble oligomers under physiological conditions: a possible general mechanism for familial ALS. Proc Natl Acad Sci U S A 2007;104(27):11263-7.

23. Sasaki S, Warita H, Murakami T, Shibata N, Komori T, Abe K, Kobayashi M, Iwata M. Ultrastructural study of aggregates in the spinal cord of transgenic mice with a G93A mutant SOD1 gene. Acta Neuropathol 2005;109(3):247-55.

24. Kato S, Shimoda M, Watanabe Y, Nakashima K, Takahashi K, Ohama E. Familial amyotrophic lateral sclerosis with a two base pair deletion in superoxide dismutase 1: gene multisystem degeneration with intracytoplasmic hyaline inclusions in astrocytes. J Neuropathol Exp Neurol 1996;55(10):1089-101.

25. Allen MJ, Lacroix JJ, Ramachandran S, Capone R, Whitlock JL, Ghadge GD, Arnsdorf MF, Roos RP, Lal R. Mutant SOD1 forms ion channel: implications for ALS pathophysiology. Neurobiol Dis 2012;45(3):831-8.

26. Rabizadeh S, Gralla EB, Borchelt DR, Gwinn R, Valentine JS, Sisodia S, Wong P, Lee M, Hahn H, Bredesen DE. Mutations associated with amyotrophic lateral sclerosis convert superoxide dismutase from an antiapoptotic gene to a proapoptotic gene: studies in yeast and neural cells. Proc Natl Acad Sci U S A 1995;92(7):3024-8.

27. Vehvilainen P, Koistinaho J, Gundars G. Mechanisms of mutant SOD1 induced mitochondrial toxicity in amyotrophic lateral sclerosis. Front Cell Neurosci 2014;8:126.

28. Tan W, Naniche N, Bogush A, Pedrini S, Trotti D, Pasinelli P. Small peptides against the mutant SOD1/Bcl-2 toxic mitochondrial complex restore mitochondrial function and cell viability in mutant SOD1-mediated ALS. J Neurosci 2013;33(28):11588-98.

29. Vijayvergiya C, Beal MF, Buck J, Manfredi G. Mutant superoxide dismutase 1 forms aggregates in the brain mitochondrial matrix of amyotrophic lateral sclerosis mice. J Neurosci 2005;25(10):2463-70.

30. Carri MT, Cozzolino M. SOD1 and mitochondria in ALS: a dangerous liaison. J Bioenerg Biomembr 2011;43(6):593-9.

31. Mondola P, Santillo M, Seru R, Damiano S, Alvino C, Ruggiero G, Formisano P, Terrazzano G, Secondo A, Annunziato L. Cu,Zn superoxide dismutase increases intracellular calcium levels via a phospholipase C-protein kinase C pathway in SK-N-BE neuroblastoma cells. Biochem Biophys Res Commun 2004;324(2):887-92.

32. Grad LI, Cashman NR. Prion-like activity of Cu/Zn superoxide dismutase: implications for amyotrophic lateral sclerosis. Prion 2014;8(1):33-41.

33. Neumann M, Sampathu DM, Kwong LK, Truax AC, Micsenyi MC, Chou TT, Bruce J, Schuck T, Grossman M, Clark CM and others. Ubiquitinated TDP-43 in frontotemporal lobar degeneration and amyotrophic lateral sclerosis. Science 2006;314(5796):130-3.

34. Kabashi E, Valdmanis PN, Dion P, Spiegelman D, McConkey BJ, Vande Velde C, Bouchard JP, Lacomblez L, Pochigaeva K, Salachas F and others. TARDBP mutations in individuals with sporadic and familial amyotrophic lateral sclerosis. Nat Genet 2008;40(5):572-4.

35. Gitcho MA, Baloh RH, Chakraverty S, Mayo K, Norton JB, Levitch D, Hatanpaa KJ, White CL, 3rd, Bigio EH, Caselli R and others. TDP-43 A315T mutation in familial motor neuron disease. Ann Neurol 2008;63(4):535-8.

36. Sreedharan J, Blair IP, Tripathi VB, Hu X, Vance C, Rogelj B, Ackerley S, Durnall JC, Williams KL, Buratti E and others. TDP-43 mutations in familial and sporadic amyotrophic lateral sclerosis. Science 2008;319(5870):1668-72.

37. Borroni B, Bonvicini C, Alberici A, Buratti E, Agosti C, Archetti S, Papetti A, Stuani C, Di Luca M, Gennarelli M and others. Mutation within TARDBP leads to frontotemporal dementia without motor neuron disease. Hum Mutat 2009;30(11):E974-83.

38. Kwong LK, Neumann M, Sampathu DM, Lee VM, Trojanowski JQ. TDP-43 proteinopathy: the neuropathology underlying major forms of sporadic and familial frontotemporal lobar degeneration and motor neuron disease. Acta Neuropathol 2007;114(1):63-70.

39. Baralle M, Buratti E, Baralle FE. The role of TDP-43 in the pathogenesis of ALS and FTLD. Biochem Soc Trans 2013;41(6):1536-40.

40. Janssens J, Van Broeckhoven C. Pathological mechanisms underlying TDP-43 driven neurodegeneration in FTLD-ALS spectrum disorders. Hum Mol Genet 2013;22(R1):R77-87.

41. Arai T, Hasegawa M, Nonoka T, Kametani F, Yamashita M, Hosokawa M, Niizato K, Tsuchiya K, Kobayashi Z, Ikeda K and others. Phosphorylated and cleaved TDP-43 in ALS, FTLD and other neurodegenerative disorders and in cellular models of TDP-43 proteinopathy. Neuropathology 2010;30(2):170-81.

42. Buratti E, Baralle FE. Multiple roles of TDP-43 in gene expression, splicing regulation, and human disease. Front Biosci 2008;13:867-78.

43. Lagier-Tourenne C, Polymenidou M, Cleveland DW. TDP-43 and FUS/TLS: emerging roles in RNA processing and neurodegeneration. Hum Mol Genet 2010;19(R1):R46-64.

44. Wu LS, Cheng WC, Hou SC, Yan YT, Jiang ST, Shen CK. TDP-43, a neuro-pathosignature factor, is essential for early mouse embryogenesis. Genesis 2010;48(1):56-62.

45. Sephton CF, Good SK, Atkin S, Dewey CM, Mayer P, 3rd, Herz J, Yu G. TDP-43 is a developmentally regulated protein essential for early embryonic development. J Biol Chem 2010;285(9):6826-34.

46. Colombrita C, Zennaro E, Fallini C, Weber M, Sommacal A, Buratti E, Silani V, Ratti A. TDP-43 is recruited to stress granules in conditions of oxidative insult. J Neurochem 2009;111(4):1051-61.

47. Liu-Yesucevitz L, Bilgutay A, Zhang YJ, Vanderweyde T, Citro A, Mehta T, Zaarur N, McKee A, Bowser R, Sherman M and others. Tar DNA binding protein-43 (TDP-43) associates with stress granules: analysis of cultured cells and pathological brain tissue. PLoS One 2010;5(10):e13250.

48. Dewey CM, Cenik B, Sephton CF, Johnson BA, Herz J, Yu G. TDP-43 aggregation in neurodegeneration: are stress granules the key? Brain Res 2012;1462:16-25.

49. Bentmann E, Neumann M, Tahirovic S, Rodde R, Dormann D, Haass C. Requirements for stress granule recruitment of fused in sarcoma (FUS) and TAR DNA-binding protein of 43 kDa (TDP-43). J Biol Chem 2012;287(27):23079-94.

50. Johnson BS, Snead D, Lee JJ, McCaffery JM, Shorter J, Gitler AD. TDP-43 is intrinsically aggregation-prone, and amyotrophic lateral sclerosis-linked mutations accelerate aggregation and increase toxicity. J Biol Chem 2009;284(30):20329-39.

51. Polymenidou M, Lagier-Tourenne C, Hutt KR, Huelga SC, Moran J, Liang TY, Ling SC, Sun E, Wancewicz E, Mazur C and others. Long pre-mRNA depletion and RNA missplicing contribute to neuronal vulnerability from loss of TDP-43. Nat Neurosci 2011;14(4):459-68.

52. Wegorzewska I, Bell S, Cairns NJ, Miller TM, Baloh RH. TDP-43 mutant transgenic mice develop features of ALS and frontotemporal lobar degeneration. Proc Natl Acad Sci U S A 2009;106(44):18809-14.

53. Wils H, Kleinberger G, Janssens J, Pereson S, Joris G, Cuijt I, Smits V, Ceuterick-de Groote C, Van Broeckhoven C, Kumar-Singh S. TDP-43 transgenic mice develop spastic paralysis and neuronal inclusions characteristic of ALS and frontotemporal lobar degeneration. Proc Natl Acad Sci U S A 2010;107(8):3858-63.

54. Feiguin F, Godena VK, Romano G, D'Ambrogio A, Klima R, Baralle FE. Depletion of TDP-43 affects Drosophila motoneurons terminal synapsis and locomotive behavior. FEBS Lett 2009;583(10):1586-92.

55. Li Y, Ray P, Rao EJ, Shi C, Guo W, Chen X, Woodruff EA, 3rd, Fushimi K, Wu JY. A Drosophila model for TDP-43 proteinopathy. Proc Natl Acad Sci U S A 2010;107(7):3169-74.

56. Lin MJ, Cheng CW, Shen CK. Neuronal function and dysfunction of Drosophila dTDP. PLoS One 2011;6(6):e20371.

57. Kabashi E, Lin L, Tradewell ML, Dion PA, Bercier V, Bourgouin P, Rochefort D, Bel Hadj S, Durham HD, Vande Velde C and others. Gain and loss of function of ALS-related mutations of TARDBP (TDP-43) cause motor deficits in vivo. Hum Mol Genet 2010;19(4):671-83.

58. Schmid B, Hruscha A, Hogl S, Banzhaf-Strathmann J, Strecker K, van der Zee J, Teucke M, Eimer S, Hegermann J, Kittelmann M and others. Loss of ALS-associated TDP-43 in zebrafish causes muscle degeneration, vascular dysfunction, and reduced motor neuron axon outgrowth. Proc Natl Acad Sci U S A 2013;110(13):4986-91.

59. Giordana MT, Piccinini M, Grifoni S, De Marco G, Vercellino M, Magistrello M, Pellerino A, Buccinna B, Lupino E, Rinaudo MT. TDP-43 redistribution is an early event in sporadic amyotrophic lateral sclerosis. Brain Pathol 2010;20(2):351-60.

60. Winton MJ, Igaz LM, Wong MM, Kwong LK, Trojanowski JQ, Lee VM. Disturbance of nuclear and cytoplasmic TAR DNA-binding protein (TDP-43) induces disease-like redistribution, sequestration, and aggregate formation. J Biol Chem 2008;283(19):13302-9.

61. Scotter EL, Vance C, Nishimura AL, Lee YB, Chen HJ, Urwin H, Sardone V, Mitchell JC, Rogelj B, Rubinsztein DC and others. Differential roles of the ubiquitin proteasome system and autophagy in the clearance of soluble and aggregated TDP-43 species. J Cell Sci 2014;127(Pt 6):1263-78.

62. Picher-Martel V, Dutta K, Phaneuf D, Sobue G, Julien JP. Ubiquilin-2 drives NF-kappaB activity and cytosolic TDP-43 aggregation in neuronal cells. Mol Brain 2015;8(1):71.

63. Suzuki H, Lee K, Matsuoka M. TDP-43-induced death is associated with altered regulation of BIM and Bcl-xL and attenuated by caspase-mediated TDP-43 cleavage. J Biol Chem 2011;286(15):13171-83.

64. Zhang YJ, Xu YF, Cook C, Gendron TF, Roettges P, Link CD, Lin WL, Tong J, Castanedes-Casey M, Ash P and others. Aberrant cleavage of TDP-43 enhances aggregation and cellular toxicity. Proc Natl Acad Sci U S A 2009;106(18):7607-12.

65. Tsuji H, Arai T, Kametani F, Nonaka T, Yamashita M, Suzukake M, Hosokawa M, Yoshida M, Hatsuta H, Takao M and others. Molecular analysis and biochemical classification of TDP-43 proteinopathy. Brain 2012;135(Pt 11):3380-91.

66. Nonaka T, Masuda-Suzukake M, Arai T, Hasegawa Y, Akatsu H, Obi T, Yoshida M, Murayama S, Mann DM, Akiyama H and others. Prion-like properties of pathological TDP-43 aggregates from diseased brains. Cell Rep 2013;4(1):124-34.

67. Sama RR, Ward CL, Bosco DA. Functions of FUS/TLS from DNA repair to stress response: implications for ALS. ASN Neuro 2014;6(4).

68. Kwiatkowski TJ, Jr., Bosco DA, Leclerc AL, Tamrazian E, Vanderburg CR, Russ C, Davis A, Gilchrist J, Kasarskis EJ, Munsat T and others. Mutations in the FUS/TLS gene on chromosome 16 cause familial amyotrophic lateral sclerosis. Science 2009;323(5918):1205-8.

69. Vance C, Rogelj B, Hortobagyi T, De Vos KJ, Nishimura AL, Sreedharan J, Hu X, Smith B, Ruddy D, Wright P and others. Mutations in FUS, an RNA processing protein, cause familial amyotrophic lateral sclerosis type 6. Science 2009;323(5918):1208-11.

70. Ling SC, Polymenidou M, Cleveland DW. Converging mechanisms in ALS and FTD: disrupted RNA and protein homeostasis. Neuron 2013;79(3):416-38.

71. Sun Z, Diaz Z, Fang X, Hart MP, Chesi A, Shorter J, Gitler AD. Molecular determinants and genetic modifiers of aggregation and toxicity for the ALS disease protein FUS/TLS. PLoS Biol 2011;9(4):e1000614.

72. Rogelj B, Easton LE, Bogu GK, Stanton LW, Rot G, Curk T, Zupan B, Sugimoto Y, Modic M, Haberman N and others. Widespread binding of FUS along nascent RNA regulates alternative splicing in the brain. Sci Rep 2012;2:603.

73. Andersson MK, Stahlberg A, Arvidsson Y, Olofsson A, Semb H, Stenman G, Nilsson O, Aman P. The multifunctional FUS, EWS and TAF15 proto-oncoproteins show cell type-specific expression patterns and involvement in cell spreading and stress response. BMC Cell Biol 2008;9:37.

74. Bosco DA, Lemay N, Ko HK, Zhou H, Burke C, Kwiatkowski TJ, Jr., Sapp P, McKenna-Yasek D, Brown RH, Jr., Hayward LJ. Mutant FUS proteins that cause amyotrophic lateral sclerosis incorporate into stress granules. Hum Mol Genet 2010;19(21):4160-75.

75. Gal J, Zhang J, Kwinter DM, Zhai J, Jia H, Jia J, Zhu H. Nuclear localization sequence of FUS and induction of stress granules by ALS mutants. Neurobiol Aging 2011;32(12):2323 e27-40.

76. Deng HX, Zhai H, Bigio EH, Yan J, Fecto F, Ajroud K, Mishra M, Ajroud-Driss S, Heller S, Sufit R and others. FUS-immunoreactive inclusions are a common feature in sporadic and non-SOD1 familial amyotrophic lateral sclerosis. Ann Neurol 2010;67(6):739-48.

77. Nomura T, Watanabe S, Kaneko K, Yamanaka K, Nukina N, Furukawa Y. Intranuclear aggregation of mutant FUS/TLS as a molecular pathomechanism of amyotrophic lateral sclerosis. J Biol Chem 2014;289(2):1192-202.

78. Xiao S, McLean J, Robertson J. Neuronal intermediate filaments and ALS: a new look at an old question. Biochim Biophys Acta 2006;1762(11-12):1001-12.

79. Kondo A, Iwaki T, Tateishi J, Kirimoto K, Morimoto T, Oomura I. Accumulation of neurofilaments in a sporadic case of amyotrophic lateral sclerosis. Jpn J Psychiatry Neurol 1986;40(4):677-84.

80. He CZ, Hays AP. Expression of peripherin in ubiquinated inclusions of amyotrophic lateral sclerosis. J Neurol Sci 2004;217(1):47-54.

81. Lariviere RC, Julien JP. Functions of intermediate filaments in neuronal development and disease. J Neurobiol 2004;58(1):131-48.

82. Omary MB, Coulombe PA, McLean WH. Intermediate filament proteins and their associated diseases. N Engl J Med 2004;351(20):2087-100.

83. Chou YH, Goldman RD. Intermediate filaments on the move. J Cell Biol 2000;150(3):F101-6.

84. Kang SH, Li Y, Fukaya M, Lorenzini I, Cleveland DW, Ostrow LW, Rothstein JD, Bergles DE. Degeneration and impaired regeneration of gray matter oligodendrocytes in amyotrophic lateral sclerosis. Nat Neurosci 2013;16(5):571-9.

85. Hirano A. Cytopathology of amyotrophic lateral sclerosis. Adv Neurol 1991;56:91-101.

86. Leung CL, He CZ, Kaufmann P, Chin SS, Naini A, Liem RK, Mitsumoto H, Hays AP. A pathogenic peripherin gene mutation in a patient with amyotrophic lateral sclerosis. Brain Pathol 2004;14(3):290-6.

87. Gros-Louis F, Lariviere R, Gowing G, Laurent S, Camu W, Bouchard JP, Meininger V, Rouleau GA, Julien JP. A frameshift deletion in peripherin gene associated with amyotrophic lateral sclerosis. J Biol Chem 2004;279(44):45951-6.

88. Figlewicz DA, Krizus A, Martinoli MG, Meininger V, Dib M, Rouleau GA, Julien JP. Variants of the heavy neurofilament subunit are associated with the development of amyotrophic lateral sclerosis. Hum Mol Genet 1994;3(10):1757-61.

89. Tomkins J, Usher P, Slade JY, Ince PG, Curtis A, Bushby K, Shaw PJ. Novel insertion in the KSP region of the neurofilament heavy gene in amyotrophic lateral sclerosis (ALS). Neuroreport 1998;9(17):3967-70.

90. Beaulieu JM, Nguyen MD, Julien JP. Late onset of motor neurons in mice overexpressing wild-type peripherin. J Cell Biol 1999;147(3):531-44.

91. Okamoto K, Mizuno Y, Fujita Y. Bunina bodies in amyotrophic lateral sclerosis. Neuropathology 2008;28(2):109-15.

92. Piao YS, Wakabayashi K, Kakita A, Yamada M, Hayashi S, Morita T, Ikuta F, Oyanagi K, Takahashi H. Neuropathology with clinical correlations of sporadic amyotrophic lateral sclerosis: 102 autopsy cases examined between 1962 and 2000. Brain Pathol 2003;13(1):10-22.

93. Okamoto K, Hirai S, Amari M, Watanabe M, Sakurai A. Bunina bodies in amyotrophic lateral sclerosis immunostained with rabbit anti-cystatin C serum. Neurosci Lett 1993;162(1-2):125-8.

94. Mizuno Y, Amari M, Takatama M, Aizawa H, Mihara B, Okamoto K. Transferrin localizes in Bunina bodies in amyotrophic lateral sclerosis. Acta Neuropathol 2006;112(5):597-603.

95. Li YR, King OD, Shorter J, Gitler AD. Stress granules as crucibles of ALS pathogenesis. J Cell Biol 2013;201(3):361-72.

96. Anderson P, Kedersha N. Stress granules: the Tao of RNA triage. Trends Biochem Sci 2008;33(3):141-50.

97. Kawai T, Fan J, Mazan-Mamczarz K, Gorospe M. Global mRNA stabilization preferentially linked to translational repression during the endoplasmic reticulum stress response. Mol Cell Biol 2004;24(15):6773-87.

98. Stohr N, Lederer M, Reinke C, Meyer S, Hatzfeld M, Singer RH, Huttelmaier S. ZBP1 regulates mRNA stability during cellular stress. J Cell Biol 2006;175(4):527-34.

99. Moeller BJ, Cao Y, Li CY, Dewhirst MW. Radiation activates HIF-1 to regulate vascular radiosensitivity in tumors: role of reoxygenation, free radicals, and stress granules. Cancer Cell 2004;5(5):429-41.

100. Esclatine A, Taddeo B, Roizman B. Herpes simplex virus 1 induces cytoplasmic accumulation of TIA-1/TIAR and both synthesis and cytoplasmic accumulation of tristetraprolin, two cellular proteins that bind and destabilize AU-rich RNAs. J Virol 2004;78(16):8582-92.

101. Johnson BS, McCaffery JM, Lindquist S, Gitler AD. A yeast TDP-43 proteinopathy model: Exploring the molecular determinants of TDP-43 aggregation and cellular toxicity. Proc Natl Acad Sci U S A 2008;105(17):6439-44.

102. King OD, Gitler AD, Shorter J. The tip of the iceberg: RNA-binding proteins with prion-like domains in neurodegenerative disease. Brain Res 2012;1462:61-80.

103. Kim HJ, Kim NC, Wang YD, Scarborough EA, Moore J, Diaz Z, MacLea KS, Freibaum B, Li S, Molliex A and others. Mutations in prion-like domains in hnRNPA2B1 and hnRNPA1 cause multisystem proteinopathy and ALS. Nature 2013;495(7442):467-73.

104. Couthouis J, Hart MP, Shorter J, DeJesus-Hernandez M, Erion R, Oristano R, Liu AX, Ramos D, Jethava N, Hosangadi D and others. A yeast functional screen predicts new candidate ALS disease genes. Proc Natl Acad Sci U S A 2011;108(52):20881-90.

105. Eskelinen EL, Saftig P. Autophagy: a lysosomal degradation pathway with a central role in health and disease. Biochim Biophys Acta 2009;1793(4):664-73.

106. Peters OM, Ghasemi M, Brown RH, Jr. Emerging mechanisms of molecular pathology in ALS. J Clin Invest 2015;125(5):1767-79.

107. Puri C, Renna M, Bento CF, Moreau K, Rubinsztein DC. Diverse autophagosome membrane sources coalesce in recycling endosomes. Cell 2013;154(6):1285-99.

108. Bjorkoy G, Lamark T, Brech A, Outzen H, Perander M, Overvatn A, Stenmark H, Johansen T. p62/SQSTM1 forms protein aggregates degraded by autophagy and has a protective effect on huntingtin-induced cell death. J Cell Biol 2005;171(4):603-14.

109. Zavodszky E, Vicinanza M, Rubinsztein DC. Biology and trafficking of ATG9 and ATG16L1, two proteins that regulate autophagosome formation. FEBS Lett 2013;587(13):1988-96.

110. Schreiber A, Peter M. Substrate recognition in selective autophagy and the ubiquitin-proteasome system. Biochim Biophys Acta 2014;1843(1):163-81.

111. Komatsu M, Waguri S, Chiba T, Murata S, Iwata J, Tanida I, Ueno T, Koike M, Uchiyama Y, Kominami E and others. Loss of autophagy in the central nervous system causes neurodegeneration in mice. Nature 2006;441(7095):880-4.

112. Wong YC, Holzbaur EL. Optineurin is an autophagy receptor for damaged mitochondria in parkin-mediated mitophagy that is disrupted by an ALS-linked mutation. Proc Natl Acad Sci U S A 2014;111(42):E4439-48.

113. Maruyama H, Morino H, Ito H, Izumi Y, Kato H, Watanabe Y, Kinoshita Y, Kamada M, Nodera H, Suzuki H and others. Mutations of optineurin in amyotrophic lateral sclerosis. Nature 2010;465(7295):223-6.

114. Hortobagyi T, Troakes C, Nishimura AL, Vance C, van Swieten JC, Seelaar H, King A, Al-Sarraj S, Rogelj B, Shaw CE. Optineurin inclusions occur in a minority of TDP-43 positive ALS and FTLD-TDP cases and are rarely observed in other neurodegenerative disorders. Acta Neuropathol 2011;121(4):519-27.

115. Johnson JO, Mandrioli J, Benatar M, Abramzon Y, Van Deerlin VM, Trojanowski JQ, Gibbs JR, Brunetti M, Gronka S, Wuu J and others. Exome sequencing reveals VCP mutations as a cause of familial ALS. Neuron 2010;68(5):857-64.

116. Ju JS, Fuentealba RA, Miller SE, Jackson E, Piwnica-Worms D, Baloh RH, Weihl CC. Valosin-containing protein (VCP) is required for autophagy and is disrupted in VCP disease. J Cell Biol 2009;187(6):875-88.

117. Rodriguez-Ortiz CJ, Hoshino H, Cheng D, Liu-Yescevitz L, Blurton-Jones M, Wolozin B, LaFerla FM, Kitazawa M. Neuronal-specific overexpression of a mutant valosin-containing protein associated with IBMPFD promotes aberrant ubiquitin and TDP-43 accumulation and cognitive dysfunction in transgenic mice. Am J Pathol 2013;183(2):504-15.

118. Ayaki T, Ito H, Fukushima H, Inoue T, Kondo T, Ikemoto A, Asano T, Shodai A, Fujita T, Fukui S and others. Immunoreactivity of valosin-containing protein in sporadic amyotrophic lateral sclerosis and in a case of its novel mutant. Acta Neuropathol Commun 2014;2:172.

119. Fecto F, Yan J, Vemula SP, Liu E, Yang Y, Chen W, Zheng JG, Shi Y, Siddique N, Arrat H and others. SQSTM1 mutations in familial and sporadic amyotrophic lateral sclerosis. Arch Neurol 2011;68(11):1440-6.

120. Deng HX, Chen W, Hong ST, Boycott KM, Gorrie GH, Siddique N, Yang Y, Fecto F, Shi Y, Zhai H and others. Mutations in UBQLN2 cause dominant X-linked juvenile and adult-onset ALS and ALS/dementia. Nature 2011;477(7363):211-5.

121. Cox LE, Ferraiuolo L, Goodall EF, Heath PR, Higginbottom A, Mortiboys H, Hollinger HC, Hartley JA, Brockington A, Burness CE and others. Mutations in CHMP2B in lower motor neuron predominant amyotrophic lateral sclerosis (ALS). PLoS One 2010;5(3):e9872.

122. Farg MA, Sundaramoorthy V, Sultana JM, Yang S, Atkinson RA, Levina V, Halloran MA, Gleeson PA, Blair IP, Soo KY and others. C9ORF72, implicated in amytrophic lateral sclerosis and frontotemporal dementia, regulates endosomal trafficking. Hum Mol Genet 2014;23(13):3579-95.

123. Morimoto N, Nagai M, Ohta Y, Miyazaki K, Kurata T, Morimoto M, Murakami T, Takehisa Y, Ikeda Y, Kamiya T and others. Increased autophagy in transgenic mice with a G93A mutant SOD1 gene. Brain Res 2007;1167:112-7.

124. Onesto E, Rusmini P, Crippa V, Ferri N, Zito A, Galbiati M, Poletti A. Muscle cells and motoneurons differentially remove mutant SOD1 causing familial amyotrophic lateral sclerosis. J Neurochem 2011;118(2):266-80.

125. Caccamo A, Shaw DM, Guarino F, Messina A, Walker AW, Oddo S. Reduced protein turnover mediates functional deficits in transgenic mice expressing the 25 kDa C-terminal fragment of TDP-43. Hum Mol Genet 2015;24(16):4625-35.

126. Wang IF, Guo BS, Liu YC, Wu CC, Yang CH, Tsai KJ, Shen CK. Autophagy activators rescue and alleviate pathogenesis of a mouse model with proteinopathies of the TAR DNA-binding protein 43. Proc Natl Acad Sci U S A 2012;109(37):15024-9.

127. Cheng CW, Lin MJ, Shen CK. Rapamycin alleviates pathogenesis of a new Drosophila model of ALS-TDP. J Neurogenet 2015;29(2-3):59-68.

128. Zhang X, Li L, Chen S, Yang D, Wang Y, Zhang X, Wang Z, Le W. Rapamycin treatment augments motor neuron degeneration in SOD1(G93A) mouse model of amyotrophic lateral sclerosis. Autophagy 2011;7(4):412-25.

129. Sasaki S. Autophagy in spinal cord motor neurons in sporadic amyotrophic lateral sclerosis. J Neuropathol Exp Neurol 2011;70(5):349-59.

130. Mandon EC, Trueman SF, Gilmore R. Protein translocation across the rough endoplasmic reticulum. Cold Spring Harb Perspect Biol 2013;5(2).

131. Gardner BM, Pincus D, Gotthardt K, Gallagher CM, Walter P. Endoplasmic reticulum stress sensing in the unfolded protein response. Cold Spring Harb Perspect Biol 2013;5(3):a013169.

132. Sano R, Reed JC. ER stress-induced cell death mechanisms. Biochim Biophys Acta 2013;1833(12):3460-70.

133. Hoyer-Hansen M, Jaattela M. Connecting endoplasmic reticulum stress to autophagy by unfolded protein response and calcium. Cell Death Differ 2007;14(9):1576-82.

134. Teske BF, Wek SA, Bunpo P, Cundiff JK, McClintick JN, Anthony TG, Wek RC. The eIF2 kinase PERK and the integrated stress response facilitate activation of ATF6 during endoplasmic reticulum stress. Mol Biol Cell 2011;22(22):4390-405.

135. Kanekura K, Suzuki H, Aiso S, Matsuoka M. ER stress and unfolded protein response in amyotrophic lateral sclerosis. Mol Neurobiol 2009;39(2):81-9.

136. Ilieva EV, Ayala V, Jove M, Dalfo E, Cacabelos D, Povedano M, Bellmunt MJ, Ferrer I, Pamplona R, Portero-Otin M. Oxidative and endoplasmic reticulum stress interplay in sporadic amyotrophic lateral sclerosis. Brain 2007;130(Pt 12):3111-23.

137. Walker AK, Soo KY, Sundaramoorthy V, Parakh S, Ma Y, Farg MA, Wallace RH, Crouch PJ, Turner BJ, Horne MK and others. ALS-associated TDP-43 induces endoplasmic reticulum stress, which drives cytoplasmic TDP-43 accumulation and stress granule formation. PLoS One 2013;8(11):e81170.

138. Farg MA, Soo KY, Walker AK, Pham H, Orian J, Horne MK, Warraich ST, Williams KL, Blair IP, Atkin JD. Mutant FUS induces endoplasmic reticulum stress in amyotrophic lateral sclerosis and interacts with protein disulfide-isomerase. Neurobiol Aging 2012;33(12):2855-68.

139. Nishimura AL, Mitne-Neto M, Silva HC, Richieri-Costa A, Middleton S, Cascio D, Kok F, Oliveira JR, Gillingwater T, Webb J and others. A mutation in the vesicle-trafficking protein VAPB causes late-onset spinal muscular atrophy and amyotrophic lateral sclerosis. Am J Hum Genet 2004;75(5):822-31.

140. Fasana E, Fossati M, Ruggiano A, Brambillasca S, Hoogenraad CC, Navone F, Francolini M, Borgese N. A VAPB mutant linked to amyotrophic lateral sclerosis generates a novel form of organized smooth endoplasmic reticulum. FASEB J 2010;24(5):1419-30.

141. Suzuki H, Kanekura K, Levine TP, Kohno K, Olkkonen VM, Aiso S, Matsuoka M. ALS-linked P56S-VAPB, an aggregated loss-of-function mutant of VAPB, predisposes motor neurons to ER stress-related death by inducing aggregation of co-expressed wild-type VAPB. J Neurochem 2009;108(4):973-985.

142. Moumen A, Virard I, Raoul C. Accumulation of wildtype and ALS-linked mutated VAPB impairs activity of the proteasome. PLoS One 2011;6(10):e26066.

143. De Vos KJ, Morotz GM, Stoica R, Tudor EL, Lau KF, Ackerley S, Warley A, Shaw CE, Miller CC. VAPB interacts with the mitochondrial protein PTPIP51 to regulate calcium homeostasis. Hum Mol Genet 2012;21(6):1299-311.

144. Gkogkas C, Middleton S, Kremer AM, Wardrope C, Hannah M, Gillingwater TH, Skehel P. VAPB interacts with and modulates the activity of ATF6. Hum Mol Genet 2008;17(11):1517-26.

145. Saxena S, Cabuy E, Caroni P. A role for motoneuron subtype-selective ER stress in disease manifestations of FALS mice. Nat Neurosci 2009;12(5):627-36.

146. Mondola P, Annella T, Santillo M, Santangelo F. Evidence for secretion of cytosolic CuZn superoxide dismutase by Hep G2 cells and human fibroblasts. Int J Biochem Cell Biol 1996;28(6):677-81.

147. Lee S, Kim HJ. Prion-like Mechanism in Amyotrophic Lateral Sclerosis: are Protein Aggregates the Key? Exp Neurobiol 2015;24(1):1-7.

148. Atkin JD, Farg MA, Turner BJ, Tomas D, Lysaght JA, Nunan J, Rembach A, Nagley P, Beart PM, Cheema SS and others. Induction of the unfolded protein response in familial amyotrophic lateral sclerosis and association of protein-disulfide isomerase with superoxide dismutase 1. J Biol Chem 2006;281(40):30152-65.

149. Turner BJ, Atkin JD, Farg MA, Zang DW, Rembach A, Lopes EC, Patch JD, Hill AF, Cheema SS. Impaired extracellular secretion of mutant superoxide dismutase 1 associates with neurotoxicity in familial amyotrophic lateral sclerosis. J Neurosci 2005;25(1):108-17.

150. Urushitani M, Sik A, Sakurai T, Nukina N, Takahashi R, Julien JP. Chromogranin-mediated secretion of mutant superoxide dismutase proteins linked to amyotrophic lateral sclerosis. Nat Neurosci 2006;9(1):108-18.

151. Wate R, Ito H, Zhang JH, Ohnishi S, Nakano S, Kusaka H. Expression of an endoplasmic reticulum-resident chaperone, glucose-regulated stress protein 78, in the spinal cord of a mouse model of amyotrophic lateral sclerosis. Acta Neuropathol 2005;110(6):557-62.

152. Hetz C, Thielen P, Matus S, Nassif M, Court F, Kiffin R, Martinez G, Cuervo AM, Brown RH, Glimcher LH. XBP-1 deficiency in the nervous system protects against amyotrophic lateral sclerosis by increasing autophagy. Genes Dev 2009;23(19):2294-306.

153. Neumann M, Sampathu DM, Kwong LK, Truax AC, Miscenyi MC, Chou LT, Bruce J, Schuck T, Grossman M, Clark CM and others. Ubiquitinated TDP-43 in frontotemporal lobar degeneration and amyotrophic lateral sclerosis. Science 2006;314:130-133.

154. Sreedharan J, Blair IP, Tripathi V, Hu X, Vance C, Rogeli B, Ackerley S, Durnall JC, Williams KL, Buratti E and others. TDP-43 mutations in familial and sporadic amyotrophic lateral sclerosis. Science 2008;319:1668-1672.

155. Chio A, Calvo A, Mazzini L, Cantello R, Mora G, Moglia C, Corrado L, D'Alfonso S, Majounie E, Renton AE and others. Extensive genetics of ALS: a population-based study in Italy. Neurology 2012;79(19):1983-1989.

156. Kwiatkowski TJJ, Bosco DA, LeClerc AL, Tamrazian E, Vanderburg CR, Russ C, Davis A, Gilchrist J, Kasarskis EJ, Munsat T and others. Mutations in the FUS/TLS gene on chromosome 16 cause familial amyotrophic lateral sclerosis. Science 2009;323:1205-1208.

157. Vance C, Rogeli B, Hortobagyi T, De Vos KJ, Nishimura AL, Sreedharan J, Hu X, Smith B, Ruddy D, Wright P and others. Mutations in FUS, an RNA processing protein, cause familial amyotrophic lateral sclerosis type 6. Science 2009;323:1208-1211.

158. Couthouis J, Hart MP, Shorter J, DeJesus-Hernandez M, Erion R, Oristano R, Liu AX, Ramos D, Jethava N, Hosangadi D and others. A yeast functional screen predicts new candidate ALS disease genes. Proceedings of the National Academy of Sciences 2011;108(52):20881-20890.

159. Kim HJ, Kim NC, Wang YD, Scarborough EA, Moore J, Diaz Z, MacLea KS, Freibaum B, Li S, Molliex A and others. Prion-like domain mutations in hnRNPs cause multisystem proteinopathy and ALS. Nature 2013;495:467-473.

160. Chance PF, Rabin BA, Ryan SG, Ding Y, Scavina M, Crain B, Griffin JW, Cornblath DR. Linkage of the gene for an autosomal dominant form of juvenile amyotrophic lateral sclerosis to chromosome 9q34. Am J Hum Genet 1998;62:633-640.

161. Greenway MJ, Alexander MD, Ennis S, Traynor BJ, Corr B, Frost E, Green A, Hardiman O. A novel candidate region for ALS on chromosome 14q11.2. Neurology 2004;63:1936-1938.

162. Simpson CL, Lemmens R, Miskiewicz K, Broom WJ, Hansen VK, van Vught PWJ, Landers JE, Sapp P, Van Den Bosch L, Knight J and others. Variants of the elongator protein 3 (ELP3) gene are associated with motor neuron degeneration. Human Molecular Genetics 2009;18(3):472-481.

163. Elden AC, Kim H-J, Hart MP, Chen-Plotkin AS, Johnson BS, Fang X, Armakola M, Geser F, Greene R, Lu MM and others. Ataxin-2 intermediate-length polyglutamine expansions are associated with increased risk for ALS. Nature 2010;466(7310):1069-1075.

164. Collins M, Riascos D, Kovalik T, An J, Krupa K, Hood BL, Conrads TP, Renton AE, Traynor BJ, Bowser R. The RNA-binding motif 45 (RBM45) protein accumulates in inclusion bodies in amyotrophic lateral sclerosis (ALS) and frontotemporal lobar degeneration with TDP-43 inclusions (FTLD-TDP) patients. Acta Neuropathol 2012;124(5):717-32.

165. Lagier-Tourenne C, Polymenidou M, Hutt KR, Vu AQ, Baughn M, Huelga SC, Clutario KM, Ling SC, Liang TY, Mazur C and others. Divergent roles of ALS-linked proteins FUS/TLS and TDP-43 intersect in processing long pre-mRNAs. Nat Neurosci 2012;15(11):1488-97.

166. Sephton CF, Cenik C, Kucukural A, Dammer EB, Cenik B, Han Y, Dewey CM, Roth FP, Herz J, Peng J and others. Identification of neuronal RNA targets of TDP-43-containing ribonucleoprotein complexes. J Biol Chem 2011;286(2):1204-15.

167. Tollervey JR, Curk T, Rogelj B, Briese M, Cereda M, Kayikci M, Konig J, Hortobagyi T, Nishimura AL, Zupunski V and others. Characterizing the RNA targets and position-dependent splicing regulation by TDP-43. Nat Neurosci 2011;14(4):452-8.

168. Polymenidou M, Lagier-Tourenne C, Hutt KR, Huelga SC, Moran J, Liang TY, Ling S-C, Sun E, Wancewicz E, Mazur C and others. Long pre-mRNA depletion and RNA missplicing contribute to neuronal vulnerability from loss of TDP-43. Nat Neurosci 2011;14:459-468.

169. Xiao S, Sanelli T, Dib S, Sheps D, Findlater J, Bilbao J, Keith J, Zinman L, Rogaeva E, Robertson J. RNA targets of TDP-43 identified by UV-CLIP are deregulated in ALS. Mol Cell Neurosci 2011;47(3):167-180.

170. Nishimoto Y, Nakagawa S, Hirose T, Okano HJ, Takao M, Shibata S, Suyama S, Kuwako K-I, Imai T, Murayama S and others. The long non-coding RNA nuclear-enriched abundant transcript 1_2 induces paraspeckle formation in the motor neuron during the early phase of amyotrophic lateral sclerosis. Molecular Brain 2013;6(31):doi:10.1186/1756-6606-6-31.

171. Naganuma T, Hirose T. Paraspeckle formation during the biogenesis of long non-coding RNAs. RNA Biology 2013;10(3):456-461.

172. Shelkovnikova TA, Robinson HK, Troakes C, Ninkina N, Buchman VL. Compromised paraspeckle formation as a pathogenic factor in FUSopathies. Hum Mol Genet 2014;23(9):2298-2312.

173. Wang I-F, Wu L-S, Chang H-Y, Shen CKJ. TDP-43, the signature protein of FTLD-U, is a neuronal activity-responsive factor. J Neurochem 2008;105:797-806.

174. Fujii R, Okabe S, Urushido T, Inoue K, Yoshimura A, Tachibana T, Nishikawa T, Hicks GG, Takumi T. The RNA binding protein TLS is translocated to dendritic spines by mGluR5 activation and regulates spine morphology. Curr Biol 2005;15:587-593.

175. Kwak S, Kawahara Y. Deficient RNA editing of GluR2 and neuronal death in amyotropic lateral sclerosis. J Mol Med (Berl) 2005;83(2):110-20.

176. Yamashita T, Kwak S. The molecular link between inefficient GluA2 Q/R site-RNA editing and TDP-43 pathology in motor neurons of sporadic amyotrophic lateral sclerosis patients. Brain Res 2014;1584:28-38.

177. Fabian MR, Sonenberg N, Filipowicz W. Regulation of mRNA translation and stability by microRNAs. Annu. Rev. Biochem. 2010;79:351-379.

178. Friedman RC, Farh KK, Burge CB, Bartel DP. Most mammalian mRNAs are conserved targets of microRNAs. Genome Res. 2009;19:92-105.

179. Leung AKL, Sharp PA. MicroRNA functions in stress response. Mol. Cell 2010;40(205-215).

180. Butovsky O, Siddiqui S, Gabriely G, Lanser AJ, Dake B, Murugaiyan G, Doykan CE, Wu PM, Gali RR, Iyer LK and others. Modulating inflammatory monocytes with a unique microRNA gene signature ameliorates murine ALS. J Clin Invest 2012;122(9):3063-87.

181. Parisi C, Arisi I, D'Ambrosi N, Storti AE, Brandi R, D'Onofrio M, Volonte C. Dysregulated microRNAs in amyotrophic lateral sclerosis microglia modulate genes linked to neuroinflammation. Cell Death Dis 2013;4:e959.

182. Campos-Melo D, Droppelmann CA, He Z, Volkening K, Strong MJ. Altered microRNA expression profile in Amyotrophic Lateral Sclerosis: a role in the regulation of NFL mRNA levels. Mol Brain 2013;6:26.

183. Williams AH, Valdez G, Moresi V, Qi X, McAnally J, Elliott JL, Bassel-Duby R, Sanes JR, Olson EN. MicroRNA-206 delays ALS progression and promotes regeneration of neuromuscular synapses in mice. Science 2009;326(5959):1549-54.

184. De Felice B, Annunziata A, Fiorentino G, Borra M, Biffali E, Coppola C, Cotrufo R, Brettschneider J, Giordana ML, Dalmay T and others. miR-338-3p is over-expressed in blood, CFS, serum and spinal cord from sporadic amyotrophic lateral sclerosis patients. Neurogenetics 2014;15(4):243-53.

185. Koval ED, Shaner C, Zhang P, du Maine X, Fischer K, Tay J, Chau BN, Wu GF, Miller TM. Method for widespread microRNA-155 inhibition prolongs survival in ALS-model mice. Hum Mol Genet 2013;22(20):4127-35.

186. Butovsky O, Siddiqui S, Gabriely G, Lanser AJ, Dake B, Murugaiyan G, Doykan CE, Wu PM, Gali RR, Iyer LK and others. Modulating inflammatory monocytes with a unique microRNA gene signature ameliorates murine ALS. J Clin Invest 2012;122:3063-3087.

187. Williams AH, Valdez G, Moresi V, Qi X, McAnally J, Elliott JL, Bassel-Duby R, Sanes JR, Olson EN. MicroRNA-206 delays ALS progression and promotes regeneration of neuromuscular synapses in mice. Science 2009;326:1549-1554.

188. Buratti E, De Conti L, Stuani C, Romano M, Baralle M, Baralle F. Nuclear factor TDP-43 can affect selected microRNA levels. FEBS J 2010;277(10):2268-81.

189. Morlando M, Modigliani SD, G. T, Rosa A, Di Carla V, Caffarelli E, Bozzoni I. FUS stimulates microRNA biogenesis by facilitating co-transcriptional Drosha recruitment. EMBO J 2012;31(24):4502-4510.

190. DeJesus-Hernandez M, Mackenzie IR, Boeve BF, Boxer AL, Baker M, Rutherford NJ, Nicholson AM, Finch NA, Flynn H, Adamson J and others. Expanded GGGGCC hexanucleotide repeat in noncoding region of C9ORF72 causes chromosome 9p-linked FTD and ALS. Neuron 2011;72(2):245-256.

191. Renton AE, Majounie E, Waite A, Simon-Sanchez J, Rollinson S, Gibbs JR, Schymick JC, Laaksovirta H, van Swieten JC, Myllykangas L and others. A hexanucleotide repeat expansion in C9ORF72 is the cause of chromosome 9p21-linked ALS-FTD. Neuron 2011;72(2):257-268.

192. Rademakers R. C9orf72 repeat expansion in patients with ALS and FTLD. Lancet Neurol 2012;11:297-298.

193. Al-Sarraj S, King A, Troakes C, Smith B, Maekawa S, Bodi I, Rogelj B, Al-Chalabi A, Hortobagyi T, Shaw CE. p62 positive, TDP-43 negative, neuronal cytoplasmic and intranuclear inclusions in the cerebellum and hippocampus define the pathology of C9orf72-linked FTLD and MND/ALS. Acta Neuropathol 2011;122:691-702.

194. Levine TP, Daniels RD, Gatta AT, Wong LH, Hayes MJ. The product of C9orf72, a gene strongly implicated in neurodegeneration, is structurally related to DENN Rab-GEFs. Bioinformatics 2013;29(4):499-503.

195. Koppers M, Blokhuis AM, Westeneng H-J, Terpstra ML, Zundel CAC, Vieira de Sá R, Schellevis RD, Waite AJ, Blake DJ, Veldink JH and others. C9orf72 ablation in mice does not cause motor neuron degeneration or motor deficits. Ann Neurol 2015;78(3):426-438.

196. Ciura S, Lattante S, Le Ber J, Latouche M, Tostivint H, Brice A, Kabashi E. Loss of function of C9orf72 causes motor deficits in a zebrafish model of amyotrophic lateral sclerosis. Ann Neurol 2013;74(2):180-187.

197. Rohrer JD, Isaacs AM, Mizielinska S, Mead S, Lashley T, Wray S, Sidle K, Fratta P, Orrell RW, Hardy J and others. C9orf72 expansions in frontotemporal dementia and amyotrophic lateral sclerosis. The Lancet Neurology 2015;14(3):291-301.

198. Vatovec S, Kovanda A, Rogeli B. Unconventional features of C9ORF72 expanded repeat in amyotrophic lateral sclerosis and frontotemporal lobar degeneration. Neurobiol Aging 2014;35(10):2421.e1-2421.e12.

199. Simone R, Fratta P, Neidle S, Parkinson GN, Isaacs AM. G-quadruplexes: Emerging roles in neurodegenerative diseases and the non-coding transcriptome. FEBS Lett 2015;589(14):1653-1668.

200. Wen X, Tan W, Westergard T, Krishnamurthy K, Markandaiah SS, Shi Y, Lin S, Shneider Neil A, Monaghan J, Pandey Udai B and others. Antisense Proline-Arginine RAN Dipeptides Linked to C9ORF72-ALS/FTD Form Toxic Nuclear Aggregates that Initiate In Vitro and In Vivo Neuronal Death. Neuron 2014;84(6):1213-1225.

201. Meyer K, Ferraiuolo L, Miranda CJ, Likhite S, McElroy S, Renusch S, Ditsworth D, Lagier-Tourenne C, Smith RA, Ravits J and others. Direct conversion of patient fibroblasts demonstrates non-cell autonomous toxicity of astrocytes to motor neurons in familial and sporadic ALS. Proc Natl Acad Sci USA 2014;111(2):829-832.

202. Mackenzie I, Arzberger T, Kremmer E, Troost D, Lorenzl S, Mori K, Weng S-M, Haass C, Kretzschmar H, Edbauer D and others. Dipeptide repeat protein pathology in C9ORF72 mutation cases: clinico-pathological correlations. Acta Neuropathol 2013;126(6):859-879.

203. Freibaum BD, Lu Y, Lopez-Gonzalez R, Kim NC, Almeida S, Lee K-H, Badders N, Valentine M, Miller BL, Wong PC and others. GGGGCC repeat expansion in C9orf72 compromises nucleocytoplasmic transport. Nature 2015;525(7567):129-133.

204. Zhang K, Donnelly CJ, Haeusler AR, Grima JC, Machamer JB, Steinwald P, Daley EL, Miller SJ, Cunningham KM, Vidensky S and others. The C9orf72 repeat expansion disrupts nucleocytoplasmic transport. Nature 2015;525(7567):56-61.

205. Su Z, Zhang Y, Gendron TF, Bauer PO, Chew J, Yang WY, Fostvedt E, Jansen-West K, Belzil VV, Desaro P and others. Discovery of a biomarker and lead small molecules to target r(GGGGCC)-associated defects in c9FTD/ALS. Neuron 2014;83(5):1043-50.

206. Zu T, Liu Y, Banez-Coronel M, Reid T, Pletnikova O, Lewis J, Miller TM, Harms MB, Falchook AE, Subramony SH and others. RAN proteins and RNA foci from antisense transcripts in C9ORF72 ALS and frontotemporal dementia. Proc Natl Acad Sci U S A 2013;110(51):E4968-77.

207. Weber B, Barros LF. The Astrocyte: Powerhouse and Recycling Center. Cold Spring Harb Perspect Biol 2015.

208. Bayraktar OA, Fuentealba LC, Alvarez-Buylla A, Rowitch DH. Astrocyte development and heterogeneity. Cold Spring Harb Perspect Biol 2015;7(1):a020362.

209. Parpura V, Heneka MT, Montana V, Oliet SH, Schousboe A, Haydon PG, Stout RF, Jr., Spray DC, Reichenbach A, Pannicke T and others. Glial cells in (patho)physiology. J Neurochem 2012;121(1):4-27.

210. Abbott NJ. Astrocyte-endothelial interactions and blood-brain barrier permeability. J Anat 2002;200(6):629-38.

211. Phatnani H, Maniatis T. Astrocytes in neurodegenerative disease. Cold Spring Harb Perspect Biol 2015;7(6).

212. Dong Y, Benveniste EN. Immune function of astrocytes. Glia 2001;36(2):180-90.

213. Vargas MR, Johnson JA. Astrogliosis in amyotrophic lateral sclerosis: role and therapeutic potential of astrocytes. Neurotherapeutics 2010;7(4):471-81.

214. Philips T, Robberecht W. Neuroinflammation in amyotrophic lateral sclerosis: role of glial activation in motor neuron disease. Lancet Neurol 2011;10(3):253-63.

215. Pekny M, Pekna M. Astrocyte reactivity and reactive astrogliosis: costs and benefits. Physiol Rev 2014;94(4):1077-98.

216. Valori CF, Brambilla L, Martorana F, Rossi D. The multifaceted role of glial cells in amyotrophic lateral sclerosis. Cell Mol Life Sci 2014;71(2):287-97.

217. Schiffer D, Cordera S, Cavalla P, Migheli A. Reactive astrogliosis of the spinal cord in amyotrophic lateral sclerosis. J Neurol Sci 1996;139 Suppl:27-33.

218. Almer G, Vukosavic S, Romero N, Przedborski S. Inducible nitric oxide synthase up-regulation in a transgenic mouse model of familial amyotrophic lateral sclerosis. J Neurochem 1999;72(6):2415-25.

219. Poloni M, Facchetti D, Mai R, Micheli A, Agnoletti L, Francolini G, Mora G, Camana C, Mazzini L, Bachetti T. Circulating levels of tumour necrosis factor-alpha and its soluble receptors are increased in the blood of patients with amyotrophic lateral sclerosis. Neurosci Lett 2000;287(3):211-4.

220. Veglianese P, Lo Coco D, Bao Cutrona M, Magnoni R, Pennacchini D, Pozzi B, Gowing G, Julien JP, Tortarolo M, Bendotti C. Activation of the p38MAPK cascade is associated with upregulation of TNF alpha receptors in the spinal motor neurons of mouse models of familial ALS. Mol Cell Neurosci 2006;31(2):218-31.

221. Frakes AE, Ferraiuolo L, Haidet-Phillips AM, Schmelzer L, Braun L, Miranda CJ, Ladner KJ, Bevan AK, Foust KD, Godbout JP and others. Microglia induce motor neuron death via the classical NF-kappaB pathway in amyotrophic lateral sclerosis. Neuron 2014;81(5):1009-23.

222. Borasio GD, Robberecht W, Leigh PN, Emile J, Guiloff RJ, Jerusalem F, Silani V, Vos PE, Wokke JH, Dobbins T. A placebo-controlled trial of insulin-like growth factor-I in amyotrophic lateral sclerosis. European ALS/IGF-I Study Group. Neurology 1998;51(2):583-6.

223. A controlled trial of recombinant methionyl human BDNF in ALS: The BDNF Study Group (Phase III). Neurology 1999;52(7):1427-33.

224. Cudkowicz ME, Shefner JM, Schoenfeld DA, Zhang H, Andreasson KI, Rothstein JD, Drachman DB. Trial of celecoxib in amyotrophic lateral sclerosis. Ann Neurol 2006;60(1):22-31.

225. Klivenyi P, Kiaei M, Gardian G, Calingasan NY, Beal MF. Additive neuroprotective effects of creatine and cyclooxygenase 2 inhibitors in a transgenic mouse model of amyotrophic lateral sclerosis. J Neurochem 2004;88(3):576-82.

226. Kaspar BK, Llado J, Sherkat N, Rothstein JD, Gage FH. Retrograde viral delivery of IGF-1 prolongs survival in a mouse ALS model. Science 2003;301(5634):839-42.

227. Sagot Y, Tan SA, Baetge E, Schmalbruch H, Kato AC, Aebischer P. Polymer encapsulated cell lines genetically engineered to release ciliary neurotrophic factor can slow down progressive motor neuronopathy in the mouse. Eur J Neurosci 1995;7(6):1313-22.

228. Sasaki S, Warita H, Abe K, Iwata M. Inducible nitric oxide synthase (iNOS) and nitrotyrosine immunoreactivity in the spinal cords of transgenic mice with a G93A mutant SOD1 gene. J Neuropathol Exp Neurol 2001;60(9):839-46.

229. Hensley K, Floyd RA, Gordon B, Mou S, Pye QN, Stewart C, West M, Williamson K. Temporal patterns of cytokine and apoptosis-related gene expression in spinal cords of the G93A-SOD1 mouse model of amyotrophic lateral sclerosis. J Neurochem 2002;82(2):365-74.

230. Elliott JL. Cytokine upregulation in a murine model of familial amyotrophic lateral sclerosis. Brain Res Mol Brain Res 2001;95(1-2):172-8.

231. Seeburger JL, Tarras S, Natter H, Springer JE. Spinal cord motoneurons express p75NGFR and p145trkB mRNA in amyotrophic lateral sclerosis. Brain Res 1993;621(1):111-5.

232. Lowry KS, Murray SS, McLean CA, Talman P, Mathers S, Lopes EC, Cheema SS. A potential role for the p75 low-affinity neurotrophin receptor in spinal motor neuron degeneration in murine and human amyotrophic lateral sclerosis. Amyotroph Lateral Scler Other Motor Neuron Disord 2001;2(3):127-34.

233. Frade JM, Rodriguez-Tebar A, Barde YA. Induction of cell death by endogenous nerve growth factor through its p75 receptor. Nature 1996;383(6596):166-8.

234. Pehar M, Cassina P, Vargas MR, Castellanos R, Viera L, Beckman JS, Estevez AG, Barbeito L. Astrocytic production of nerve growth factor in motor neuron apoptosis: implications for amyotrophic lateral sclerosis. J Neurochem 2004;89(2):464-73.

235. Turner BJ, Murray SS, Piccenna LG, Lopes EC, Kilpatrick TJ, Cheema SS. Effect of p75 neurotrophin receptor antagonist on disease progression in transgenic amyotrophic lateral sclerosis mice. J Neurosci Res 2004;78(2):193-9.

236. Tortarolo M, Vallarola A, Lidonnici D, Battaglia E, Gensano F, Spaltro G, Fiordaliso F, Corbelli A, Garetto S, Martini E and others. Lack of TNF-alpha receptor type 2 protects motor neurons in a cellular model of amyotrophic lateral sclerosis and in mutant SOD1 mice but does not affect disease progression. J Neurochem 2015;135(1):109-24.

237. Beschorner R, Dietz K, Schauer N, Mittelbronn M, Schluesener HJ, Trautmann K, Meyermann R, Simon P. Expression of EAAT1 reflects a possible neuroprotective function of reactive astrocytes and activated microglia following human traumatic brain injury. Histol Histopathol 2007;22(5):515-26.

238. Beschorner R, Simon P, Schauer N, Mittelbronn M, Schluesener HJ, Trautmann K, Dietz K, Meyermann R. Reactive astrocytes and activated microglial cells express EAAT1, but not EAAT2, reflecting a neuroprotective potential following ischaemia. Histopathology 2007;50(7):897-910.

239. Lin CL, Bristol LA, Jin L, Dykes-Hoberg M, Crawford T, Clawson L, Rothstein JD. Aberrant RNA processing in a neurodegenerative disease: the cause for absent EAAT2, a glutamate transporter, in amyotrophic lateral sclerosis. Neuron 1998;20(3):589-602.

240. Meyer T, Fromm A, Munch C, Schwalenstocker B, Fray AE, Ince PG, Stamm S, Gron G, Ludolph AC, Shaw PJ. The RNA of the glutamate transporter EAAT2 is variably spliced in amyotrophic lateral sclerosis and normal individuals. J Neurol Sci 1999;170(1):45-50.

241. Wong PC, Pardo CA, Borchelt DR, Lee MK, Copeland NG, Jenkins NA, Sisodia SS, Cleveland DW, Price DL. An adverse property of a familial ALS-linked SOD1 mutation causes motor neuron disease characterized by vacuolar degeneration of mitochondria. Neuron 1995;14(6):1105-16.

242. Hall ED, Oostveen JA, Gurney ME. Relationship of microglial and astrocytic activation to disease onset and progression in a transgenic model of familial ALS. Glia 1998;23(3):249-56.

243. Haidet-Phillips AM, Gross SK, Williams T, Tuteja A, Sherman A, Ko M, Jeong YH, Wong PC, Maragakis NJ. Altered astrocytic expression of TDP-43 does not influence motor neuron survival. Exp Neurol 2013;250:250-9.

244. Correia AS, Patel P, Dutta K, Julien JP. Inflammation Induces TDP-43 Mislocalization and Aggregation. PLoS One 2015;10(10):e0140248.

245. Ferraiuolo L. The non-cell-autonomous component of ALS: new in vitro models and future challenges. Biochem Soc Trans 2014;42(5):1270-4.

246. Wirenfeldt M, Babcock AA, Vinters HV. Microglia - insights into immune system structure, function, and reactivity in the central nervous system. Histol Histopathol 2011;26(4):519-30.

247. Hanisch UK, Kettenmann H. Microglia: active sensor and versatile effector cells in the normal and pathologic brain. Nat Neurosci 2007;10(11):1387-94.

248. Wu Y, Dissing-Olesen L, MacVicar BA, Stevens B. Microglia: Dynamic Mediators of Synapse Development and Plasticity. Trends Immunol 2015;36(10):605-13.

249. Olah M, Biber K, Vinet J, Boddeke HW. Microglia phenotype diversity. CNS Neurol Disord Drug Targets 2011;10(1):108-18.

250. Engelhardt JI, Appel SH. IgG reactivity in the spinal cord and motor cortex in amyotrophic lateral sclerosis. Arch Neurol 1990;47(11):1210-6.

251. Maihofner C, Probst-Cousin S, Bergmann M, Neuhuber W, Neundorfer B, Heuss D. Expression and localization of cyclooxygenase-1 and -2 in human sporadic amyotrophic lateral sclerosis. Eur J Neurosci 2003;18(6):1527-34.

252. Henkel JS, Engelhardt JI, Siklos L, Simpson EP, Kim SH, Pan T, Goodman JC, Siddique T, Beers DR, Appel SH. Presence of dendritic cells, MCP-1, and activated microglia/macrophages in amyotrophic lateral sclerosis spinal cord tissue. Ann Neurol 2004;55(2):221-35.

253. Henkel JS, Beers DR, Zhao W, Appel SH. Microglia in ALS: the good, the bad, and the resting. J Neuroimmune Pharmacol 2009;4(4):389-98.

254. Clement AM, Nguyen MD, Roberts EA, Garcia ML, Boillee S, Rule M, McMahon AP, Doucette W, Siwek D, Ferrante RJ and others. Wild-type nonneuronal cells extend survival of SOD1 mutant motor neurons in ALS mice. Science 2003;302(5642):113-7.

255. Weydt P, Yuen EC, Ransom BR, Moller T. Increased cytotoxic potential of microglia from ALS-transgenic mice. Glia 2004;48(2):179-82.

256. Roberts K, Zeineddine R, Corcoran L, Li W, Campbell IL, Yerbury JJ. Extracellular aggregated Cu/Zn superoxide dismutase activates microglia to give a cytotoxic phenotype. Glia 2013;61(3):409-19.

257. Zhao W, Beers DR, Bell S, Wang J, Wen S, Baloh RH, Appel SH. TDP-43 activates microglia through NF-kappaB and NLRP3 inflammasome. Exp Neurol 2015;273:24-35.

258. Gonzalez-Velasquez F, Reed JW, Fuseler JW, Matherly EE, Kotarek JA, Soto-Ortega DD, Moss MA. Activation of brain endothelium by soluble aggregates of the amyloid-beta protein involves nuclear factor-kappaB. Curr Alzheimer Res 2011;8(1):81-94.

259. Xia Q, Hu Q, Wang H, Yang H, Gao F, Ren H, Chen D, Fu C, Zheng L, Zhen X and others. Induction of COX-2-PGE2 synthesis by activation of the MAPK/ERK pathway contributes to neuronal death triggered by TDP-43-depleted microglia. Cell Death Dis 2015;6:e1702.

260. Zhao W, Xie W, Xiao Q, Beers DR, Appel SH. Protective effects of an anti-inflammatory cytokine, interleukin-4, on motoneuron toxicity induced by activated microglia. J Neurochem 2006;99(4):1176-87.

261. Villacampa N, Almolda B, Vilella A, Campbell IL, Gonzalez B, Castellano B. Astrocyte-targeted production of IL-10 induces changes in microglial reactivity and reduces motor neuron death after facial nerve axotomy. Glia 2015;63(7):1166-84.

262. Kobayashi M, Konishi H, Takai T, Kiyama H. A DAP12-dependent signal promotes pro-inflammatory polarization in microglia following nerve injury and exacerbates degeneration of injured neurons. Glia 2015;63(6):1073-82.

263. Lee Y, Morrison BM, Li Y, Lengacher S, Farah MH, Hoffman PN, Liu Y, Tsingalia A, Jin L, Zhang PW and others. Oligodendroglia metabolically support axons and contribute to neurodegeneration. Nature 2012;487(7408):443-8.

264. Mackenzie IR, Ansorge O, Strong M, Bilbao J, Zinman L, Ang LC, Baker M, Stewart H, Eisen A, Rademakers R and others. Pathological heterogeneity in amyotrophic lateral sclerosis with FUS mutations: two distinct patterns correlating with disease severity and mutation. Acta Neuropathol 2011;122(1):87-98.

265. Seilhean D, Cazeneuve C, Thuries V, Russaouen O, Millecamps S, Salachas F, Meininger V, Leguern E, Duyckaerts C. Accumulation of TDP-43 and alpha-actin in an amyotrophic lateral sclerosis patient with the K17I ANG mutation. Acta Neuropathol 2009;118(4):561-73.

266. Philips T, Bento-Abreu A, Nonneman A, Haeck W, Staats K, Geelen V, Hersmus N, Kusters B, Van Den Bosch L, Van Damme P and others. Oligodendrocyte dysfunction in the pathogenesis of amyotrophic lateral sclerosis. Brain 2013;136(Pt 2):471-82.

267. Niebroj-Dobosz I, Rafalowska J, Fidzianska A, Gadamski R, Grieb P. Myelin composition of spinal cord in a model of amyotrophic lateral sclerosis (ALS) in SOD1G93A transgenic rats. Folia Neuropathol 2007;45(4):236-41.

268. Rinholm JE, Hamilton NB, Kessaris N, Richardson WD, Bergersen LH, Attwell D. Regulation of oligodendrocyte development and myelination by glucose and lactate. J Neurosci 2011;31(2):538-48.

269. Karetko M, Skangiel-Kramska J. Diverse functions of perineuronal nets. Acta Neurobiol Exp (Wars) 2009;69(4):564-77.

270. Kwok JC, Dick G, Wang D, Fawcett JW. Extracellular matrix and perineuronal nets in CNS repair. Dev Neurobiol 2011;71(11):1073-89.

271. Reimers S, Hartlage-Rubsamen M, Bruckner G, Rossner S. Formation of perineuronal nets in organotypic mouse brain slice cultures is independent of neuronal glutamatergic activity. Eur J Neurosci 2007;25(9):2640-8.

272. Deepa SS, Umehara Y, Higashiyama S, Itoh N, Sugahara K. Specific molecular interactions of oversulfated chondroitin sulfate E with various heparin-binding growth factors. Implications as a physiological binding partner in the brain and other tissues. J Biol Chem 2002;277(46):43707-16.

273. Collins MA, An J, Hood BL, Conrads TP, Bowser RP. Label-Free LC-MS/MS Proteomic Analysis of Cerebrospinal Fluid Identifies Protein/Pathway Alterations and Candidate Biomarkers for Amyotrophic Lateral Sclerosis. J Proteome Res 2015;14(11):4486-501.

274. Forostyak S, Homola A, Turnovcova K, Svitil P, Jendelova P, Sykova E. Intrathecal delivery of mesenchymal stromal cells protects the structure of altered perineuronal nets in SOD1 rats and amends the course of ALS. Stem Cells 2014;32(12):3163-72.

275. Lim GP, Backstrom JR, Cullen MJ, Miller CA, Atkinson RD, Tokes ZA. Matrix metalloproteinases in the neocortex and spinal cord of amyotrophic lateral sclerosis patients. J Neurochem 1996;67(1):251-9.

276. Lorenzl S, Narr S, Angele B, Krell HW, Gregorio J, Kiaei M, Pfister HW, Beal MF. The matrix metalloproteinases inhibitor Ro 28-2653 [correction of Ro 26-2853] extends survival in transgenic ALS mice. Exp Neurol 2006;200(1):166-71.

277. Brkic M, Balusu S, Libert C, Vandenbroucke RE. Friends or Foes: Matrix Metalloproteinases and Their Multifaceted Roles in Neurodegenerative Diseases. Mediators Inflamm 2015;2015:620581.

278. Brockington A, Ning K, Heath PR, Wood E, Kirby J, Fusi N, Lawrence N, Wharton SB, Ince PG, Shaw PJ. Unravelling the enigma of selective vulnerability in neurodegeneration: motor neurons resistant to degeneration in ALS show distinct gene expression characteristics and decreased susceptibility to excitotoxicity. Acta Neuropathol 2013;125(1):95-109.

279. Rabin SJ, Kim JM, Baughn M, Libby RT, Kim YJ, Fan Y, Libby RT, La Spada A, Stone B, Ravits J. Sporadic ALS has compartment-specific aberrant exon splicing and altered cell-matrix adhesion biology. Hum Mol Genet 2010;19(2):313-28.

280. Berry JD, Shefner JM, Conwit R, Schoenfeld D, Keroack M, Felsenstein D, Krivickas L, David WS, Vriesendorp F, Pestronk A and others. Design and initial results of a multi-phase randomized trial of ceftriaxone in amyotrophic lateral sclerosis. PLoS One 2013;8(4):e61177.

281. Cudkowicz M, Shefner J, Schoenfeld DA, Zhang H, Andreasson KL, Rothstein JD, Drachman DB. Trial of celecoxib in amyotrophic lateral sclerosis. Ann Neurol 2006;60(1):22-31.

282. Gordon PH, Moore DH, Miller RG, Florence JM, Verheijde JL, Doorish C, Hilton JF, Spitalny GM, MacArthur RB, Mitsumoto H and others. Efficacy of minocyline in patients with amyotrophic lateral sclerosis: a phase III randomized trial. Lancet Neurol 2007;6(12):1045-1053.

283. Beers DR, Henkel JS, Xiao Q, Zhao W, Wang J, Yen AA, Siklos L, McKercher SR, Appel SH. Wild-type microglia extend survival in PU.1 knockout mice with familial amyotrophic lateral sclerosis. Proc Natl Acad Sci U S A 2006;103(43):16021-16026.

284. Chiu IM, Chen A, Zheng Y, Kosaras B, Tsiftsoglou SA, Vartanian TK, Brown RH, Jr., Carroll MC. T lymphocytes potentiate endogenous neuroprotective inflammation in a mouse model of ALS. Proc Natl Acad Sci U S A 2008;105(46):17913-17918.

285. Beers DR, Henkel JS, Zhao W, Wang J, Huang A, Wen S, Liao B, Appel SH. Endogenous regulatory T lymphocytes ameliorate amyotrophic lateral sclerosis in mice and correlate with disease progression in patients with amyotrophic lateral sclerosis. Brain 2011;134(5):1293-1314.

286. Henkel JS, Beers DR, Wen S, Rivera AL, Toennis KM, Appel JE, Zhao W, Moore DH, Powell SZ, Appel SH. Regulatory T-lymphocytes mediate amyotrophic lateral sclerosis progression and survival. EMBO Mol Med 2013;5(1):64-79.

287. Schwartz M, Baruch K. The resolution of neuroinflammation in neurodegeneration: leukocyte recruitment via the choroid plexus. EMBO J 2014;33(1):7-22.

288. Baruch K, Schwartz M. CNS-specific T cells shape brain function via the choroid plexus. Brain, Behavior and Immunity 2013;34:11-16.

289. Kunis G, Baruch K, Rosenzweig N, Kertser A, Miller O, Berkutzki T, Schwartz M. IFN-γ-dependent activation of the brain's choroid plexus for CNS immune surveillance and repair. Brain 2013;136:3427-3440.

290. Smith R, Myers K, Ravits J, Bowser R. Amyotrophic lateral sclerosis: Is the spinal fluid pathway involved in seeding and spread? Med Hypotheses 2015;85(5):576-583.

291. Hirokawa N, Noda Y. Intracellular transport and kinesin superfamily proteins, KIFs: structure, function, and dynamics. Physiol Rev 2008;88(3):1089-118.

292. Millecamps S, Julien JP. Axonal transport deficits and neurodegenerative diseases. Nat Rev Neurosci 2013;14(3):161-76.

293. Hirokawa N, Takemura R. Molecular motors in neuronal development, intracellular transport and diseases. Curr Opin Neurobiol 2004;14(5):564-73.

294. Vallee RB, Williams JC, Varma D, Barnhart LE. Dynein: An ancient motor protein involved in multiple modes of transport. J Neurobiol 2004;58(2):189-200.

295. Liu G, Dwyer T. Microtubule dynamics in axon guidance. Neurosci Bull 2014;30(4):569-83.

296. Conradi S, Ronnevi LO, Vesterberg O. Increased plasma levels of lead in patients with amyotrophic lateral sclerosis compared with control subjects as determined by flameless atomic absorption spectrophotometry. J Neurol Neurosurg Psychiatry 1978;41(5):389-93.

297. Breuer AC, Lynn MP, Atkinson MB, Chou SM, Wilbourn AJ, Marks KE, Culver JE, Fleegler EJ. Fast axonal transport in amyotrophic lateral sclerosis: an intra-axonal organelle traffic analysis. Neurology 1987;37(5):738-48.

298. Kato T, Kurita K, Seino T, Kadoya T, Horie H, Wada M, Kawanami T, Daimon M, Hirano A. Galectin-1 is a component of neurofilamentous lesions in sporadic and familial amyotrophic lateral sclerosis. Biochem Biophys Res Commun 2001;282(1):166-72.

299. Julien JP, Cote F, Collard JF. Mice overexpressing the human neurofilament heavy gene as a model of ALS. Neurobiol Aging 1995;16(3):487-90; discussion 490-2.

300. Collard JF, Cote F, Julien JP. Defective axonal transport in a transgenic mouse model of amyotrophic lateral sclerosis. Nature 1995;375(6526):61-4.

301. LaMonte BH, Wallace KE, Holloway BA, Shelly SS, Ascano J, Tokito M, Van Winkle T, Howland DS, Holzbaur EL. Disruption of dynein/dynactin inhibits axonal transport in motor neurons causing late-onset progressive degeneration. Neuron 2002;34(5):715-27.

302. Warita H, Itoyama Y, Abe K. Selective impairment of fast anterograde axonal transport in the peripheral nerves of asymptomatic transgenic mice with a G93A mutant SOD1 gene. Brain Res 1999;819(1-2):120-31.

303. Williamson TL, Cleveland DW. Slowing of axonal transport is a very early event in the toxicity of ALS-linked SOD1 mutants to motor neurons. Nat Neurosci 1999;2(1):50-6.

304. De Vos KJ, Chapman AL, Tennant ME, Manser C, Tudor EL, Lau KF, Brownlees J, Ackerley S, Shaw PJ, McLoughlin DM and others. Familial amyotrophic lateral sclerosis-linked SOD1 mutants perturb fast axonal transport to reduce axonal mitochondria content. Hum Mol Genet 2007;16(22):2720-8.

305. Bilsland LG, Sahai E, Kelly G, Golding M, Greensmith L, Schiavo G. Deficits in axonal transport precede ALS symptoms in vivo. Proc Natl Acad Sci U S A 2010;107(47):20523-8.

306. Zhang F, Strom AL, Fukada K, Lee S, Hayward LJ, Zhu H. Interaction between familial amyotrophic lateral sclerosis (ALS)-linked SOD1 mutants and the dynein complex. J Biol Chem 2007;282(22):16691-9.

307. Perlson E, Jeong GB, Ross JL, Dixit R, Wallace KE, Kalb RG, Holzbaur EL. A switch in retrograde signaling from survival to stress in rapid-onset neurodegeneration. J Neurosci 2009;29(31):9903-17.

308. Landers JE, Melki J, Meininger V, Glass JD, van den Berg LH, van Es MA, Sapp PC, van Vught PW, McKenna-Yasek DM, Blauw HM and others. Reduced expression of the Kinesin-Associated Protein 3 (KIFAP3) gene increases survival in sporadic amyotrophic lateral sclerosis. Proc Natl Acad Sci U S A 2009;106(22):9004-9.

309. Traynor BJ, Nalls M, Lai SL, Gibbs RJ, Schymick JC, Arepalli S, Hernandez D, van der Brug MP, Johnson JO, Dillman A and others. Kinesin-associated protein 3 (KIFAP3) has no effect on survival in a population-based cohort of ALS patients. Proc Natl Acad Sci U S A 2010;107(27):12335-8.

310. Pantelidou M, Zographos SE, Lederer CW, Kyriakides T, Pfaffl MW, Santama N. Differential expression of molecular motors in the motor cortex of sporadic ALS. Neurobiol Dis 2007;26(3):577-89.

311. Alami NH, Smith RB, Carrasco MA, Williams LA, Winborn CS, Han SS, Kiskinis E, Winborn B, Freibaum BD, Kanagaraj A and others. Axonal transport of TDP-43 mRNA granules is impaired by ALS-causing mutations. Neuron 2014;81(3):536-43.

312. Keller MF, Ferrucci L, Singleton AB, Tienari PJ, Laaksovirta H, Restagno G, Chio A, Traynor BJ, Nalls MA. Genome-Wide Analysis of the Heritability of Amyotrophic Lateral Sclerosis. JAMA Neurol 2014.

313. Cady J, Allred P, Bali T, Pestronk A, Goate A, Miller TM, Mitra RD, Ravits J, Harms MB, Baloh RH. Amyotrophic lateral sclerosis onset is influenced by the burden of rare variants in known amyotrophic lateral sclerosis genes. Ann Neurol 2015;77(1):100-113.

314. Majoor-Krakauer D, Willems PJ, Hofman A. Genetic epidemiology of amyotrophic lateral sclerosis. Clin Genet 2003;63(2):83-101.

315. Talbot K. Amyotrophic lateral sclerosis: cell vulnerability or system vulnerability? J Anat 2014;224(1):45-51.

316. Renton AE, Chio A, Traynor BJ. State of play in amyotrophic lateral sclerosis genetics. Nat Neurosci 2014;17(1):17-23.

317. Bowser R, Turner MR, Shefner J. Biomarkers in amyotrophic lateral sclerosis: opportunities and limitations. Nat Rev Neurol 2011;7(11):631-8.

318. Bowser R, Lacomis D. Applying proteomics to the diagnosis and treatment of ALS and related diseases. Muscle Nerve 2009;40(5):753-62.

319. Teng PN, Bateman NW, Hood BL, Conrads TP. Advances in proximal fluid proteomics for disease biomarker discovery. J Proteome Res 2010;9(12):6091-100.

320. Schutzer SE, Liu T, Natelson BH, Angel TE, Schepmoes AA, Purvine SO, Hixson KK, Lipton MS, Camp DG, Coyle PK and others. Establishing the Proteome of Normal Human Cerebrospinal Fluid. PLoS ONE 2010;5(6):e10980.

321. Perrin RJ, Payton JE, Malone JP, Gilmore P, Davis AE, Xiong C, Fagan AM, Townsend RR, Holtzman DM. Quantitative label-free proteomics for discovery of biomarkers in cerebrospinal fluid: assessment of technical and inter-individual variation. PLoS One 2013;8(5):e64314.

322. Kuhle J, Lindberg RL, Regeniter A, Mehling M, Steck AJ, Kappos L, Czaplinski A. Increased levels of inflammatory chemokines in amyotrophic lateral sclerosis. Eur J Neurol 2009;16(6):771-4.

323. Ganesalingam J, An J, Shaw CE, Shaw G, Lacomis D, Bowser R. Combination of neurofilament heavy chain and complement C3 as CSF biomarkers for ALS. J Neurochem 2011;117(3):528-37.

324. Geser F, Prvulovic D, O'Dwyer L, Hardiman O, Bede P, Bokde AL, Trojanowski JQ, Hampel H. On the development of markers for pathological TDP-43 in amyotrophic lateral sclerosis with and without dementia. Prog Neurobiol 2011;95(4):649-62.

325. Logroscino G, Traynor BJ, Hardiman O, Chio A, Mitchell D, Swingler RJ, Millul A, Benn E, Beghi E. Incidence of amyotrophic lateral sclerosis in Europe. Journal of Neurology, Neurosurgery & Psychiatry 2009;81(4):385-390.

326. Wolf J, Wöhrle JC, Palm F, Nix WA, Maschke M, Safer A, Becher H, Grau AJ. Incidence of amyotrophic lateral sclerosis in Rhineland-Palatinate, Germany. Amyotrophic Lateral Sclerosis and Frontotemporal Degeneration 2014;15(3-4):269-274.

327. Kiernan MC, Vucic S, Cheah BC, Turner MR, Eisen A, Hardiman O, Burrell JR, Zoing MC. Amyotrophic lateral sclerosis. The Lancet 2011;377(9769):942-955.

328. Stambler N, Charatan M, Cedarbaum JM. Prognostic indicators of survival in ALS. Neurology 1998;50(1):66-72.

329. Alčaz S, Jarebinski M, Pekmezović T, Stević-Marinković Z, Pavlović S, Apostolski S. Epidemiological and clinical characteristics of ALS in Belgrade, Yugoslavia. Acta Neurologica Scandinavica 1996;94(4):264-268.

330. Martínez HR, Molina-López JF, Cantú-Martínez L, González-Garza MT, Moreno-Cuevas JE, Couret-Alcaraz P, Treviño SA, Webb-Vargas Y, Caro E, Gil-Valadez A and others. Survival and clinical features in Hispanic amyotrophic lateral sclerosis patients. Amyotrophic Lateral Sclerosis 2011;12(3):199-205.

331. Bensimon G, Lacomblez L, Meininger V. A Controlled Trial of Riluzole in Amyotrophic Lateral Sclerosis. New England Journal of Medicine 1994;330(9):585-591.

332. Sabatelli M, Conte A, Zollino M. Clinical and genetic heterogeneity of amyotrophic lateral sclerosis. Clin Genet 2013;83(5):408-416.

333. Iguchi Y, Katsuno M, Ikenaka K, Ishigaki S, Sobue G. Amyotrophic lateral sclerosis: an update on recent genetic insights. Journal of Neurology 2013;260(11):2917-2927.

334. Turner MR, Hardiman O, Benatar M, Brooks BR, Chio A, de Carvalho M, Ince PG, Lin C, Miller RG, Mitsumoto H and others. Controversies and priorities in amyotrophic lateral sclerosis. The Lancet Neurology 2013;12(3):310-322.

335. Rossi L, Valle C, Carrì MT. Altered Gene Expression, Mitochondrial Damage and Oxidative Stress: Converging Routes in Motor Neuron Degeneration. International Journal of Cell Biology 2012;2012:1-9.

336. Turner MR, Swash M. The expanding syndrome of amyotrophic lateral sclerosis: a clinical and molecular odyssey. Journal of Neurology, Neurosurgery & Psychiatry 2015;86(6):667-673.

337. Neumann M. Frontotemporal lobar degeneration and amyotrophic lateral sclerosis: Molecular similarities and differences. Revue Neurologique 2013;169(10):793-798.

338. Teng P-n, Bateman NW, Hood BL, Conrads TP. Advances in Proximal Fluid Proteomics for Disease Biomarker Discovery. J. Proteome Res. 2010;9(12):6091-6100.

339. Ogata Y, Charlesworth MC, Muddiman DC. Evaluation of Protein Depletion Methods for the Analysis of Total-, Phospho- and Glycoproteins in Lumbar Cerebrospinal Fluid. J. Proteome Res. 2005;4(3):837-845.

340. Ramström M, Zuberovic A, Grönwall C, Hanrieder J, Bergquist J, Hober S. Development of affinity columns for the removal of high-abundance proteins in cerebrospinal fluid. Biotechnol. Appl. Biochem. 2009;52(2):159.

341. Hosokawa M, Arai T, Yamashita M, Tsuji H, Nonaka T, Masuda-Suzukake M, Tamaoka A, Hasegawa M, Akiyama H. Differential diagnosis of amyotrophic lateral sclerosis from Guillain–Barré syndrome by quantitative determination of TDP-43 in cerebrospinal fluid. International Journal of Neuroscience 2013;124(5):344-349.

342. Kasai T, Tokuda T, Ishigami N, Sasayama H, Foulds P, Mitchell DJ, Mann DMA, Allsop D, Nakagawa M. Increased TDP-43 protein in cerebrospinal fluid of patients with amyotrophic lateral sclerosis. Acta Neuropathologica 2008;117(1):55-62.

343. Noto Y-I, Shibuya K, Sato Y, Kanai K, Misawa S, Sawai S, Mori M, Uchiyama T, Isose S, Nasu S and others. Elevated CSF TDP-43 levels in amyotrophic lateral sclerosis: Specificity, sensitivity, and a possible prognostic value. Amyotrophic Lateral Sclerosis 2010;12(2):140-143.

344. Harari O, Cruchaga C, Kauwe JSK, Ainscough BJ, Bales K, Pickering EH, Bertelsen S, Fagan AM, Holtzman DM, Morris JC and others. Phosphorylated Tau-Aβ42 Ratio as a Continuous Trait for Biomarker Discovery for Early-Stage Alzheimer's Disease in Multiplex Immunoassay Panels of Cerebrospinal Fluid. Biological Psychiatry 2014;75(9):723-731.

345. Parnetti L, Castrioto A, Chiasserini D, Persichetti E, Tambasco N, El-Agnaf O, Calabresi P. Cerebrospinal fluid biomarkers in Parkinson disease. Nature Reviews Neurology 2013;9(3):131-140.

346. Awad A, Hemmer B, Hartung H-P, Kieseier B, Bennett JL, Stuve O. Analyses of cerebrospinal fluid in the diagnosis and monitoring of multiple sclerosis. Journal of Neuroimmunology 2010;219(1-2):1-7.

347. Bowser R, Turner MR, Shefner J. Biomarkers in amyotrophic lateral sclerosis: opportunities and limitations. Nature Reviews Neurology 2011;7(11):631-638.

348. Lange DJ, Andersen PM, Remanan R, Marklund S, Benjamin D. Pyrimethamine decreases levels of SOD1 in leukocytes and cerebrospinal fluid of ALS patients: A phase I pilot study. Amyotrophic Lateral Sclerosis and Frontotemporal Degeneration 2012;14(3):199-204.

349. Liu H, Sadygov RG, Yates JR. A Model for Random Sampling and Estimation of Relative Protein Abundance in Shotgun Proteomics. Analytical Chemistry 2004;76(14):4193-4201.

350. Gokce E, Shuford CM, Franck WL, Dean RA, Muddiman DC. Evaluation of Normalization Methods on GeLC-MS/MS Label-Free Spectral Counting Data to Correct for Variation during Proteomic Workflows. J. Am. Soc. Mass Spectrom. 2011;22(12):2199-2208.

351. Eng JK, McCormack AL, Yates JR. An approach to correlate tandem mass spectral data of peptides with amino acid sequences in a protein database. J Am Soc Mass Spectrom 1994;5(11):976-989.

352. Old WM. Comparison of Label-free Methods for Quantifying Human Proteins by Shotgun Proteomics. Molecular & Cellular Proteomics 2005;4(10):1487-1502.

353. Ashburner M, Ball CA, Blake JA, Botstein D, Butler H, Cherry JM, Davis AP, Dolinski K, Dwight SS, Eppig JT and others. Gene Ontology: tool for the unification of biology. Nature Genetics 2000;25(1):25-29.

354. Saeys Y, Inza I, Larranaga P. A review of feature selection techniques in bioinformatics. Bioinformatics 2007;23(19):2507-2517.

355. Liu Q. Support vector machines coupled with proteomics approaches for detecting biomarkers predicting chemotherapy resistance in small cell lung cancer. Oncology Reports 2012.

356. Gollapalli K, Ray S, Srivastava R, Renu D, Singh P, Dhali S, Bajpai Dikshit J, Srikanth R, Moiyadi A, Srivastava S. Investigation of serum proteome alterations in human glioblastoma multiforme. Proteomics 2012;12(14):2378-2390.

357. Cima I, Schiess R, Wild P, Kaelin M, Schuffler P, Lange V, Picotti P, Ossola R, Templeton A, Schubert O and others. Cancer genetics-guided discovery of serum biomarker signatures for diagnosis and prognosis of prostate cancer. Proceedings of the National Academy of Sciences 2011;108(8):3342-3347.

358. Silvestre D, Zoppis I, Brambilla F, Bellettato V, Mauri G, Mauri P. Availability of MudPIT data for classification of biological samples. J Clin Bioinformatics 2013;3(1):1.

359. Ranganathan S, Williams E, Ganchev P, Gopalakrishnan V, Lacomis D, Urbinelli L, Newhall K, Cudkowicz ME, Brown RH, Bowser R. Proteomic profiling of cerebrospinal fluid identifies biomarkers for amyotrophic lateral sclerosis. Journal of Neurochemistry 2005;95(5):1461-1471.

360. Pasinetti GM, Ungar LH, Lange DJ, Yemul S, Deng H, Yuan X, Brown RH, Cudkowicz ME, Newhall K, Peskind E and others. Identification of potential CSF biomarkers in ALS. Neurology 2006;66(8):1218-1222.

361. Ramström M, Ivonin I, Johansson A, Askmark H, Markides KE, Zubarev R, Håkansson P, Aquilonius S-M, Bergquist J. Cerebrospinal fluid protein patterns in neurodegenerative disease revealed by liquid chromatography-Fourier transform ion cyclotron resonance mass spectrometry. Proteomics 2004;4(12):4010-4018.

362. Brettschneider J, Lehmensiek V, Mogel H, Pfeifle M, Dorst J, Hendrich C, Ludolph AC, Tumani H. Proteome analysis reveals candidate markers of disease progression in amyotrophic lateral sclerosis (ALS). Neuroscience Letters 2010;468(1):23-27.

363. von Neuhoff N, Oumeraci T, Wolf T, Kollewe K, Bewerunge P, Neumann B, Brors B, Bufler J, Wurster U, Schlegelberger B and others. Monitoring CSF Proteome Alterations in Amyotrophic Lateral Sclerosis: Obstacles and Perspectives in Translating a Novel Marker Panel to the Clinic. PLoS ONE 2012;7(9):e44401.

364. You J-S, Gelfanova V, Knierman MD, Witzmann FA, Wang M, Hale JE. The impact of blood contamination on the proteome of cerebrospinal fluid. Proteomics 2005;5(1):290-296.

365. Elias JE, Gygi SP. Target-decoy search strategy for increased confidence in large-scale protein identifications by mass spectrometry. Nature Methods 2007;4(3):207-214.

366. Gregori J, Villarreal L, Sánchez A, Baselga J, Villanueva J. An effect size filter improves the reproducibility in spectral counting-based comparative proteomics. Journal of Proteomics 2013;95:55-65.

367. Pham TV, Piersma SR, Warmoes M, Jimenez CR. On the beta-binomial model for analysis of spectral count data in label-free tandem mass spectrometry-based proteomics. Bioinformatics 2009;26(3):363-369.

368. Kwong KS, Holland B, Cheung SH. A modified Benjamini–Hochberg multiple comparisons procedure for controlling the false discovery rate. Journal of Statistical Planning and Inference 2002;104(2):351-362.

369. Storey JD, Tibshirani R. Statistical significance for genomewide studies. Proceedings of the National Academy of Sciences 2003;100(16):9440-9445.

370. Storey JD, Taylor JE, Siegmund D. Strong control, conservative point estimation and simultaneous conservative consistency of false discovery rates: a unified approach. Journal of the Royal Statistical Society: Series B (Statistical Methodology) 2004;66(1):187-205.

371. Storey JD. A direct approach to false discovery rates. Journal of the Royal Statistical Society: Series B (Statistical Methodology) 2002;64(3):479-498.

372. Tusher VG, Tibshirani R, Chu G. Significance analysis of microarrays applied to the ionizing radiation response. Proceedings of the National Academy of Sciences 2001;98(9):5116-5121.

373. Karp NA, McCormick PS, Russell MR, Lilley KS. Experimental and Statistical Considerations to Avoid False Conclusions in Proteomics Studies Using Differential In-gel Electrophoresis. Molecular & Cellular Proteomics 2007;6(8):1354-1364.

374. Hendrickson EL, Xia Q, Wang T, Leigh JA, Hackett M. Comparison of spectral counting and metabolic stable isotope labeling for use with quantitative microbial proteomics. The Analyst 2006;131(12):1335.

375. Bhatia VN, Perlman DH, Costello CE, McComb ME. Software Tool for Researching Annotations of Proteins: Open-Source Protein Annotation Software with Data Visualization. Analytical Chemistry 2009;81(23):9819-9823.

376. Shannon P. Cytoscape: A Software Environment for Integrated Models of Biomolecular Interaction Networks. Genome Research 2003;13(11):2498-2504.

377. Bindea G, Mlecnik B, Hackl H, Charoentong P, Tosolini M, Kirilovsky A, Fridman WH, Pages F, Trajanoski Z, Galon J. ClueGO: a Cytoscape plug-in to decipher functionally grouped gene ontology and pathway annotation networks. Bioinformatics 2009;25(8):1091-1093.

378. Rivals I, Personnaz L, Taing L, Potier MC. Enrichment or depletion of a GO category within a class of genes: which test? Bioinformatics 2006;23(4):401-407.

379. Khatri P, Draghici S. Ontological analysis of gene expression data: current tools, limitations, and open problems. Bioinformatics 2005;21(18):3587-3595.

380. Tilford CA, Siemers NO. Gene Set Enrichment Analysis. Methods in Molecular Biology: Springer Science + Business Media; 2009. p 99-121.

381. Bindea G, Galon J, Mlecnik B. CluePedia Cytoscape plugin: pathway insights using integrated experimental and in silico data. Bioinformatics 2013;29(5):661-663.

382. Snel B. STRING: a web-server to retrieve and display the repeatedly occurring neighbourhood of a gene. Nucleic Acids Research 2000;28(18):3442-3444.

383. Mering Cv. STRING: a database of predicted functional associations between proteins. Nucleic Acids Research 2003;31(1):258-261.

384. Hall M, Frank E, Holmes G, Pfahringer B, Reutemann P, Witten IH. The WEKA data mining software. SIGKDD Explor. Newsl. 2009;11(1):10.

385. Golub TR, Slonim DK, Tamayo P, Huard C, Gaasenbeek M, Mesirov JP, Coller H, Loh ML, Downing JR, Caligiuri MA and others. Molecular classification of cancer: class discovery and class prediction by gene expression monitoring. Science 1999;286(5439):531-7.

386. Carvalho PC, Hewel J, Barbosa VC, Yates Iii JR. Identifying differences in protein expression levels by spectral counting and feature selection. Genetics and Molecular Research 2008;7(2):342-356.

387. Guyon I, Weston J, Barnhill S, Vapnik V. Machine Learning 2002;46(1/3):389-422.

388. Collins MA, An J, Peller D, Bowser R. Total protein is an effective loading control for cerebrospinal fluid western blots. Journal of Neuroscience Methods 2015;251:72-82.

389. Degasperi A, Birtwistle MR, Volinsky N, Rauch J, Kolch W, Kholodenko BN. Evaluating Strategies to Normalise Biological Replicates of Western Blot Data. PLoS ONE 2014;9(1):e87293.

390. Ganesalingam J, An J, Shaw CE, Shaw G, Lacomis D, Bowser R. Combination of neurofilament heavy chain and complement C3 as CSF biomarkers for ALS. Journal of Neurochemistry 2011;117(3):528-537.

391. Wilson ME, Boumaza I, Lacomis D, Bowser R. Cystatin C: A Candidate Biomarker for Amyotrophic Lateral Sclerosis. PLoS ONE 2010;5(12):e15133.

392. Collins M, Riascos D, Kovalik T, An J, Krupa K, Krupa K, Hood BL, Conrads TP, Renton AE, Traynor BJ and others. The RNA-binding motif 45 (RBM45) protein accumulates in inclusion bodies in amyotrophic lateral sclerosis (ALS) and frontotemporal lobar degeneration with TDP-43 inclusions (FTLD-TDP) patients. Acta Neuropathologica 2012;124(5):717-732.

393. Suzuki Y, Minami M, Suzuki M, Abe K, Zenno S, Tsujimoto M, Matsumoto K, Minami Y. The Hsp90 Inhibitor Geldanamycin Abrogates Colocalization of eIF4E and eIF4E-Transporter into Stress Granules and Association of eIF4E with eIF4G. Journal of Biological Chemistry 2009;284(51):35597-35604.

394. Liu-Yesucevitz L, Bilgutay A, Zhang Y-J, Vanderwyde T, Citro A, Mehta T, Zaarur N, McKee A, Bowser R, Sherman M and others. Tar DNA Binding Protein-43 (TDP-43) Associates with Stress Granules: Analysis of Cultured Cells and Pathological Brain Tissue. PLoS ONE 2010;5(10):e13250.

395. Cushing H. Studies on the Cerebro-Spinal Fluid : I. Introduction. J Med Res 1914;31(1):1-19.

396. Conly JM, Ronald AR. Cerebrospinal fluid as a diagnostic body fluid. The American Journal of Medicine 1983;75(1):102-108.

397. Tsuji-Akimoto S, Yabe I, Niino M, Kikuchi S, Sasaki H. Cystatin C in cerebrospinal fluid as a biomarker of ALS. Neuroscience Letters 2009;452(1):52-55.

398. Bartolomucci A, Pasinetti GM, Salton SRJ. Granins as disease-biomarkers: translational potential for psychiatric and neurological disorders. Neuroscience 2010;170(1):289-297.

399. Van Hoecke A, Schoonaert L, Lemmens R, Timmers M, Staats KA, Laird AS, Peeters E, Philips T, Goris A, Dubois B and others. EPHA4 is a disease modifier of amyotrophic lateral sclerosis in animal models and in humans. Nature Medicine 2012;18(9):1418-1422.

400. Brockington A, Ning K, Heath PR, Wood E, Kirby J, Fusi N, Lawrence N, Wharton SB, Ince PG, Shaw PJ. Unravelling the enigma of selective vulnerability in neurodegeneration: motor neurons resistant to degeneration in ALS show distinct gene expression characteristics and decreased susceptibility to excitotoxicity. Acta Neuropathologica 2012;125(1):95-109.

401. Annunziata P, Volpi N. High levels of C3c in the cerebrospinal fluid from amyotrophic lateral sclerosis patients. Acta Neurologica Scandinavica 2009;72(1):61-64.

402. Mantovani S, Gordon R, Macmaw JK, Pfluger CMM, Henderson RD, Noakes PG, McCombe PA, Woodruff TM. Elevation of the terminal complement activation products C5a and C5b-9 in ALS patient blood. Journal of Neuroimmunology 2014;276(1-2):213-218.

403. Goldknopf IL, Sheta EA, Bryson J, Folsom B, Wilson C, Duty J, Yen AA, Appel SH. Complement C3c and related protein biomarkers in amyotrophic lateral sclerosis and Parkinson's disease. Biochemical and Biophysical Research Communications 2006;342(4):1034-1039.

404. Lee JD, Kamaruzaman NA, Fung JNT, Taylor SM, Turner BJ, Atkin JD, Woodruff TM, Noakes PG. Dysregulation of the complement cascade in the hSOD1G93A transgenic mouse model of amyotrophic lateral sclerosis. Journal of Neuroinflammation 2013;10(1):119.

405. Heurich B, el Idrissi NB, Donev RM, Petri S, Claus P, Neal J, Morgan BP, Ramaglia V. Complement upregulation and activation on motor neurons and neuromuscular junction in the SOD1 G93A mouse model of familial amyotrophic lateral sclerosis. Journal of Neuroimmunology 2011;235(1-2):104-109.

406. Woodruff TM, Costantini KJ, Taylor SM, Noakes PG. Role of Complement in Motor Neuron Disease: Animal Models and Therapeutic Potential of Complement Inhibitors. Advances in Experimental Medicine and Biology: Springer Science + Business Media; 2008. p 136-151.

407. Dadon-Nachum M, Melamed E, Offen D. The "Dying-Back" Phenomenon of Motor Neurons in ALS. Journal of Molecular Neuroscience 2010;43(3):470-477.

408. Fischer LR, Glass JD. Axonal Degeneration in Motor Neuron Disease. Neurodegenerative Diseases 2007;4(6):431-442.

409. Sasaki S, Iwata M. Dendritic synapses of anterior horn neurons in amyotrophic lateral sclerosis: an ultrastructural study. Acta Neuropathologica 1996;91(3):278-283.

410. Sasaki S, Iwata M. Ultrastructural study of synapses in the anterior horn neurons of patients with amyotrophic lateral sclerosis. Neuroscience Letters 1996;204(1-2):53-56.

411. Venkova K, Christov A, Kamaluddin Z, Kobalka P, Siddiqui S, Hensley K. Semaphorin 3A Signaling Through Neuropilin-1 Is an Early Trigger for Distal Axonopathy in the SOD1G93A Mouse Model of Amyotrophic Lateral Sclerosis. Journal of Neuropathology & Experimental Neurology 2014;73(7):702-713.

412. Winter FD, Vo T, Stam FJ, Wisman LAB, Bär PR, Niclou SP, van Muiswinkel FL, Verhaagen J. The expression of the chemorepellent Semaphorin 3A is selectively induced in terminal Schwann cells of a subset of neuromuscular synapses that display limited anatomical plasticity and enhanced vulnerability in motor neuron disease. Molecular and Cellular Neuroscience 2006;32(1-2):102-117.

413. Rabin SJ, Kim JMH, Baughn M, Libby RT, Kim YJ, Fan Y, Libby RT, La Spada A, Stone B, Ravits J. Sporadic ALS has compartment-specific aberrant exon splicing and altered cell-matrix adhesion biology. Human Molecular Genetics 2009;19(2):313-328.

414. Forostyak S, Homola A, Turnovcova K, Svitil P, Jendelova P, Sykova E. Intrathecal Delivery of Mesenchymal Stromal Cells Protects the Structure of Altered Perineuronal Nets in SOD1 Rats and Amends the Course of ALS. STEM CELLS 2014;32(12):3163-3172.

415. Karetko-Sysa M, Skangiel-Kramska J, Nowicka D. Aging somatosensory cortex displays increased density of WFA-binding perineuronal nets associated with GAD-negative neurons. Neuroscience 2014;277:734-746.

416. Wang D, Fawcett J. The perineuronal net and the control of CNS plasticity. Cell Tissue Res 2012;349(1):147-160.

417. Suttkus A, Rohn S, Weigel S, Glöckner P, Arendt T, Morawski M. Aggrecan, link protein and tenascin-R are essential components of the perineuronal net to protect neurons against iron-induced oxidative stress. Cell Death Dis 2014;5(3):e1119.

418. Robinson JL, Geser F, Stieber A, Umoh M, Kwong LK, Van Deerlin VM, Lee VMY, Trojanowski JQ. TDP-43 skeins show properties of amyloid in a subset of ALS cases. Acta Neuropathologica 2012;125(1):121-131.

419. Al-Sarraj S, King A, Troakes C, Smith B, Maekawa S, Bodi I, Rogelj B, Al-Chalabi A, Hortobágyi T, Shaw CE. p62 positive, TDP-43 negative, neuronal cytoplasmic and intranuclear inclusions in the cerebellum and hippocampus define the pathology of C9orf72-linked FTLD and MND/ALS. Acta Neuropathologica 2011;122(6):691-702.

420. Komori M, Matsuyama Y, Nirasawa T, Thiele H, Becker M, Alexandrov T, Saida T, Tanaka M, Matsuo H, Tomimoto H and others. Proteomic pattern analysis discriminates among multiple sclerosis-related disorders. Annals of Neurology 2012;71(5):614-623.

421. Cousins SL, Dai W, Stephenson FA. APLP1 and APLP2, members of the APP family of proteins, behave similarly to APP in that they associate with NMDA receptors and enhance NMDA receptor surface expression. J. Neurochem. 2015;133(6):879-885.

422. Klevanski M, Saar M, Baumkötter F, Weyer SW, Kins S, Müller UC. Differential role of APP and APLPs for neuromuscular synaptic morphology and function. Molecular and Cellular Neuroscience 2014;61:201-210.

423. Hambrock HO, Nitsche DP, Hansen U, Bruckner P, Paulsson M, Maurer P, Hartmann U. SC1/Hevin: AN EXTRACELLULAR CALCIUM-MODULATED PROTEIN THAT BINDS COLLAGEN I. Journal of Biological Chemistry 2003;278(13):11351-11358.

424. Kucukdereli H, Allen NJ, Lee AT, Feng A, Ozlu MI, Conatser LM, Chakraborty C, Workman G, Weaver M, Sage EH and others. Control of excitatory CNS synaptogenesis by astrocyte-secreted proteins Hevin and SPARC. Proceedings of the National Academy of Sciences 2011;108(32):E440-E449.

425. Kakunaga S. Nectin-like molecule-1/TSLL1/SynCAM3: a neural tissue-specific immunoglobulin-like cell-cell adhesion molecule localizing at non-junctional contact sites of presynaptic nerve terminals, axons and glia cell processes. Journal of Cell Science 2005;118(6):1267-1277.

426. Gao J, Chen T, Hu G, Gong Y, Qiang B, Yuan J, Peng X. Nectin-like molecule 1 is a glycoprotein with a single N-glycosylation site at N290KS which influences its adhesion activity. Biochimica et Biophysica Acta (BBA) - Biomembranes 2008;1778(6):1429-1435.

427. Hunter PR, Nikolaou N, Odermatt B, Williams PR, Drescher U, Meyer MP. Localization of Cadm2a and Cadm3 proteins during development of the zebrafish nervous system. The Journal of Comparative Neurology 2011;519(11):2252-2270.

428. Tanabe Y, Fujita E, Hayashi YK, Zhu X, Lubbert H, Mezaki Y, Senoo H, Momoi T. Synaptic adhesion molecules in Cadm family at the neuromuscular junction. Cell Biology International 2013;37(7):731-736.

429. Yu L, Smith TF, Gaitatzes C. Thirty-plus functional families from a single motif. Protein Sci. 2000;9(12):2470-2476.

430. Smith TF. Diversity of WD-Repeat proteins. Subcellular Biochemistry: Springer Science + Business Media. p 20-30.

431. Dubitsky A, DeCollibus D, Ortolano GA. Sensitive fluorescent detection of protein on nylon membranes. Journal of Biochemical and Biophysical Methods 2002;51(1):47-56.

432. Gingrich JC, Davis DR, Nguyen Q. Multiplex detection and quantitation of proteins on western blots using fluorescent probes. Biotechniques 2000;29(3):636-42.

433. Sternberg. Biomedical Image Processing. Computer 1983;16(1):22-34.

434. Taylor SC, Berkelman T, Yadav G, Hammond M. A Defined Methodology for Reliable Quantification of Western Blot Data. Molecular Biotechnology 2013;55(3):217-226.

435. Pepe MS, Etzioni R, Feng Z, Potter JD, Thompson ML, Thornquist M, Winget M, Yasui Y. Phases of Biomarker Development for Early Detection of Cancer. JNCI Journal of the National Cancer Institute 2001;93(14):1054-1061.

436. Barker PE. Cancer Biomarker Validation: Standards and Process. Annals of the New York Academy of Sciences 2003;983(1):142-150.

437. Cummings J, Ward TH, Greystoke A, Ranson M, Dive C. Biomarker method validation in anticancer drug development. British Journal of Pharmacology 2008;153(4):646-656.

438. Köhler K, Seitz H. Validation Processes of Protein Biomarkers in Serum—A Cross Platform Comparison. Sensors 2012;12(12):12710-12728.

439. Gao J, Garulacan L-A, Storm SM, Opiteck GJ, Dubaquie Y, Hefta SA, Dambach DM, Dongre AR. Biomarker discovery in biological fluids. Methods 2005;35(3):291-302.

440. Greer S, Honeywell R, Geletu M, Arulanandam R, Raptis L. Housekeeping genes; expression levels may change with density of cultured cells. Journal of Immunological Methods 2010;355(1-2):76-79.

441. Ferguson RE, Carroll HP, Harris A, Maher ER, Selby PJ, Banks RE. Housekeeping proteins: A preliminary study illustrating some limitations as useful references in protein expression studies. Proteomics 2005;5(2):566-571.

442. Sikand K, Singh J, Ebron JS, Shukla GC. Housekeeping Gene Selection Advisory: Glyceraldehyde-3-Phosphate Dehydrogenase (GAPDH) and β-Actin Are Targets of miR-644a. PLoS ONE 2012;7(10):e47510.

443. Eaton SL, Roche SL, Llavero Hurtado M, Oldknow KJ, Farquharson C, Gillingwater TH, Wishart TM. Total Protein Analysis as a Reliable Loading Control for Quantitative Fluorescent Western Blotting. PLoS ONE 2013;8(8):e72457.

444. Pérez-Pérez R, López JA, García-Santos E, Camafeita E, Gómez-Serrano M, Ortega-Delgado FJ, Ricart W, Fernández-Real JM, Peral B. Uncovering Suitable Reference Proteins for Expression Studies in Human Adipose Tissue with Relevance to Obesity. PLoS ONE 2012;7(1):e30326.

445. Moritz CP, Marz SX, Reiss R, Schulenborg T, Friauf E. Epicocconone staining: A powerful loading control for Western blots. Proteomics 2014;14(2-3):162-168.

446. Liu N-K, Xu X-M. β -Tubulin Is a More Suitable Internal Control than β -Actin in Western Blot Analysis of Spinal Cord Tissues after Traumatic Injury. Journal of Neurotrauma 2006;23(12):1794-1801.

447. Krzystek-Korpacka M, Diakowska D, Bania J, Gamian A. Expression Stability of Common Housekeeping Genes Is Differently Affected by Bowel Inflammation and Cancer. Inflammatory Bowel Diseases 2014;20(7):1147-1156.

448. Welinder C, Ekblad L. Coomassie Staining as Loading Control in Western Blot Analysis. J. Proteome Res. 2011;10(3):1416-1419.

449. Zeng L, Guo J, Xu H-B, Huang R, Shao W, Yang L, Wang M, Chen J, Xie P. Direct Blue 71 staining as a destaining-free alternative loading control method for Western blotting. ELECTROPHORESIS 2013;34(15):2234-2239.

450. Gilda JE, Gomes AV. Stain-Free total protein staining is a superior loading control to β-actin for Western blots. Analytical Biochemistry 2013;440(2):186-188.

451. Aldridge GM, Podrebarac DM, Greenough WT, Weiler IJ. The use of total protein stains as loading controls: An alternative to high-abundance single-protein controls in semi-quantitative immunoblotting. Journal of Neuroscience Methods 2008;172(2):250-254.

452. Rivero-Gutiérrez B, Anzola A, Martínez-Augustin O, de Medina FS. Stain-free detection as loading control alternative to Ponceau and housekeeping protein immunodetection in Western blotting. Analytical Biochemistry 2014;467:1-3.

453. Romero-Calvo I, Ocón B, Martínez-Moya P, Suárez MD, Zarzuelo A, Martínez-Augustin O, de Medina FS. Reversible Ponceau staining as a loading control alternative to actin in Western blots. Analytical Biochemistry 2010;401(2):318-320.

454. Boyd W. LUTEIN IN THE CEREBRO-SPINAL FLUID. BMJ 1914;1(2786):1158-1158.

455. Zappaterra MW, Lehtinen MK. The cerebrospinal fluid: regulator of neurogenesis, behavior, and beyond. Cell. Mol. Life Sci. 2012;69(17):2863-2878.

456. Rosenmann H. CSF Biomarkers for Amyloid and Tau Pathology in Alzheimer's Disease. Journal of Molecular Neuroscience 2011;47(1):1-14.

457. Hu WT, Watts K, Grossman M, Glass J, Lah JJ, Hales C, Shelnutt M, Van Deerlin V, Trojanowski JQ, Levey AI. Reduced CSF p-Tau181 to Tau ratio is a biomarker for FTLD-TDP. Neurology 2013;81(22):1945-1952.

458. LeWitt P. Recent advances in CSF biomarkers for Parkinson's disease. Parkinsonism & Related Disorders 2012;18:S49-S51.

459. Madeddu R, Farace C, Tolu P, Solinas G, Asara Y, Sotgiu MA, Delogu LG, Prados JC, Sotgiu S, Montella A. Cytoskeletal proteins in the cerebrospinal fluid as biomarker of multiple sclerosis. Neurological Sciences 2012;34(2):181-186.

460. Kalinina J, Peng J, Ritchie JC, Van Meir EG. Proteomics of gliomas: Initial biomarker discovery and evolution of technology. Neuro-Oncology 2011;13(9):926-942.

461. Schwarz E, Bahn S. Cerebrospinal fluid: identification of diagnostic markers for schizophrenia. Expert Review of Molecular Diagnostics 2008;8(2):209-216.

462. Suon S, Zhao J, Villarreal SA, Anumula N, Liu M, Carangia LM, Renger JJ, Zerbinatti CV. Systemic treatment with liver X receptor agonists raises apolipoprotein E, cholesterol, and amyloid-β peptides in the cerebral spinal fluid of rats. Molecular Neurodegeneration 2010;5(1):44.

463. Khwaja FW, Duke-Cohan JS, Brat DJ, Van Meir EG. Attractin Is Elevated in the Cerebrospinal Fluid of Patients with Malignant Astrocytoma and Mediates Glioma Cell Migration. Clinical Cancer Research 2006;12(21):6331-6336.

464. Light M, Minor KH, DeWitt P, Jasper KH, Davies SJA. Multiplex array proteomics detects increased MMP-8 in CSF after spinal cord injury. Journal of Neuroinflammation 2012;9(1):122.

465. Castañeyra-Ruiz L, González-Marrero I, González-Toledo JM, Castañeyra-Ruiz A, de Paz-Carmona H, Castañeyra-Perdomo A, Carmona-Calero EM. Aquaporin-4 expression in the cerebrospinal fluid in congenital human hydrocephalus. Fluids Barriers CNS 2013;10(1):18.

466. Ditzen C, Tang N, Jastorff AM, Teplytska L, Yassouridis A, Maccarrone G, Uhr M, Bronisch T, Miller CA, Holsboer F and others. Cerebrospinal Fluid Biomarkers for Major Depression Confirm Relevance of Associated Pathophysiology. Neuropsychopharmacology 2011;37(4):1013-1025.

467. Hong Z, Shi M, Chung KA, Quinn JF, Peskind ER, Galasko D, Jankovic J, Zabetian CP, Leverenz JB, Baird G and others. DJ-1 and -synuclein in human cerebrospinal fluid as biomarkers of Parkinson's disease. Brain 2010;133(3):713-726.

468. Otter T, King SM, Witman GB. A two-step procedure for efficient electrotransfer of both high-molecular-weight (>400,000) and low-molecular-weight (<20,000) proteins. Analytical Biochemistry 1987;162(2):370-377.

469. Schneider CA, Rasband WS, Eliceiri KW. NIH Image to ImageJ: 25 years of image analysis. Nature Methods 2012;9(7):671-675.

470. Gassmann M, Grenacher B, Rohde B, Vogel J. Quantifying Western blots: Pitfalls of densitometry. ELECTROPHORESIS 2009;30(11):1845-1855.

471. Šidák Z. Rectangular Confidence Regions for the Means of Multivariate Normal Distributions. Journal of the American Statistical Association 1967;62(318):626-633.

472. Wong M, Schlaggar BL, Buller RS, Storch GA, Landt M. Cerebrospinal Fluid Protein Concentration in Pediatric Patients. Arch Pediatr Adolesc Med 2000;154(8):827.

473. Katila O, Lappalainen A. [Fluctuations in the total protein content of the cerebrospinal fluid in patients with neurosyphilis]. Duodecim 1960;76:61-8.

474. Lush B, Crowley MF, Fletcher E, Buchan JF. Total and Differential Protein Levels in the Blood and Cerebrospinal Fluid in Rheumatoid Arthritis. Annals of the Rheumatic Diseases 1951;10(2):153-162.

475. Roberts-Thomson PJ, Esiri MM, Young AC, Maclennan IC. Cerebrospinal fluid immunoglobulin quotients, kappa/lambda ratios, and viral antibody titres in neurological disease. Journal of Clinical Pathology 1976;29(12):1105-1115.

476. Ghasemzadeh N, Nyberg F, Hjertén S. Highly selective artificial gel antibodies for detection and quantification of biomarkers in clinical samples. II. Albumin in body fluids of patients with neurological disorders. J. Sep. Sci. 2008;31(22):3954-3958.

477. Li X, Miyajima M, Mineki R, Taka H, Murayama K, Arai H. Analysis of potential diagnostic biomarkers in cerebrospinal fluid of idiopathic normal pressure hydrocephalus by proteomics. Acta Neurochir (Wien) 2006;148(8):859-864.

478. Sidor MM, Sakic B, Malinowski PM, Ballok DA, Oleschuk CJ, Macri J. Elevated immunoglobulin levels in the cerebrospinal fluid from lupus-prone mice. Journal of Neuroimmunology 2005;165(1-2):104-113.

479. Davidsson P, Sjögren M, Andreasen N, Lindbjer M, Nilsson CL, Westman-Brinkmalm A, Blennow K. Studies of the pathophysiological mechanisms in frontotemporal dementia by proteome analysis of CSF proteins. Molecular Brain Research 2002;109(1-2):128-133.

480. Guldbrandsen A, Vethe H, Farag Y, Oveland E, Garberg H, Berle M, Myhr K-M, Opsahl JA, Barsnes H, Berven FS. In-depth Characterization of the Cerebrospinal Fluid (CSF) Proteome Displayed Through the CSF Proteome Resource (CSF-PR). Mol Cell Proteomics 2014;13(11):3152-3163.

481. Roche S, Gabelle A, Lehmann S. Clinical proteomics of the cerebrospinal fluid: Towards the discovery of new biomarkers. Prot. Clin. Appl. 2008;2(3):428-436.

482. Simonsen AH, Bahl JMC, Danborg PB, Lindstrom V, Larsen SO, Grubb A, Heegaard NHH, Waldemar G. Pre-analytical factors influencing the stability of cerebrospinal fluid proteins. Journal of Neuroscience Methods 2013;215(2):234-240.

483. Toombs J, Paterson RW, Schott JM, Zetterberg H. Amyloid-beta 42 adsorption following serial tube transfer. Alzheimers Res Ther 2014;6(1):5.

484. Boillée S, Vande Velde C, Cleveland DW. ALS: a disease of motor neurons and their nonneuronal neighbors. Neuron 2006;52(1):39-59.

485. Mackenzie IR, Neumann M, Bigio EH, Cairns NJ, Alafuzoff I, Kril J, Kovacs GG, Ghetti B, Halliday G, Holm IE and others. Nomenclature and nosology for neuropathologic subtypes of frontotemporal lobar degeneration: an update. Acta Neuropathol 2010;119:1-4.

486. McKhann G, Albert M, Grossman M, Miller B, Dickson D, Trojanowski J. Clinical and pathological diagnosis of frontotemporal dementia: report of the Work Group on Frontotemporal Dementia and Pick's Disease. Arch Neurol 2001;58(11):1803-9.

487. Leigh P, Whitwell H, Garofalo O, Buller J, Swash M, Martin J, Gallo JM, Weller R, Anderton B. Ubiquitin-immunoreactive intraneuronal inclusions in amyotrophic lateral sclerosis. Brain 1991;114(2):775-88.

488. Katsuse O, Dickson DW. Ubiquitin immunohistochemistry of frontotemporal lobar degeneration differentiates cases with and without motor neuron disease. Alzheimer Dis Assoc Disord 2005;19:S37-43.

489. Lomen-Hoerth C, Anderson T, Miller B. The overlap of amyotrophic lateral sclerosis and frontotemporal dementia. Neurology 2002;59(7):1077-1079.

490. Murphy J, Henry R, Langmore S, Kramer J, Miller B, Lomen-Hoerth C. Continuum of frontal lobe impairment in amyotrophic lateral sclerosis. Arch Neurol 2007;64(4):530-4.

491. Wojciechowska M, Krzyzosiak WJ. Cellular toxicity of expanded RNA repeats: focus on RNA foci. Hum Mol Genet 2011;20:3811-3821.

492. Mackenzie IR, Bigio EH, Ince PG, Geser F, Neumann M, Cairns NJ, Kwong LK, Forman MS, Ravits J, Stewart H and others. Pathological TDP-43 distinguishes sporadic amyotrophic lateral sclerosis from amyotrophic lateral sclerosis with SOD1 mutations. Ann Neurol 2007;61(5):427-434.

493. Arai T, Hasegawa M, Akiyama H, Ikeda K, Nonaka T, Mori H, Mann D, Tsuchiya K, Yoshida M, Hashizume Y and others. TDP-43 is a component of ubiquitin-positive tau-negative inclusions in frontotemporal lobar degeneration and amyotrophic lateral sclerosis. Biochem Biophys Res Commun 2006;351:602-611.

494. Neumann M, Rademakes R, Roeber S, Baker M, Kretzschmar HA, Mackenzie IRA. A new subtype of frontotemporal lobar degeneration with FUS pathology. Brain 2009;132(11):2922-2931.

495. Lagier-Tourenne C, Polymenidou M, Cleveland DW. TDP-43 and FUS/TLS: emerging roles in RNA processing and neurodegeneration. Human Mol Genet 2010;19(R1):R46-64.

496. Mackenzie IRA, Rademakers R, Neumann M. TDP-43 and FUS in amyotrophic lateral sclerosis and frontotemporal dementia. Lancet Neurol 2010;9(10):995-1007.

497. Strong MJ, Volkening K. TDP-43 and FUS/TLS: sending a complex message about messenger RNA in amyotrophic lateral sclerosis? FEBS Lett 2011;278:3569-3577.

498. Tamada H, Sakashita E, Shimazaki K, Ueno E, Hamamoto T, Kagawa Y, Endo H. cDNA cloning and characterization of Drb1, a new member of RRM-type neural RNA-binding protein* 1. Biochem Biophys Res Commun 2002;297(1):96-104.

499. Mladinic M, Lefèvre C, Del Bel E, Nicholls J, Digby M. Developmental changes of gene expression after spinal cord injury in neonatal opossums. Brain Res 2010;Dec 2(1363):20-39.

500. Mackenzie IR, Neumann M, Baborie A, Sampathu DM, Du Plessis D, Jaros E, Perry RH, Trojanowski JQ, Mann DMA, Lee VMY. A harmonized classification system for FTLD-TDP pathology. Acta Neuropathol 2011;122:111-113.

501. Mirra SS, Heyman A, McKeel D. The Consortium to Establish a Registry for Alzheimer's Disease (CERAD). II. Standardization of the neuropathological assessment of Alzheimer's disease. Neurology 1991;41:479-486.

502. Mirra S. The CERAD neuropathology protocol and consensus recommendations for the postmortem diagnosis of Alzheimer's disease: a commentary. Neurobiol Aging 1997;18(Suppl 4):S91-94.

503. Ma K, Inglis JD, Sharkey A, Bickmore WA, Hill RE, Prosser EJ, Speed RM, Thomson EJ, Jobling M, Taylor K and others. A Y-chromosome gene family with RNA-binding protein homology - candidates for the azoospermia factor AZF controlling human spermatogenesis. Cell 1993;75:1287-1295.

504. Cooper-Knock J, Hewitt C, Highley JR, Brockington A, Milano A, Man S, Martindale J, Hartley J, Walsh T, Gelsthorpe C and others. Clinico-pathological features in amyotrophic lateral sclerosis with expansions in C9ORF72. Brain 2012;135:751-764.

505. Josephs KA, Holton JL, Rossor MN, Godbolt AK, Ozawa T, Strand K, Khan N, Al-Sarraj S, Revesz T. Frontotemporal lobar degeneration and ubiquitin immunohistochemistry. Neuropathol Appl Neurobiol 2004;30(4):369-373.

506. Mackenzie IRA, Baborie A, Pickering-Brown S, Plessis DD, Jaros E, Perry RH, Neary D, Snowden JS, Mann DMA. Heterogeneity of ubiquitin pathology in frontotemporal lobar degeneration: classification and relation to clinical phenotype. Acta Neuropathol 2006;112(5):539-549.

507. Tamada H, Sakashita E, Shimazaki K, Ueno E, Hamamoto T, Kagawa Y, Endo H. cDNA cloning and characterization of Drb1, a new member of RRM-type neural RNA-binding protein. Biochem Biophys Res Comm 2002;297:96-104.

508. Lamond AI, Spector DL. Nuclear Speckles: A model for nuclear organelles. Nat Rev Mol Cell Biol 2003;4:605-612.

509. Spector DL, Lamond AI. Nuclear speckles. Cold Spring Harb Perspect Biol 2011;3:a000646.

510. Mintz PJ, Spector DL. Compartmentalization of RNA processig factors within nuclear speckles. J Struct Biol 2000;129:241-251.

511. Hall LL, Smith KP, Byron M, Lawrence JB. Molecular anatomy of a speckle. Anat Rec A Discov Mol Cell Evol Biol 2006;288(7):664-675.

512. Kopreski MS, Benko FA, Kwak LW, Gocke CD. Detection of tumor messenger RNA in the serum of patients with malignant melanoma. Clin Cancer Res 1999;5:1961-1965.

513. Cogswell JP, Ward J, Taylor IA, Waters M, Shi Y, Cannon B, Kelnar K, Kemppainen J, Brown D, Chen C and others. Indentification of miRNA changes in Alzheimer's disease brain and CSF yields putative biomarkers and insights into disease pathways. J Alzheimers Dis 2008;14(1):27-41.

514. Wang K, Zhang S, Weber J, Baxter D, Galas DJ. Export of microRNAs and microRNA-protective protein by mammalian cells. Nucleic Acids Res 2010;38:7248-7259.

515. Deng H-X, Zhai H, Bigio EH, Yan J, Fecto F, Ajroud K, Mishra M, Ajroud-Driss S, Heller S, Sufit R and others. FUS-immunoreactive inclusions are a common feature in sporadic and non-SOD1 familial amyotrophic lateral sclerosis. Ann Neurol 2010;67:739-748.

516. Hewitt C, Kirby J, Highley JR, Hartley J, Hibberd R, Hollinger HC, Williams TL, Ince PG, McDermott CJ, Shaw PJ. Novel FUS/TLS mutations and pathology in familial and sporadic amyotrophic lateral sclerosis. Arch Neurol 2010;67:455-461.

517. Stewart H, Rutherford NJ, Briemberg H, Krieger C, Cashman N, Fabros M, Baker M, Fok A, DeJesus-Hernandez M, Eisen A and others. Clinical and pathological features of amyotrophic lateral sclerosis caused by mutation in the *C9ORF72* gene on crhomosome 9p. Acta Neuropathol 2012;123:409-417.

518. Murray ME, DeJesus-Hernandez M, Rutherford NJ, Baker M, Duara R, Graff-Radford NR, Wszolek ZK, Ferman TJ, Josephs KA, Boylan KB and others. Clinical and neuropathologic heterogeneity of c9FTD/ALS associated with hexanucleotide repeat expansion in C9ORF72. Acta Neuropathol 2011;122:673-690.

519. Andersen PM, Al-Chalabi A. Clinical genetics of amyotrophic lateral sclerosis: what do we really know? Nat Rev Neurol 2011;7:603-615.

520. Sephton CF, Cenik C, Kucukural A, Dammer EB, Cenik B, Han Y, Dewey CM, Roth FP, Herz J, Peng J and others. Identification of neuronal RNA targets of TDP-43-containing ribonucleoprotein complexes. J Biol Chem 2011;286(2):1204-1215.

521. King OD, Gitler AD, Shorter J. The tip of the iceberg: RNA-binding proteins with prion-like domains in neurodegenerative disease. Brain research 2012;1462:61-80.

522. Gitler AD, Shorter J. RNA-binding proteins with prion-like domains in ALS and FTLD-U. Prion 2011;5(3):179-87.

523. Dammer EB, Fallini C, Gozal YM, Duong DM, Rossoll W, Xu P, Lah JJ, Levey AI, Peng J, Bassell GJ and others. Coaggregation of RNA-binding proteins in a model of TDP-43 proteinopathy with selective RGG motif methylation and a role for RRM1 ubiquitination. PLoS One 2012;7(6):e38658.

524. Shelkovnikova TA, Robinson HK, Troakes C, Ninkina N, Buchman VL. Compromised paraspeckle formation as a pathogenic factor in FUSopathies. Hum Mol Genet 2014;23(9):2298-312.

525. Yamazaki T, Chen S, Yu Y, Yan B, Haertlein TC, Carrasco MA, Tapia JC, Zhai B, Das R, Lalancette-Hebert M and others. FUS-SMN protein interactions link the motor neuron diseases ALS and SMA. Cell Rep 2012;2(4):799-806.

526. Vance C, Scotter EL, Nishimura AL, Troakes C, Mitchell JC, Kathe C, Urwin H, Manser C, Miller CC, Hortobagyi T and others. ALS mutant FUS disrupts nuclear localisation and sequesters wild-type FUS within cytoplasmic stress granules. Human molecular genetics 2013.

527. Takanashi K, Yamaguchi A. Aggregation of ALS-linked FUS mutant sequesters RNA binding proteins and impairs RNA granules formation. Biochem Biophys Res Commun 2014;452(3):600-7.

528. Li Y, Collins M, Geiser R, Bakkar N, Riascos D, Bowser R. RBM45 homo-oligomerization mediates association with ALS-linked proteins and stress granules. Sci Rep 2015;5:14262.

529. Nittis T, Guittat L, LeDuc RD, Dao B, Duxin JP, Rohrs H, Townsend RR, Stewart SA. Revealing novel telomere proteins using in vivo cross-linking, tandem affinity purification, and label-free quantitative LC-FTICR-MS. Mol Cell Proteomics 2010;9(6):1144-56.

530. Pahlich S, Quero L, Roschitzki B, Leemann-Zakaryan RP, Gehring H. Analysis of Ewing sarcoma (EWS)-binding proteins: interaction with hnRNP M, U, and RNA-helicases p68/72 within protein-RNA complexes. J Proteome Res 2009;8(10):4455-65.

531. Law WJ, Cann KL, Hicks GG. TLS, EWS and TAF15: a model for transcriptional integration of gene expression. Brief Funct Genomic Proteomic 2006;5(1):8-14.

532. Mackenzie IR, Neumann M. FET proteins in frontotemporal dementia and amyotrophic lateral sclerosis. Brain Res 2012;1462:40-3.

533. Collins M, Riascos D, Kovalik T, An J, Krupa K, Hood BL, Conrads TP, Renton AE, Traynor BJ, Bowser R. The RNA-binding motif 45 (RBM45) protein accumulates in inclusion bodies in amyotrophic lateral sclerosis (ALS) and frontotemporal lobar degeneration with TDP-43 inclusions (FTLD-TDP) patients. Acta neuropathologica 2012;124(5):717-32.

534. Bakkar N, Kousari A, Kovalik T, Li Y, Bowser R. RBM45 Modulates the Antioxidant Response in Amyotrophic Lateral Sclerosis through Interactions with KEAP1. Mol Cell Biol 2015;35(14):2385-99.

535. Tamada H, Sakashita E, Shimazaki K, Ueno E, Hamamoto T, Kagawa Y, Endo H. cDNA cloning and characterization of Drb1, a new member of RRM-type neural RNA-binding protein. Biochemical and biophysical research communications 2002;297(1):96-104.

536. Shevchenko A, Tomas H, Havlis J, Olsen JV, Mann M. In-gel digestion for mass spectrometric characterization of proteins and proteomes. Nat Protoc 2006;1(6):2856-60.

537. Choi H, Glatter T, Gstaiger M, Nesvizhskii AI. SAINT-MS1: protein-protein interaction scoring using label-free intensity data in affinity purification-mass spectrometry experiments. J Proteome Res 2012;11(4):2619-24.

538. Teo G, Liu G, Zhang J, Nesvizhskii AI, Gingras AC, Choi H. SAINTexpress: improvements and additional features in Significance Analysis of INTeractome software. J Proteomics 2014;100:37-43.

539. Shannon P, Markiel A, Ozier O, Baliga NS, Wang JT, Ramage D, Amin N, Schwikowski B, Ideker T. Cytoscape: a software environment for integrated models of biomolecular interaction networks. Genome Res 2003;13(11):2498-504.

540. Staudt T, Lang MC, Medda R, Engelhardt J, Hell SW. 2,2'-thiodiethanol: a new water soluble mounting medium for high resolution optical microscopy. Microsc Res Tech 2007;70(1):1-9.

541. Schneider CA, Rasband WS, Eliceiri KW. NIH Image to ImageJ: 25 years of image analysis. Nat Methods 2012;9(7):671-5.

542. Bolte S, Cordelieres FP. A guided tour into subcellular colocalization analysis in light microscopy. J Microsc 2006;224(Pt 3):213-32.

543. Costes SV, Daelemans D, Cho EH, Dobbin Z, Pavlakis G, Lockett S. Automatic and quantitative measurement of protein-protein colocalization in live cells. Biophys J 2004;86(6):3993-4003.

544. Li Q, Lau A, Morris TJ, Guo L, Fordyce CB, Stanley EF. A syntaxin 1, Galpha(o), and N-type calcium channel complex at a presynaptic nerve terminal: analysis by quantitative immunocolocalization. J Neurosci 2004;24(16):4070-81.

545. Mellacheruvu D, Wright Z, Couzens AL, Lambert JP, St-Denis NA, Li T, Miteva YV, Hauri S, Sardiu ME, Low TY and others. The CRAPome: a contaminant repository for affinity purification-mass spectrometry data. Nat Methods 2013;10(8):730-6.

546. Peters OM, Ghasemi M, Brown RH, Jr. Emerging mechanisms of molecular pathology in ALS. J Clin Invest 2015;125(6):2548.

547. Dreyfuss G, Kim VN, Kataoka N. Messenger-RNA-binding proteins and the messages they carry. Nat Rev Mol Cell Biol 2002;3(3):195-205.

548. Walsh MJ, Cooper-Knock J, Dodd JE, Stopford MJ, Mihaylov SR, Kirby J, Shaw PJ, Hautbergue GM. Invited review: decoding the pathophysiological mechanisms that underlie RNA dysregulation in neurodegenerative disorders: a review of the current state of the art. Neuropathol Appl Neurobiol 2015;41(2):109-34.

549. Lagier-Tourenne C, Polymenidou M, Hutt KR, Vu AQ, Baughn M, Huelga SC, Clutario KM, Ling SC, Liang TY, Mazur C and others. Divergent roles of ALS-linked proteins FUS/TLS and TDP-43 intersect in processing long pre-mRNAs. Nature neuroscience 2012;15(11):1488-97.

550. Kim VN, Dreyfuss G. Nuclear mRNA binding proteins couple pre-mRNA splicing and post-splicing events. Mol Cells 2001;12(1):1-10.

551. Jean-Philippe J, Paz S, Caputi M. hnRNP A1: the Swiss army knife of gene expression. Int J Mol Sci 2013;14(9):18999-9024.

552. Fukuda H, Katahira M, Tsuchiya N, Enokizono Y, Sugimura T, Nagao M, Nakagama H. Unfolding of quadruplex structure in the G-rich strand of the minisatellite repeat by the binding protein UP1. Proc Natl Acad Sci U S A 2002;99(20):12685-90.

553. Cooper-Knock J, Walsh MJ, Higginbottom A, Robin Highley J, Dickman MJ, Edbauer D, Ince PG, Wharton SB, Wilson SA, Kirby J and others. Sequestration of multiple RNA recognition motif-containing proteins by C9orf72 repeat expansions. Brain 2014;137(Pt 7):2040-51.

554. Mori K, Lammich S, Mackenzie IR, Forne I, Zilow S, Kretzschmar H, Edbauer D, Janssens J, Kleinberger G, Cruts M and others. hnRNP A3 binds to GGGGCC repeats and is a constituent of p62-positive/TDP43-negative inclusions in the hippocampus of patients with C9orf72 mutations. Acta Neuropathol 2013;125(3):413-23.

555. Hui J, Stangl K, Lane WS, Bindereif A. HnRNP L stimulates splicing of the eNOS gene by binding to variable-length CA repeats. Nat Struct Biol 2003;10(1):33-7.

556. Hui J, Reither G, Bindereif A. Novel functional role of CA repeats and hnRNP L in RNA stability. RNA 2003;9(8):931-6.

557. Majumder M, Yaman I, Gaccioli F, Zeenko VV, Wang C, Caprara MG, Venema RC, Komar AA, Snider MD, Hatzoglou M. The hnRNA-binding proteins hnRNP L and PTB are required for efficient translation of the Cat-1 arginine/lysine transporter mRNA during amino acid starvation. Mol Cell Biol 2009;29(10):2899-912.

558. Hung LH, Heiner M, Hui J, Schreiner S, Benes V, Bindereif A. Diverse roles of hnRNP L in mammalian mRNA processing: a combined microarray and RNAi analysis. RNA 2008;14(2):284-96.

559. Chiou NT, Shankarling G, Lynch KW. hnRNP L and hnRNP A1 induce extended U1 snRNA interactions with an exon to repress spliceosome assembly. Mol Cell 2013;49(5):972-82.

560. Ma AS, Moran-Jones K, Shan J, Munro TP, Snee MJ, Hoek KS, Smith R. Heterogeneous nuclear ribonucleoprotein A3, a novel RNA trafficking response element-binding protein. J Biol Chem 2002;277(20):18010-20.

561. Huang PR, Hung SC, Wang TC. Telomeric DNA-binding activities of heterogeneous nuclear ribonucleoprotein A3 in vitro and in vivo. Biochim Biophys Acta 2010;1803(10):1164-74.

562. Tanaka E, Fukuda H, Nakashima K, Tsuchiya N, Seimiya H, Nakagama H. HnRNP A3 binds to and protects mammalian telomeric repeats in vitro. Biochem Biophys Res Commun 2007;358(2):608-14.

563. Papadopoulou C, Boukakis G, Ganou V, Patrinou-Georgoula M, Guialis A. Expression profile and interactions of hnRNP A3 within hnRNP/mRNP complexes in mammals. Arch Biochem Biophys 2012;523(2):151-60.

564. Wang IF, Wu LS, Chang HY, Shen CK. TDP-43, the signature protein of FTLD-U, is a neuronal activity-responsive factor. J Neurochem 2008;105(3):797-806.

565. Narayanan RK, Mangelsdorf M, Panwar A, Butler TJ, Noakes PG, Wallace RH. Identification of RNA bound to the TDP-43 ribonucleoprotein complex in the adult mouse brain. Amyotroph Lateral Scler Frontotemporal Degener 2013;14(4):252-60.

566. Lautenschlaeger J, Prell T, Grosskreutz J. Endoplasmic reticulum stress and the ER mitochondrial calcium cycle in amyotrophic lateral sclerosis. Amyotroph Lateral Scler 2012;13(2):166-77.

567. Gautrey H, McConnell J, Hall J, Hesketh J. Polarised distribution of the RNA-binding protein Staufen in differentiated intestinal epithelial cells. FEBS Lett 2005;579(10):2226-30.

568. Stepanenko AA, Dmitrenko VV. HEK293 in cell biology and cancer research: phenotype, karyotype, tumorigenicity, and stress-induced genome-phenotype evolution. Gene 2015;569(2):182-90.

569. Wolozin B, Apicco D. RNA binding proteins and the genesis of neurodegenerative diseases. Adv Exp Med Biol 2015;822:11-5.

570. Mili S, Steitz JA. Evidence for reassociation of RNA-binding proteins after cell lysis: implications for the interpretation of immunoprecipitation analyses. RNA 2004;10(11):1692-4.

571. Klockenbusch C, Kast J. Optimization of formaldehyde cross-linking for protein interaction analysis of non-tagged integrin beta1. J Biomed Biotechnol 2010;2010:927585.

572. Sutherland BW, Toews J, Kast J. Utility of formaldehyde cross-linking and mass spectrometry in the study of protein-protein interactions. J Mass Spectrom 2008;43(6):699-715.

573. Miernyk JA, Thelen JJ. Biochemical approaches for discovering protein-protein interactions. Plant J 2008;53(4):597-609.

574. Zhang H, Tang X, Munske GR, Tolic N, Anderson GA, Bruce JE. Identification of protein-protein interactions and topologies in living cells with chemical cross-linking and mass spectrometry. Mol Cell Proteomics 2009;8(3):409-20.

575. Corgiat BA, Nordman JC, Kabbani N. Chemical crosslinkers enhance detection of receptor interactomes. Front Pharmacol 2014;4:171.

576. Vanderweyde T, Youmans K, Liu-Yesucevitz L, Wolozin B. Role of stress granules and RNA-binding proteins in neurodegeneration: a mini-review. Gerontology 2013;59(6):524-33.

577. Capitini C, Conti S, Perni M, Guidi F, Cascella R, De Poli A, Penco A, Relini A, Cecchi C, Chiti F. TDP-43 inclusion bodies formed in bacteria are structurally amorphous, non-amyloid and inherently toxic to neuroblastoma cells. PLoS One 2014;9(1):e86720.

578. Miguel L, Avequin T, Delarue M, Feuillette S, Frebourg T, Campion D, Lecourtois M. Accumulation of insoluble forms of FUS protein correlates with toxicity in Drosophila. Neurobiol Aging 2012;33(5):1008 e1-15.

579. Xu ZS. Does a loss of TDP-43 function cause neurodegeneration? Mol Neurodegener 2012;7:27.

580. Halliday G, Bigio EH, Cairns NJ, Neumann M, Mackenzie IR, Mann DM. Mechanisms of disease in frontotemporal lobar degeneration: gain of function versus loss of function effects. Acta Neuropathol 2012;124(3):373-82.

581. Lanson NA, Jr., Pandey UB. FUS-related proteinopathies: lessons from animal models. Brain Res 2012;1462:44-60.

582. Kato M, Han TW, Xie S, Shi K, Du X, Wu LC, Mirzaei H, Goldsmith EJ, Longgood J, Pei J and others. Cell-free formation of RNA granules: low complexity sequence domains form dynamic fibers within hydrogels. Cell 2012;149(4):753-67.

583. Murakami T, Qamar S, Lin JQ, Schierle GS, Rees E, Miyashita A, Costa AR, Dodd RB, Chan FT, Michel CH and others. ALS/FTD Mutation-Induced Phase Transition of FUS Liquid Droplets and Reversible Hydrogels into Irreversible Hydrogels Impairs RNP Granule Function. Neuron 2015;88(4):678-90.

584. Zhou Y, Liu S, Liu G, Ozturk A, Hicks GG. ALS-associated FUS mutations result in compromised FUS alternative splicing and autoregulation. PLoS Genet 2013;9(10):e1003895.

585. Cauchi RJ. Gem depletion: amyotrophic lateral sclerosis and spinal muscular atrophy crossover. CNS Neurosci Ther 2014;20(7):574-81.

586. Biamonti G, Vourc'h C. Nuclear stress bodies. Cold Spring Harb Perspect Biol 2010;2(6):a000695.

587. Jolly C, Konecny L, Grady DL, Kutskova YA, Cotto JJ, Morimoto RI, Vourc'h C. In vivo binding of active heat shock transcription factor 1 to human chromosome 9 heterochromatin during stress. J Cell Biol 2002;156(5):775-81.

588. Jolly C, Usson Y, Morimoto RI. Rapid and reversible relocalization of heat shock factor 1 within seconds to nuclear stress granules. Proc Natl Acad Sci U S A 1999;96(12):6769-74.

589. Li Y, Collins M, An J, Geiser R, Tegeler T, Tsantilas K, Garcia K, Pirrotte P, Bowser R. Immunoprecipitation and Mass Spectrometry Defines an Extensive RBM45 Protein-Protein Interaction Network. Brain Res 2016.

590. Denegri M, Chiodi I, Corioni M, Cobianchi F, Riva S, Biamonti G. Stress-induced nuclear bodies are sites of accumulation of pre-mRNA processing factors. Mol Biol Cell 2001;12(11):3502-14.

591. Valgardsdottir R, Chiodi I, Giordano M, Rossi A, Bazzini S, Ghigna C, Riva S, Biamonti G. Transcription of Satellite III non-coding RNAs is a general stress response in human cells. Nucleic Acids Res 2008;36(2):423-34.

592. Busa R, Geremia R, Sette C. Genotoxic stress causes the accumulation of the splicing regulator Sam68 in nuclear foci of transcriptionally active chromatin. Nucleic Acids Res 2010;38(9):3005-18.

593. Burns TC, Li MD, Mehta S, Awad AJ, Morgan AA. Mouse models rarely mimic the transcriptome of human neurodegenerative diseases: A systematic bioinformatics-based critique of preclinical models. Eur J Pharmacol 2015;759:101-17.

594. Mackenzie IR, Neumann M, Bigio EH, Cairns NJ, Alafuzoff I, Kril J, Kovacs GG, Ghetti B, Halliday G, Holm IE and others. Nomenclature and nosology for neuropathologic subtypes of frontotemporal lobar degeneration: an update. Acta Neuropathol 2010;119(1):1-4.

595. Mitsumoto H, Brooks BR, Silani V. Clinical trials in amyotrophic lateral sclerosis: why so many negative trials and how can trials be improved? Lancet Neurol 2014;13(11):1127-38.

596. Kjellin KG, Stibler H. Isoelectric focusing and electrophoresis of cerebrospinal fluid proteins in muscular dystrophies and spinal muscular atrophies. J Neurol Sci 1976;27(1):45-57.

597. Ganesalingam J, An J, Bowser R, Andersen PM, Shaw CE. pNfH is a promising biomarker for ALS. Amyotroph Lateral Scler Frontotemporal Degener 2013;14(2):146-9.

598. Lu CH, Macdonald-Wallis C, Gray E, Pearce N, Petzold A, Norgren N, Giovannoni G, Fratta P, Sidle K, Fish M and others. Neurofilament light chain: A prognostic biomarker in amyotrophic lateral sclerosis. Neurology 2015;84(22):2247-57.

599. Mitchell RM, Freeman WM, Randazzo WT, Stephens HE, Beard JL, Simmons Z, Connor JR. A CSF biomarker panel for identification of patients with amyotrophic lateral sclerosis. Neurology 2009;72(1):14-9.

600. Weydt P, Oeckl P, Huss A, Muller K, Volk AE, Kuhle J, Knehr A, Andersen PM, Prudlo J, Steinacker P and others. Neurofilament levels as biomarkers in asymptomatic and symptomatic familial amyotrophic lateral sclerosis. Ann Neurol 2016;79(1):152-8.

601. Feneberg E, Steinacker P, Lehnert S, Schneider A, Walther P, Thal DR, Linsenmeier M, Ludolph AC, Otto M. Limited role of free TDP-43 as a diagnostic tool in neurodegenerative diseases. Amyotroph Lateral Scler Frontotemporal Degener 2014;15(5-6):351-6.

602. de Carvalho M, Turkman A, Swash M. Sensitivity of MUP parameters in detecting change in early ALS. Clin Neurophysiol 2014;125(1):166-9.

603. Zetterstrom P, Andersen PM, Brannstrom T, Marklund SL. Misfolded superoxide dismutase-1 in CSF from amyotrophic lateral sclerosis patients. J Neurochem 2011;117(1):91-9.

604. Munch C, O'Brien J, Bertolotti A. Prion-like propagation of mutant superoxide dismutase-1 misfolding in neuronal cells. Proc Natl Acad Sci U S A 2011;108(9):3548-53.

605. May S, Hornburg D, Schludi MH, Arzberger T, Rentzsch K, Schwenk BM, Grasser FA, Mori K, Kremmer E, Banzhaf-Strathmann J and others. C9orf72 FTLD/ALS-associated Gly-Ala dipeptide repeat proteins cause neuronal toxicity and Unc119 sequestration. Acta Neuropathol 2014;128(4):485-503.

606. Berry JD, Cudkowicz ME, Shefner JM. Predicting success: optimizing phase II ALS trials for the transition to phase III. Amyotroph Lateral Scler Frontotemporal Degener 2014;15(1-2):1-8.

607. Mizwicki MT, Fiala M, Magpantay L, Aziz N, Sayre J, Liu G, Siani A, Chan D, Martinez-Maza O, Chattopadhyay M and others. Tocilizumab attenuates inflammation in ALS patients through inhibition of IL6 receptor signaling. Am J Neurodegener Dis 2012;1(3):305-15.

608. Lobsiger CS, Cleveland DW. Reply to Woodruff et al.: C1q and C3-dependent complement pathway activation does not contribute to disease in SOD1 mutant ALS mice. Proc Natl Acad Sci U S A 2014;111(1):E5.

609. Miller TM, Pestronk A, David W, Rothstein J, Simpson E, Appel SH, Andres PL, Mahoney K, Allred P, Alexander K and others. An antisense oligonucleotide against SOD1 delivered intrathecally for patients with SOD1 familial amyotrophic lateral sclerosis: a phase 1, randomised, first-in-man study. Lancet Neurol 2013;12(5):435-42.

610. Rohrer JD, Isaacs AM, Mizielinska S, Mead S, Lashley T, Wray S, Sidle K, Fratta P, Orrell RW, Hardy J and others. C9orf72 expansions in frontotemporal dementia and amyotrophic lateral sclerosis. Lancet Neurol 2015;14(3):291-301.

611. Al-Chalabi A, Fang F, Hanby MF, Leigh PN, Shaw CE, Ye W, Rijsdijk F. An estimate of amyotrophic lateral sclerosis heritability using twin data. J Neurol Neurosurg Psychiatry 2010;81(12):1324-6.

612. van Blitterswijk M, van Es MA, Hennekam EA, Dooijes D, van Rheenen W, Medic J, Bourque PR, Schelhaas HJ, van der Kooi AJ, de Visser M and others. Evidence for an oligogenic basis of amyotrophic lateral sclerosis. Hum Mol Genet 2012;21(17):3776-84.

613. Wroe R, Wai-Ling Butler A, Andersen PM, Powell JF, Al-Chalabi A. ALSOD: the Amyotrophic Lateral Sclerosis Online Database. Amyotroph Lateral Scler 2008;9(4):249-50.

614. Oskarsson B, Horton DK, Mitsumoto H. Potential Environmental Factors in Amyotrophic Lateral Sclerosis. Neurol Clin 2015;33(4):877-88.

615. Prudencio M, Belzil VV, Batra R, Ross CA, Gendron TF, Pregent LJ, Murray ME, Overstreet KK, Piazza-Johnston AE, Desaro P and others. Distinct brain transcriptome profiles in C9orf72-associated and sporadic ALS. Nat Neurosci 2015;18(8):1175-82.

616. Bandyopadhyay U, Cotney J, Nagy M, Oh S, Leng J, Mahajan M, Mane S, Fenton WA, Noonan JP, Horwich AL. RNA-Seq profiling of spinal cord motor neurons from a presymptomatic SOD1 ALS mouse. PLoS One 2013;8(1):e53575.

617. Kirby J, Halligan E, Baptista MJ, Allen S, Heath PR, Holden H, Barber SC, Loynes CA, Wood-Allum CA, Lunec J and others. Mutant SOD1 alters the motor neuronal transcriptome: implications for familial ALS. Brain 2005;128(Pt 7):1686-706.

618. Fukada Y, Yasui K, Kitayama M, Doi K, Nakano T, Watanabe Y, Nakashima K. Gene expression analysis of the murine model of amyotrophic lateral sclerosis: studies of the Leu126delTT mutation in SOD1. Brain Res 2007;1160:1-10.

619. Evans TG. Considerations for the use of transcriptomics in identifying the 'genes that matter' for environmental adaptation. J Exp Biol 2015;218(Pt 12):1925-35.

620. Hazelett DJ, Chang JC, Lakeland DL, Morton DB. Comparison of parallel high-throughput RNA sequencing between knockout of TDP-43 and its overexpression reveals primarily nonreciprocal and nonoverlapping gene expression changes in the central nervous system of Drosophila. G3 (Bethesda) 2012;2(7):789-802.

621. Seyfried NT, Gozal YM, Donovan LE, Herskowitz JH, Dammer EB, Xia Q, Ku L, Chang J, Duong DM, Rees HD and others. Quantitative analysis of the detergent-insoluble brain proteome in frontotemporal lobar degeneration using SILAC internal standards. J Proteome Res 2012;11(5):2721-38.

622. Acquadro E, Caron I, Tortarolo M, Bucci EM, Bendotti C, Corpillo D. Human SOD1-G93A specific distribution evidenced in murine brain of a transgenic model for amyotrophic lateral sclerosis by MALDI imaging mass spectrometry. J Proteome Res 2014;13(4):1800-9.

623. Bruijn LI, Cleveland DW. Mechanisms of selective motor neuron death in ALS: insights from transgenic mouse models of motor neuron disease. Neuropathol Appl Neurobiol 1996;22(5):373-87.

624. Peviani M, Caron I, Pizzasegola C, Gensano F, Tortarolo M, Bendotti C. Unraveling the complexity of amyotrophic lateral sclerosis: recent advances from the transgenic mutant SOD1 mice. CNS Neurol Disord Drug Targets 2010;9(4):491-503.

625. Tsao W, Jeong YH, Lin S, Ling J, Price DL, Chiang PM, Wong PC. Rodent models of TDP-43: recent advances. Brain Res 2012;1462:26-39.

626. Koppers M, Blokhuis AM, Westeneng HJ, Terpstra ML, Zundel CA, Vieira de Sa R, Schellevis RD, Waite AJ, Blake DJ, Veldink JH and others. C9orf72 ablation in mice does not cause motor neuron degeneration or motor deficits. Ann Neurol 2015;78(3):426-38.

627. Peters OM, Cabrera GT, Tran H, Gendron TF, McKeon JE, Metterville J, Weiss A, Wightman N, Salameh J, Kim J and others. Human C9ORF72 Hexanucleotide Expansion Reproduces RNA Foci and Dipeptide Repeat Proteins but Not Neurodegeneration in BAC Transgenic Mice. Neuron 2015;88(5):902-9.

628. O'Rourke JG, Bogdanik L, Muhammad AK, Gendron TF, Kim KJ, Austin A, Cady J, Liu EY, Zarrow J, Grant S and others. C9orf72 BAC Transgenic Mice Display Typical Pathologic Features of ALS/FTD. Neuron 2015;88(5):892-901.

629. O'Rourke JG, Bogdanik L, Yanez A, Lall D, Wolf AJ, Muhammad AK, Ho R, Carmona S, Vit JP, Zarrow J and others. C9orf72 is required for proper macrophage and microglial function in mice. Science 2016;351(6279):1324-9.

630. Atanasio A, Decman V, White D, Ramos M, Ikiz B, Lee HC, Siao CJ, Brydges S, LaRosa E, Bai Y and others. C9orf72 ablation causes immune dysregulation characterized by leukocyte expansion, autoantibody production, and glomerulonephropathy in mice. Sci Rep 2016;6:23204.

631. Schwartz JC, Podell ER, Han SS, Berry JD, Eggan KC, Cech TR. FUS is sequestered in nuclear aggregates in ALS patient fibroblasts. Mol Biol Cell 2014;25(17):2571-8.

632. Lee S, Huang EJ. Modeling ALS and FTD with iPSC-derived neurons. Brain Res 2015.

633. Kiskinis E, Sandoe J, Williams LA, Boulting GL, Moccia R, Wainger BJ, Han S, Peng T, Thams S, Mikkilineni S and others. Pathways disrupted in human ALS motor neurons identified through genetic correction of mutant SOD1. Cell Stem Cell 2014;14(6):781-95.

634. Burkhardt MF, Martinez FJ, Wright S, Ramos C, Volfson D, Mason M, Garnes J, Dang V, Lievers J, Shoukat-Mumtaz U and others. A cellular model for sporadic ALS using patient-derived induced pluripotent stem cells. Mol Cell Neurosci 2013;56:355-64.

635. Li M, Suzuki K, Kim NY, Liu GH, Izpisua Belmonte JC. A cut above the rest: targeted genome editing technologies in human pluripotent stem cells. J Biol Chem 2014;289(8):4594-9.